U.S.NRC
United States Nuclear Regulatory Commission
Protecting People and the Environment

NUREG/CR-7276

Primary Water Stress Corrosion Cracking of High-Chromium Nickel-Base Welds – 2018

Office of Nuclear Regulatory Research

AVAILABILITY OF REFERENCE MATERIALS IN NRC PUBLICATIONS

NRC Reference Material

As of November 1999, you may electronically access NUREG-series publications and other NRC records at the NRC's Library at www.nrc.gov/reading-rm.html. Publicly released records include, to name a few, NUREG-series publications; *Federal Register* notices; applicant, licensee, and vendor documents and correspondence; NRC correspondence and internal memoranda; bulletins and information notices; inspection and investigative reports; licensee event reports; and Commission papers and their attachments.

NRC publications in the NUREG series, NRC regulations, and Title 10, "Energy," in the *Code of Federal Regulations* may also be purchased from one of these two sources:

1. **The Superintendent of Documents**
   U.S. Government Publishing Office
   Washington, DC 20402-0001
   Internet: https://bookstore.gpo.gov/
   Telephone: (202) 512-1800
   Fax: (202) 512-2104

2. **The National Technical Information Service**
   5301 Shawnee Road
   Alexandria, VA 22312-0002
   Internet: https://www.ntis.gov/
   1-800-553-6847 or, locally, (703) 605-6000

A single copy of each NRC draft report for comment is available free, to the extent of supply, upon written request as follows:

Address: **U.S. Nuclear Regulatory Commission**
Office of Administration
Digital Communications and Administrative Services Branch
Washington, DC 20555-0001
E-mail: Reproduction.Resource@nrc.gov
Facsimile: (301) 415-2289

Some publications in the NUREG series that are posted at the NRC's Web site address www.nrc.gov/reading-rm/doc-collections/nuregs are updated periodically and may differ from the last printed version. Although references to material found on a Web site bear the date the material was accessed, the material available on the date cited may subsequently be removed from the site.

Non-NRC Reference Material

Documents available from public and special technical libraries include all open literature items, such as books, journal articles, transactions, *Federal Register* notices, Federal and State legislation, and congressional reports. Such documents as theses, dissertations, foreign reports and translations, and non-NRC conference proceedings may be purchased from their sponsoring organization.

Copies of industry codes and standards used in a substantive manner in the NRC regulatory process are maintained at—

The NRC Technical Library
Two White Flint North
11545 Rockville Pike
Rockville, MD 20852-2738

These standards are available in the library for reference use by the public. Codes and standards are usually copyrighted and may be purchased from the originating organization or, if they are American National Standards, from—

American National Standards Institute
11 West 42nd Street
New York, NY 10036-8002
Internet: www.ansi.org
(212) 642-4900

Legally binding regulatory requirements are stated only in laws; NRC regulations; licenses, including technical specifications; or orders, not in NUREG-series publications. The views expressed in contractor prepared publications in this series are not necessarily those of the NRC.

The NUREG series comprises (1) technical and administrative reports and books prepared by the staff (NUREG–XXXX) or agency contractors (NUREG/CR–XXXX), (2) proceedings of conferences (NUREG/CP–XXXX), (3) reports resulting from international agreements (NUREG/IA–XXXX),(4) brochures (NUREG/BR–XXXX), and (5) compilations of legal decisions and orders of the Commission and the Atomic and Safety Licensing Boards and of Directors' decisions under Section 2.206 of the NRC's regulations (NUREG-0750), (6) Knowledge Management prepared by NRC staff or agency contractors (NUREG/KM-XXXX).

U.S.NRC
United States Nuclear Regulatory Commission
Protecting People and the Environment

NUREG/CR-7276

Primary Water Stress Corrosion Cracking of High-Chromium Nickel-Base Welds – 2018

Manuscript Completed: October 2018
Date Published: April 2023

Prepared by:
B. Alexandreanu, Y. Chen, and K. Natesan

Argonne National Laboratory
Argonne, IL 60439

M. Audrain, NRC Project Manager

Office of Nuclear Regulatory Research

ABSTRACT

Nickel-base Alloy 690 and the associated weld Alloys 52 and 152 are typically used for nozzle penetrations in replacement heads for pressurized water reactor (PWR) vessels, because of their increased resistance to stress corrosion cracking (SCC) relative to Alloys 600, 82, and 182. The report presents the results of a confirmatory research program conducted with the purpose of evaluating the susceptibility of Nickel-base Alloy 52/152 and variant welds to stress corrosion cracking (SCC). Several areas have been of particular interest: heat to heat variability, the effect of welding parameters, and the effect of cold work on SCC CGR response. An Alloy 152 weld heat (WC04F6) used in the production of two early weldments by ANL Central Shops was found to be particularly susceptible to IG SCC. This data set was found to have an average SCC CGR approximately 17x lower than the disposition curve for Alloy 182. SCC CGR testing of an Alloy 152 mock-up produced by MHI for the Kewaunee reactor was found to occasionally result in elevated levels of IG fracture, especially at high stress intensity factors. The SCC CGR for this latter weldment were not as high as those measured for the ANL-produced welds. A systematic study on the effect of welding parameters on the SCC CGR response was conducted on three weldments produced by ANL Central Shops with the same Alloy 152 heat code and in the same geometry. The welding parameters tested do not seem to affect the SCC CGR response. In addition, testing also involved an Alloy 52M weld produced at EPRI with high heat input. Although this weld was also found also appears to be resistant, concern remains with susceptibility to SCC at high stress intensity where one SCC CGR measurement was as high as those measured in the early ANL-produced Alloy 152 weldments. The effect of cold-work was evaluated on an Alloy 52 weld in both as-welded and 20% cold-forged (CF) conditions, and all the SCC CGRs were found to be very small. Overall, it was found that the Alloy 52/152 SCC CGR disposition curve proposed in MRP-386 [13] bounds hardly any data presented in this report. The likely explanation lies with the fact that the MRP-386 curve [13] relies on a database of which 60% of the data were obtained at 350-360°C, and to which an unproven dependence on temperature was applied, resulting in an artificially low curve. By contrast, the ANL data were obtained at 320°C, hence, they did not need to be adjusted for temperature.

FOREWORD

This report describes a study sponsored by the NRC Office of Nuclear Regulatory Research (RES) to investigate the stress corrosion cracking (SCC) susceptibility of alloy 690 weld metals including alloys 152, 52 and its many variants. SCC of nickel-based weld metals, such as those used for reactor vessel head penetration nozzles and reactor coolant system nozzles, is a degradation mechanism that can affect the operational safety of pressurized water reactors (PWRs). For instance, through-wall cracking was detected in an Alloy 82 and 182 hot leg nozzle weld at the V.C. Summer plant in 2000. Alloys 52 and 152 are more resistant to SCC than Alloys 82 and 182 because of higher chromium content, and there is no operational experience of their cracking in service. In light of the positive service history and low crack growth rates measured in laboratory testing sponsored by the industry, utilities have submitted requests to the Office of Nuclear Reactor Regulation (NRR) for relief from the inspection requirements found in Title 10 of the Code of Federal Regulations, Part 50.55a, including a 10 year interval for volumetric examination of pressure vessel head nozzles.

In the course of reviewing the relief requests and test results from industry-sponsored research, RES and NRR staff raised questions with respect to the potential for SCC due to higher strains associated with the welds and the weld metal's complex microstructure. These higher chromium weld metals are also susceptible to segregation and weld cracking including solidification cracking and ductility dip cracking. Limited testing has been performed on dissimilar metal (DM) welds where complex compositions and microstructure can be produced at interfaces between Fe-bases alloys (e.g., low allow steel, carbon steel and stainless steels) and the high-Cr, Ni-base weld metal.

This report presents the results of a confirmatory research program conducted with the purpose of evaluating the susceptibility of Nickel-base Alloy 52/152 and variant welds to stress corrosion cracking (SCC). Several areas have been of particular interest: heat to heat variability, the effect of welding parameters, and the effect of cold work on SCC CGR response. A systematic study on the effect of welding parameters on the SCC CGR response was conducted on three weldments produced by ANL Central Shops with the same Alloy 152 heat code and in the same geometry. Also tested was an Alloy 152M weldment produced by IHI with two fillers, one of which exhibited weldability problems. The effect of cold-work was evaluated on an Alloy 52 weld produced by MHI on a piece of Alloy 690 CRDM tubing. Tests were conducted on both as-welded conditions and 20% cold-forged (CF) conditions. Overall, these results support the excellent SCC resistance of the high Cr welds in the as-welded condition.

The application of the test results to plant components is particularly challenging given the large number of potential variations in weld designs and configurations that are found in service. Such tests are ongoing and will continue to inform the evaluations by NRR to determine whether inspection requirement for components with Alloy 52 and 152 welds provide a reasonable assurance of safety.

TABLE OF CONTENTS

LIST OF FIGURES

LIST OF TABLES

EXECUTIVE SUMMARY

Nickel-base Alloy 690 and the associated weld Alloys 52 and 152 are typically used for nozzle penetrations in replacement heads for pressurized water reactor (PWR) vessels, and for mitigation or repairs for dissimilar metal butt welds in the reactor coolant system, and nozzle penetration welds for instrumentation lines in both the reactor vessel and reactor coolant system, because of their increased resistance to stress corrosion cracking (SCC) relative to Alloys 600, 82, and 182. This report summarizes the results of a confirmatory research program performed at ANL to investigate the SCC susceptibility of Ni-base Alloy 52/152 and variant welds. Several areas have been of particular interest: heat to heat variability, the effect of welding parameters, and the effect of cold work on SCC CGR response.

An Alloy 152 weld heat (WC04F6) used in the production of two early weldments by ANL Central Shops was found to be particularly susceptible to IG SCC. This data set was found to have an average SCC CGR approximately 17x lower than the disposition curve for Alloy 182. In addition, these SCC CGRs also exhibited a response to temperature change consistent with that observed for Alloy 182. SCC CGR testing of an Alloy 152 mock-up produced by MHI for the Kewaunee reactor was found to occasionally result in elevated levels of IG fracture, especially at higher stress intensity factors. Overall, the SCC CGR for this latter weldment were not as high as those measured for the ANL-produced welds.

A systematic study on the effect of welding parameters on the SCC CGR response was conducted on three weldments produced by ANL Central Shops with the same Alloy 152 heat code and in the same geometry. SCC CGR data were obtained on a weld produced using “normal” welding parameters (qualified to ASME IX), one produced using “high current”, and another produced using a “high heat input”. The welding parameters tested do not seem to affect the SCC CGR response. In addition to the ANL-produced welds, testing also involved an Alloy 52M weld produced at EPRI with high heat input. Overall, this weld appears to be resistant, however, at high stress intensity one SCC CGR measurement was as high as those measured in the early ANL-produced Alloy 152 weldments.

The effect of cold-work was evaluated on an Alloy 52 weld produced by MHI on a piece of Alloy 690 CRDM tubing. Tests were conducted on both as-welded conditions and 20% cold-forged (CF) conditions, and all the SCC CGRs were found to be very small.

It was found that the Alloy 52/152 SCC CGR disposition curve proposed in MRP-386 [13] bounds a limited set of the data (7%) presented in this report. The likely explanation lies with the fact that the MRP-386 curve [13] relies on a database of which 60% of the data were obtained at 350-360°C, and to which a temperature dependence similar to that of Alloy 182 was applied with little actual data to support its applicability to the Alloy 52/152 weld materials, resulting in an artificially low curve. By contrast, the ANL data were obtained at 320°C, hence, they did not need to be adjusted for temperature.

ACKNOWLEDGMENTS

The authors thank E. Listwan and Z. Zheng for their contributions to the experimental effort, as well as the ANL Electron Microscopy Center. This work is sponsored by the Office of Nuclear Regulatory Research, U.S. Nuclear Regulatory Commission, under EWA NRC-HQ-25-14-D003, Task Order NRC-HQ-60-16-T-0001; Program Manager: M. Audrain.

ABBREVIATIONS AND ACRONYMS

ANL	Argonne National Laboratory
ASTM	American Society for Testing and Materials
B&W	Babcock and Wilcox
BPR	Back Pressure Regulator
BWR	Boiling Water Reactor
CGR	Crack Growth Rate
CL	Constant Load
CMTR	Certified Material Test Report
CRDM	Control Rod Drive Mechanism
CT	Compact Tension
DO	Dissolved Oxygen
ECP	Electrochemical Potential
EDX	Energy Dispersive X-ray Spectroscopy
EPRI MRP	Electric Power Research Institute Materials Reliability Program
GTAW	Gas Tungsten Arc Welding
HAZ	Heat Affected Zone
HX	Heat Exchanger
IG	Intergranular
LAS	Low Alloy Steel
LWR	Light Water Reactor
NRC	Nuclear Regulatory Commission
PNNL	Pacific Northwest National Laboratory
PPU	Partial Periodic Unloading
PWR	Pressurized Water Reactor
PWHT	Post Weld Heat Treatment
PWSCC	Primary Water Stress Corrosion Cracking
SCC	Stress Corrosion Cracking
SEM	Scanning Electron Microscopy
SMAW	Shielded Metal Arc Welding
SS	Stainless Steel
S	Side
T	Transverse
TC	Thermocouple
TG	Transgranular
WOL	Weld Overlay
WPS	Weld Procedure Specification

1 INTRODUCTION

Alloy 600, a nickel-based alloy, was used at the time of construction in light water reactors (LWRs) and has over the years proven to be susceptible to stress corrosion cracking (SCC). Such cracking was first observed in steam generator tubes, but it has also occurred in components such as instrument nozzles and heater thermal sleeves in the pressurizer and control-rod drive mechanism (CRDM) housings in reactor pressure vessel upper closure heads, as in the notable case of the Davis-Besse plant in 2002. In operating plants, the nickel-based weld Alloys 82 and 182 are used with Alloy 600 and are themselves also susceptible to SCC. Through-wall cracking was detected in an Alloy 82 and 182 hot leg nozzle weld at the V.C. Summer plant in 2000. Alloy 690, which has higher chromium (Cr) content than Alloy 600, has been widely used since the 1990s to repair, mitigate or replace Alloy 600 components in pressurized water reactors (PWRs), beginning with thin-walled steam generator tubes, and eventually including thick-section nozzle penetrations in reactor pressure vessel heads. This choice was made following numerous laboratory studies worldwide which established an excellent resistance to SCC in reactor coolant primary water for this alloy [2-4]. Alloys 52 and 152 are the higher Cr content nickel-based weld metals that are used for joining Alloy 690 components, and which are also used for overlays (WOLs), inlays, or onlays to mitigate the SCC susceptibility of Alloy 82 and 182 welds. To date, there are no known cases of in-service SCC of Alloys 690, 52, and 152. This report summarizes the confirmatory testing performed at ANL to investigate the SCC susceptibility of Ni-base Alloy 52/152 and variant welds. Several areas have been of particular interest: heat to heat variability, the effect of welding parameters, and the effect of cold work on SCC CGR response.

Chapter 2 of this report describes the mockups used for testing, including the materials of fabrication, the schematic design of the welds, and the weld fabrication processes. It was intended that the materials and welding parameters should be representative of those used for actual welds used in service. Chapter 2 also discusses the SCC testing equipment and experimental approach. ANL generally followed well-established testing practices that have been employed for a number of years and were reported in previous ANL reports.

Chapter 3 provides the testing results for Alloy 52/152 and variants. Complete CGR data sets are provided as a function of testing conditions, crack advance vs. time plots show the crack extension as a function of time, and photographs and micrographs are given to document the appearances of the fracture surfaces. SCC CGR testing included an Alloy 152 weld heat (WC04F6) used in the production of two early weldments by ANL Central Shops that was found to be particularly susceptible to IG SCC as well as an Alloy 152 mock-up produced by MHI for the Kewaunee reactor that was found to occasionally result in elevated levels of IG fracture, especially at higher stress intensity factors. A systematic study on the effect of welding parameters on the SCC CGR response was conducted on three weldments produced by ANL Central Shops with the same Alloy 152 heat code and in the same geometry. A weld produced by EPRI with high heat input was part of the test program. The effect of cold-work was evaluated on an Alloy 52 weld produced by MHI on a piece of Alloy 690 CRDM tubing. Tests were conducted on both as-welded conditions and 20% cold-forged (CF) conditions

Chapter 4 provides a discussion of the testing results in the framework provided by the industry-proposed disposition curves for Alloys 182 [1] and 52/152 [13]. Finally, Chapter 5 gives a summary of the main findings and conclusions.

2 EXPERIMENTAL

This section describes the Alloy 52/152 weldments used in this study, the configuration of test specimens, and the CGR test apparatus and experimental approach.

2.1 Alloy 690 to Alloy 690 double-J Joint (Alloy 152 weld produced by ANL)

The Alloy 152 shielded-metal-arc weld (SMAW) was fabricated at ANL Central Shops in a double-J geometry (Figure 2) following ASME Boiler and Pressure Vessel Code, Section IX. The double-J weld was produced by joining two Alloy 690 plates (Heat NX3297HK12) and was prepared by 96 weld passes. Root passes 1 to 5 were made by gas tungsten arc welding (GTAW) with Alloy 52 filler, and the other passes were made by SMAW with Alloy 152 filler. The conditions for each weld pass are listed in Table 1. During welding, the maximum inter-pass temperature was ≈120°C (250°F), and the weld surfaces were cleaned by wire brushing and grinding, and were rinsed with de-mineralized water or alcohol. The chemical compositions of the Alloy 152 weld wire supplied by the vendor and those obtained by ICP-OES analysis of the as-deposited weld are given in Table 2.

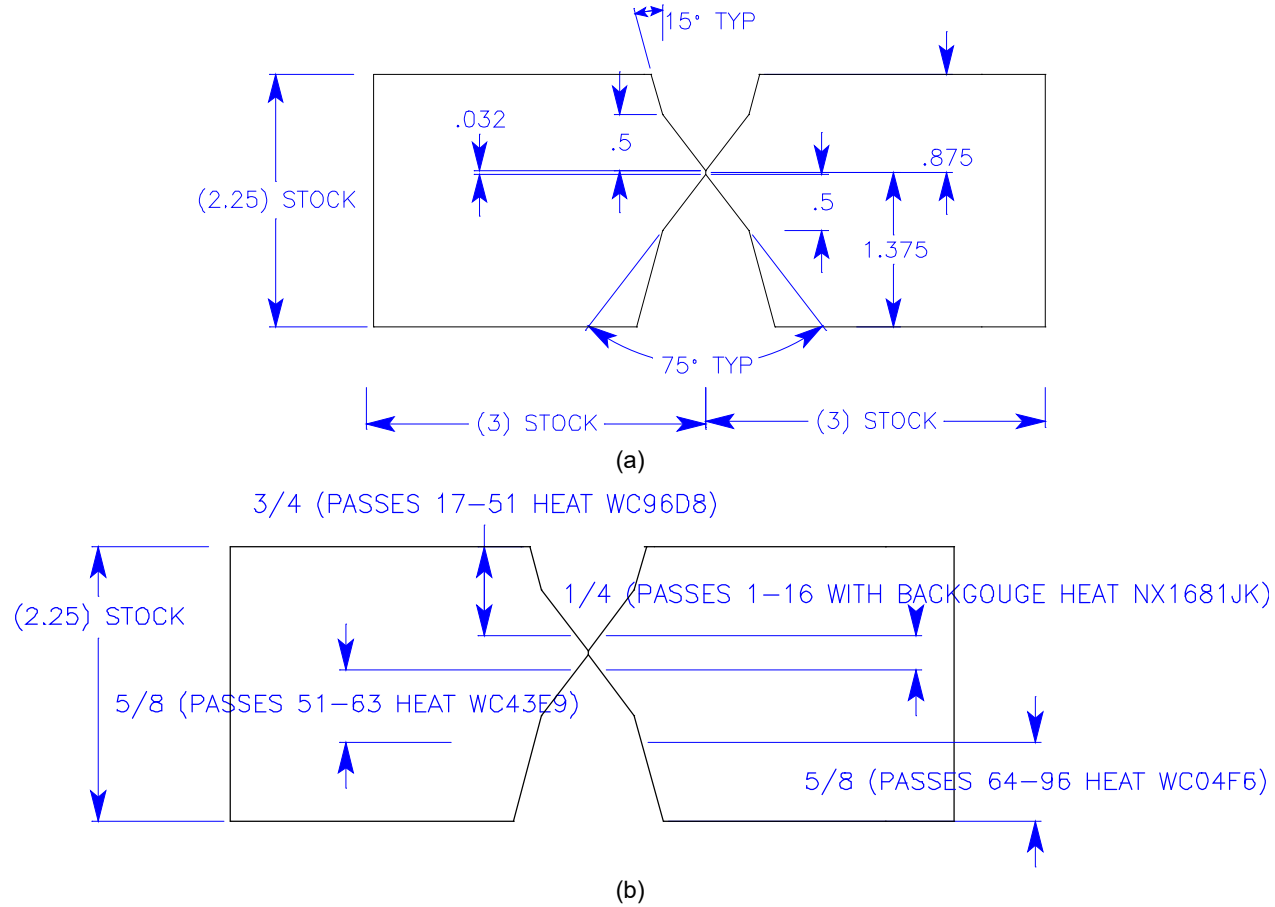

Figure 2 (a) Schematic of the weld joint design for the Alloy 152 double-J weld, and (b) weld passes and filler heats used.

Table 1 Welding process and conditions for various weld passes used for fabricating the A152 weld.

Weld Pass	Process	Filler Metal	Heat Code	Filler Size, in.	Current, A	Voltage, V	Travel Speed, in./min
1 - 16	GTA	Alloy 52 (A5.14M-97 ERNiCrFe-7)	NX1681JK	3/32	55 - 60	21 - 23	6 - 7
17 - 51	SMA	Alloy 152 (A5.11M-97 ENiCrFe-7)	WC96D8	1/8	100 - 110	22 - 25	7 -9
51 - 63	SMA	Alloy 152 (A5.11M-97 ENiCrFe-7)	WC43E9	3/32	55 - 60	21 - 23	6 - 7
64 - 96	SMA	Alloy 152 (A5.11M-97 ENiCrFe-7)	WC04F6	1/8	100 - 110	22 - 25	7 - 9

Table 2 Chemical composition (wt%) of Alloy 152 weld - wire (vendor) and as-deposited (ANL).

Alloy ID (Heat)	Analysis	C	Mn	Fe	S	P	Si	Cu	Ni	Cr	Ti	Nb	Co
A52 (NX168IJK)	Vendor	0.02	0.24	10.40	<0.001	0.005	0.12	0.01	59.30	28.68	0.52	<0.01	0.00
A152 (WC96D8)	Vendor	0.04	3.88	9.16	0.007	0.008	0.54	0.01	55.88	29.35	0.07	1.81	0.01
A152 (WC43E9)	Vendor	<0.03	3.95	10.25	<0.003	<0.005	0.51	0.01	54.16	28.60	0.08	1.93	0.01
A152 (WC04F6)	Vendor	0.048	3.48	10.39	0.003	0.003	0.41	<0.01	55.20	28.70	0.09	1.54	<0.005
	ANL	-	3.88	9.56	-	<0.08	0.52	<0.04	53.70	28.40	0.10	1.80	<0.04

The size of the double-J weld allowed for 1-T CT specimens. These were cut from the bottom weld shown schematically in Figure 2 in the transverse side (TS) orientation, with the notch about 5 mm into the weld. This specimen geometry ensured that the CGR tests were conducted in the region of the weld made with a single Alloy 152 heat, WC04F6. These specimens are designated A152-orientation-number, and initial test results are given in [5].

2.2 Alloy 690 to Alloy 533 Grade B Joint (Alloy 152 weld produced by ANL)

As a large amount of the weld described in the previous section was used to generate tensile data on a temperature range 77-1598°F (25-870°C) [5], a new Alloy 152 weldment was needed for testing purposes. However, the geometry selected for this weldment reflects additional testing priorities: weld HAZ and weld dilution zones. This subsection documents the steps taken to produce a 3-inch thick butt weld for Alloy 690 (Heat NX3297HK12) welded to SA-533 Gr B class 1 steel (Heat A5466-2 from the Midland reactor lower head [8]) buttered with Alloy 152 filler metal. The geometry of the joint is shown in Figure 3. The joint was designed with a straight edge on the Alloy 690 side to facilitate SCC CGR testing of the Alloy 690 heat affected zone (HAZ) which was also of interest in the research program. The SMAW welding procedure was qualified to ASME Section IX by ANL Central Shops [6].

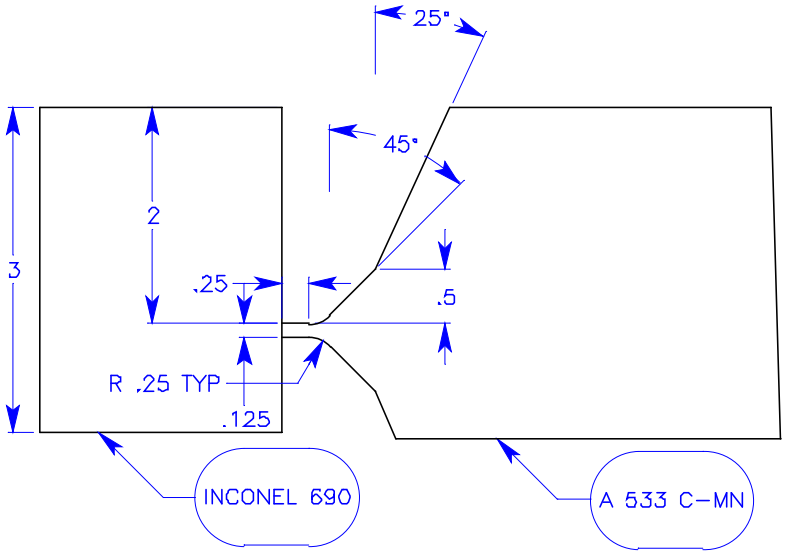

Figure 3 Joint design, Alloy 690 to SA-533 Gr B. Units are in inch.

2.2.1 Alloy 152 Weld Buttering

The LAS plate was machined with a bevel on one end. The beveled end was buttered with Alloy 152 F43 filler metal. A record was kept of the number and location of weld passes together with the heat code of the filler metal used, and the welding parameters that were used [6]. This record is shown in Table 3. After each layer, a liquid penetrant (LP) check was performed. After buttering, the LAS piece was stress relieved at 1150 ± 25ºF for 3h. The chemical composition of the Alloy 152 filler heat 720129 that was used to produce the first layer of buttering is given in Table 4.

Table 3 Welding process and conditions for various weld passes used for fabricating the A152 butter

Weld Pass	Process	Filler Metal	Filler Size, in.	Heat Code	Type Polarity	Current, A	Voltage, V	Travel Speed, in./min	Notes
1 – 23	SMAW	Alloy 152, EniCrFe-7	1/8	720129	DCRP	97-102	21 – 23	5	Layer 1 LP
24-44	SMAW	Alloy 152, EniCrFe-7	5/32	146444	DCRP	113-117	25 – 26	5	Layer 2 LP
45-65	SMAW	Alloy 152, EniCrFe-7	5/32	146444	DCRP	113-117	25 – 26	5	Layer 3 LP

DCRP = direct current reverse polarity

Table 4 Chemical composition (wt.%) of Alloy 152 heats used to produce the weld buttering.

Alloy ID	Analysis	C	Mn	Fe	S	P	Si	Cu	Ni	Cr	Ti	Nb+Ta	Co
A152 (720129)	CMTR	0.037	3.70	9.28	<0.001	<0.003	0.51	0.01	55.26	28.92	0.12	1.92	<0.01
A152 (146444)	CMTR	0.040	3.56	9.36	<0.001	<0.003	0.46	<0.01	55.25	29.04	0.15	1.84	<0.01

2.2.2 Alloy 152 Butt Weld

The buttered LAS piece described in the previous sub-section was beveled on the buttered edge leaving ¼" of Alloy 152 F43 weld material on the face, and a section of Alloy 690 plate was used to make the opposing part of the butt weld. A double bevel J-grove weld was produced according to the design shown in Figure 3, and the number and location of weld passes together with the heat code of the filler metal used, as well as the welding parameters are given in Table 5 [6]. The root pass of the weld and back grind was LP tested, and the final weld surface was also LP tested. The final weld was radiographed per ASME Section IX.

Table 5 Welding process and conditions for various weld passes used for fabricating the A152 butt weld.

Weld Pass	Process	Filler Metal	Filler Size, in.	Heat Code	Type Polarity	Current, A	Voltage, V	Travel Speed, in./min	Notes
1 – 8	SMAW	Alloy 152, EniCrFe-7	1/8	720129	DCRP	97-102	21 – 23	5	
9-14	SMAW	Alloy 152, EniCrFe-7	1/8	146444	DCRP	97-102	25 – 26	5	Root LP BG LP
15-26	SMAW	Alloy 152, EniCrFe-7	5/32	146444	DCRP	113-117	25 – 26	5	Final LP
27-76	SMAW	Alloy 152, EniCrFe-7	1/8	WCO4F6	DCRP	97-102	25 – 26	5	Final LP

DCRP = direct current reverse polarity

The size of this weld allowed for fabrication large 1-T CT specimens. These were cut from the top weld shown schematically in Figure 3 in the transverse side (TS) orientation. This specimen geometry ensured that the CGR tests were conducted in the region of the weld made with a single Alloy 152 heat, WC04F6, just like in the weld described in the previous section. These specimens are designated N152-orientation-number.

2.3 "Kewaunee" mock-up weld (Alloy 152 produced by Mitsubishi Heavy Industries, Japan)

This Alloy 152 weld mock-up was produced by Mitsubishi Heavy Industries (MHI) for the Kewaunee reactor. No other information is available except for weld wire heat code (307380). Sufficient material was provided by EPRI to produce one 1T CT specimen, Figure 4. Great care was taken to machine the specimen notch beyond the solidification crack indicated with a red arrow in the figure. As additional testing (specimens) were desired, an Alloy 690 piece was EB-welded to the end of the tested 1T CT specimen to produce two more 1/2T CT specimens, Fig. Figure 5.

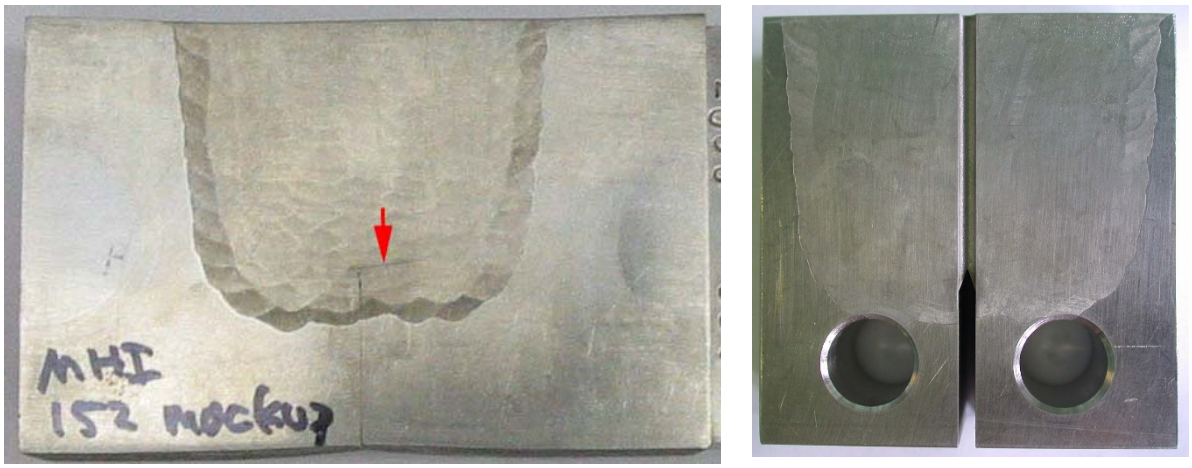

(a) (b)

Figure 4 **Alloy 152 "Kewaunee" mock-up weld produced by Mitsubishi Heavy Industries, Japan (a) and (b) resulting 1T CT specimen. The red arrow indicates a solidification crack.**

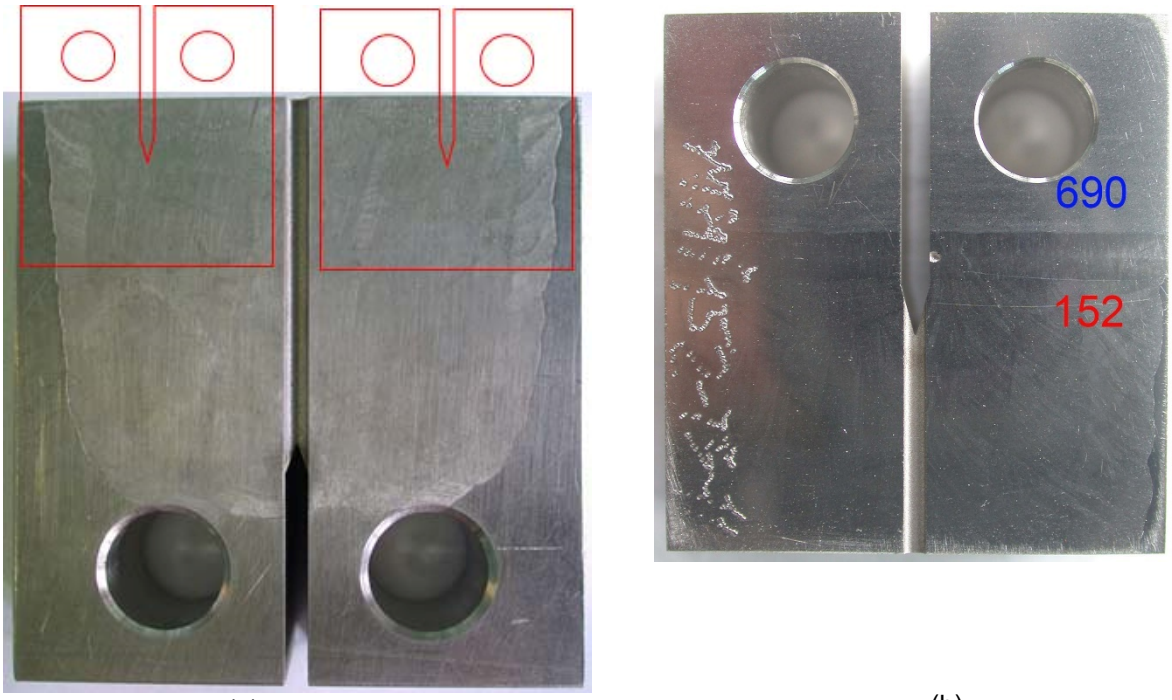

(a) (b)

Figure 5 **(a) original 1T CT specimen fabricated from the Alloy 152 "Kewaunee" mock-up weld produced by Mitsubishi Heavy Industries, Japan, and (b) additional 1/2T CT specimens obtained after the initial test was completed.**

2.4 Effect of welding parameters (Alloy 152 welds produced by ANL)

In order to study the effect of welding parameters on the SCC response of Alloy 152 weld, three weldments were produced on the same piece of Alloy 690 CRDM tubing (Heat WP016) with the same Alloy 152 filler (Heat 509528, Table 6). A weld geometry with a straight edge was favored because that would also facilitate the CGR testing of the Alloy 690 HAZ if desired.

Table 6 Chemical composition (wt. %) of Alloy 152 heat 509528 used to produce the welds for the study of the effect of the welding parameters on SCC.

Alloy ID	Analysis	C	Mn	Fe	S	P	Si	Cu	Ni	Cr	Ti	Nb+Ta	Co
A152 (509528)	CMTR	0.046	3.78	9.02	0.005	<0.003	0.41	<0.01	55.97	28.79	0.07	1.78	<0.01

Three welds were produced in sequence as described in Figure 6 and Figure 7. First, a groove was EDM cut, and the weld with "normal" parameters (weld A) was made. This corresponds to the procedure that was qualified to ASME IX by ANL (see Section 2.2). Then, a diametrically-opposed groove was EDM cut, and a weld with a higher current (weld B) was made. The travel speed was also increased, so the heat input for weld B was practically equivalent to that for weld A. Finally, the sequence was repeated to produce the "high heat input" weld C. As the request from the sponsor for all of these welds was to pass inspection, the allowable parameters limited the heat input of weld C to approximately 20% higher than those for the previous two welds. Table 7 summarizes the welding parameters and the resulting heat inputs for each of the three welds that were produced for this study.

Table 7 Welding conditions used for producing the three Alloy 152 welds used for the study of the effects of welding parameters on SCC

Weld Joint	Process	Filler Metal	Filler Size, in.	Heat Code	Type Polarity	Current, A	Voltage, V	Travel Speed, in./min	Heat Input kJ/cm	Heat input kJ/in.
A	SMAW	Alloy 152, EniCrFe-7	1/8	509528	DCRP	97-102	25–26	3.5-4.5	15.1	38.3
B	SMAW	Alloy 152, EniCrFe-7	1/8	509528	DCRP	125-135	29–32	5.5-6.5	15.4	39.0
C	SMAW	Alloy 152, EniCrFe-7	1/8	509528	DCRP	134-136	30–32	5.4-5.6	18.0	48.5

DCRP = direct current reverse polarity

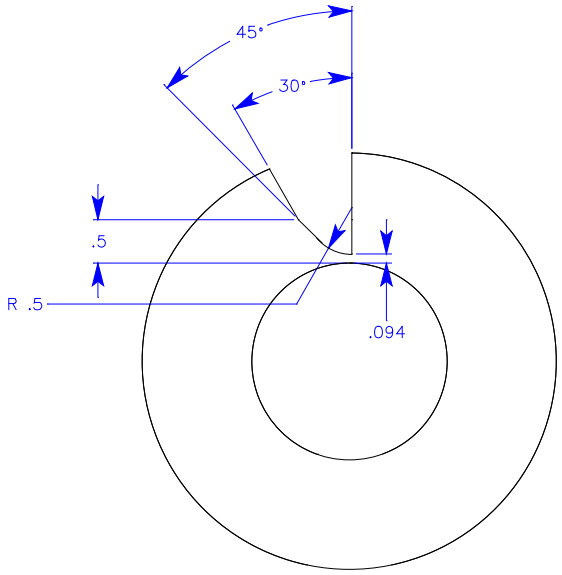

(a)

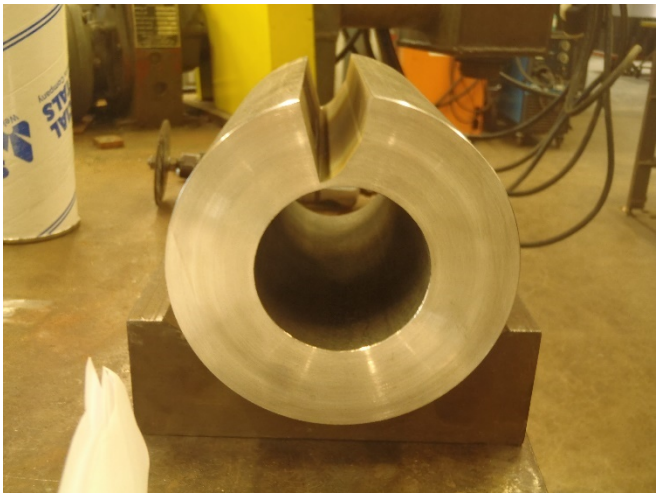

(b)

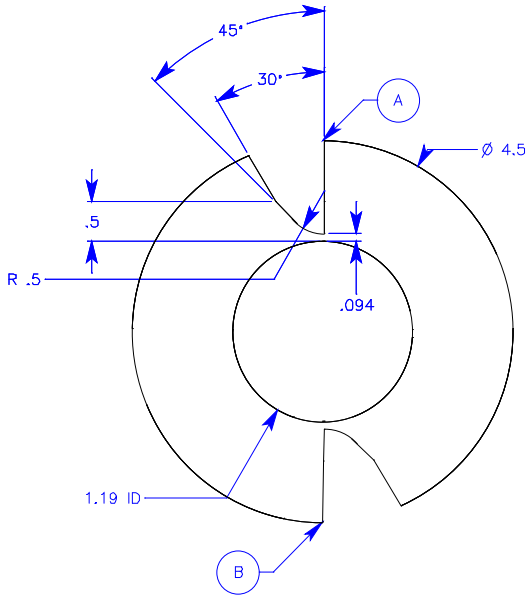

(c)

(d)

Figure 6 **Fabrication of the welds used in the study of the effect of the welding parameters on SCC: (a) schematic for the weld groove (units in inch), and (b) machined weld groove; (c) schematic for two weld grooves (units in inch), and (d) completed welds.**

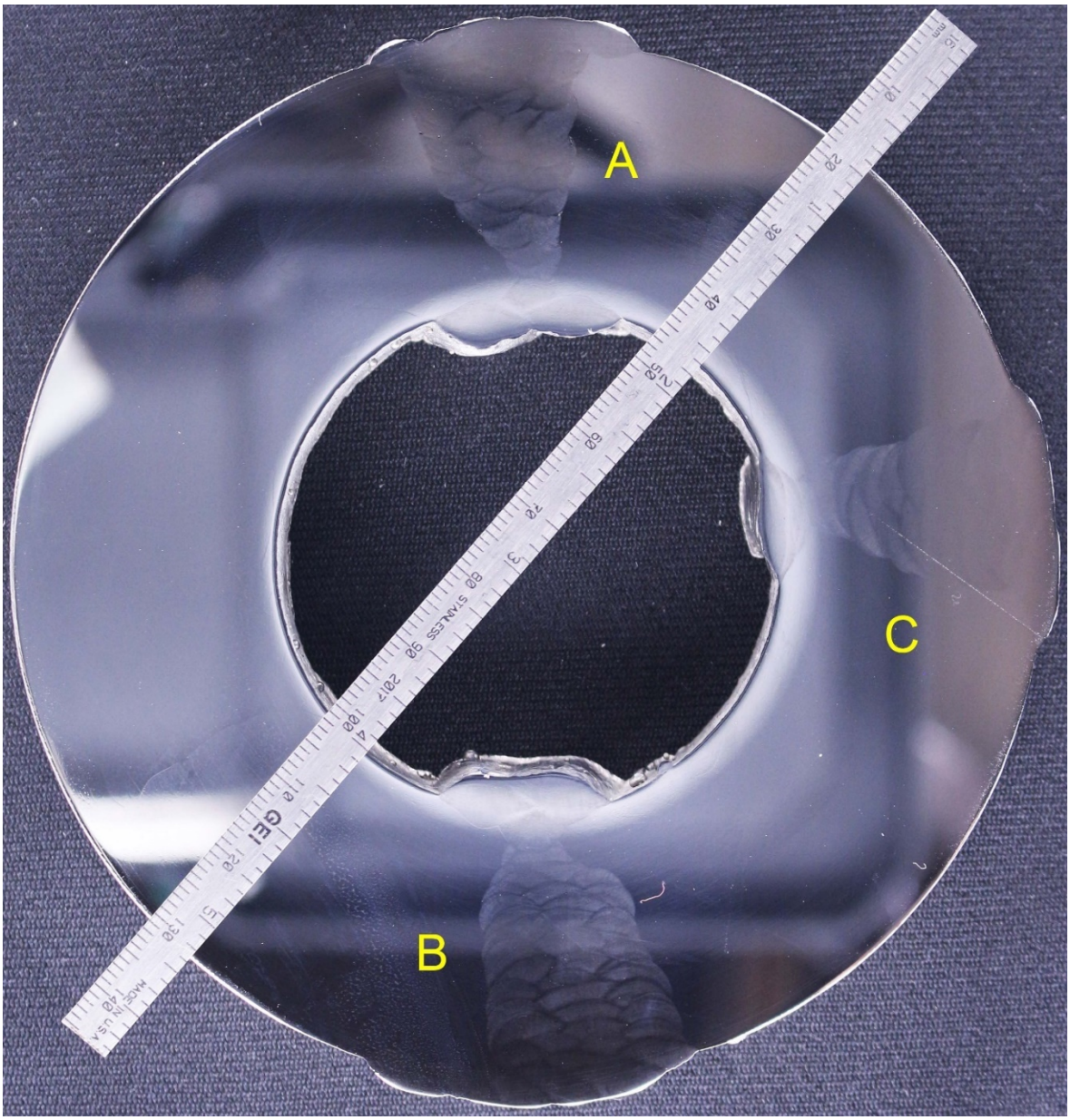

Figure 7 **All three welds used in the study of the effect of the welding parameters on SCC: "normal" weld (A) made with using a procedure qualified to ASME IX, (b) "high current" weld (B), and (c) "high heat input" weld (C).**

2.5 Effect of welding parameters (high heat input Alloy 52M weld produced by EPRI)

This high heat input GTAW Alloy 52M weld was produced by EPRI under contract with ANL. Unlike the weld produced by ANL where the parameters for the high heat input weld were chosen by experimentation, the parameters for the EPRI-produced weld were chosen after a survey of four vendors was conducted. The results of the survey are shown in Table 8. Based

on this survey, EPRI proposed a heat input in the 48 to 55 KJ/in. range. This exceeded or was very close to the maximum for three of the four vendors and they believed it was representative of a high heat input weld.

Table 8 Summary of heat input and power ratio for the four vendors surveyed by EPRI

	Calculated – nominal		Maximum per WPS	
	Heat Input (kJ/in.)	Power Ratio (kW/in.^{2})	Heat Input (kJ/in.)	Power Ratio (kW/in.^{2})
Vendor 1	35.6	74.7	38.9	82.5
Vendor 2	33.6	86.3	48.4	-
Vendor 3	41.1	77.3	44.3	-
Vendor 4	66.0	105.8	66.0	105.8

A schematic of the EPRI-produced high heat input weld is shown in Figure 8. The Alloy 52M dissimilar metal weld (DMW) joins SA-508 to Type 304L. The SA-508 Gr 3 Class 2 is heat T1835-T1836, and the Type 304L is Specification A-240 heat X7P2. Prior to joining, the SA-508 was buttered with Alloy 152M weld.

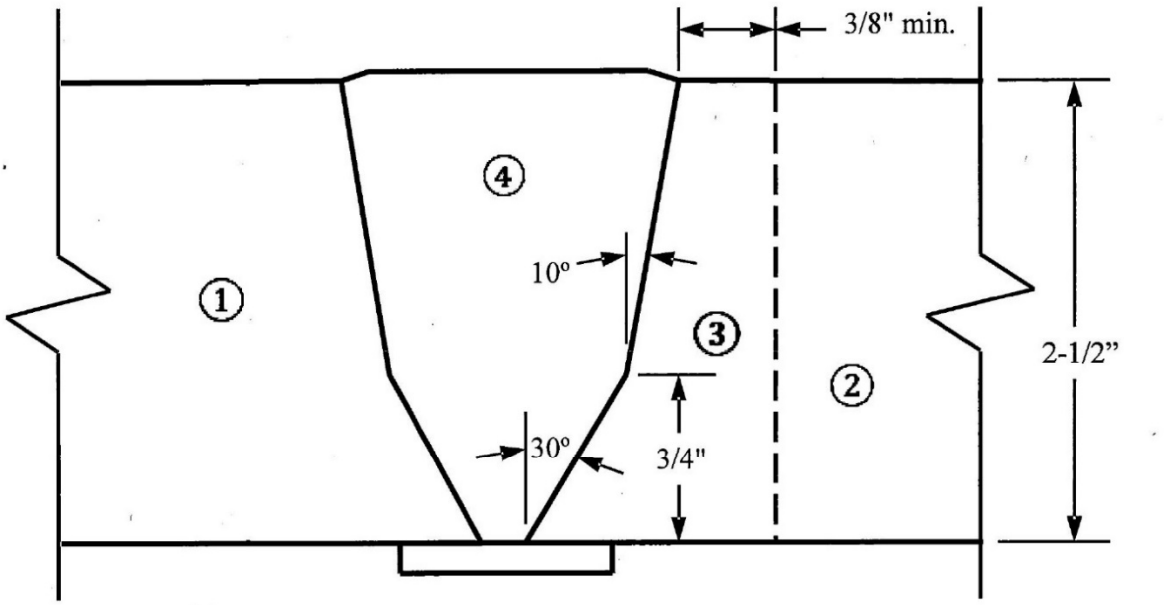

Notes:

1. Type 304L Plate (2-1/2" thick)
2. SA-508 Plate (2-1/2" thick)
3. 152M butter with PWHT
4. High Heat-input GTAW (cold wire) with 52M

Figure 8 Schematic of the EPRI-produced high heat input Alloy 52M weld dissimilar metal weld (DMW) joining SA-508 to Type 304L. The SA-508 was buttered with Alloy 152M weld.

2.5.1 Alloy 152M Weld Butter on SA-508 plate

The Alloy 152M butter was welded manually on the SA-508 joint. The butter welding parameters are shown in Table 9. The interpass temperature was maintained at 450°F.

Table 9 Welding process and conditions for various weld passes used for fabricating the Alloy 152M butter

Layer	Process	Filler Size, in.	Heat Code	Current, A	Voltage, V	Travel Speed, in./min
1	SMAW	3/32	135143	60	24.8	7.695
2	SMAW	1/8	633865	92	27.0	8.438
3	SMAW	5/32	162663 265010	118.5	25.8	8.8

Following buttering, the buttered SA-508 plate was given a PWHT at 1175°F±50°F for 2.5 h.

2.5.2 Installing the high heat input Alloy 52M Weld Joint

Prior to joining, a narrow groove J-prep was machined (see Figure 8 for bevel details). Minimum Alloy 152M buildup thickness after machining was 3/8 in. The high heat input Alloy 52M weld (heat NX79W5TW) was deposited with machine GTAW. The parameters are given in Table 10:

Table 10 Welding parameters for Alloy 52M groove weld.

Layer	Current, Pri/Bkg A	Voltage, Pri/Bkg V	Travel Speed, Pri/Bkg in./min	Wire Feed Speed Pri/Bkg in./min	Pulse Freq. Hz	Pulse Width, %
1 (root)	190/120	10.8/0	2.4/2.4	26/20	1.6	50
2-13	235/175	11.4/0	2.4/2.4	44/32	1.6	50
14-30	235/175	11.4/0	2.4/2.4	40/36	1.6	50

2.6 Effect of weldability (Alloy 152M weld produced by IHI Corporation, Japan)

The Alloy 152M weld produced by IHI with two filler heats, WC83F8 and 444537 on an Alloy 600 plate. The SMA weld was produced with an average current of 130 A, a voltage range of 15 to 40V, and a min. travel speed of 3 cm/min. The maximum interpass temperature was 176°C. This weld was included in the experimental program because the first heat (WC83F8) had to be abandoned because according to the WPS it showed poor weldability. Hence, the interest was to determine whether poor weldability translates into susceptibility to SCC. The dotted line in Figure 9 is an approximate separation of the regions made with each heat. The red contour in the figure illustrates the specimen that was actually tested, positioned to sample the two filler metals.

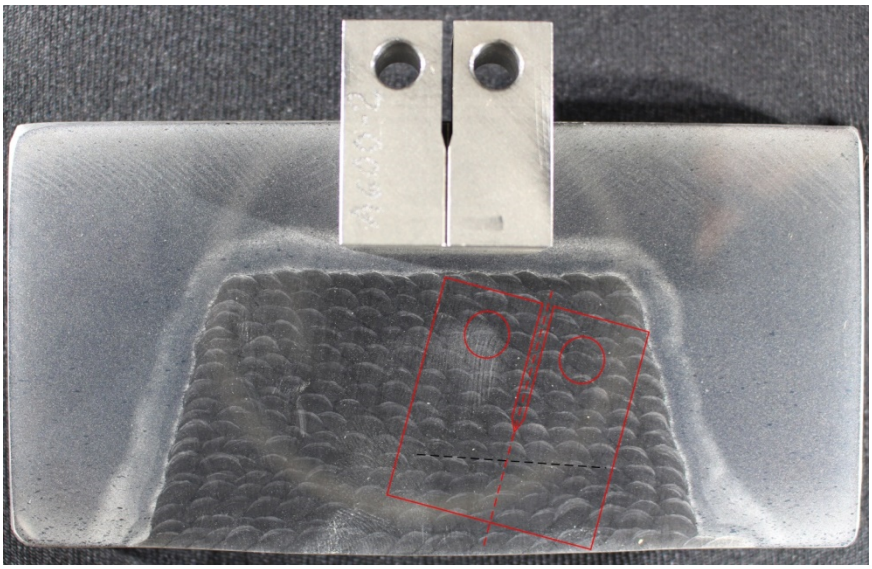

Figure 9 Alloy 152M weld produced by IHI. The red contour illustrates the specimen that was actually tested, positioned to sample two filler metals (separated by the dotted line). The first filler showed weldability issues.

2.7 Effect of cold work (Alloy 52 weld produced by Mitsubishi Heavy Industries, Japan)

The Alloy 52 GTAW weld was produced by MHI on a piece of CRDM tubing in similar fashion to the ANL-produced welds described previously (See Section 2.4, Figure 7). As such, two apparently identical welds were produced with Alloy 52 heat NX4467JK on a CRDM tube made of Alloy 690 Heat S670743, Figure 10. The power ration for these welds was 191 W/mm^2, and the heat input was 9.6 kJ/cm. The interpass temperature was maintained below 134°C.

Figure 10 Alloy 52 welds produced by MHI on a piece of CRDM tubing.

CGR testing of this weld was conducted on both as as-received and 20% cold-forged condition. CGR testing of the as-received condition was conducted in the CR orientation. For forging, a ring was cut from the tube, and this was cold forged to achieve a 20% reduction in thickness.

The forged condition was tested in both CR and LR orientations, Figure 11. Both these orientations allow for CGR testing along the dendritic grains, however, CR orientation is normal to forging plane, while LR orientation is in the forging plane. For a butt weld, the CR orientation corresponds to a circumferential crack, and the LR orientation corresponds to an axial crack.

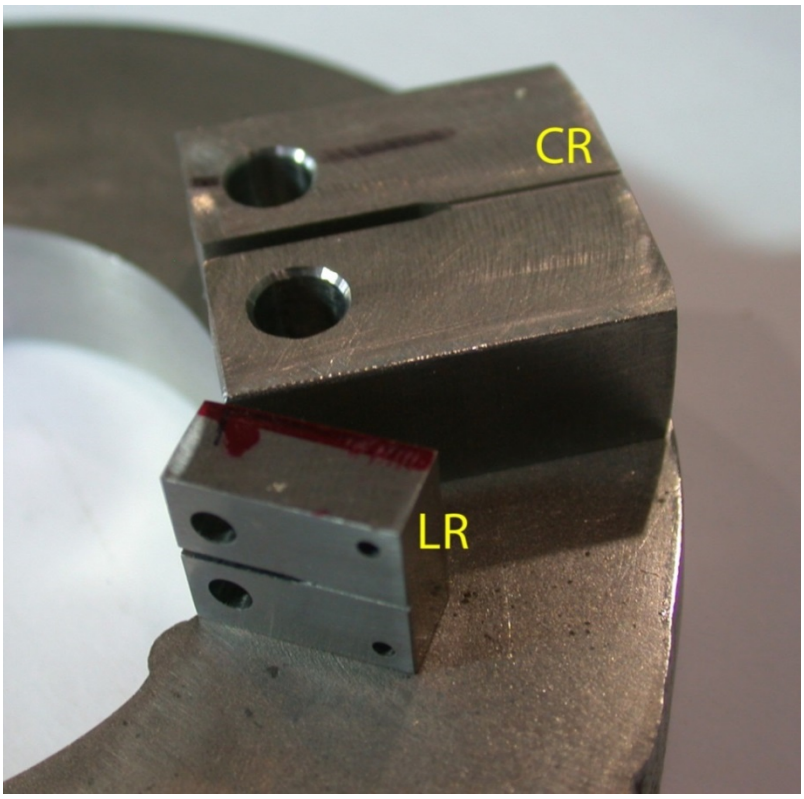

Figure 11 Test specimens in the CR and LR orientation set on top of a ring cut from a CRDM tube containing Alloy 52 welds. The ring was cold-forged to achieve a 20% reduction in thickness.

2.8 CT Specimens

All CGR tests were conducted in simulated PWR environments at 320°C. The testing protocol was in accordance with ASTM E-647, "Standard Test Method for Measurement of Fatigue Crack Growth Rates," [9] and ASTM E-1681, "Standard Test Method for Determining a Threshold Stress Intensity Factor for Environment-Assisted Cracking of Metallic Materials under Constant Load" [10]. Depending on the dimensions of the available materials, the tests were performed on either 1-T or ½-T compact tension (CT) specimens; the geometries of the CT specimens are shown in Figure 12.

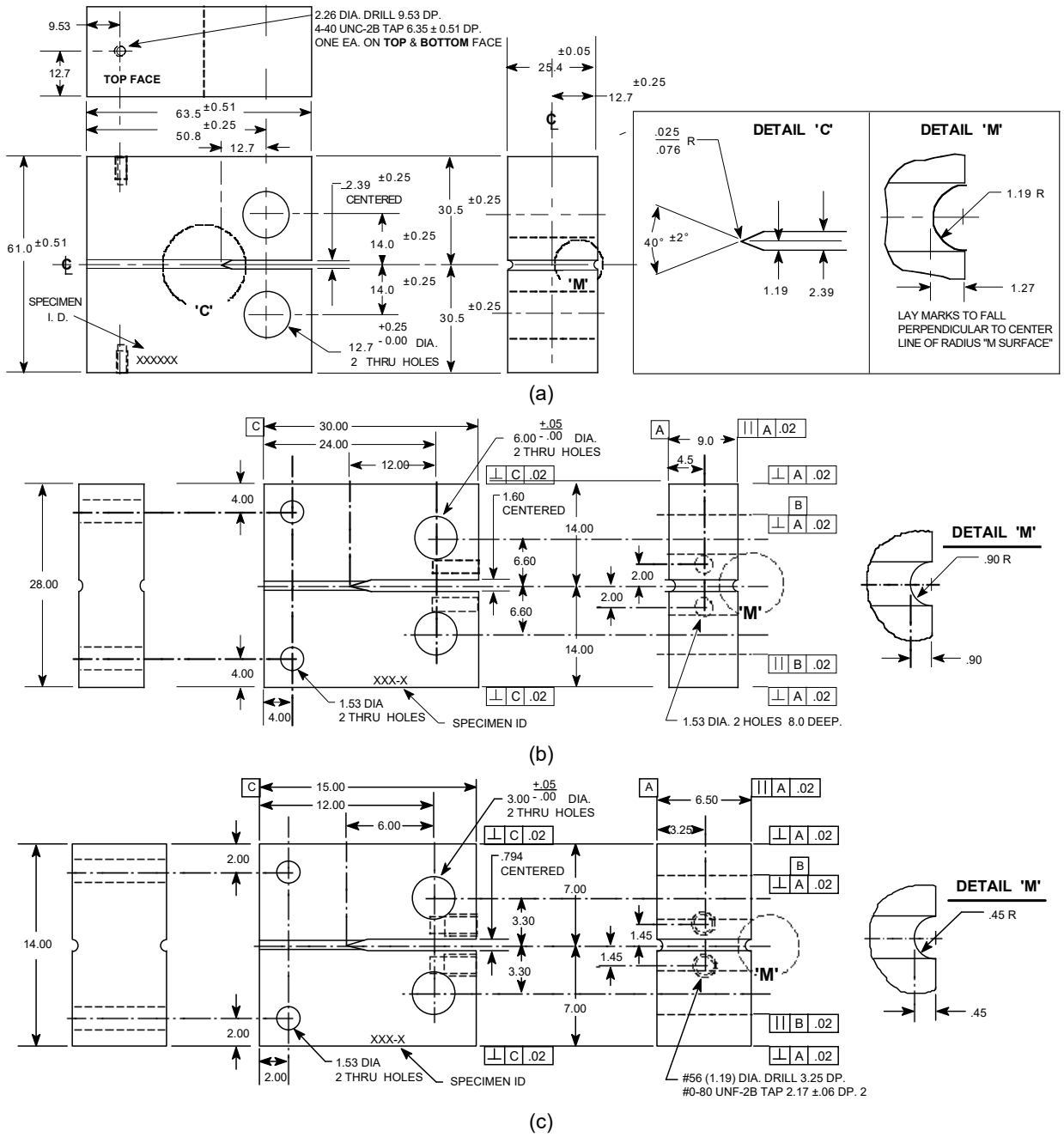

Figure 12 Configuration of the (a) 1-T, (b) ½-T CT, and (c) ¼-T CT specimens used for this study. Dimensions are in mm.

2.9 PWSCC Test Facilities

The CGR tests were conducted in test facilities equipped with either 2 or 6-liter stainless steel (SS) autoclaves. Each system has a suite of calibrated instrumentation, including digitally controlled hydraulic loading and load cells, and an independent water loop to maintain a simulated PWR environment with water chemistry monitoring. The test systems are nearly

identical except for the maximum load rating of the test frame and the volume of the autoclave vessel. A detailed description of the test system with the 2-liter autoclave is provided in this section.

The 2-liter autoclave test facility allows test temperatures of up to 350°C [662°F]. Figure 13 is a photograph showing the entire test system. The servo-hydraulic test frame consists of a load train, an autoclave support frame, and autoclave. The hydraulic actuator is mounted on bottom of the test frame, with the load train components located above it. The load cell is located at the bottom of the pull rod. An Instron Model 8800 system is used to control the load on the specimen. The test temperature is maintained by heater bands mounted on the autoclave body.

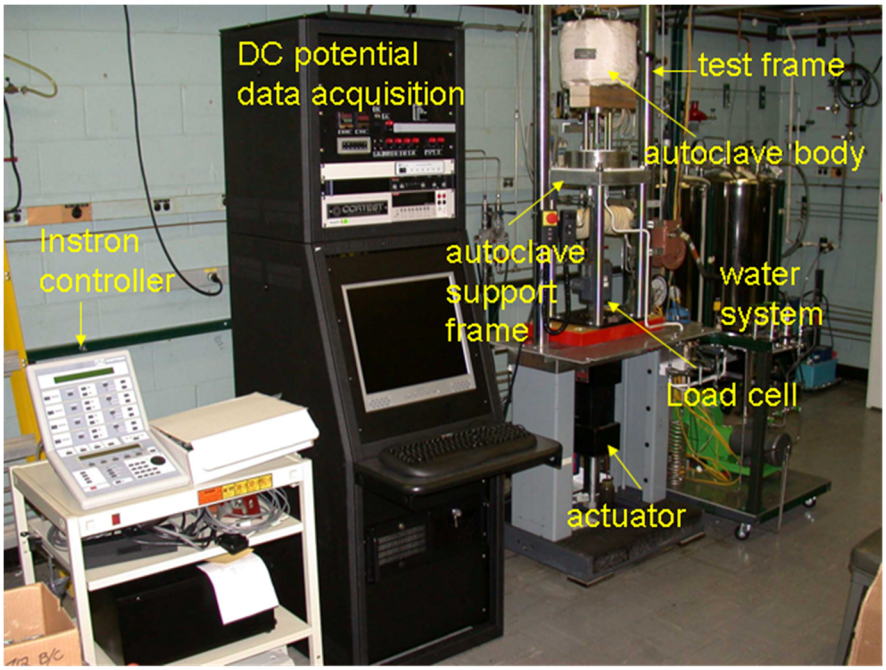

Figure 13 Layout of the 2-liter SCC test system.

The autoclave support frame consists of a thick plate supported by four compression rods (Figure 14). The internal load frame that contains the test specimen consists of a top plate supported by three rods. The upper two-piece clevis assembly is fastened to the top plate of the internal load frame, and the lower piece clevis assembly is connected to the pull rod. The specimen to be tested is mounted between the clevises. The specimen and clevises are kept electrically insulated from the load train by using oxidized Zircaloy pins and mica washers to connect the clevises to the rest of the load train. Water is circulated through a port in the autoclave head, which serves both as inlet and outlet. A schematic diagram of the recirculating water system is shown in Figure 15.

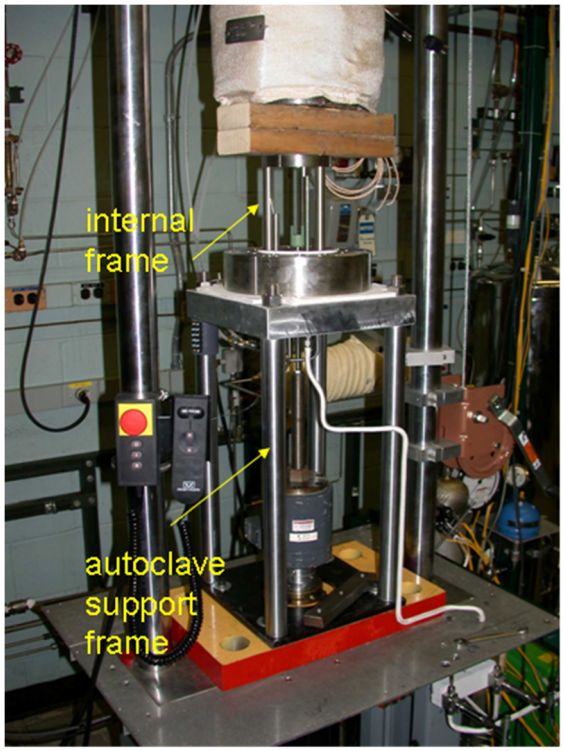

Figure 14 Photograph of the specimen load train for the 2-liter autoclave

The simulated PWR feedwater contains 2 ppm Li as LiOH, 1000 ppm B as HBO_3, ≈2 ppm dissolved hydrogen (≈23 cm^3/kg), and less than 10 ppb dissolved oxygen (DO) [11]. Water is circulated at relatively low flow rates (15-25 mL/min). The test temperatures were 320°C [608°F].

Crack extensions are monitored by the reversing-direct current (DC) potential difference method, Figure 16. In this method, a constant DC current is passed through the test specimen and the crack length is measured through the changes in the electrical voltage at the crack mouth. The electrical voltage measured across the crack mouth is related to the unbroken crack ligament resistance through the Ohm's law. Thus, as the crack advances, the length of the unbroken ligament decreases and its resistance increases. In short, as the crack advances the voltage measured across the crack mouth increases. Figure 16 shows a typical configuration of a CT specimen instrumented for crack growth measurements by the DC potential method: the current leads are welded on the top and bottom surfaces of the specimen, and potential leads are welded on the front face of the specimen across the machined notch but on diagonal ends. Also, to compensate for the effects of changes in resistivity of the material with time, an internal reference bar of the same material being tested is installed in series, near the test specimen. The voltage readings across the reference bar are used to normalize potential drop measurements for the CT test specimen. The changes in potential drop measurements for the CT test specimen are transformed into crack advance data using correlations developed for the specimen geometry that is tested. In practice, voltage readings are taken successively as the current is reversed, and, typically, 800 voltage readings are needed to generate 1 crack advance data point, approximately every 4 min. with a resolution of approximately 1-2 μm [0.039-0.079 mils].

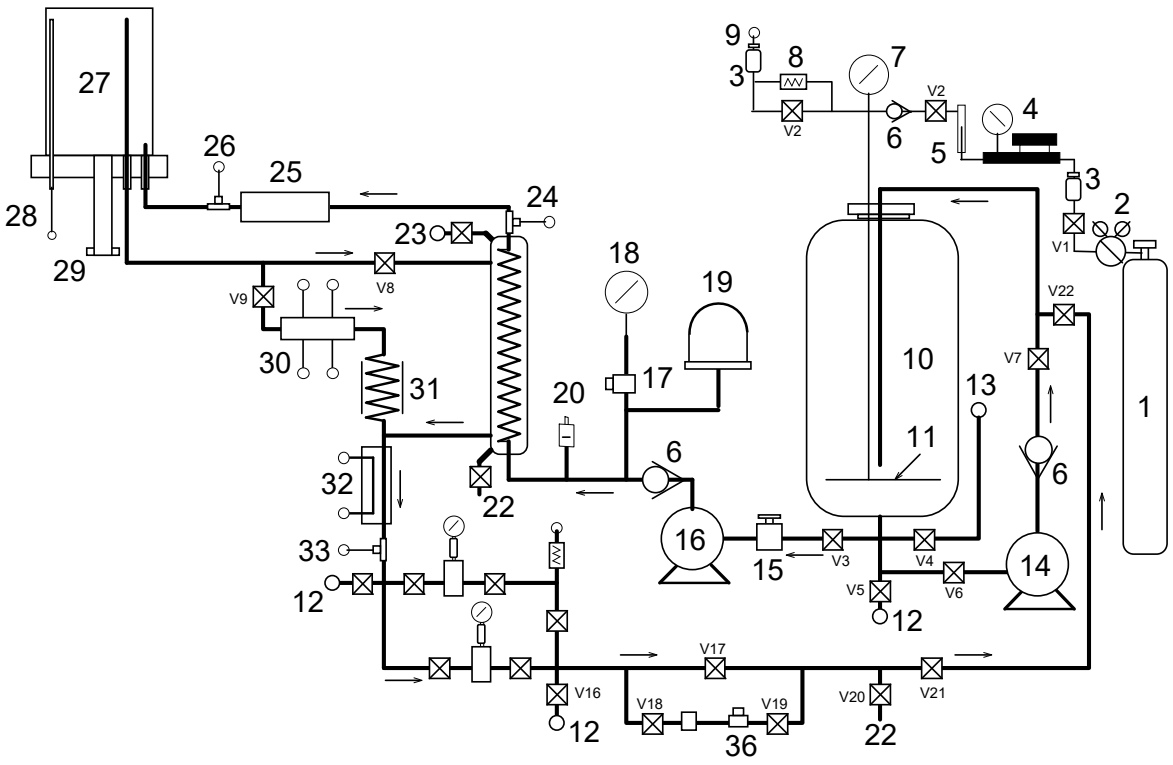

1. COVER GASS SUPPLY TANK
2. TWO-STAGE HIGH-PRESSURE REGULATOR
3. FLASH ARRESTOR
4. LOW-PRESSURE REGULATOR
5. FLOW METER
6. CHECK VALVE
7. COMPOUND VACUUM & PRESSURE GAUGE
8. PRESSURE RELIEF VALVE
9. VENT TO AIR & FLASH ARRESTOR
10. FEEDWATER STORAGE TANK
11. SPARGE TUBE
12. WATER SAMPLE PORT
13. FEEDWATER FILL PORT
14. FEEDWATER TANK RECIRCULATION PUMP
15. SOLENOID VALVE
16. HIGH-PRESSURE PUMP
17. PRESSURE TRANSDUCER
18. HIGH-PRESSURE GAUGE
19. ACCUMULATOR
20. RUPTURE DISC
21. HEAT EXCHANGER (HX)
22. DRAIN
23. SYSTEM BLEED PORT
24. HEAT EXCHANGER OUTLET TC
25. AUTOCLAVE PREHEATER
26. PREHEATER OUTLET TC
27. COMMERCIAL AUTOCLAVE
28. THERMOWELL
29. “BAL SEAL” RETAINER
30. ECP CELL
31. AIR-COOLED COIL
32. WATER COOLED HEAT EXCHANGER
33. BACK-PRESSURE REGULATOR (BPR) INLET TC
34. BPR
35. PH METER
36. CONDUCTIVITY METER

Figure 15 Schematic diagram of the recirculating 2-liter autoclave system.

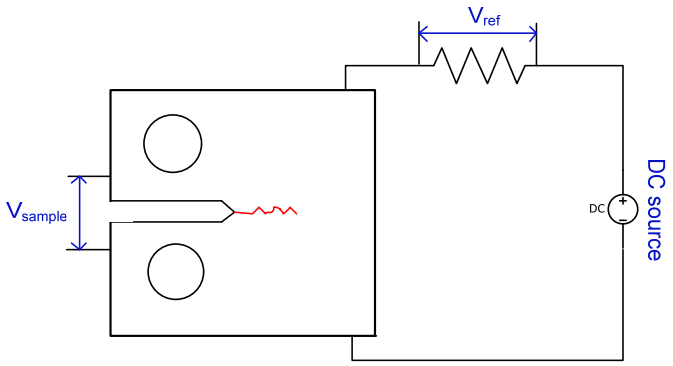

Figure 16 Principle of crack length measurement by the DC potential method.

2.10 CGR Test Methodology

A typical CGR test at ANL consists of three stages: in-situ precracking, transitioning to SCC, and the SCC growth stage. At the end of the test the specimen is broken open, and the fracture surface is examined. The objective of each stage will be highlighted next.

The objective of precracking is to produce a sharp crack tip. This is typically achieved by fatigue cracking, using a triangular waveform at load ratio R = 0.3[1], frequency of ≈1 Hz, and maximum stress intensity factor (K_{max}) of 20-25 MPa·$m^{1/2}$ [18.2-22.8 ksi·$in^{1/2}$]. Under rapid cyclic loading, the crack growth is dominated by mechanical fatigue; hence, the known fatigue behavior of the alloy being tested is expected to be reproduced. In turn, this step ensures that a straight crack front has been produced.

After approximately 0.5-mm (20 mils) extension in fatigue, the transitioning stage is initiated. The purpose of this stage is to transition from the fatigue/transgranular (TG) fracture mode to an SCC/intergranular (IG) fracture mode. As such, cycling is continued under loading conditions expected to foster environmental effects. In general, environmental enhancement of cyclic rates is typically observed under loading conditions that would lead to CGRs between 10^{-11} and 10^{-9} m/s in air. To generate these rates, the load ratio R is increased incrementally to 0.5-0.7, and the loading waveform is changed to a slow/fast sawtooth with rise times of 30-1000 s and an unload time of 12 s. Transitioning to an IG SCC fracture mode is assessed by analyzing the cyclic response. The analysis, described in detail in the subsequent section, relies in principle on superposition. Under cyclic loading, the measured CGR is the superposition of mechanical fatigue, corrosion fatigue, and SCC components. Thus, a crack is considered “transitioned” when the SCC component is non-zero, that is, the measured CGR is larger than the sum of the fatigue and corrosion fatigue components. Once the crack is transitioned to IG SCC, the specimen is set at constant load. By eliminating the mechanical fatigue and corrosion fatigue components, constant load allows for the SCC CGR to be measured directly. However, as the crack grows in an IG fracture mode, it typically follows the least resistant grain boundary path. As such, crack branching develops, and that in turn results in unbroken/uncracked ligaments.

As described in the previous section, the DC potential method measures the potential drop across the unbroken ligament in the sample; hence, the ligaments formed during the preferential SCC path often confound the DC potential measurement by making the crack appear shorter

[1] Load ratio R = K_{min}/K_{max}

than it is in reality. As a result, the crack advance measured on the fracture surface of the specimen at the end of the test is almost always longer than that measured in-situ. Therefore, a correction of the DC potential data is almost always needed after the test is completed, and the DC potential data is compared to the actual crack advance measured on the fracture surface. The downside of this approach is that in the case of SCC tests conducted under multiple conditions resulting in the same fracture mode, e.g., multiple stress intensity factors or multiple test temperatures, the fracture surface cannot be used to distinguish between the various test periods. Hence, in complex tests, there is almost always an uncertainty in correlating the test conditions to the resulting fracture surface. Nevertheless, the uncertainty regarding the amount of crack growth during a test period at constant load can be minimized by introducing cyclic loading at the end of that test period. This cyclic loading is typically a well-known condition for which the CGR is known precisely. If ligaments form during constant load, the resulting CGR during this subsequent test period is typically higher than the known rate. This is the case for as long as ligaments are broken, then the CGR eventually settles to the known rate once that process is complete. The point at which the rate settles to the known rate can be conservatively interpreted to signal the actual extent of crack advance during the previous test period at constant load. This approach results in a conservative CGR as it does not take into account the growth due to cyclic loading.

As an alternative to the purely constant loading described previously, some form of cycling or partial periodic unloading (PPU) is introduced during the constant load test period with the purpose of breaking the ligaments as they form, and allow for a more realistic SCC CGR to be measured in real time. As a guideline, the cycle/periodic unloading is chosen to be subtle enough not to advance the crack by itself, but aggressive enough to be effective at breaking the ligaments. These experimental challenges have been recognized in industry publications [1,12], and periodic unloading is, in fact, recommended [1]. Such conditions have been used to generate a portion of the database used for generating the industry disposition curves [1,12]. The data generated at ANL conform to these guidelines. In addition, for each test conducted at ANL, the fatigue behavior is confirmed at the beginning of the test during precracking; this way the contributions from fatigue during constant load with periodic unloading or cycling plus hold conditions are calculated with precision during each test. Nevertheless, to increase confidence in the results, the objective of each ANL test is to measure the SCC CGR under not just one, but under several loading conditions.

There are two types of PPU used at ANL to supplement and/or confirm the SCC CGR determinations under constant load: “constant load with periodic unloading” and “cycle + hold”. They are in principle similar, in that the constant load is interrupted periodically (“hold” time) by a unload/reload cycle. However, the nature of the loading cycle is different in each case, hence a different approach is undertaken in the interpretation of the response. For constant load with periodic unloading, the cycle is essentially an aggressive fatigue cycle, e.g. R = 0.5, 12 s rise / 12 s unload times. This type of cycling results by itself in a transgranular (TG) fracture mode. Hence, if the resulting fracture mode is verified at the end on the test to be intergranular (IG), then it is assumed that most of the growth occurred at constant load during the hold time. The actual hold time under constant load can be set to result in a fatigue CGR less than the SCC CGR to be measured; for Alloy 52/152 weldments hold times of minimum 2h have typically been used to result in a CGR_{air} of approx. 5×10^{-12} m/s. By contrast, “cycle + hold” involves a gentle cycle, e.g. R = 0.5, 600 s rise / 12 s unload times. This type of cycle is used during transitioning from TG to IG, and by itself usually results in an IG fracture mode. Hence, under “cycle + hold” IG SCC growth occurs under both cyclic loading and constant load (hold). In this case, in order

to calculate the SCC CGR component (SCC growth under constant load), the cyclic contribution to the total growth is subtracted. As before, hold times of minimum 2h have typically been used.

In addition to the calculations described previously, another technique used to check for the presence or to evaluate the magnitude of the SCC CGR component, is to alternate the hold times between K_{max} and K_{min} in otherwise identical loading waveforms, Figure 17. In the first scenario with the hold time at K_{max}, the measured CGR consists of a corrosion fatigue component plus an SCC component during the 2h hold time at K_{max}. In the subsequent test period, with the hold at K_{min}, the CGR is only due to corrosion fatigue due to cyclic loading; during the hold time, the specimen is practically unloaded, so no SCC growth is expected. In this framework, the SCC CGR component is a simple subtraction between the CGRs measured under the two loading schemes. The advantage vs. simple superposition is that this approach eliminates the synergistic effects that might exist between cyclic and constant loading.

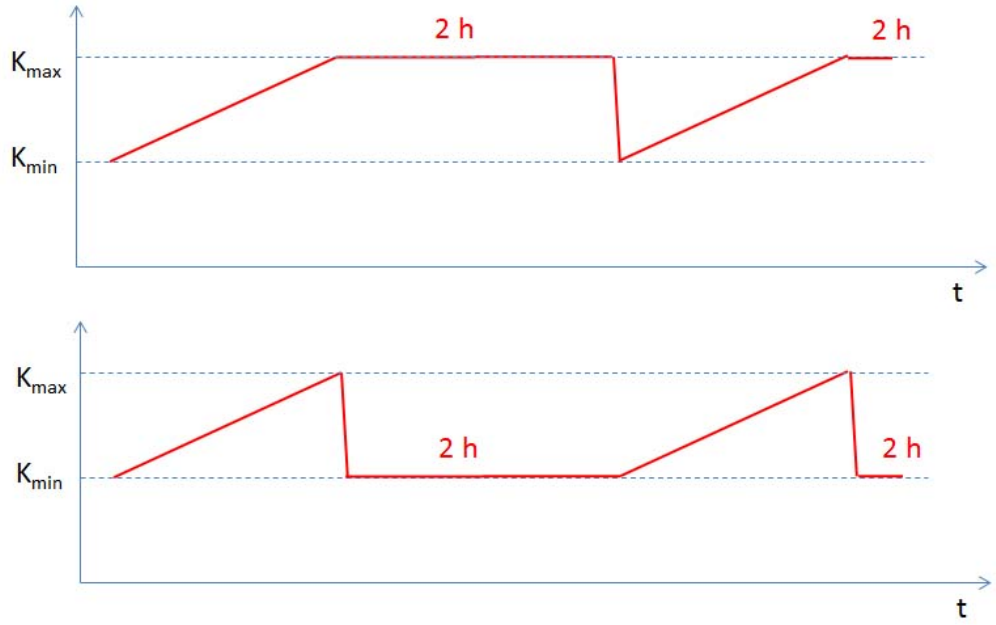

Figure 17 Schematic of the loading waveform with the 2 h – hold time at K_{max} and K_{min}.

A post-test examination of the specimen is always conducted. Typically, all specimens are examined microscopically at the fracture surface and sometimes in the cross section. For the cross section examination, the two side surfaces are ground to remove the side grooves. The cross sections are then polished and etched. They are examined by scanning electron microscopy (SEM) to verify the planarity of the crack front and to determine the extent of crack branching. Next, the specimens are fractured to expose the fracture surface obtained during the test. The fracture surface is examined by SEM to measure the crack extension and to determine the fracture mode(s). The crack length measurements obtained on the fracture surface are used to correct the data obtained in-situ by the DC potential method. As described in the previous paragraph, the DC potential method typically underestimates the full extent of the crack, particularly during intergranular cracking. Hence, during the correction stage, the DC potential data is adjusted to match the measurements obtained on the fracture surface. The

known relationships between the loading conditions and the expected fracture mode are used to the extent possible to substantiate the correction approach.

2.11 Analysis of Crack Growth Rate Data

Under cyclic loading, the CGR (m/s) in the environment, $\dot{a}_{env}$, can be expressed as the superposition of the rate in air (i.e., mechanical fatigue) and the rates due to corrosion fatigue and SCC ($\dot{a}_{CF}$ and $\dot{a}_{SCC}$, respectively), given in previous reports [14-16] as:

$$\dot{a}_{env} = \dot{a}_{air} + \dot{a}_{CF} + \dot{a}_{SCC} \quad (1)$$

The cyclic CGRs for Ni alloys and welds in air were determined from correlations developed earlier at Argonne [14-16]:

$$\dot{a}_{air} = \left(\frac{da}{dN}\right)/t_r = \left[C \cdot (1 - 0.82 \cdot R)^{-2.2} \cdot (\Delta K)^{4.1}\right]/t_r \quad (2)$$

where da/dN is the growth rate per cycle, t_r is the rise time for the loading cycle, R is the load ratio (i.e., ratio of the minimum and maximum stress intensity factors K_{min}/K_{max}), ΔK is $K_{max} - K_{min}$ in MPa $m^{1/2}$, and the constant C depends on the material and temperature. For Alloy 600, the constant (C_{A600}) is a third-order polynomial with respect to temperature T (°C) [14-16],

$$C_{A600} = 4.835\times10^{-14} + (1.622\times10^{-17})T - (1.490\times10^{-18})T^2 + (4.355\times10^{-21})T^3 \quad (3)$$

In LWR coolant environments, the CGRs of Alloy 600 show frequency-dependent enhancement under cyclic loading conditions. In high-DO water [i.e., normal water chemistry in boiling water reactor (BWR)], the environmental enhancement of the growth rates does not appear to depend on the material composition (e.g., C content) or material heat treatment. In contrast, environmental enhancement of CGRs of Alloy 600 in low-DO water does seem to be strongly dependent on material conditions. In the literature [17-21], such variability has been attributed to thermomechanically controlled parameters, such as yield strength and grain boundary coverage of carbides, although the evidence for this dependence is more substantial for steam generator tubing than for structural components.

For Alloy 690, the constant C_{A690} is given by a third-order polynomial of temperature T (°C), expressed as [14]:

$$C_{A690} = 5.423\times10^{-14} + (1.83\times10^{-16})T - (1.725\times10^{-18})T^2 + (5.490\times10^{-21})T^3. \quad (4)$$

For Ni-alloy welds, including Alloys 82/182 and 52/152, the constant $C_{Ni\text{-}weld}$ is given by a fourth-order polynomial with respect to temperature T (°C), expressed as [22]:

$$C_{Ni\text{-}weld} = 8.659\times10^{-14} - (5.272\times10^{-17})T + (2.129\times10^{-18})T^2 - (1.965\times10^{-20})T^3 + (6.038\times10^{-23})T^4 \quad (5)$$

In earlier ANL work, correlations were developed to estimate the enhancement of cyclic CGRs in LWR environments relative to the CGRs in air under the same loading conditions. In the absence of any significant contribution of SCC to growth rate, the cyclic CGRs for Alloy 600, either in the solution annealed (SA) condition or the SA plus thermally treated (TT) condition, in ≈300 ppb DO water at 289°C are given by the expression [14]:

$$\dot{a}_{env,A600} = \dot{a}_{air,A600} + 4.4\times10^{-7}\cdot\left(\dot{a}_{air,A600}\right)^{0.33} \quad (6)$$

In low-DO environments (e.g., hydrogen water chemistry for the BWR or PWR environment) at 320°C (608°F), some alloys show little enhancement, while others show enhancement comparable to that predicted by Eq. (6). The environmental enhancement of Alloy 690 [14] was found to be almost always less that that predicted by Eq. (6).

Similarly, correlations describing the cyclic CGRs of Ni-alloy welds (e.g., Alloys 182 and 82) have been developed [23, 24]. Under similar loading conditions, the CGRs of Ni-alloy welds are a factor of 2-3 higher than those of Alloy 600. The analysis indicated that the cyclic CGRs of Ni-alloy welds in PWR water are represented by the expression:

$$\dot{a}_{env,Ni-weld} = \dot{a}_{air,Ni-weld} + 0.018\cdot\left(\dot{a}_{air,Ni-weld}\right)^{0.78} \quad (7)$$

Figure 18 summarizes the expected behaviors for cyclic rates in air and environment for Alloys 600, 690 and Ni-base welds as described by Eqs. (2)-(7). All data is plotted as a function of the predicted behavior for Alloy 600 in air.

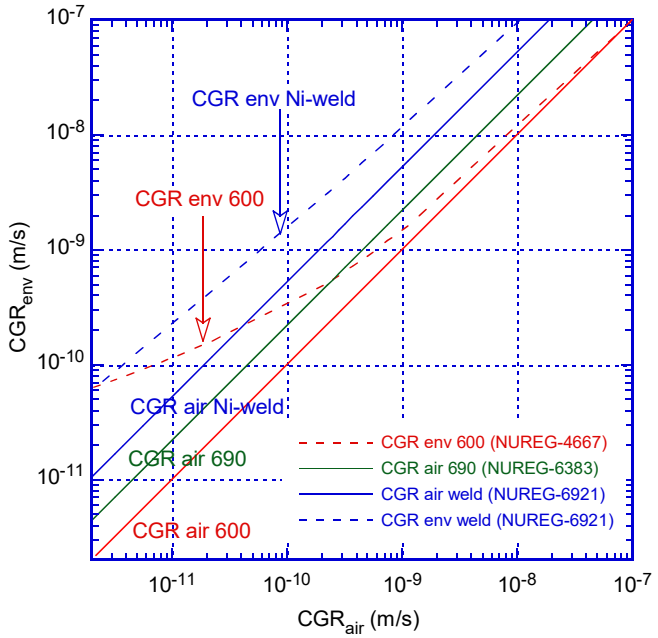

Figure 18 Crack growth rates in air and environment for Alloys 600, 690 and Ni-base welds as a function of predicted rates in air for Alloy 600 (data taken from Refs. 14, 15, 22).

The SCC growth rate data for Alloy 600 and its weld metals have been reviewed in MRP-55 [12] and MRP-115 [1] to determine the effects of critical parameters such as stress intensity factor, temperature, material heat treatment, cold work, and water chemistry on growth rates. For Alloy 600, the CGR (m/s) under SCC conditions is represented by the expression [12],

$$\dot{a}_{A600} = \alpha \exp\left[-\frac{Q}{R}\left(\frac{1}{T}-\frac{1}{T_{ref}}\right)\right](K-K_{th})^{\beta} \qquad (8)$$

where:
- Q = activation energy for crack growth (130 kJ/mol for Alloy 600)
- R = universal gas constant (8.314×10^{-3} kJ/mol K)
- T = absolute operating temperature in units of K
- T_{ref} = absolute reference temperature to normalize the CGR data (598 K)
- α = crack growth amplitude (2.67×10^{-12} at 325°C),
- K = crack tip stress intensity factor in units of MPa·m$^{1/2}$,
- K_{th} = crack tip stress intensity factor threshold (9 MPa·m$^{1/2}$), and
- β = exponent 1.16.

The effect of K on the SCC growth rate for Ni-alloy Alloy 182 welds in PWR environments has been represented by a modified [1] version of the above relationship. Unlike the CGR relationship for Alloy 600, the relationship for Ni-alloy welds has no threshold value for the stress intensity factor K,

$$\dot{a}_{Ni-weld} = \alpha \exp\left[-\frac{Q}{R}\left(\frac{1}{T}-\frac{1}{T_{ref}}\right)\right] K^{\beta} \quad (9)$$

where Q, R, T, and T_{ref} are the same as in Eq. (8), the crack growth amplitude α is 1.5×10^{-12} at 325°C, and exponent β is 1.6. Also, unlike Alloy 600, for which a reliable value for the activation energy for crack growth was determined, no such number is available for the Ni-weld alloys. Thus, for Ni-weld alloys, the activation energy is assumed to be the same as that for Alloy 600.

More recently, a similar effort [13] was made for high-Cr Ni-base Alloys 690 and 52/152. As the data did not display any dependencies typical of SCC growth such as K or temperature, these were assumed to exist and, moreover, be identical for those for Alloys 600 and 182. The improved resistance to SCC for the high-Cr alloys is captured by factors on improvement (FOI) applied to above Eq. (8) and Eq. (9): 38 for Alloy 690 and 324 for Alloy 52/152. As such, as Figure 19 shows, the SCC CGR average for 75% of the Alloy 52/152 heats should be in the 10^{-13} m/s range. Of concern with this outcome is that there was no actual data to support the assumed dependencies or the proposed curve. The MRP-386 curve relies on a database of which 60% of the data were obtained at 360°C to which the assumed temperature dependency was applied. Most of this data was low/no growth.

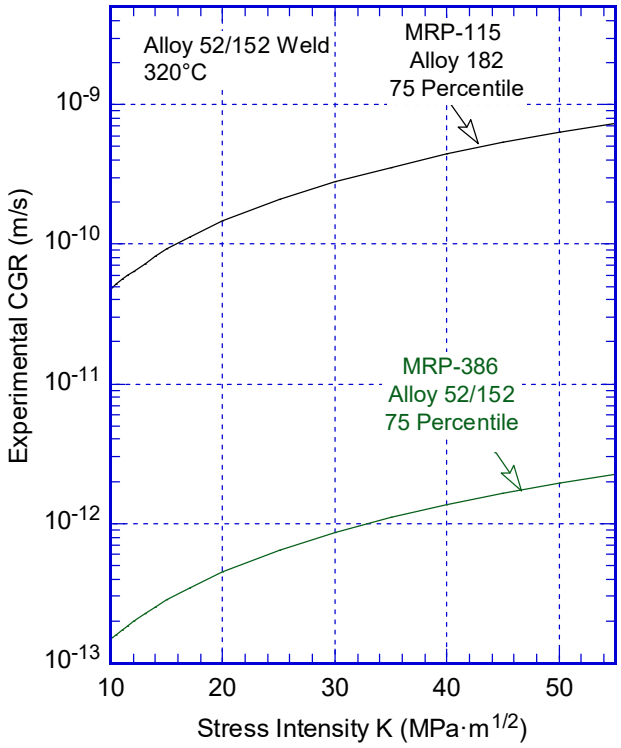

Figure 19 Proposed disposition curves for Alloys 182 [1] and 52/152 [13].

Figure 20 illustrates how the superposition concept introduced earlier is used to analyze the cyclic CGR data generated in a SCC test on Alloy 182 weld. A typical test at ANL consists of three stages: in-situ precracking, transitioning to SCC, and the SCC growth stage. The

precracking stage is dominated by mechanical fatigue, hence, in this stage of the test where CGR rates are typically larger than 10^{-9}m/s, the expectation is that the measured CGRs are close to those expected under the same loading conditions in air, $\dot{a}_{air}$ (often called the "air line"), and is calculated using Eqs. (2) and (5). During the transitioning to IG SCC stage, cyclic loading is continued under loading conditions and is expected to induce environmental enhancement. The environmental enhancement is typically observed under loading conditions that lead to CGRs between 10^{-11} and 10^{-9} m/s in air, and the effect of the additional corrosion fatigue component is labeled $\dot{a}_{air} + \dot{a}_{CF}$ in the figure. For a typical Ni-base weld, the corrosion fatigue behavior is expressed by Eq. (7). Finally, if an SCC component is also present, the specimen response is expected to follow the curve labeled $\dot{a}_{air} + \dot{a}_{CF} + \dot{a}_{SCC}$ in the figure. For the purpose of the illustration shown in Figure 20, the $\dot{a}_{SCC}$ component was calculated using Eq. (9), and represents the SCC CGR of an alloy with a cracking susceptibility ranking at the 75th percentile [1].

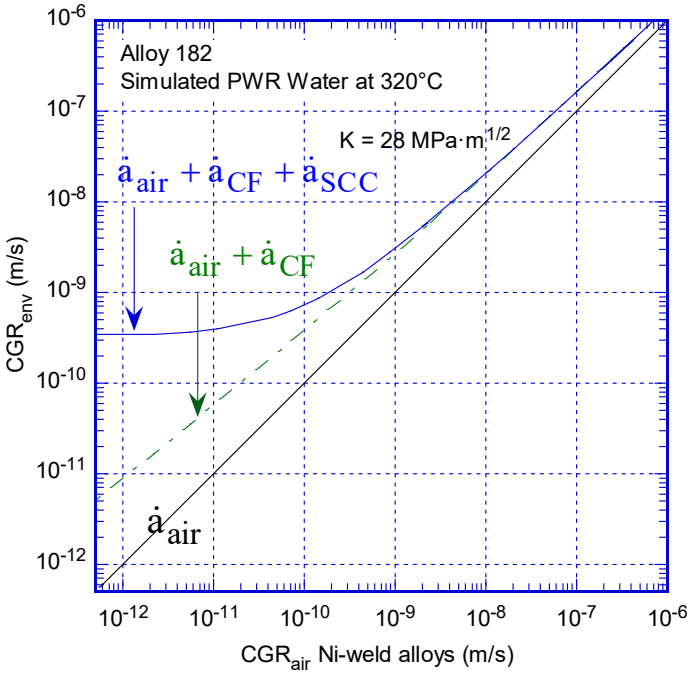

Figure 20 Cyclic CGRs for typical Ni-base weld tested in a PWR environment. Expected corrosion fatigue (Eq. (7), green) and SCC (Eq. (9), blue) curves are included.

3 RESULTS

This section presents the SCC CGR test data obtained on Alloy 52/152 (and variants) weld specimens. The tests are presented in a somewhat loose chronological order, as "lessons learned" from the early tests were used to inform the management of the subsequent tests. The tests are also grouped by topics on interest such as the "effects of welding parameters" or the "effect of cold work" to give the report some continuity. Unless otherwise specified, all specimens and areas that were tested were selected randomly in the regions of interest in order for the test results to be representative of the entire material tested. As described previously, the post-test examination included the crack path where it was deemed necessary. The fracture surface was examined for all tested specimens.

3.1 SCC CGR Testing of Alloy 152 Welds produced at ANL

The SCC CGR testing presented in this section focused on two Alloy 152 weldments produced at ANL. Two early tests of the first weldment (A152-series, Section 2.1) found relatively high levels of IG fracture morphology and moderate (10^{-11} m/s) SCC CGRs [5]. As most of this first weld was used to obtain tensile data in the 77-1598°F (25-870°C) temperature range [5], a new Alloy 152 weldment was developed (N152-series, Section 2.2). Testing was focused on one Alloy 152 filler heat (WC04F6, Special Metals).

3.1.1 Specimen A152M-TS-5

Following two successful tests on the same weldment, [5] with relatively high levels of IG engagement resulting in moderate SCC CGRs, the objective of the test on A152-TS-5 was trifold: 1) confirm prior SCC CGR results at moderate stress intensity factors, 2) obtain SCC CGR data at higher stress intensity factors and attempt to establish the K-dependence of SCC CGRs, and 3) determine the activation energy for SCC crack growth.

The testing conditions are given in Table 11, and the changes in crack length and K_{max} with time are shown in Figure 21. The specimen was fatigue precracked using a triangular waveform at K_{max} = 20-26 MPa $m^{1/2}$, R = 0.30, then cycled with a sawtooth waveform at R = 0.5. These were followed by transitioning steps similar to those that proved to be successful on the previous two Alloy 152 specimens. After environmental enhancement was established (period 17), the specimen was set at constant load with periodic unloading. The hold time was 8h. Apparently, the effect of the long hold time was to suppress the environmental enhancement, and the subsequent decrease of the hold time (periods 19, 20) did not help either. As such, cycling was restarted to re-establish the environmentally-enhanced conditions. After observing that the CGR rate did not appear to change when the hold time was doubled (period 23 vs. 22) - suggesting that an SCC mode was dominant - the specimen was set at constant load (period 24). The average rate for approximately 800h was 6.5 10^{-12}m/s. Next, periodic unloading (2h) was introduced in an attempt to break the ligaments that might have formed. The measured CGR for period 25 are about 3 times higher those measured in period 20 when environmental enhancement had been lost. As such, the first 100h into period 25 saw a CGR of 3.8 10^{-11} m/s that eventually decreased to approx. 1.7 10^{-11}m/s after approx. 1500h; this rate is in good agreement with previous measurements on this alloy. As this latter rate stayed relatively unchanged, the observations, taken together, seem to suggest that it took approximately 100h to break the ligaments formed during the approx. 30 µm of growth seen in period 24. The stress intensity factor was next increased slightly and the loading condition maintained similar to that of

period 25. As the measured rate increased to 3.9 10^{-11} m/s, the specimen was set at constant load (period 27). The measured rate remained at 3.9 10^{-11} m/s for the first 100 h, reinforcing the fact that the two loading conditions are practically equivalent. After approx. 500h, the specimen was accidentally unloaded during a routine load shedding. Nevertheless, the crack grew a statistically significant 65 μm, and the average CGR was approx. 3.3 10^{-11} m/s. After a period of limited growth, periodic unloading was reintroduced for approx. 100 h (period 28) in order to reactivate the crack. Next, the sample was set at constant load. When a CGR less than that measured in previous period 27 was observed, periodic unloading was re-introduced (period 30) aiming for a longer crack advance.

Next it was decided to increase the stress intensity factor to a larger value. As such, the specimen was set at constant load, and when growth was detected (period 31), the load was increased by 500 lb (new K_{max} = 26 MPa $m^{1/2}$). While this increase was done in a controlled fashion, it apparently overstrained the crack tip, and the CGR did not show the expected response. Next, periodic unloading was introduced, and a CGR of 3.3 10^{-11} m/s was measured, less than what was expected for this loading condition. The specimen was next set at constant load, and, the measured CGR was again smaller than expected. Constant load with periodic unloading (2h) was reintroduced (period 35), and the rate is similar to that observed previously in the same loading condition. The hold time was further increased to 4h (period 36) and the rate stayed largely unchanged suggesting that the SCC mode is dominant.

Next, the crack was advanced by fatigue with the purpose of increasing the stress intensity factor to K_{max} = 45 MPa $m^{1/2}$. This was accomplished in test periods 37-53. Next, transitioning steps were undertaken with no substantial environmental enhancement. Constant load with periodic unloading (period 60) resulted in a rates slightly higher than measured previously at the lower K_{max} values. Next, hold time was doubled (period 61), and the CGR rate initially stayed largely the same, but subsequently diminished. Cyclic loading was re-introduced (periods 62 and 63) and, again, no environmental enhancement was observed. One interesting observation is that the measured rate did not change between periods 62 and 63, suggesting that, perhaps, larger rise times are needed under the current loading conditions in order to achieve environmental enhancement.

The approach suggested above implying longer rise times was tried next. After the rise time was increased briefly to 4000 s (period 64), R was reduced to 0.3, and the rise time was increased as needed to preserve the mechanical fatigue component (period 65). On average, the result was an improvement in environmental enhancement over the previous period, and because the rates appeared to increase towards the end of the period to levels expected based on previous experience with this alloy, the specimen was set at constant load (period 67). Initially the measured CGR appeared rather low (2.2 10^{-11} m/s), but subsequently appeared to accelerate, and a CGR of 4.0 10^{-11} m/s was measured for the next 350 hours, Figure 21i. Then, the measured crack length appeared to decrease, suggesting that the two fracture surfaces were touching - most likely the effect of an unbroken ligament or a flake, thus causing the DC potential to underestimate the crack length. The situation was overcome by cycling (period 68) and constant load with periodic unloading (periods 69-71). The CGR measured in period 68 is larger than that measured in period 65, suggesting that some ligaments were indeed being broken. Once the previous crack length high was reached, loading was changed to constant load with periodic unloading to clear any remaining ligaments, and eliminate the mechanical component as the main driving force for the crack. After observing that the CGR did not change with hold time (periods 70 and 71), the specimen was set at constant load (period 72) and, the

SCC growth resumed at the 4.1 10^{-11} m/s rate measured previously. As the measured rate appeared to decrease (16,300h, Fig. Figure 21j), periodic unloading every 4h was introduced in period 73. The SCC CGR of approx. 4.0 10^{-11} m/s was re-established, however, this rate began to diminish, too, suggesting that 4h periodic unloading was too gentle for the case at hand, and did not prevent the formation of ligaments. Hence, the period was reduced to 2h in test period 74. Once a well-behaved growth was re-established, the temperature was decreased to 300°C (while maintaining the 2h periodic unload/reload cycle) to allow for a determination of the activation energy for SCC growth in this alloy. The hydrogen overpressure was also adjusted to maintain constant the potential vs. the Ni/NiO line. The SCC CGR measured in period 75 was approx. one order of magnitude lower than that measured at 320°C in the previous test period. In period 76, the specimen was set at constant load. The SCC CGR was initially consistent with that measured in the previous period, then appeared to decrease. Overall, the SCC CGR dependence on temperature is consistent with that observed previously on Alloy 182 welded in a similar double-J geometry [7]. For the final period of this test (77), the specimen was fast cycled to transition back to a TG fracture mode and mark the fracture surface.

Table 11 Crack growth data for specimen A152-TS-5 of Alloy 152 Weld in PWR water[a].

Test Period	Test Time, h	Temp. °C	Load Ratio R	Rise Time, s	Down Time, s	Hold Time, s	K_{max}, MPa·m$^{1/2}$	ΔK, MPa·m$^{1/2}$	CGR_{env}, m/s	Estimated CGR_{air}, m/s	Crack Length, mm
Pre a	152	319.7	0.3	0.5	0.5		19.3	13.5	3.59E-08	4.47E-08	12.877
Pre b	168	319.2	0.3	50	50		19.4	13.6	1.22E-09	4.49E-10	12.916
Pre c	176	319.2	0.3	0.5	0.5		20.1	14.1	5.40E-08	5.27E-08	13.682
Pre d	192	318.4	0.3	50	50		20.1	14.1	1.05E-09	5.17E-10	13.700
Pre e	200	318.8	0.3	0.5	0.5		21.3	14.9	7.18E-08	6.57E-08	14.768
Pre f	216	318.7	0.3	50	50		21.3	14.9	1.90E-09	6.57E-10	14.823
Pre g	223	319.0	0.3	0.5	0.5		22.7	15.9	9.79E-08	8.64E-08	16.063
Pre h	288	318.4	0.3	50	50		23.0	16.1	2.14E-09	9.02E-10	16.331
Pre i	296	319.3	0.3	0.5	0.5		25.1	17.6	1.15E-07	1.29E-07	18.028
Pre j	312	318.9	0.3	50	50		25.2	17.6	3.04E-09	1.31E-09	18.128
Pre k	316	319.5	0.3	0.5	0.5		26.7	18.7	1.46E-07	1.67E-07	19.181
1	320	319.1	0.49	12	12		26.9	13.7	5.47E-09	3.27E-09	19.217
2	336	318.8	0.49	50	12		27.0	13.8	1.73E-09	7.88E-10	19.296
3	391	319.3	0.49	300	12		27.1	13.8	3.97E-10	1.34E-10	19.378
4	456	319.6	0.49	600	12		27.1	13.8	2.70E-10	6.78E-11	19.439
5	555	319.3	0.49	1000	12		27.2	13.9	1.61E-10	4.11E-11	19.480
6	676	319.9	0.49	1000	12	7200	27.2	13.9	2.41E-11	5.07E-12	19.496
7	727	319.5	0.49	600	12		27.3	13.9	1.81E-10	6.93E-11	19.539
8	846	319.9	0.49	600	12	1200	27.3	13.9	1.46E-10	2.34E-11	19.564
9	972	319.6	0.49	600	12	2400	27.1	13.8	5.78E-11	1.35E-11	19.585
10	1,637	320.5	0.49	600	12	4800	27.3	13.9	2.48E-11	7.86E-12	19.651
11	1,900	318.4	1	0	0		27.3	0.0	2.04E-12	-	19.655
12	1,997	318.9	0.49	600	12		27.4	14.0	3.06E-10	6.98E-11	19.749
13	2,086	318.8	0.49	1000	12		27.5	14.0	1.92E-10	4.27E-11	19.814
14	2,110	318.1	0.49	300	12		27.6	14.1	5.40E-10	1.43E-10	19.819
15	2,134	318.0	0.49	600	12		27.5	14.0	3.19E-10	7.01E-11	19.739
16	2,208	317.8	0.49	1000	12		27.7	14.1	1.96E-10	4.32E-11	19.894
17	2,232	318.8	0.49	1000	12		27.7	14.1	2.07E-10	4.38E-11	19.919
18	2,594	318.3	1	12	12	28800	27.8	14.2	4.18E-12	-	19.916
19	2,616	318.5	1	12	12	14400	27.8	14.2	1.18E-11	-	19.927
20	2,688	319.5	1	12	12	7200	27.8	14.2	4.78E-12	-	19.930
21	2,769	318.5	0.49	600	12		27.9	14.2	1.88E-10	7.56E-11	19.954
22	2,902	318.8	0.49	600	12	3600	27.9	14.2	3.43E-11	1.07E-11	19.988
23	3,173	318.4	0.49	600	12	7200	27.9	14.2	3.64E-11	5.78E-12	20.034
24	3891	319.0	1	0	0		27.9	0.0	6.51E-12	-	20.065
25	4,926	319.2	1	12	12	7200	28.5	14.6	1.65E-11	-	20.102
26	5,520	320.1	1	12	12	7200	31.7	16.2	3.91E-11	-	20.153

Table 11 (cont.)

Test Period	Test Time, h	Temp. °C	Load Ratio R	Rise Time, s	Down Time, s	Hold Time, s	K_{max}, MPa·m$^{1/2}$	ΔK, MPa·m$^{1/2}$	CGR_{env}, m/s	Estimated CGR_{air}, m/s	Crack Length, mm
27	6,021	319.2	1	0	0		32.0	0.0	3.34E-11	-	20.218
28	6,526	319.3	1	12	12	7200	32.3	16.5	4.49E-11	-	20.235
29	6,957	319.4	1	0	0		32.8	0.0	1.37E-11	-	20.246
30	7,769	319.4	1	12	12	7200	33.3	16.9	2.46E-11	-	20.315
31	7,960	319.1	1	0	0		33.6	0.0	2.06E-11	-	20.319
32	8,299	318.8	1	0	0		36.6	0.0	6.11E-12	-	20.333
33	9,183	319.8	1	12	12	7200	36.9	0.0	3.34E-11	-	20.434
34	9,954	319.1	1	0	0		37.5	0.0	3.30E-12	-	20.448
35	11,337	319.1	1	12	12	7200	38.8	0.0	3.35E-11	-	20.619
36	12,251	318.5	1	12	12	14400	39.0	19.5	2.27E-11	-	20.697
37	12,273	318.6	0.5	100	12		37.6	18.8	1.91E-09	1.45E-09	20.805
38	12,282	318.5	0.5	12	12		37.9	19.0	1.38E-08	1.25E-08	20.967
39	12,927	318.6	0.5	100	12		38.0	19.0	1.99E-09	1.52E-09	21.055
40	12,308	318.6	0.5	12	12		38.8	19.4	2.04E-08	1.38E-08	21.434
41	12,322	318.6	0.5	100	12		39.0	19.5	1.96E-09	1.69E-09	21.534
42	12,330	318.7	0.5	12	12		39.6	19.8	1.89E-08	1.51E-08	21.825
43	12,345	318.5	0.5	100	12		39.9	20.0	1.83E-09	1.86E-09	21.952
44	12,352	319.1	0.5	12	12		40.5	20.3	2.44E-08	1.66E-08	22.198
45	12,465	318.6	0.5	300	12		41.3	20.6	8.66E-10	7.12E-10	22.532
46	12,473	318.8	0.5	12	12		41.7	20.8	1.18E-08	1.85E-08	22.704
47	12,491	318.7	0.5	100	12		42.0	21.0	2.32E-09	2.29E-09	22.848
48	12,496	318.6	0.5	12	12		42.0	21.0	1.21E-08	1.91E-08	22.928
49	12,513	318.4	0.5	100	12		42.3	21.2	2.51E-09	2.37E-09	23.085
50	12,519	318.6	0.5	12	12		42.8	21.4	1.72E-08	2.06E-08	23.250
51	12,585	316.6	0.5	300	12		42.8	21.4	1.02E-09	8.08E-10	23.273
52	12,594	318.3	0.5	12	12		43.8	21.9	1.45E-08	2.27E-08	23.697
53	12,612	318.3	0.5	100	12		44.2	22.1	2.33E-09	2.81E-09	23.834
54	12,633	318.3	0.5	300	12		44.4	22.2	9.83E-10	9.59E-10	23.927
55	12,687	318.4	0.5	600	12		44.6	22.3	5.71E-10	4.88E-10	24.024
56	12,803	318.4	0.5	1000	12		45.0	22.5	3.94E-10	3.03E-10	24.169
57	12,923	318.1	0.5	600	12		45.8	22.9	6.41E-10	5.41E-10	24.446
58	13,091	318.4	0.5	1000	12		45.3	22.7	4.16E-10	3.14E-10	24.690
59	13,477	317.1	0.5	1000	12	7200	45.7	22.9	7.61E-11	3.89E-11	24.771
60	13,954	318.3	1	12	12	7200	45.7	22.8	4.34E-11		24.833
61	14,698	318.8	1	12	12	14400	46.1	23.1	2.80E-11		24.899
62	14,770	318.7	0.5	600	12		46.4	23.2	5.72E-10	5.78E-10	25.037
63	14,800	318.7	0.5	1000	12		46.6	23.3	5.67E-10	3.51E-10	25.085
64	14,826	318.8	0.5	2000	12		46.6	23.3	2.28E-10	1.77E-10	25.105
65	14,844	319.1	0.5	4000	12		46.6	23.3	7.23E-11	8.86E-11	25.108
66	15,300	318.9	0.3	12000	12		47.4	33.2	1.27E-10	7.32E-11	25.300
67	15,874	320.1	1	0	0		47.7	0.0	4.05E-11		25.356
68	15,944	320.0	0.5	4000	12		47.9	24.0	1.66E-10	1.00E-10	25.370
69	15,973	319.4	1	12	12	28800	48.0	24.0	3.62E-11		25.375
70	16,046	319.2	1	12	12	14400	48.0	24.0	5.77E-11		25.381
71	16,163	319.4	1	12	12	7200	48.1	24.0	6.16E-11		25.390
72	16,431	319.3	1	0	0		48.4	0.0	4.13E-11		25.402
73	16,624	319.6	1	12	12	14400	48.2	24.1	4.94E-11		25.444
74	16,766	319.0	1	12	12	7200	48.2	24.1	6.50E-11		25.465
75	17,080	299.7	1	12	12	7200	48.3	24.2	1.55E-11		25.498
76	17,316	300.1	1	0	0		48.4	0.0	7.32E-12		25.501
77	17,324	300.6	1	12	12		48.8	24.4	1.02E-08	2.88E-8	25.639

[a]Simulated PWR water with 2 ppm Li, 1100 ppm B, and 2 ppm. DO<10 ppb. Conductivity was 21±3 μS/cm, and pH 6.4.

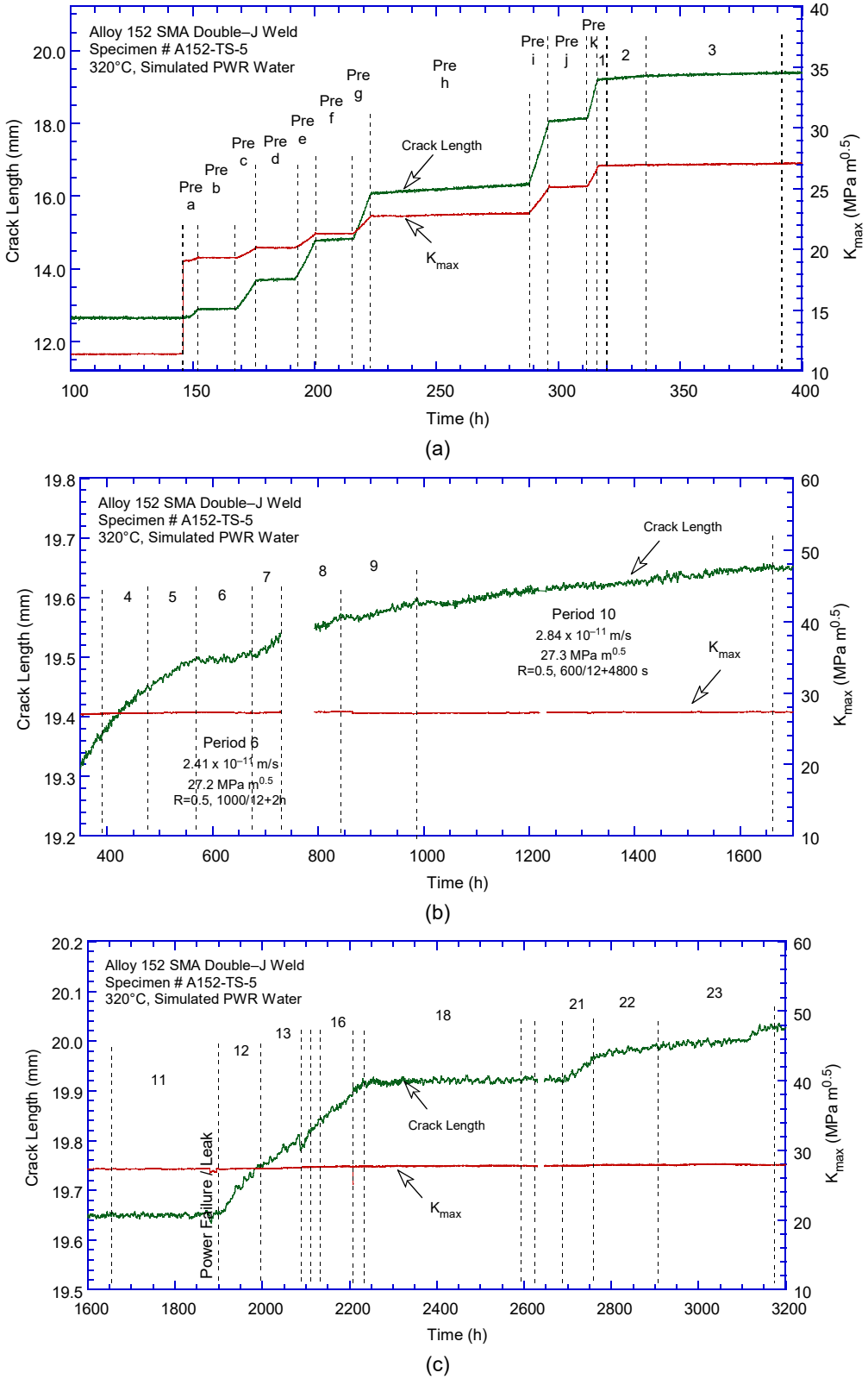

Figure 21 Crack–length–vs.–time for Alloy 152 weld specimen A152-TS-5 in simulated PWR environment during test periods: (a) precracking-3, (b) 4-10, (c) 11-23, (d) 24-27, (e) 28-33, (f) 34-36, (g) 37-52, (h) 57-64, (i) 65-72, and (j) 72-77.

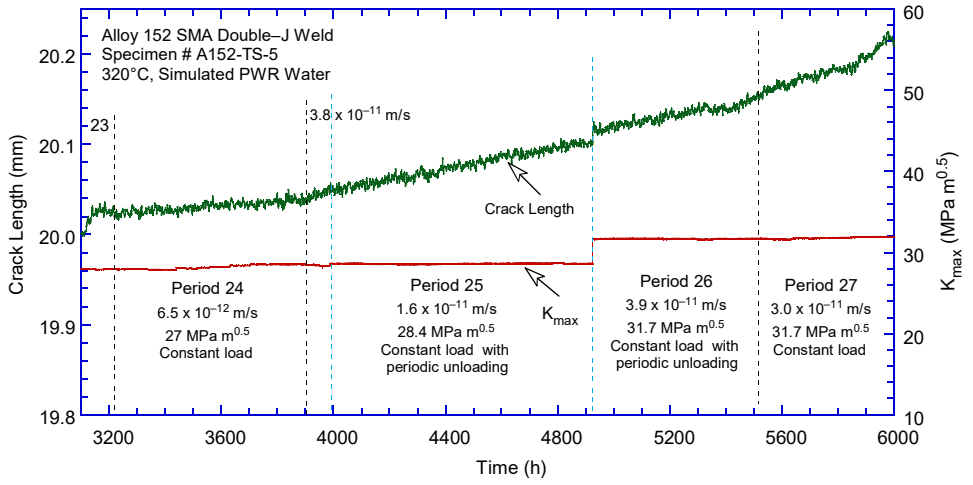

(d)

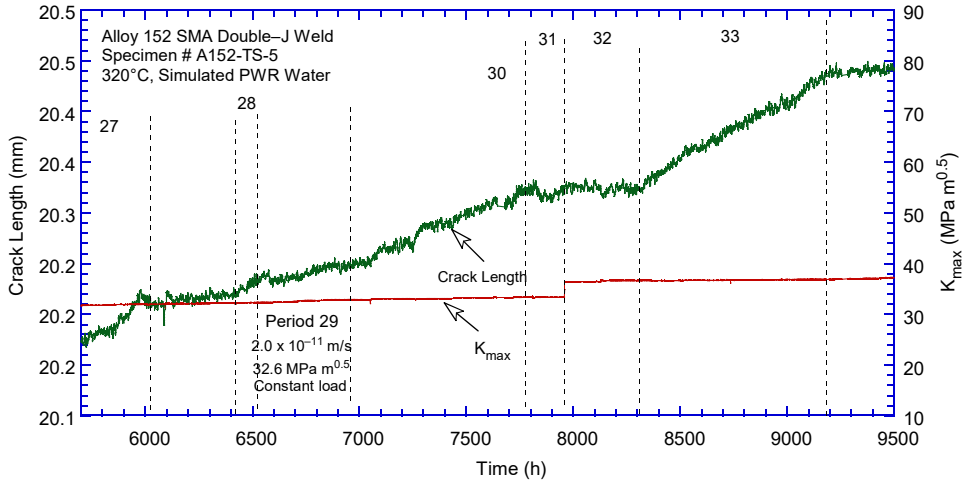

(e)

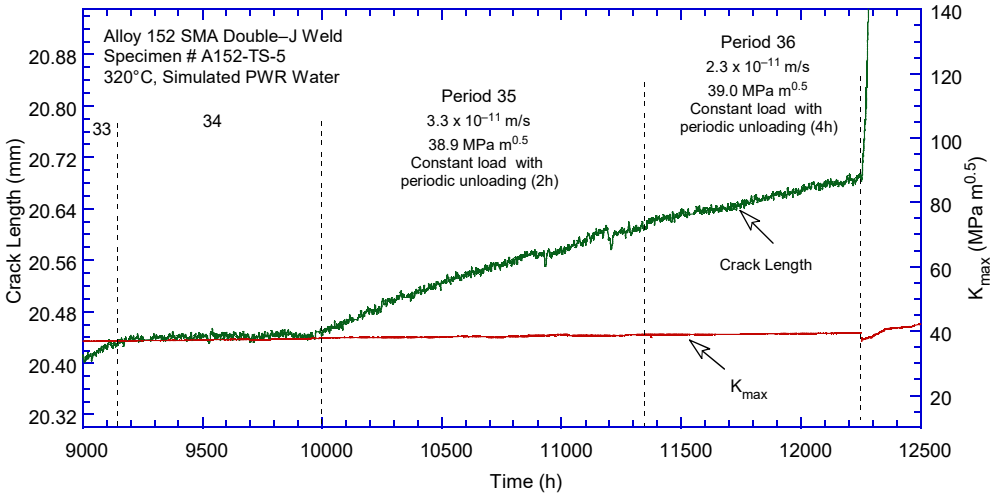

(f)

Figure 21 (cont.)

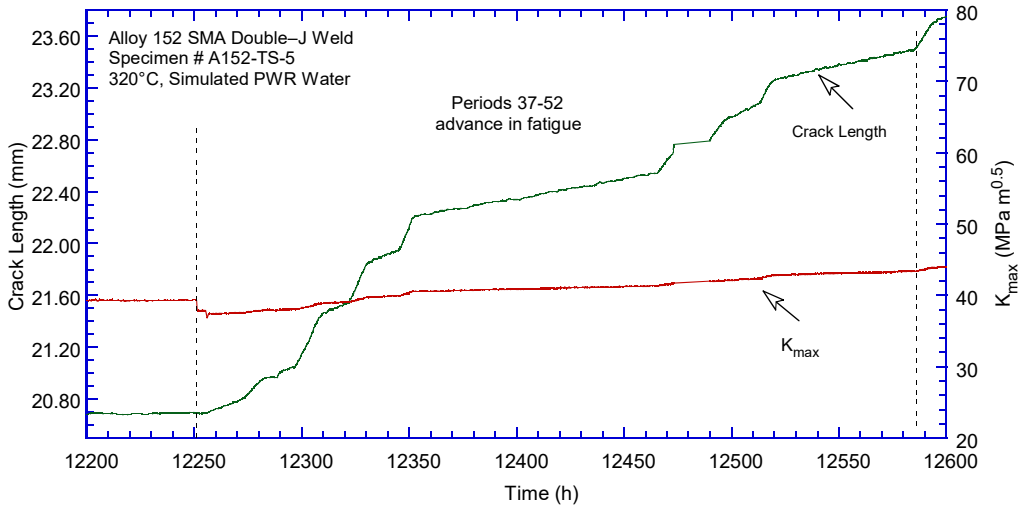

(g)

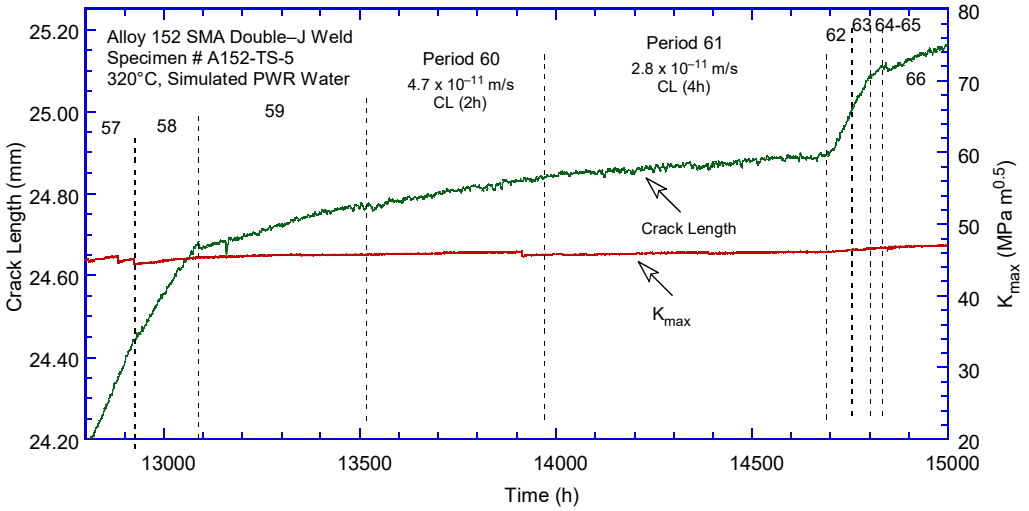

(h)

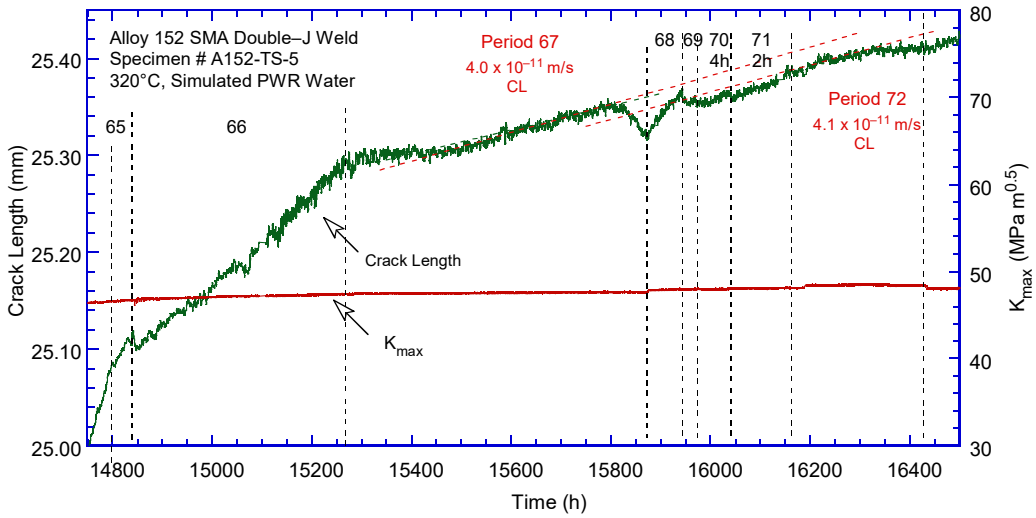

(i)

Figure 21 (cont.)

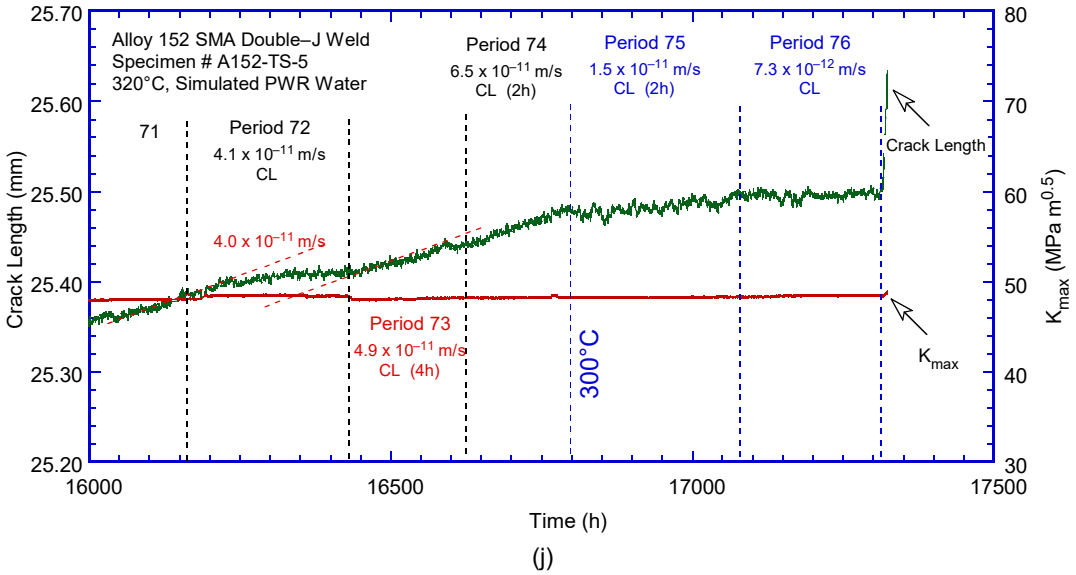

(j)

Figure 21 (cont.)

Figure 22 puts the cyclic CGR data obtained in this test into perspective. For comparison, Figure 22a shows the data from the two completed tests (A152-TS-2 and A152-TS-4) on the same Alloy 152 weld [5] as well as additional data on Alloy 152 from Babcock & Wilcox [25]. The corrosion fatigue curve for Alloy 182 is included for comparison. The cyclic CGR data for the two specimens tested at ANL and the B&W data appear to be in very good agreement. The previous ANL data – who was used to optimize the transitioning conditions for the current test - also suggests that there are conditions that show environmental enhancement, with an optimum loading ratio of R = 0.5. Moreover, one observes that by further increasing R and rise time the environmental enhancement begins to diminish. When R is 0.7 and rise time is 1000s, the rate in the environment equals that in air, that is, the environmental enhancement appears to be completely lost. Figure 22b shows the cyclic CGR data for the two Alloy 152 tests already completed and that from the current test. The cyclic data for the current specimen (A152-TS-5) agrees very well with previous data, and periods involving a hold time (open red symbols) seem to preserve the environmental enhancement once that was achieved.

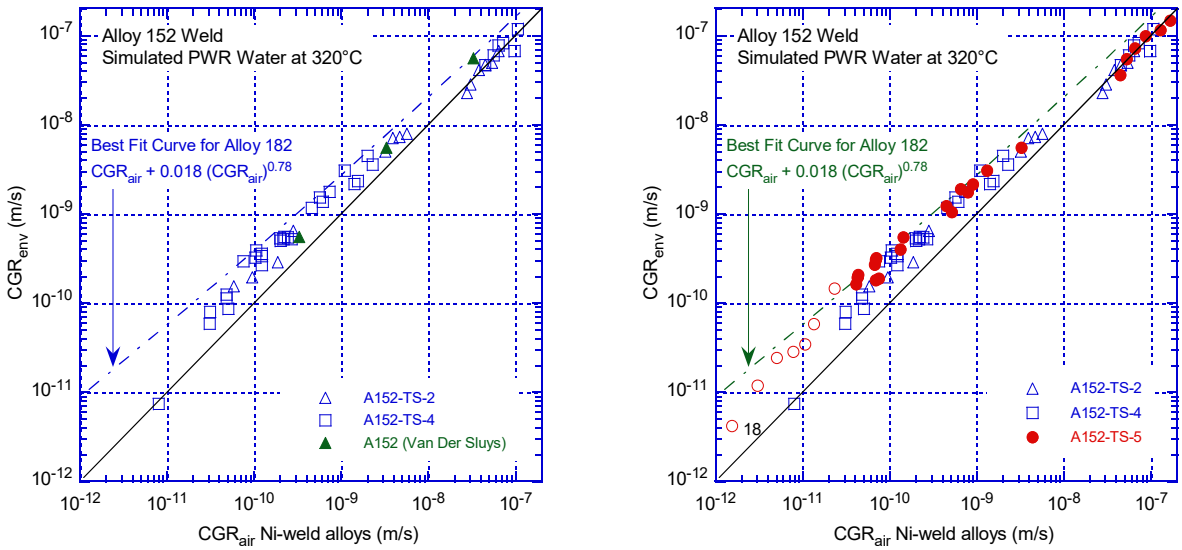

Figure 22 Cyclic CGR data for Alloy 152 specimens in PWR environment (a) ANL and B&W tests; (b) ANL specimens (two tested previously, A152-TS-2 and A152-TS-4, and the current one, A152-TS-5).

Figure 23 shows the cyclic CGR data for Alloy 152 weld specimen A152-TS-5 for periods 37-53. As these were conducted with the purpose of advancing the crack, thus, at relatively high frequencies, no environmental enhancement was observed. Additional transitioning steps (62-64) which normally result in environmental enhancement in this alloy provided no environmental enhancement under the current testing conditions. However, further lowering R to 0.3 and increasing the rise time to maintain the prior mechanical component (period 66) seemed to help with environmental enhancement. The environmental enhancement observed in test period 68 appears to be higher than that observed previously in period 65, however, that may also be a result of breaking the ligaments formed during constant load growth in period 67.

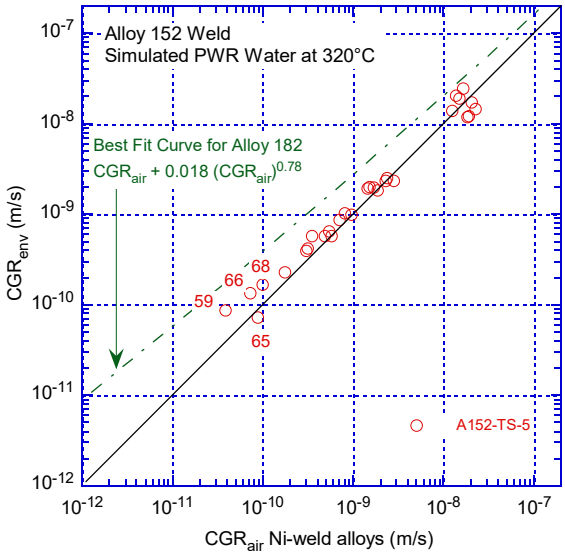

Figure 23 Cyclic CGR data for periods 37-53 for Alloy 152 specimen A152-TS-5 in PWR environment.

Figure 24 shows the SCC CGR data obtained from this specimen. There seems to be a good agreement between that data obtained at CL (solid symbols) and the data obtained from PPU conditions (open symbols), particularly for longer crack increments. The data from two identical specimens tested previously are included, and all data appear to be in good agreement.

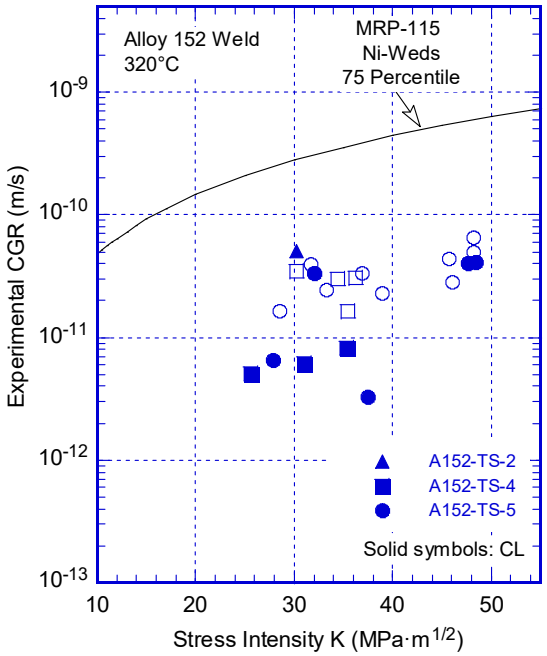

Figure 24 SCC CGRs for Alloy 152 specimen A152-TS-5 as a function of stress intensity factor. Also included are data from two identical specimens, A152-TS-2 and A152-TS-4, tested previously [5].

Figure 25 shows the Alloy 152 SCC CGR data obtained in test periods 72-76 as a function of temperature. For this plot all (PPU and constant load) data was included and the implications and alternative ways of interpretation will be discussed further in Section 4.

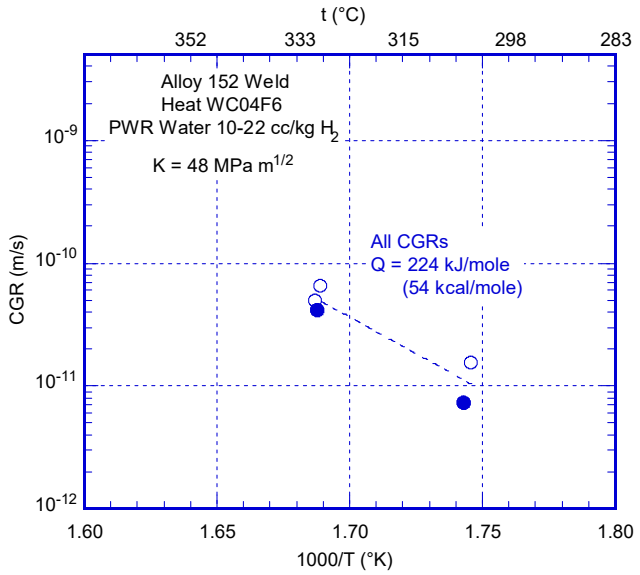

Figure 25 SCC CGRs as a function of temperature for Alloys 152 and 182 welded in double-J geometries.

Following the completion of the test, the fracture surface was examined by optical microscopy and SEM. This following section describes and discusses the findings of that examination.

The resulting fracture surface was examined by both optical microscopy and SEM, and Figure 26, the full fracture surface, is used to explain the experimental approach undertaken in order to meet the objectives. The specimen was precracked in the PWR environment, and the crack was transitioned to IG SCC at a moderate stress intensity factor, similar to those used in previous tests. The resulting cyclic (fatigue and corrosion fatigue) rates were similar to those measured previously. Once IG SCC conditions were achieved (region marked IG-1 in Figure 26), the SCC CGRs were sampled at both constant load and constant load with periodic unloading conditions. The results show that irrespective of the type of loading, the measured rates were similar, as it would be expected in a condition where the IG SCC mode was dominant. These IG SCC CGRs are also similar to those obtained previously on this alloy. Next, the crack was advanced in fatigue to achieve a higher stress intensity factor, then the crack was again transitioned from a fatigue TG fracture mode to an IG SCC fracture mode (region marked IG-2 in Figure 26). As before, the SCC CGRs were sampled under both constant load and constant load with periodic unloading conditions. Finally, the test temperature was decreased to obtain a measure of the activation energy for SCC crack growth in this alloy.

The image shown in Figure 26– with markings for the various regions and fracture modes - was used to determine the correction for the DC potential data. The difference was small (9.5%), thus, no correction was applied to the DC potential data. The small difference is not unexpected (or unusual for Alloy 152 specimens) because growth under constant load (where ligaments that confound the DC potential measurements are expected to form) was small when compared with

the total crack advance. Also, in many test periods an unload/reload cycle, introduced with the specific purpose of breaking the ligaments, was present. The overall appearance of the fracture surface indicates that the testing procedure resulted in a straight, uniformly IG-engaged fracture surface.

The two intergranular regions, IG-1 and IG-2 are shown in additional detail in Figure 27 and Figure 28. In each figure, the crack front is divided in two regions. In both cases, the IG engagement is very large, 95% in IG-1 and 100% in IG-2. The crack advance was 1.1 mm and 0.8 mm, respectively. The uninterrupted fracture mode suggests that the gentle unload/reload periods did not alter the IG fracture mode. The same observation holds true for the lower temperature.

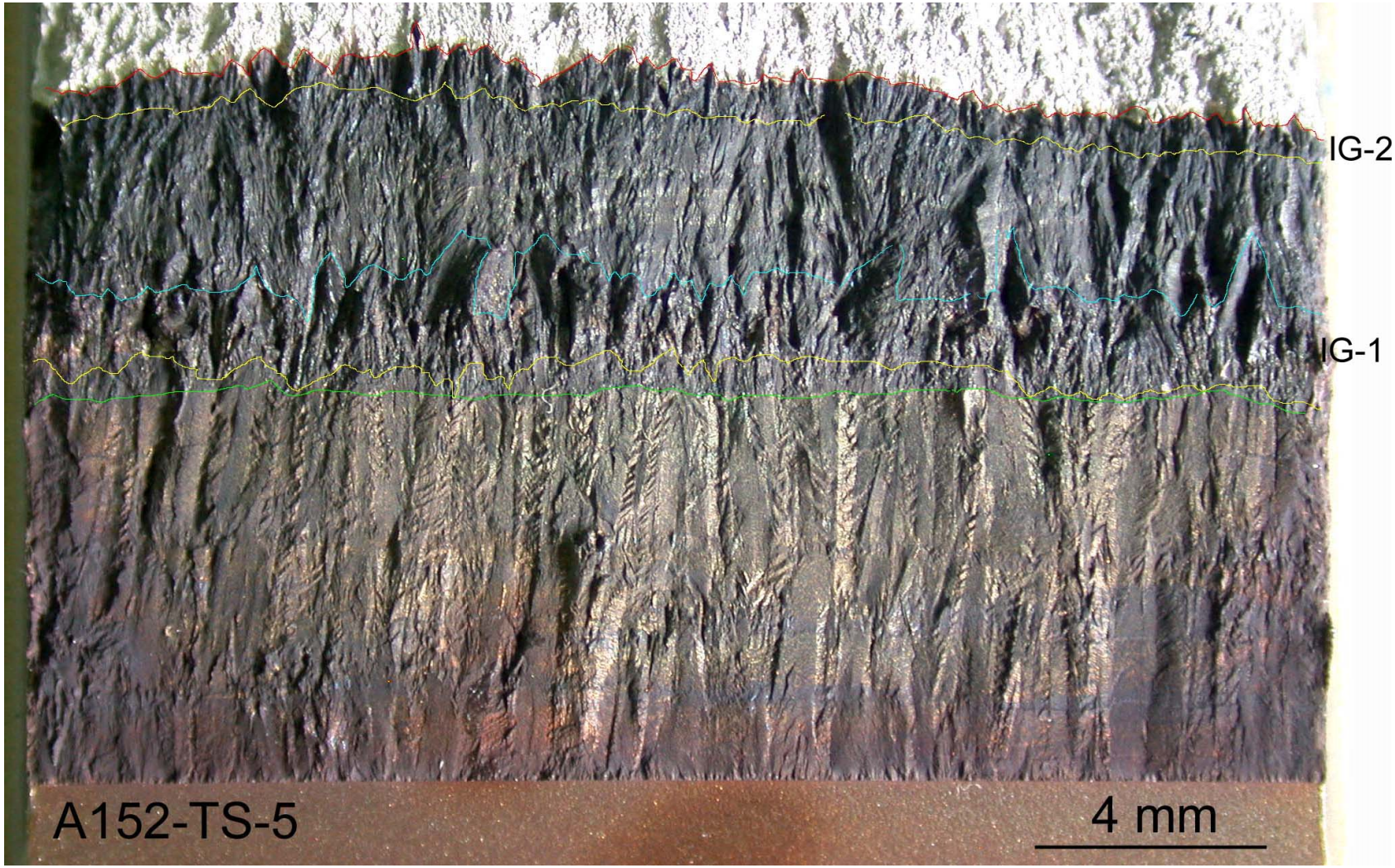

Figure 26 **Fracture surface of Specimen A152-TS-5: tested in primary water environment Crack advance is from bottom to top.**

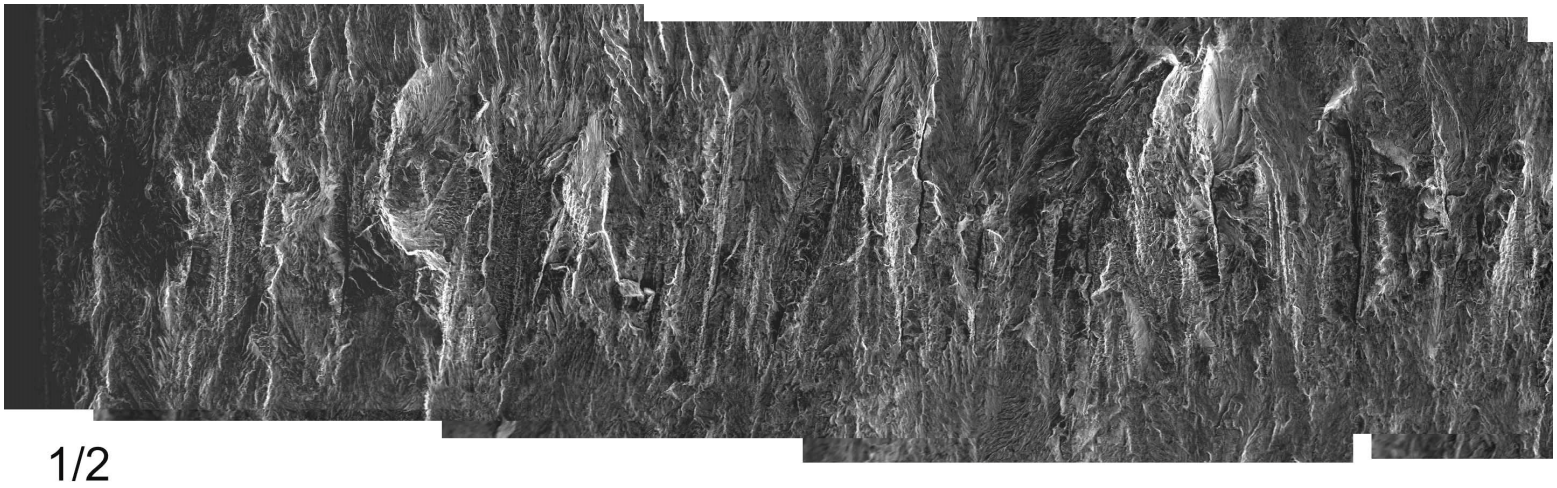

(a)

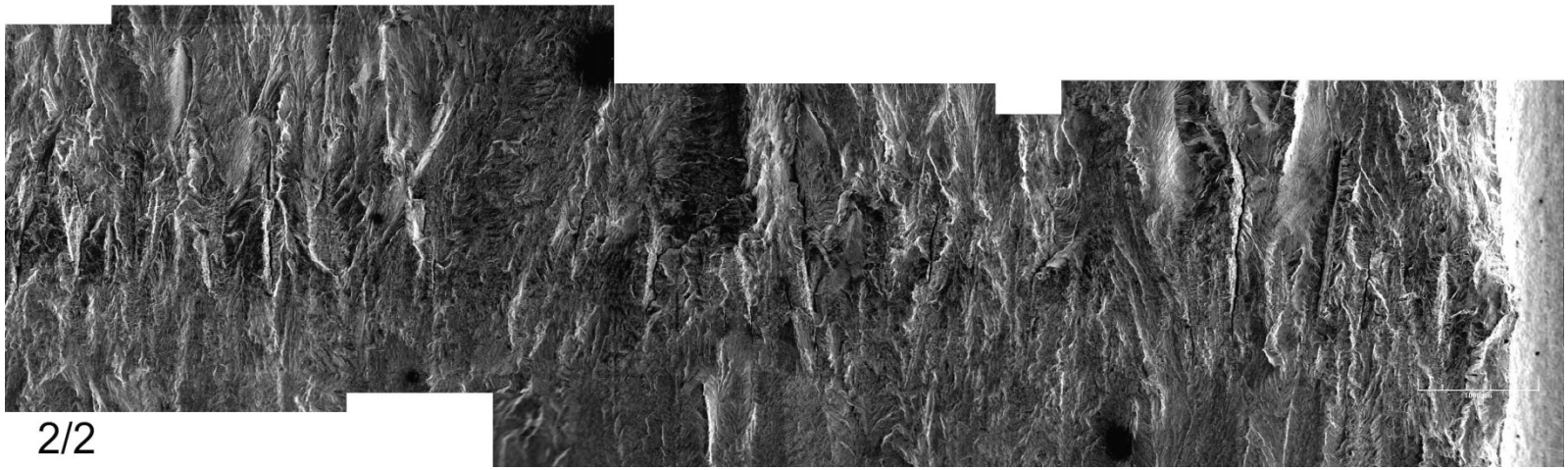

(b)

Figure 27 **Specimen A152-TS-5: (a) first half, and (b) second half of the first intergranular region (IG-1). Crack advance is from bottom to top.**

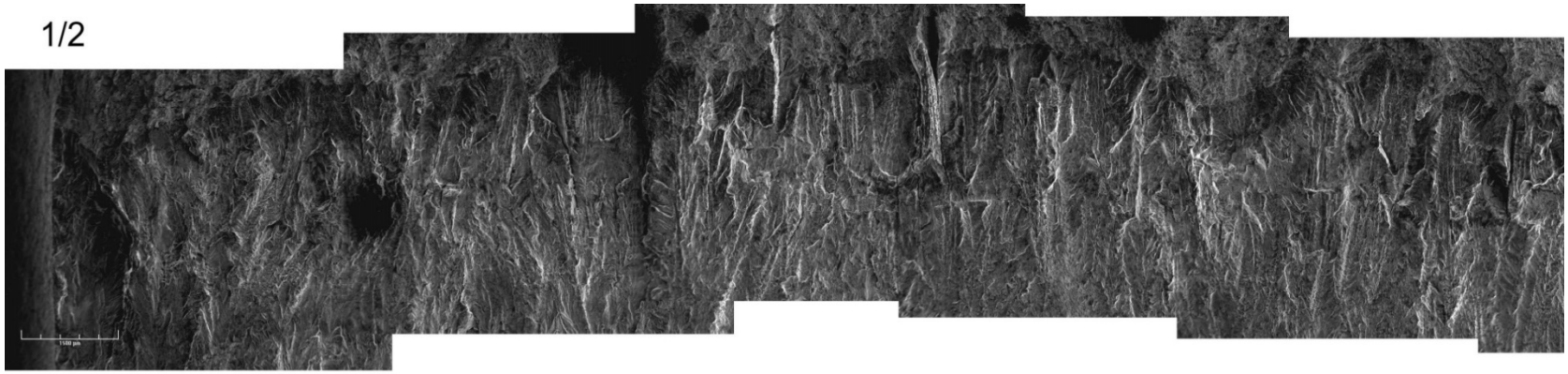

(a)

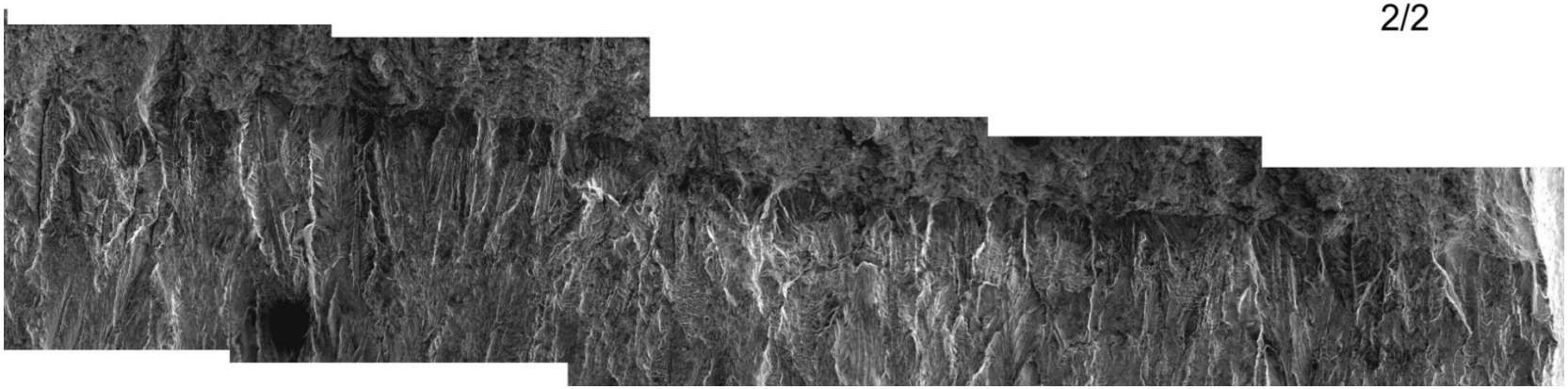

(b)

Figure 28 **Specimen A152-TS-5: (a) first half, and (b) second half of the second intergranular region (IG-2). Crack advance is from bottom to top.**

A common feature observed on the fracture surfaces of Alloy 152 (and Alloy 182) specimens is the presence of secondary IG cracks. These types of cracks seem to develop during transitioning and signal the onset of IG/interdendritic cracking. Figure 29 shows examples from current specimen A152-TS-5, region IG-1. These cases are similar to that observed on the previous specimen A152-TS-2 (Figure 30), where the IG crack indicated by an arrow seems to have initiated well ahead of the IG region; however, it apparently propagated sideways, toward the side groove of the specimen. The reverse also seems true, i.e., a lack of secondary IG cracking appears to be associated with a lack of IG engagement later on. Hence, finding and fine-tuning those transitioning conditions to produce secondary IG cracks uniformly distributed on the fracture surface appears to be key to an eventually successful, uniform transitioning.

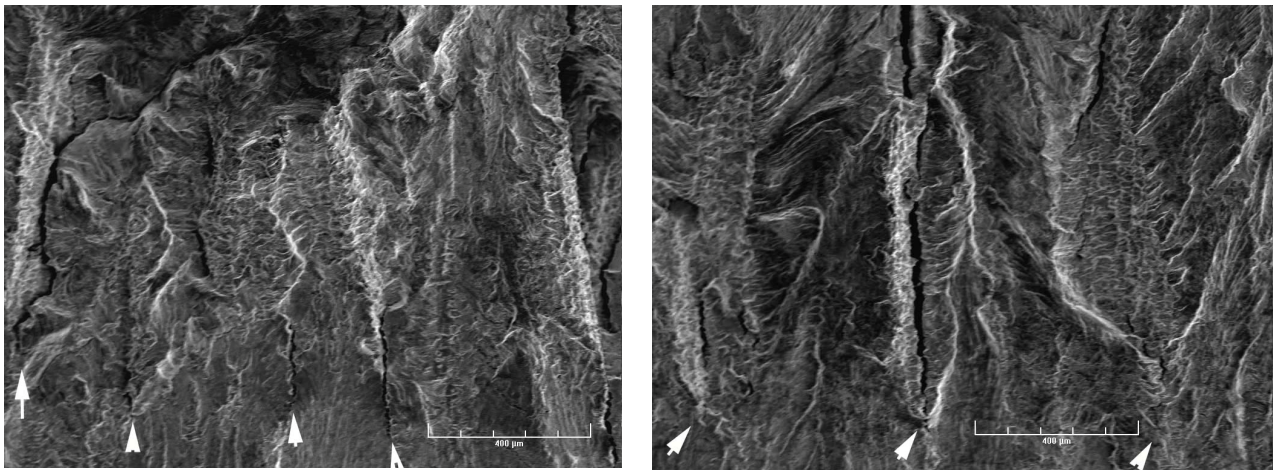

Figure 29 Secondary, out of plane cracks are indicated by white arrows on the fracture surface of specimen A152-TS-5, region IG-1. Crack advance is from bottom to top.

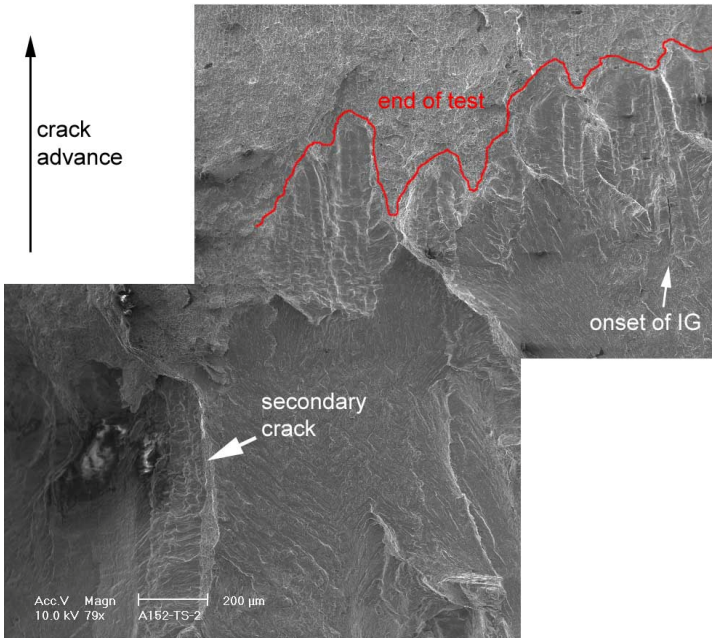

Figure 30 Region of fracture surface of specimen A152-TS-2. White arrows indicate secondary IG cracks. Crack advance is from bottom to top.

As expected, secondary IG cracks were also observed in region IG-2, Fig. Figure 31. As such, Figure 31a provides additional examples of secondary IG cracks that seem to precede the full-blown IG crack front. In addition, at the end of the test, the fracture surface was also examined for evidence of ligaments (TG in appearance) to provide additional validity to the rationale behind the test management involving PPU described previously. Two such examples are shown in Figure 31b. The figure shows a predominantly IG fracture mode, with a high density of secondary IG cracks. In the center-right of the image, the IG crack went out of plane, forming the ligament indicated by the arrow. This example is strikingly similar to the one observed previously on the fracture surface of Specimen A152-TS-4, Figure 32a. Figure 32b shows a high magnification micrograph of the ligament showing the two fracture modes: IG on the left side and TG on the right side. Interdendritic features are also recognizable on the TG side, suggesting a crack-resistant grain. Striations are also visible, consistent with a fatigue-driven crack advance. In other words, the cyclic component broke through such resistant grains ("ligaments") and enabled the SCC CGR to be measured in real time. In general, there appears that in such cases finding the right balance between the fatigue and SCC components of the CGR is critical. Specifically, the crack needs to be SCC-driven, and the fracture mode should reflect that.

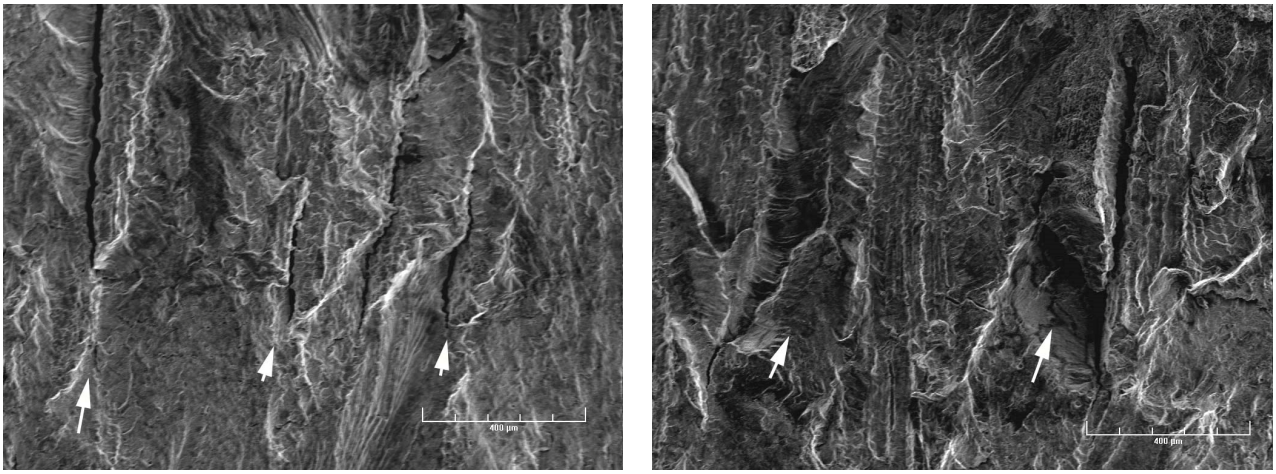

Figure 31 (a) Out of plane, secondary IG cracks and (b) ligaments on the fracture surface of specimen A152-TS-5, IG-2. White arrows indicate secondary IG cracks and ligaments. Crack advance is from bottom to top.

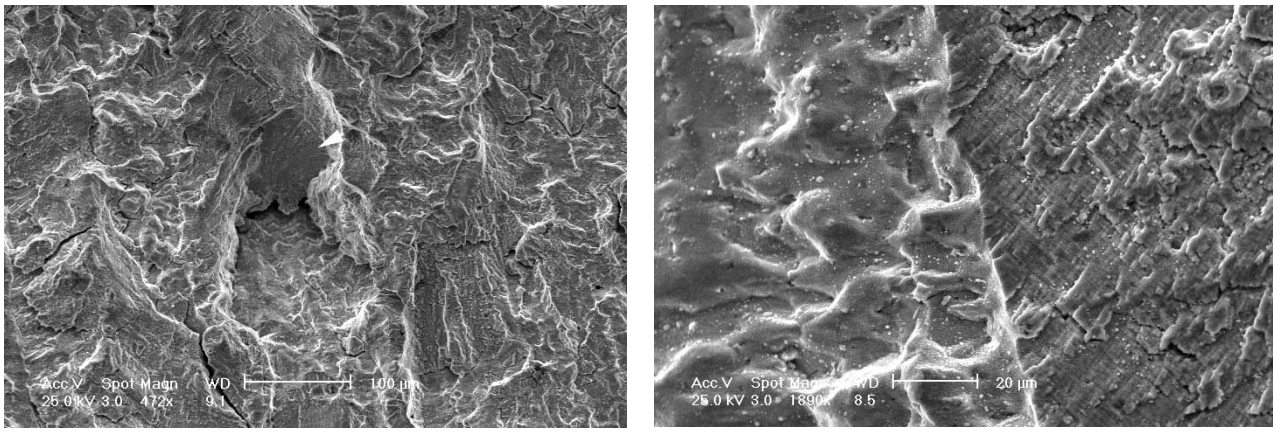

Figure 32 Ligaments on the fracture surface of specimen A152-TS-4: (a) out of plane crack and (b) interdendritic (left) and TG (right) fracture modes. Crack advance is from bottom to top.

It is also important to note that once transitioned, the crack propagated in an IG SCC mode at both 320°C and 300°C. As such, Figure 33 shows the fracture surface of specimen A152-TS-5 in the IG-2 region. As described previously, the crack front apparently initiated from/as secondary IG cracks and continued to propagate in an IG fracture mode irrespective of temperature until the loading was changed to aggressive fatigue in test period 77 at the end on the test. The implication of this finding is that the activation energy estimated from the several test periods at the end of this test is for IG SCC growth.

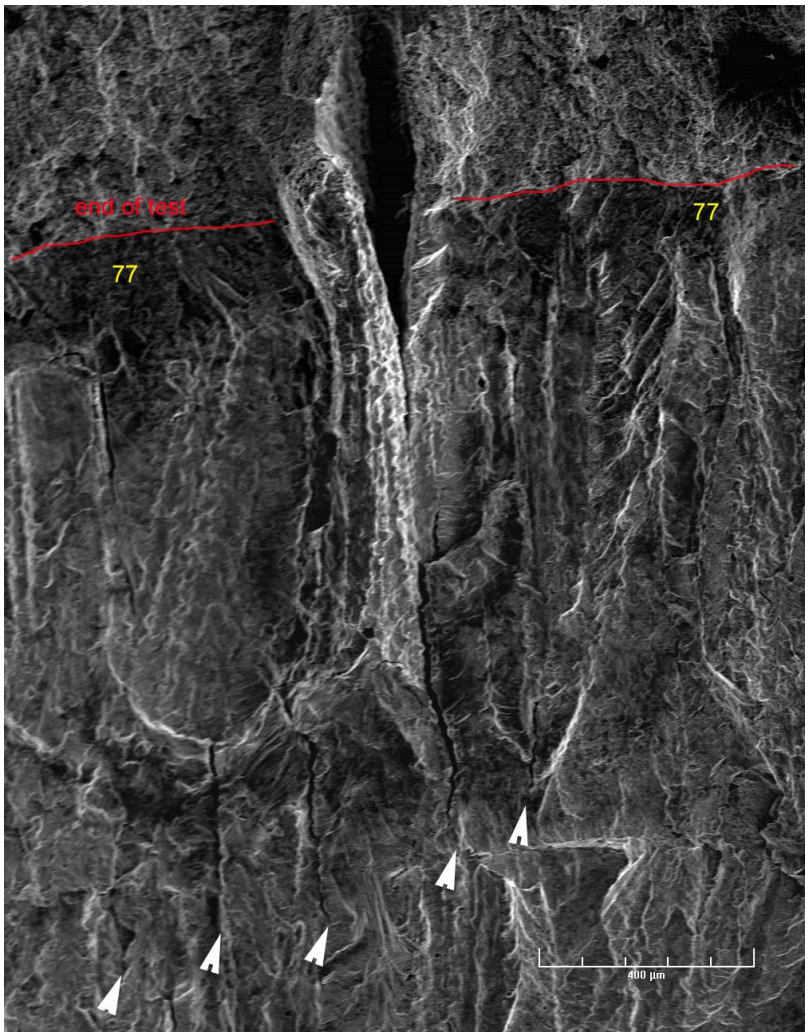

Figure 33 Fracture surface of specimen A152-TS-5 in the IG-2 region. Arrows show the secondary IG cracks preceding the IG crack front. Also indicated is the TG region corresponding to fatigue growth in the last period (77) of the test. Crack advance is from bottom to top.

In summary, the experimental approach used in this test resulted in a straight, uniformly IG-engaged fracture surface. The IG regions are continuous and suggest that the periodic unloading or temperature did not alter the propagation mode. The IG crack advance was substantial (1.1 mm and 0.8 mm). SCC CGRs were sampled at both constant load and constant load with periodic unloading conditions, and, irrespective of the type of loading, the measured rates were similar. All these features meet the criteria used by industry in MRP-115,

and, as such, make this data set directly comparable with the disposition curves proposed for Alloy 182/82.

3.1.2 Specimen N152-TS-1

The objective of the test on specimen N152-TS-1 from the newly-produced Alloy 152 weld (designated N152) was to determine SCC CGRs at several stress intensity factors. In order to allow for testing at the higher stress intensity factors, the specimen was machined in a 1T CT configuration, similar to that used for the specimens from the A152 series discussed previously. Also, in order to reproduce the specimen location vs. weld geometry used previously, an additional piece of Alloy 690 was EB-welded on top of the existing weld, allowing the notch of the specimen to be positioned near the crown of the weld. The resulting test specimen is shown in 33.

Figure 34 Photograph of Alloy 152 weld specimen N152-TS-1.

The testing conditions for specimen N152-TS-1 are given in Table 12, and the changes in crack length and K_{max} with time are shown in Figure 35. In the first part of the test, the objective was to determine the SCC CGR at a moderate stress intensity factor. As such, after transitioning at $K \approx 26$ MPa $m^{1/2}$, the sample was set at constant load in test period 4. The resulting CGR was negligible. This early attempt was followed by additional transitioning test periods, and by constant load with periodic unloading for approx. 500h in test period 7, and the resulting CGR was very small ($4.7\ 10^{-12}$ m/s) for this loading condition, suggesting that transitioning to an IG SCC fracture mode had not occurred. The test continued with additional gentle cyclic test periods. A 2h hold was introduced in period 9 and the result suggests that the SCC CGR component is approx. $1.5\ 10^{-11}$ m/s. The decrease in crack length observed at approx. 2350h suggests the formation of a flake; such a behavior was observed previously in tests involving welds. The hold was decreased to 1h in period 10, and the measured rate stayed largely unchanged (rather than doubling), suggesting that fatigue is not the major contributor to the observed rates. In period 11, the loading was changed to constant load with periodic unloading (2h hold) and the crack advance seemed to continue at the same rate, however, the crack did not overcome the previous high value for crack advance set previously at approx. 2350h, and illustrated with a horizontal red dotted line in Figure 35d. While the flake was finally overcome in period 13 by gentle cyclic, the behavior observed in periods 9-12 is atypical of fatigue growth.

The same holds true for the rather irregular growth observed in period 13. Hence, a 2h hold was introduced in period 14, and the resulting initial CGR (2.5 10^{-11} m/s) suggests that this crack was finally engaged. The un-provoked jump observed at 3280h suggests that possible additional ligament(s) may have broken, but this development only substantiates the previous inference. The rate measured after 3300h is 6.5 10^{-11} m/s. It is interesting to note that this rate can be extended all the way to the beginning of test period 14, Figure 35e. Since the mechanical component in period 14 is 5.0 10^{-12} m/s, approximately one order of magnitude less than the measured rate, it implies that most of the growth in this condition is SCC. The fact the SCC CGR measured in period 14 continues to decrease (Figure 35e) is also suggestive of SCC growth rather than fatigue growth, with the decrease attributable to crack branching and formation of ligaments. Nevertheless, the sustained growth suggests that the period of unload is appropriate for the measured rate and loading conditions. In summary, there appears that a SCC CGR of approx. 5 10^{-11} m/s was finally obtained in this specimen; the next challenge was to measure it given that this weld has proven particularly prone to formation of ligaments and flaking. To substantiate the previous observation, the specimen was set at constant load, period 15. Under this condition growth was maintained at a similar rate for approx. 32 μm, confirming that the growth observed in period 14 and the resulting SCC CGR were indeed due to SCC. In addition, both data points resulting from test periods 14 and 15 are in very good agreement with SCC CGR data obtained in previous tests on this Alloy 152 heat.

After the 32 μm of growth measured in test period 15, the rate appears to diminish, suggesting that a new ligament was formed, and began to affect (underestimate) the DC potential measurement. Cyclic with R= 0.5 (600/12) was reintroduced in period 16 in an effort to break this ligament. After lingering for approx. 24 h (another indication of a ligament/flake effect), some growth was detected and loading was changed to constant load with periodic unloading. The resulting rate was negligible, suggesting that the previous period did not break the ligament. Cyclic with R= 0.5 (600/12) was reintroduced in period 18, and constant load with periodic unloading (2h) in period 19. As the measured rate begins to diminish, the hold is decreased to 1h with no effect in period 20. Cyclic with R= 0.5 (600/12) was reintroduced in period 21, and then directly to constant load in period 22. Period 22 was ended after approx. 1500h by a 3h laboratory-wide power outage. Nevertheless, the crack advance in period 22 was approx. 100 μm, and the average SCC CGR was 2.0 10^{-11} m/s, consistent with previous measurements. After the pressure and temperature were restored, loading was changed to cycle+hold (period 23), and the resulting SCC CGR component was calculated by superposition to be approx. 1.7 10^{-11} m/s. This rate was consistent with that observed previously under constant load in test period 14. The sample was set at constant load one more time at this stress intensity factor, and the initial rate seemed to confirm the prior observations.

Next, the crack was advanced in fatigue in test periods 25-29 and re-transitioning to SCC at K ≈ 45 MPa $m^{1/2}$ was initiated. The known fatigue behavior was reproduced, and an initial loading condition at R=0.7 (1000/12) was chosen for re-transitioning. This condition is equivalent to the earlier R= 0.5 (600/12) condition, and allows for maintaining the same ΔK. As such, it was expected that the environmental enhancement to also be maintained. A 2h hold was introduced, followed by constant load with periodic unloading. The resulting rates was smaller than expected suggesting that the crack has not transitioned to IG SCC. As the testing time allotted to this test was coming to an end, one final attempt was made at R = 0.3 (9500/12) in test period 33. This condition was chosen because it was successful in a previous test on Alloy 152. As with the previous test, period 33 was followed directly by constant load. The initial CGR measured in period 34, Figure 35n, was relatively high (5.0 10^{-11} m/s), then appeared to diminish. At this stage it was decided to stop the test. A final fatigue test period was completed

in test period 34, and the fatigue response was consistent with that measured previously in test 27 and 30. Next, the test was stopped and the fracture surface was examined.

Table 12 Crack growth data for Alloy 152 specimen N152-TS-1 in PWR water[a].

Test Period	Test Time, h	Temp. °C	Load Ratio R	Rise Time, s	Down Time, s	Hold Time, s	K_{max}, MPa·m$^{1/2}$	ΔK, MPa·m$^{1/2}$	CGR_{env}, m/s	Estimated CGR_{air}, m/s	Crack Length, mm
Pre a	127	320.9	0.3	0.5	0.5		18.8	13.2	3.49E-08	4.06E-08	12.702
Pre b	144	320.0	0.3	50	50		18.8	13.2	1.15E-09	4.04E-10	12.732
Pre c	150	321.5	0.3	0.5	0.5		19.4	13.5	4.13E-08	4.59E-08	13.200
Pre d	215	320.0	0.3	100	100		19.4	13.6	5.07E-10	2.27E-10	13.262
Pre e	222	321.6	0.3	0.5	0.5		19.9	13.9	3.99E-08	5.15E-08	13.719
Pre f	239	320.9	0.3	50	50		19.9	13.9	1.10E-09	5.11E-10	13.770
Pre g	243	321.0	0.3	1	1		20.0	14.0	2.84E-08	2.62E-08	13.916
Pre h	263	320.9	0.3	50	50		20.1	14.1	1.18E-09	5.31E-10	13.979
Pre i	271	320.7	0.3	0.5	0.5		20.8	14.6	5.14E-08	6.12E-08	14.673
Pre j	288	320.1	0.3	50	50		20.9	14.6	1.41E-09	6.15E-10	14.731
Pre k	295	320.4	0.3	5	5		21.0	14.7	7.70E-09	6.33E-09	14.838
Pre l	312	319.9	0.3	50	50		20.9	14.6	1.39E-09	6.19E-10	14.885
Pre m	319	321.1	0.3	5	5		21.1	14.8	8.85E-09	6.56E-09	14.989
Pre n	386	320.4	0.3	100	100		21.1	14.8	8.22E-10	3.26E-10	15.036
Pre o	392	321.1	0.3	2	2		21.4	15.0	1.46E-08	1.72E-08	15.251
Pre p	407	320.6	0.3	50	50		21.4	15.0	1.35E-09	6.91E-10	15.291
Pre q	416	320.3	0.3	2	2		21.8	15.3	1.97E-08	1.84E-08	15.615
Pre r	457	320.3	0.3	50	50		22.0	15.4	1.72E-08	7.64E-10	15.746
1	551	320.7	0.48	300	12		26.1	13.6	3.20E-10	1.23E-10	15.858
2	648	320.6	0.48	600	12		26.1	13.6	1.60E-10	6.18E-11	15.910
3	989	320.1	0.48	1000	12		26.3	13.7	9.32E-11	3.78E-11	16.030
4	1,081	319.9	1				26.3	0.0	negligible		16.030
5	1,122	319.6	0.48	1000	12		26.3	13.7	8.00E-11	3.77E-11	16.037
6	1,193	319.0	0.48	1000	12		26.5	13.8	1.12E-10	3.83E-11	16.076
7	1,720	319.4	1	12	12	7200	26.5	13.8	4.72E-12	-	16.089
8	2,105	320.1	0.48	600	12		26.6	13.8	1.45E-10	6.64E-11	16.260
9	2,365	320.2	0.49	600	12	7,200	26.7	13.6	1.54E-11	4.91E-12	16.278
10	2,520	320.2	0.49	600	12	3,600	26.7	13.6	1.29E-11	9.11E-12	16.273
11	2,730	320.0	1	12	12	7200	26.7	13.6	4.08E-12		16.279
12	2,859	320.0	1	12	12	3600	26.7	13.6	2.61E-12		16.276
13	3,130	320.7	0.49	600	12		26.8	13.7	1.23E-10	6.54E-11	16.396
14	3,697	320.7	0.49	600	12	7200	27.0	13.8	5.24E-11	5.17E-12	16.530
15	3,889	321.2	1	0	0		27.1	0.0	4.30E-11	-	16.562
16	3,961	320.8	0.49	600	12		27.1	13.8	1.62E-10	6.86E-11	16.572
17	4,034	320.8	1	12	12	7200	27.1	13.8	negligible	5.70E-12	16.571
18	4,239	321.0	0.49	600	12		27.3	13.9	1.66E-10	7.08E-11	16.694
19	4,399	320.8	1	12	12	7200	27.3	13.9	1.42E-11	5.89E-12	16.705
20	4,427	320.7	1	12	12	3600	27.3	13.9	negligible	1.18E-11	16.706
21	4,519	321.0	0.49	600	12		27.4	14.0	1.22E-10	7.18E-11	16.737
22	5,910	320.7	1				27.5	0.0	1.88E-11	-	16.837
23	6,417	319.3	0.49	600	12	7200	28.2	14.1	2.47E-11	5.78E-12	16.837
24	6,894	319.4	1	0	0		28.3	0.0	5.40E-12		16.895
25	6,902	319.4	0.3	1	1		30.8	21.5	1.27E-07	1.50E-07	16.907
26	6,916	318.4	0.3	50	50		31.2	21.8	6.17E-09	3.11E-09	18.530
27	6,927	319.2	0.3	1	1		37.5	26.3	2.19E-07	3.36E-07	18.774
28	6,941	318.2	0.3	50	50		38.3	26.8	1.24E-08	7.27E-09	22.322
29	6,946	319.3	0.3	1	1		43.5	30.4	2.67E-07	6.16E-07	22.703
30	7,264	318.4	0.7	1000	12		45.9	13.8	1.73E-10	8.28E-11	24.901
31	7,695	318.0	0.7	1000	12	7200	45.9	13.8	1.78E-11	1.01E-11	25.399
32	8,108	318.1	0.7	12	12	7200	46.0	13.8	1.50E-11	1.16E-11	25.438
33	8,287	319.0	0.3	9500	12		46.2	32.3	1.40E-11	8.29E-11	25.498
34	8,621	318.2	1	0	0		46.3	0.0	2.54E-11	-	25.532
35	8,622	318.3	0.3	1	1		47.8	33.5	3.04E-07	8.99E-07	26.054

[a]Simulated PWR water with 2 ppm Li, 1100 ppm B, and 2 ppm. DO<10 ppb. Conductivity was 21±3 μS/cm, and pH 6.4.

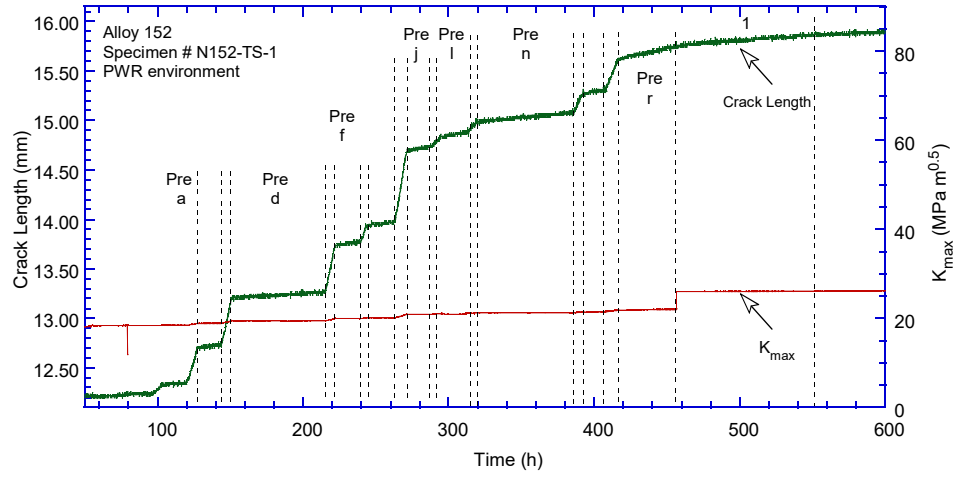

(a)

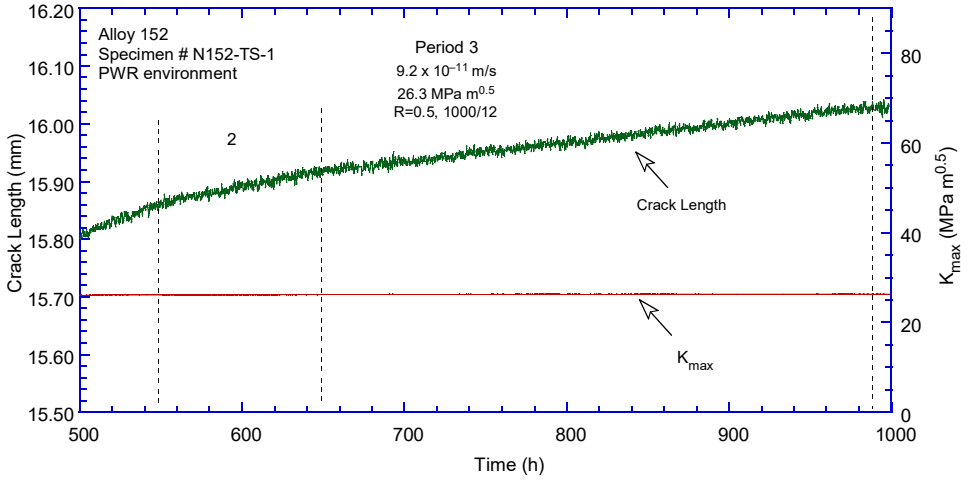

(b)

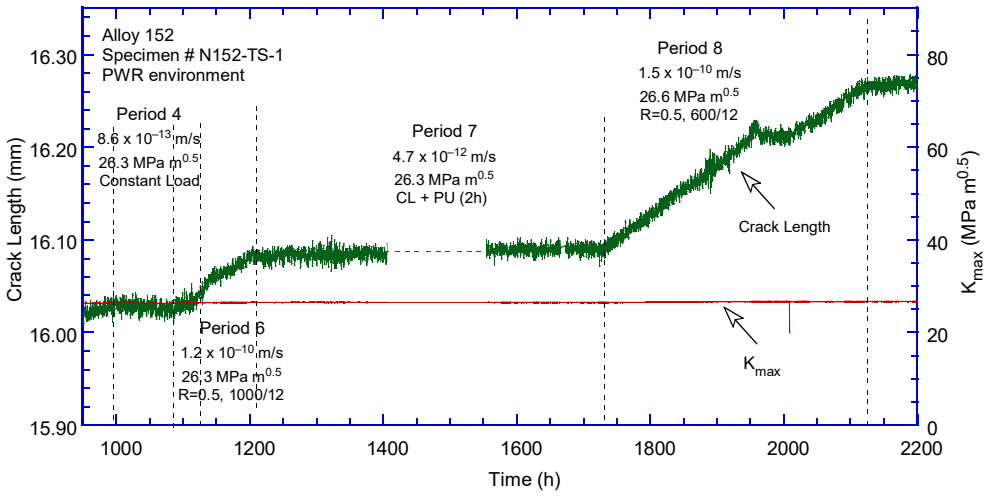

(c)

Figure 35 Crack–length–vs.–time for Alloy 152 specimen N152-TS-1 in simulated PWR environment during test periods (a) precracking-1, (b) 2-3, (c) 4-8, (d) 9-13, (e) 14, (f) 15-16, (g) 17-20, (h) 21-22, (i) 23-24, (j) 25-29, (k) 30, and (l) 31.

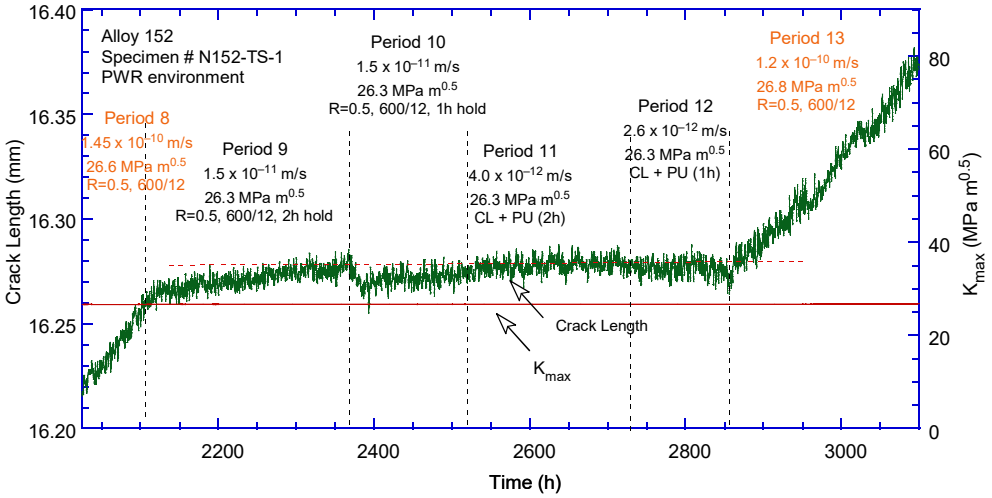

(d)

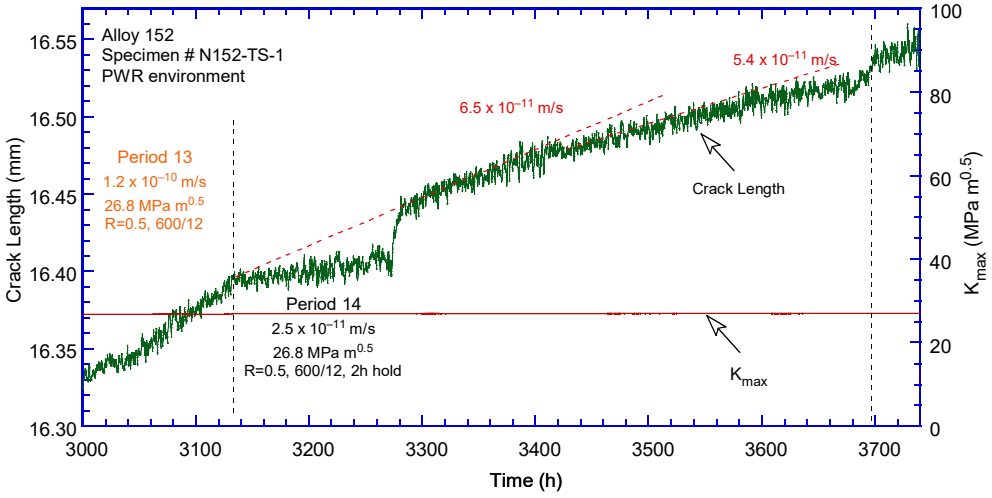

(e)

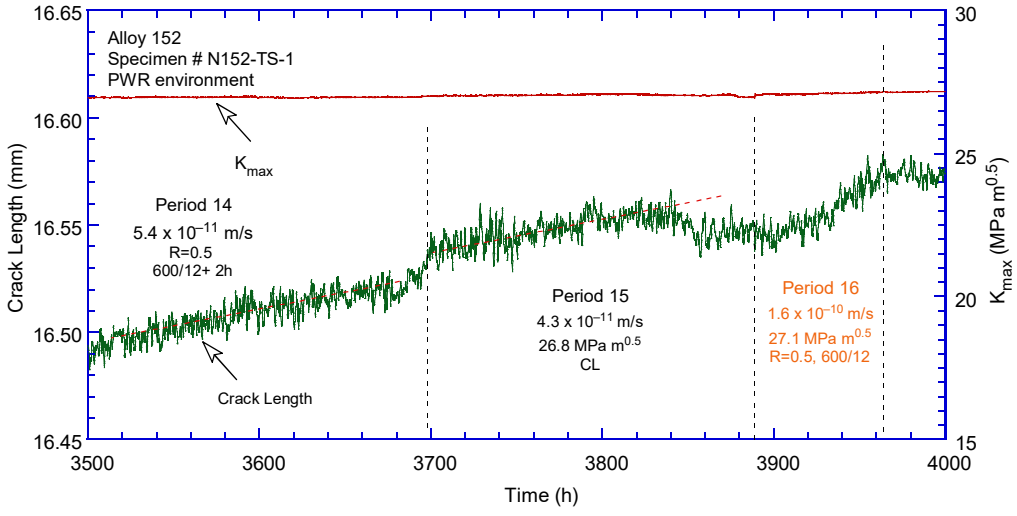

(f)

Figure 35 (cont.)

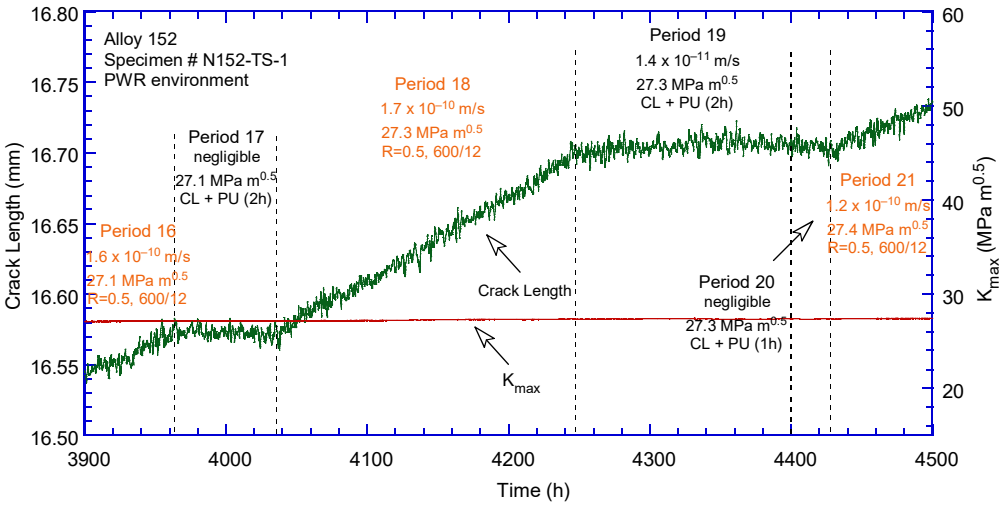

(g)

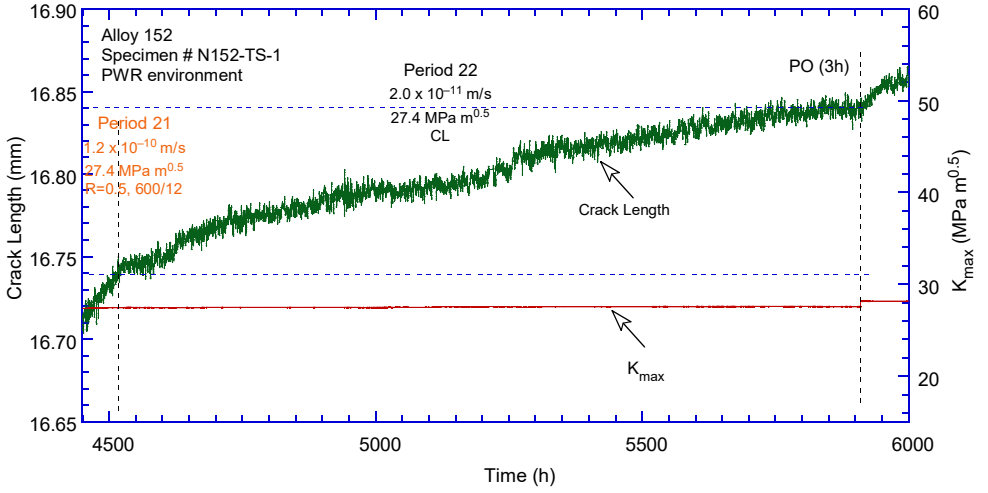

(h)

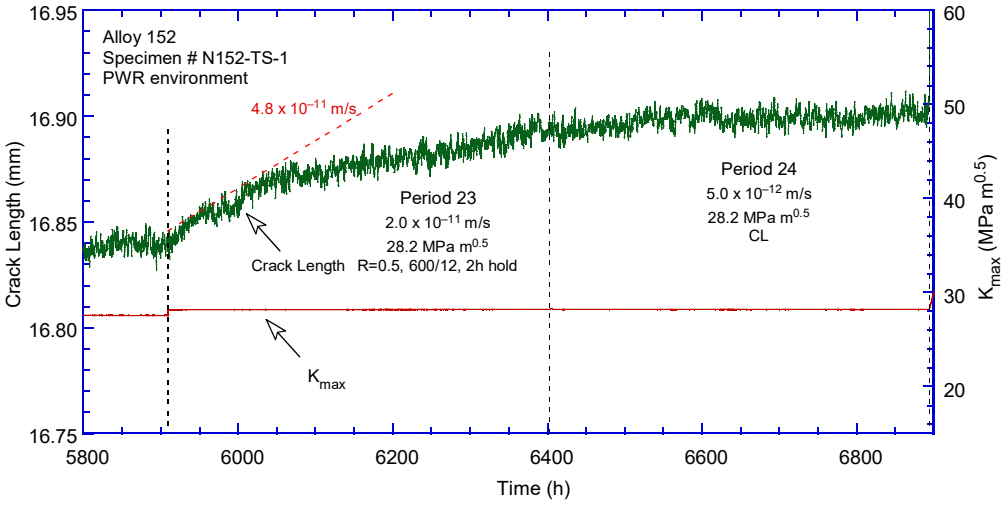

(i)

Figure 35 (cont.)

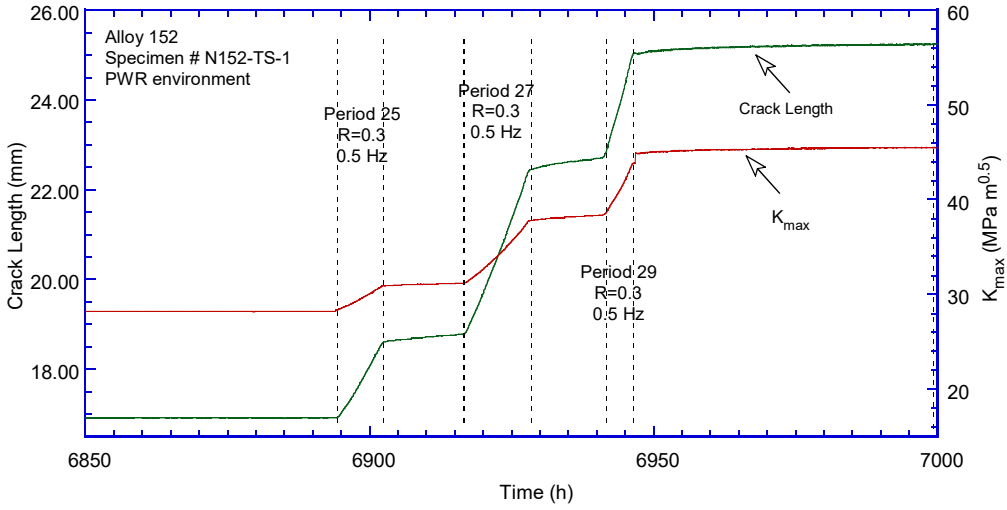

(j)

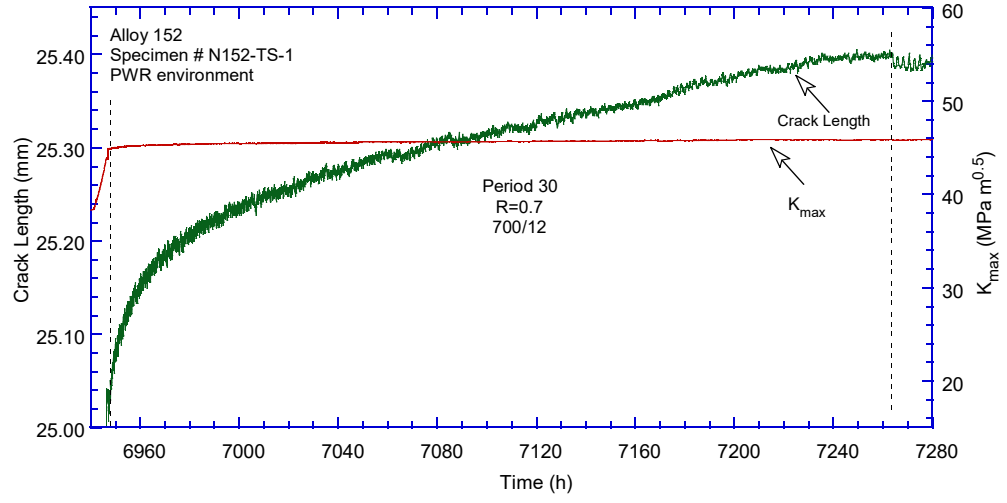

(k)

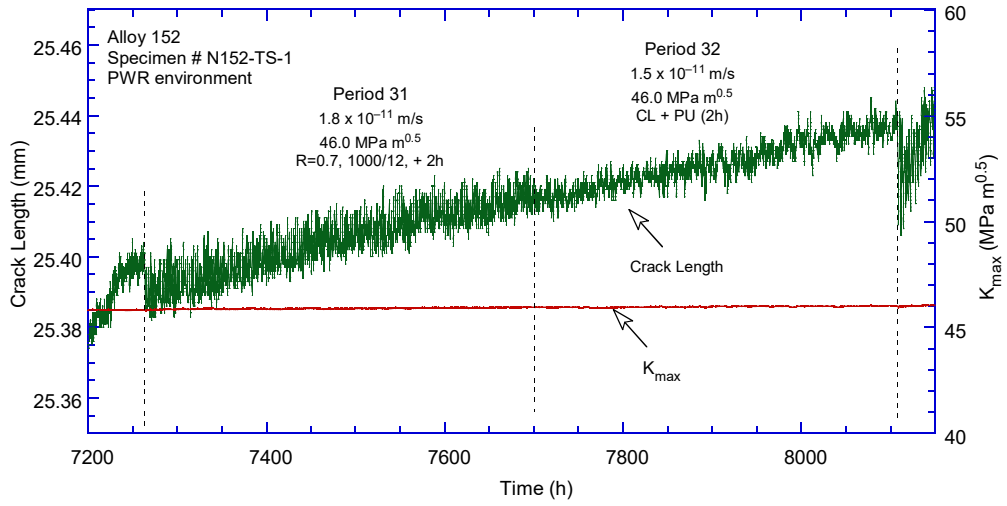

(l)

Figure 35 (cont.)

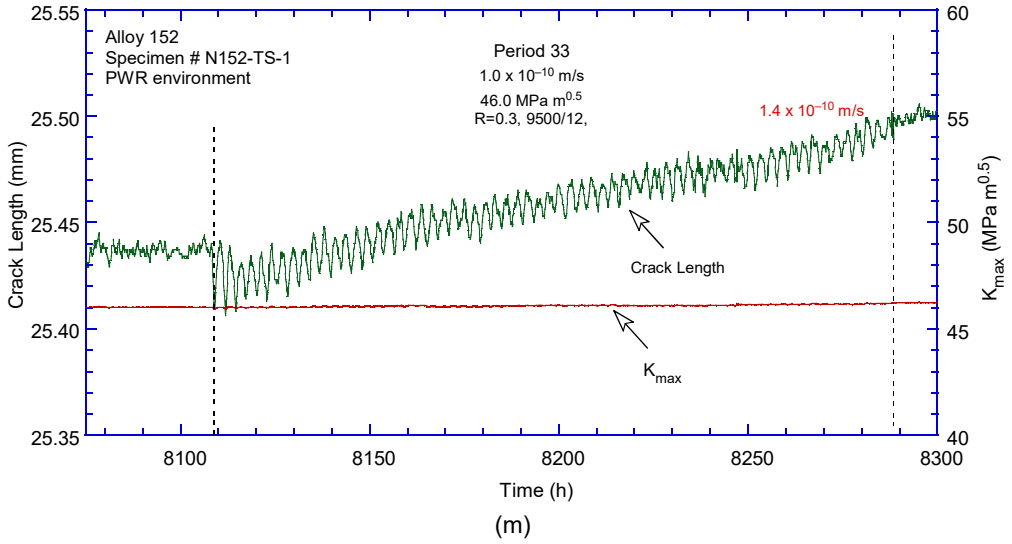

(m)

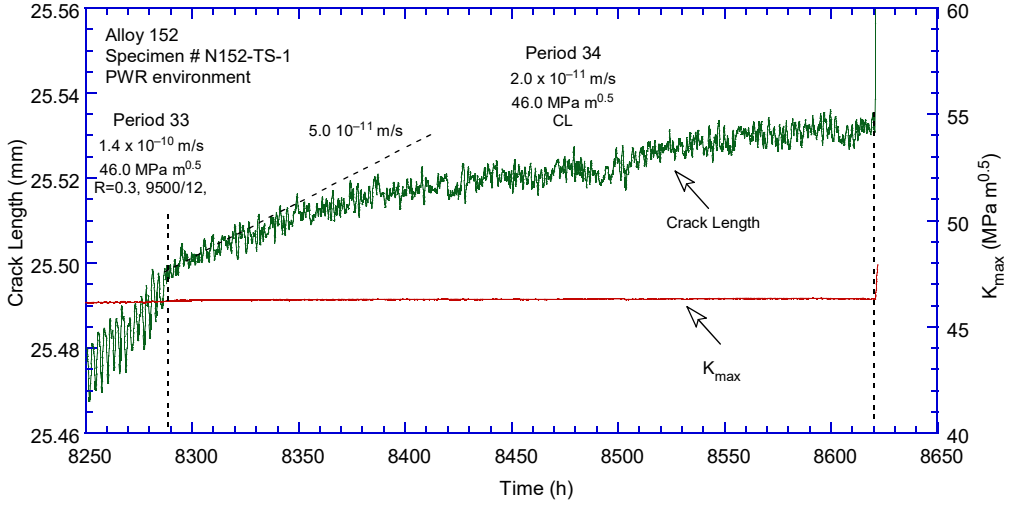

(n)

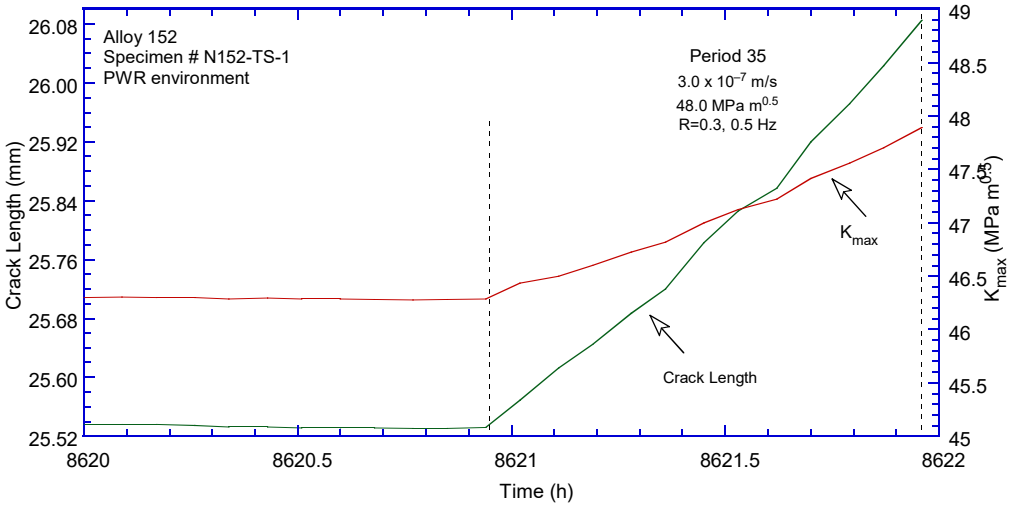

(o)

Figure 35 (cont.)

Figure 36 presents and discusses the cyclic CGR data obtained on specimen N152-TS-1. Figure 41a includes only the data obtained by the current specimen as well as the corrosion fatigue curve for Alloy 182. The Alloy 152 data is slightly below the Alloy 182 corrosion fatigue curve. The figure also indicates the preferred transitioning condition in the first part of the test, R= 0.5 (600/12), and it is important to note that this condition was reproduced multiple times during the first part of the test. Figure 41b compares the current Alloy 152 data with those obtained previously from three tests on Alloy 152 A152 series (double-J weld of the same heat) described in the previous section. These data sets are in excellent agreement. Next, as described previously, in the second part of the test on this specimen, the crack was advanced in fatigue in test periods 25-29 and re-transitioned to SCC at $K \approx 45$ MPa $m^{1/2}$. Again, it is important to note that the known fatigue behavior was reproduced, Figure 41c. CGR response during cycling at R = 0.7 - equivalent to the earlier R = 0.5 (600/12) - seemed to maintain the environmental enhancement as long as the same ΔK was maintained. However, as described previously, the introduction of hold times caused the loss of the environmental enhancement. CGR response during cycling at R = 0.3 also seemed to maintain the environmental enhancement, and allowed for transitioning to constant load directly.

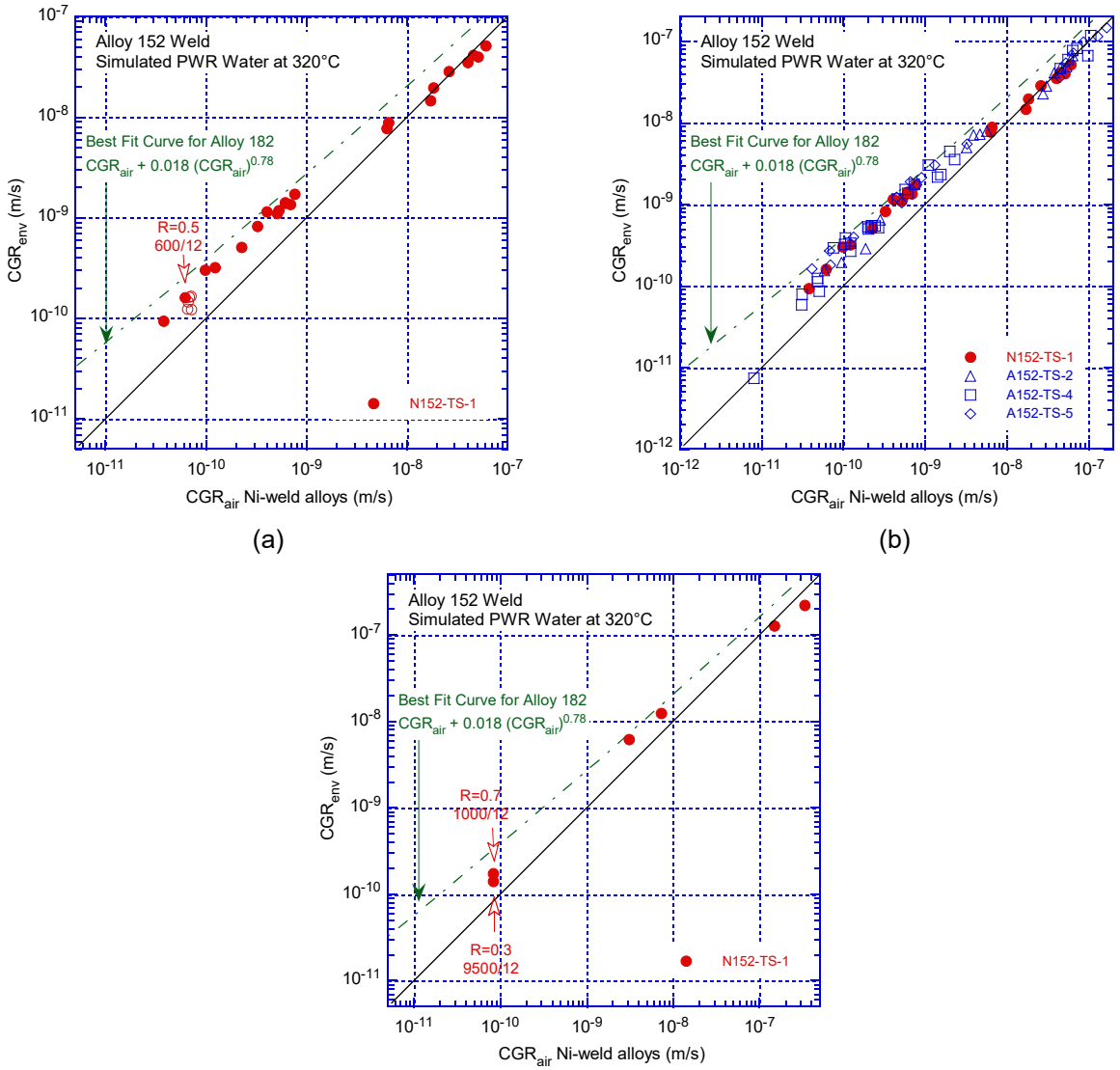

Figure 36 (a) Cyclic CGR data for Alloy 152 specimen N152-TS-1 in simulated PWR environment, (b) comparison with data obtained on the previous double-J weld (A152 series), and (c) second part of the test.

Figure 37 summarizes the SCC CGR data for Alloy 152 heat WC04F6. The data points resulting from the test on specimen N152-TS-1 appear to be in good agreement with the A152 data set. Data obtained at constant load are shown with solid symbols, while those obtained at constant load with periodic unloading or PPU are shown with open symbols. There seems to be a good agreement between that data obtained at CL and the data obtained from PPU conditions, especially for the data with the longer crack extensions. This data set meets the selection criteria of EPRI MRP-115, including the minimum IG-engagement, crack advance, and periodic unloading criteria, hence, it can be compared directly to the proposed disposition curve for Alloys 182/82.

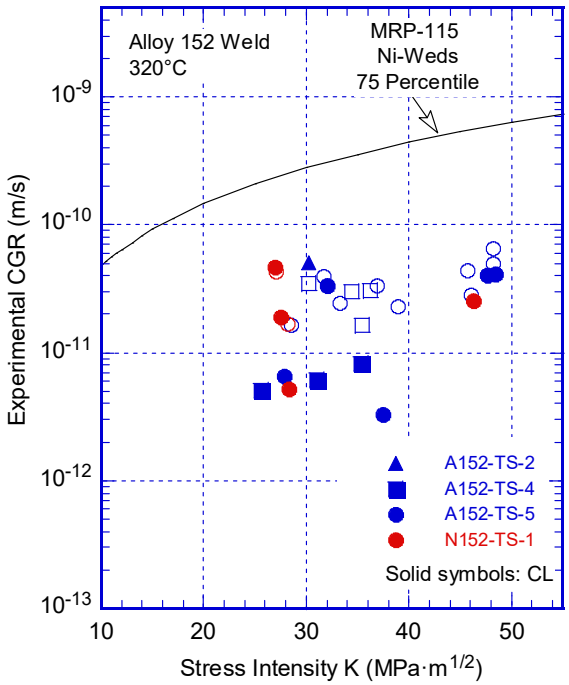

Figure 37 SCC CGR data for Alloy 152 heat WC04F6 in simulated PWR water.

Figure 38 shows the specimen N152-TS-1 after testing in simulated PWR environment, and broken apart in two pieces to expose the fracture surface. A piece containing the fracture surface – right half in the picture - was removed for examination.

Figure 38 Alloy 152 specimen N152-TS-1 after testing in simulated PWR environment. The fracture surface from one side was removed for further examination in the SEM.

The entire fracture surface of specimen N152-TS-1 is shown in Figure 39. The image indicates that the testing procedure resulted in a straight, uniform fracture surface. Measurements made on this image are in an excellent agreement (6%) with the DC potential measurements, hence no correction was performed. The milestones of this test are indicated in the figure: the specimen was fatigue precracked and transitioned in the PWR environment (notch through left yellow arrow), then the first set of SCC CGR measurements at moderate stress intensity factors were obtained in region marked IG-1 (red arrow). The specimen was next fatigued starting at the black arrow for approx. 8.5 mm, then transitioned again at the higher stress intensity factor (region marked IG-2, second red arrow).

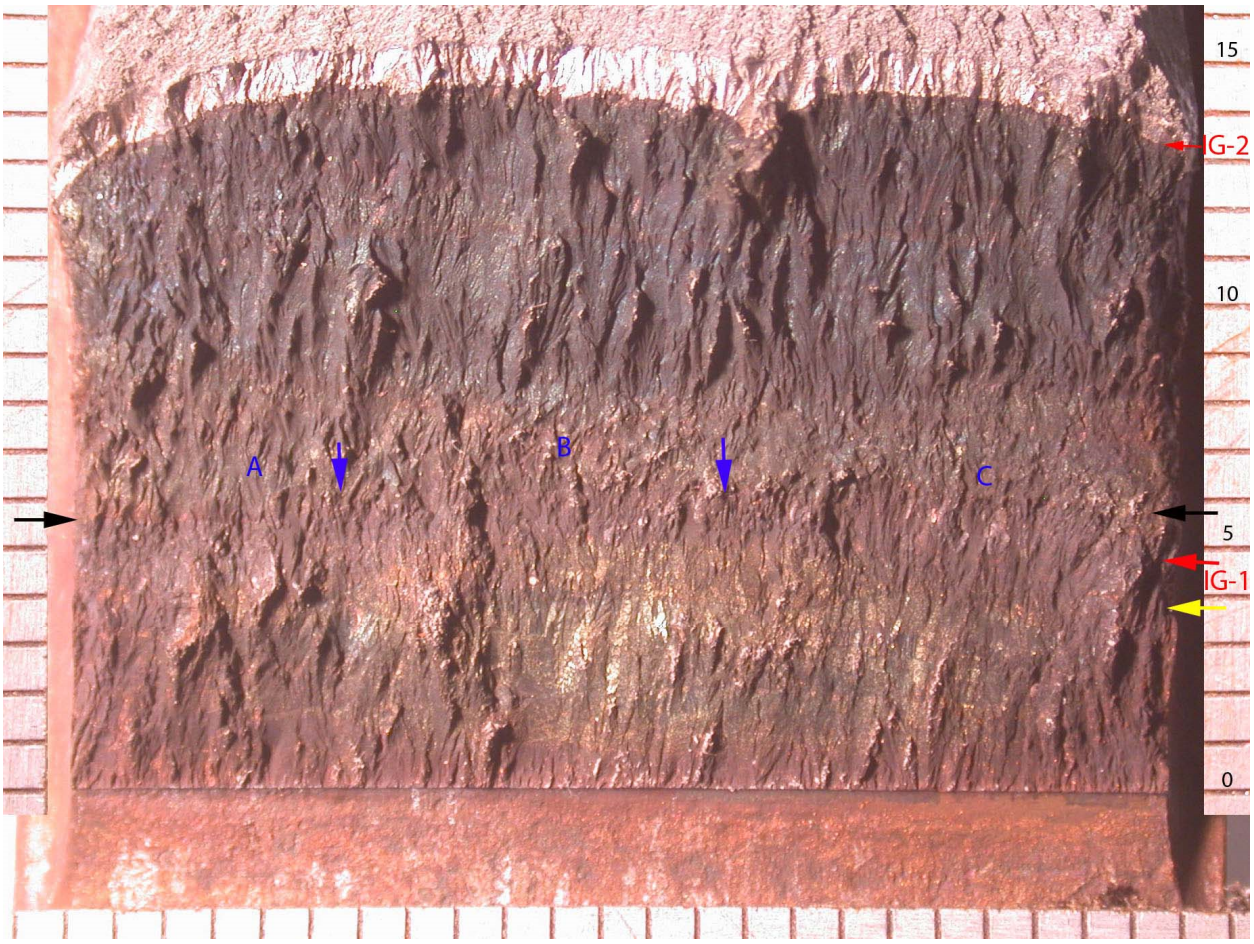

Figure 39 Fracture surface of specimen N152-TS-1. The milestones of this test are indicated in the figure. Crack advance is from bottom to top.

The IG-1 region shown in Figure 39 in was further divided into three regions, A, B, and C, and these were examined in additional detail by SEM and will be presented next.

Region A is shown in Figure 40, and represents 25% of the total width of the specimen. The IG engagement is substantial (69%), but the appearance of the crack front is irregular. Occasionally crack propagation is as long as 1 mm. Few secondary IG cracks were observed.

Region B is shown in Figure 41, and represents 34% of the total width of the specimen. The IG engagement is relatively low (46%), and the appearance of the crack front is again irregular.

The two examples of secondary cracks in a mixed IG and TG crack front shown in Figure 41b (taken at location 1 in Figure 41a) seem to suggest that the preferred IG/interdendritic cracking direction does not coincide with the main propagation front. By contrast, Figure 41c (taken at location 2 in Figure 41a) shows a predominant IG/interdendritic fracture mode.

Region C is shown in Figure 42, and represents 41% of the total width of the specimen. The IG engagement in this region is substantial (91%), and the appearance of the crack front is band-like. The band is 0.7-0.9 mm long, approximately twice the average growth measured by DC potential, suggesting that the average SCC CGR measured by the DC potential likely came from this region. This also suggests that IG propagation in this region was preferred over other modes. Figure 42b and Figure 42c show the IG/intergranular fracture mode at locations 1 and 2 in Figure 41a. Some secondary cracks are present, but the overall appearance suggests that even in this region the crack propagation is not in the most favorable direction, i.e., along the dendritic grains. The most susceptible region seems to be that at location 3 in Fig. Figure 42a, shown at higher magnification in Figure 43. The crack advance in this region was approx. 3.5 mm.

Overall, for region IG-1, the IG engagement was 70%, however, the differences between the various locations suggest that there is a SCC susceptibility difference along the specimen width. As described previously, it appears that the crack front encountered several microstructures with different dendrite orientations. Also, occasionally, out of plane cracking seems to be preferred over the direction of the main crack front, that is, the crack front is not oriented in the most SCC-susceptible orientation.

The IG-2 region was divided into two halves and both are shown in Figure 44. Additional details are provided in Figure 45 (locations 1 and 3 in Figure 44a) and Figure 46 (locations 1 and 4 in Figure 44b). Evidence of IG cracking is observed just before the last test period in fatigue. The overall IG engagement in the IG-2 region is low (40%), but otherwise remarkable considering that only four transitioning periods were used. Three of these test periods (30-32, Table 12) were at R = 0.7, with the last two showing essentially no environmental enhancement. As expected, there is no evidence of IG cracking during these test periods. The effect of the test period at R = 0.3 is unclear, however, its feasibility as a transitioning scheme appears to merit further investigation as this test was the second instance where an SCC crack grew at constant load directly from gentle cycling.

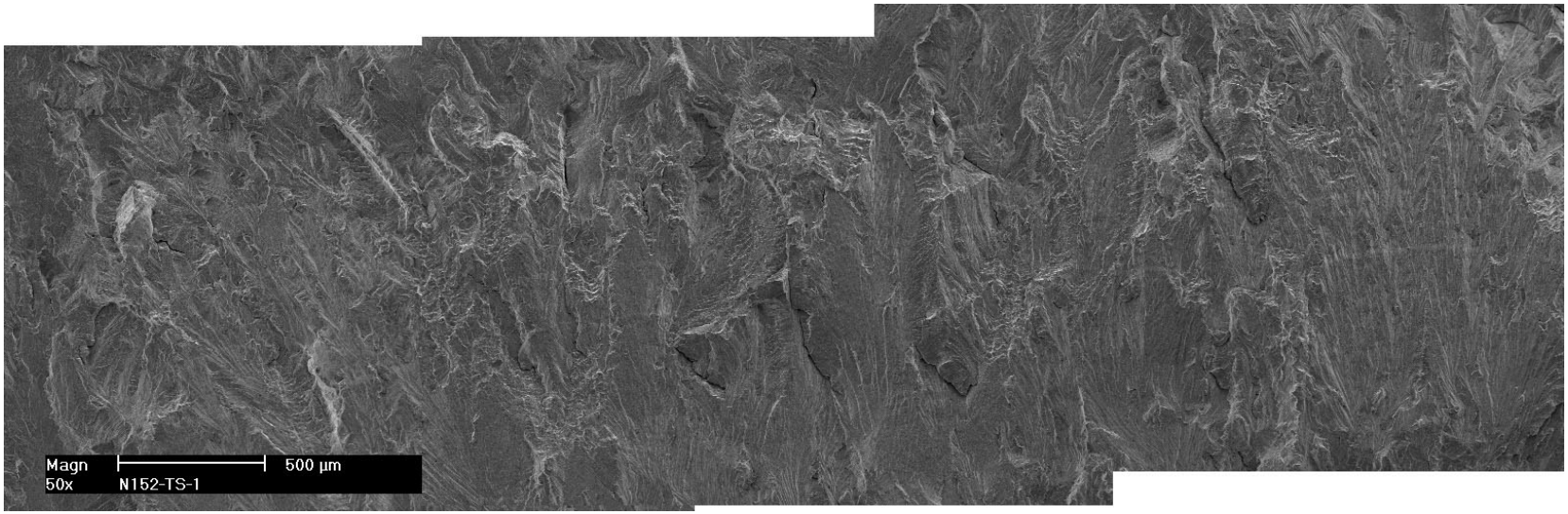

Figure 40 Specimen N152-TS-1, region A of fracture surface IG-1. Crack advance is from bottom to top.

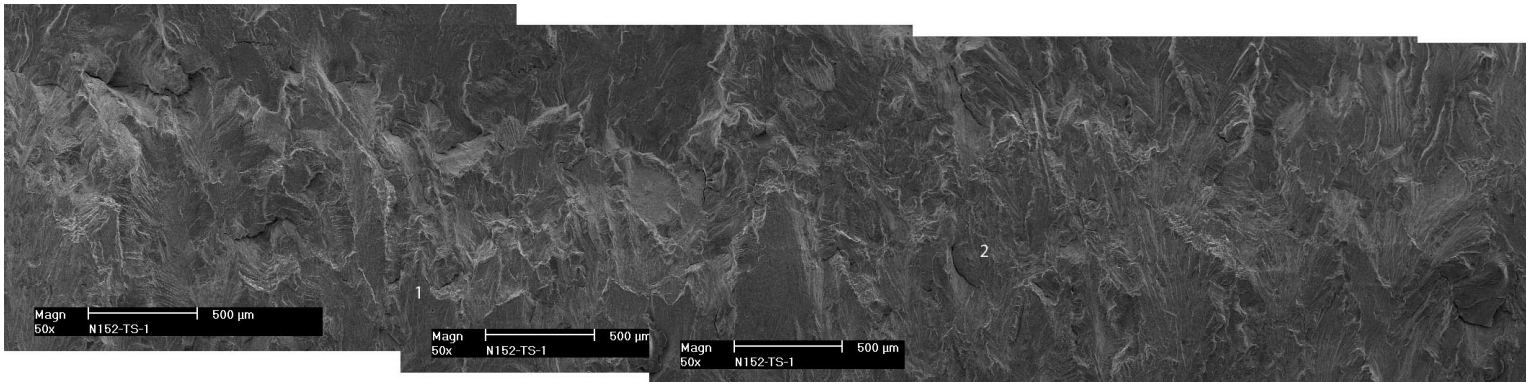

(a)

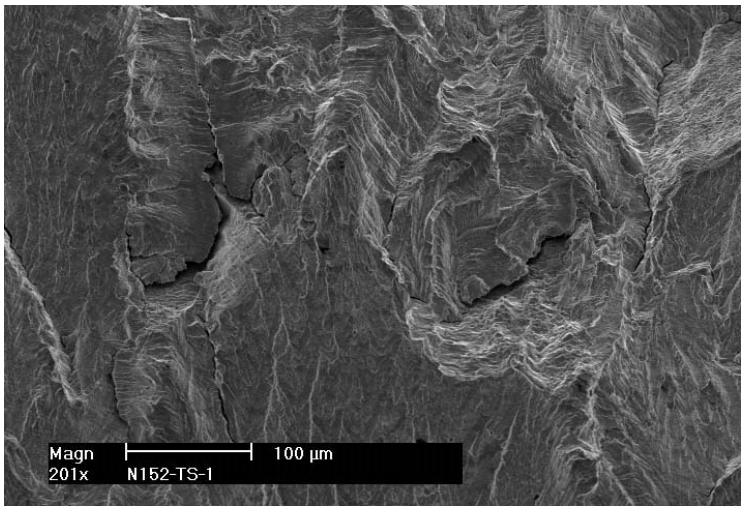

(b)

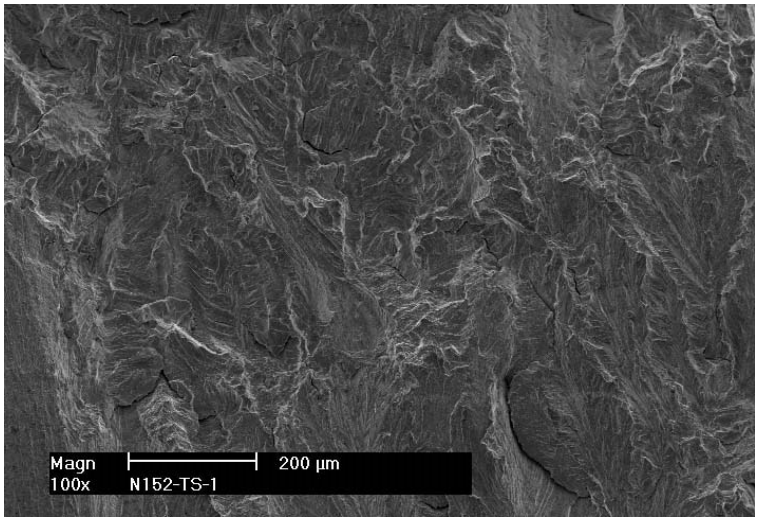

(c)

Figure 41 Specimen N152-TS-1: (a) region B of fracture surface IG-1, (b) detail at location 1, and (c) detail at location 2. Crack advance is from bottom to top.

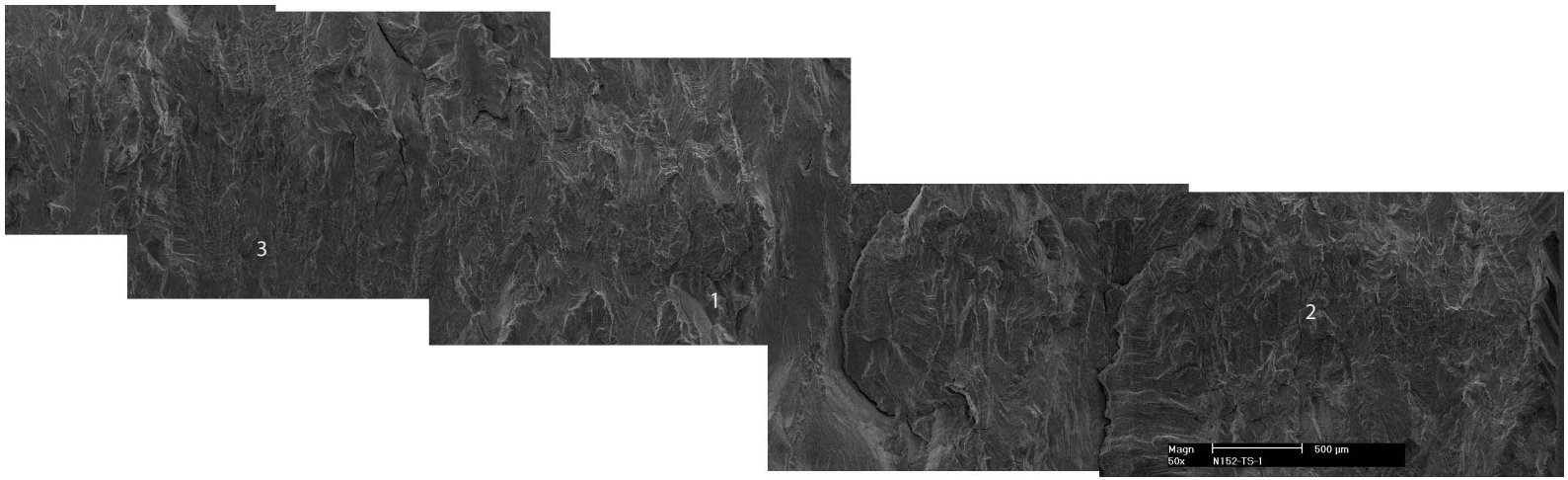

(a)

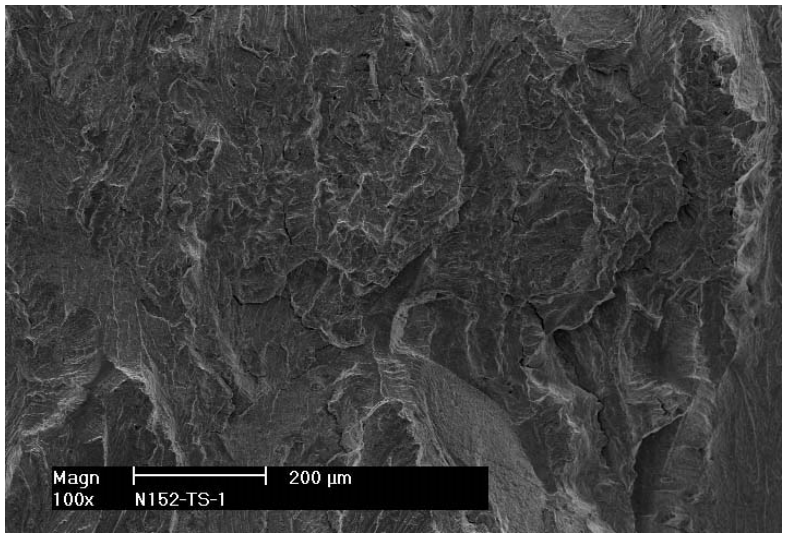

(b)

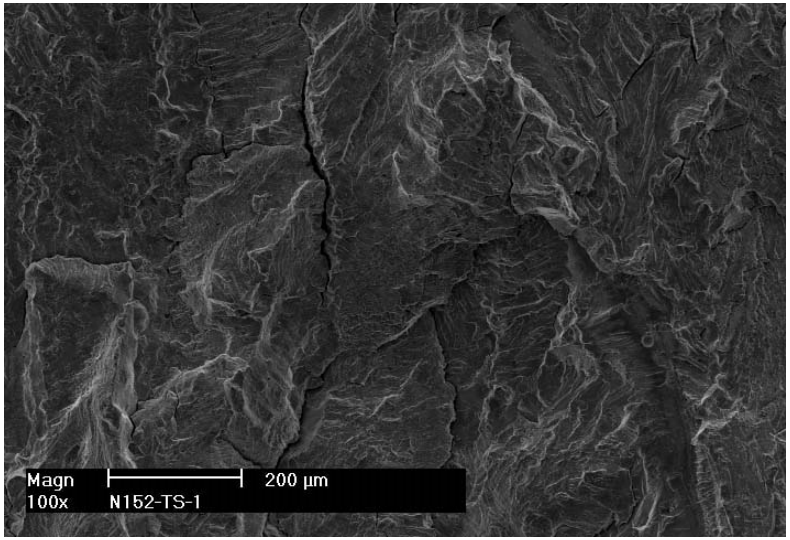

(c)

Figure 42 Specimen N152-TS-1: (a) region C of fracture surface IG-1, (b) detail at location 1, and (c) detail at location 2. Crack advance is from bottom to top.

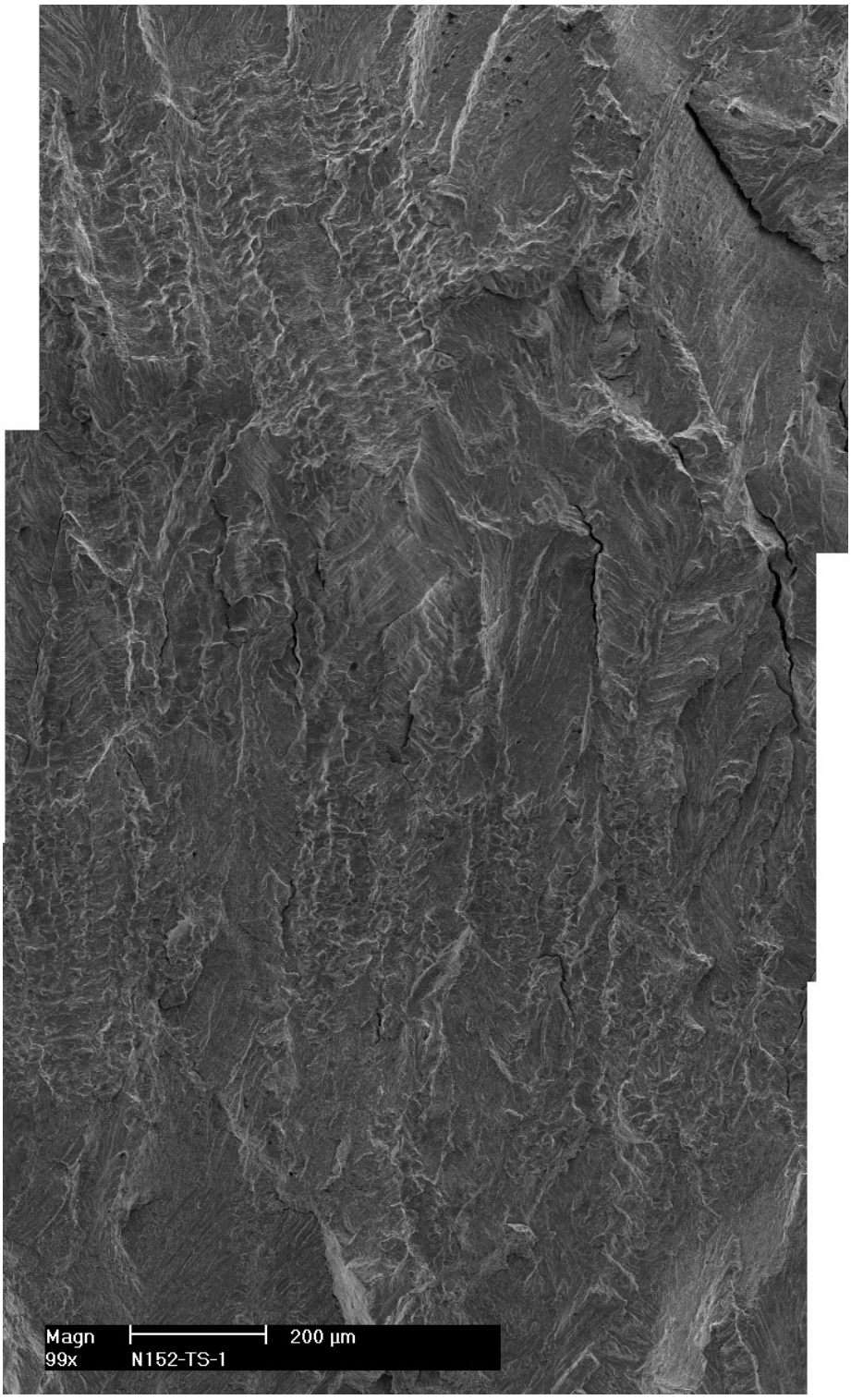

Figure 43 Specimen N152-TS-1, detail at location 3 in region C of fracture surface IG-1 (Figure 42a). Crack advance is from bottom to top.

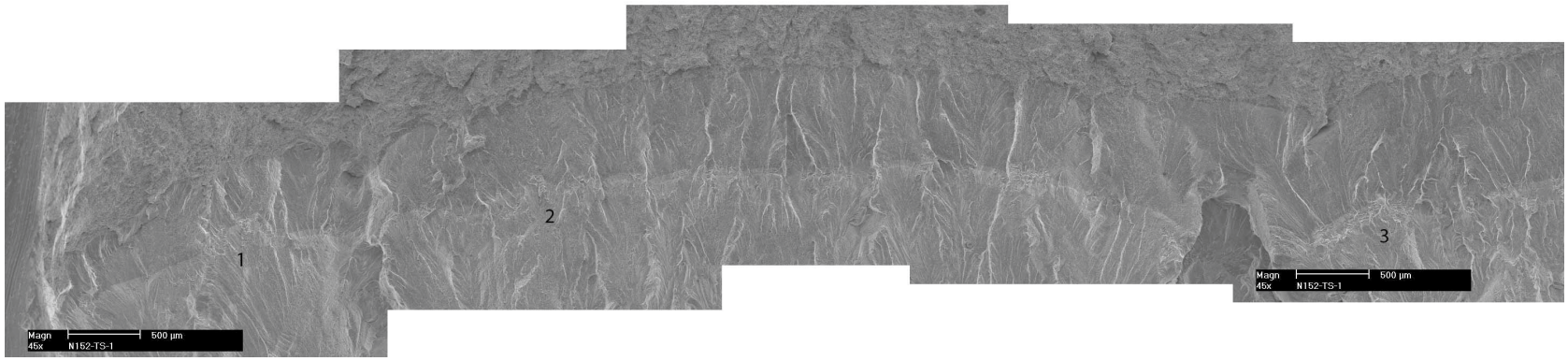

(a)

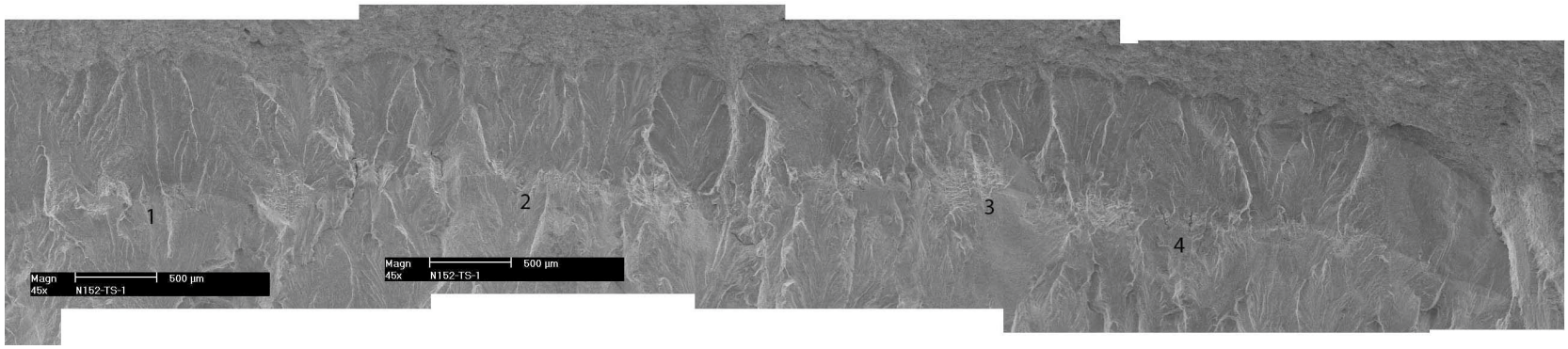

(b)

Figure 44 Specimen N152-TS-1: (a) first half of IG-2, and (b) first half of IG-2. Crack advance is from bottom to top.

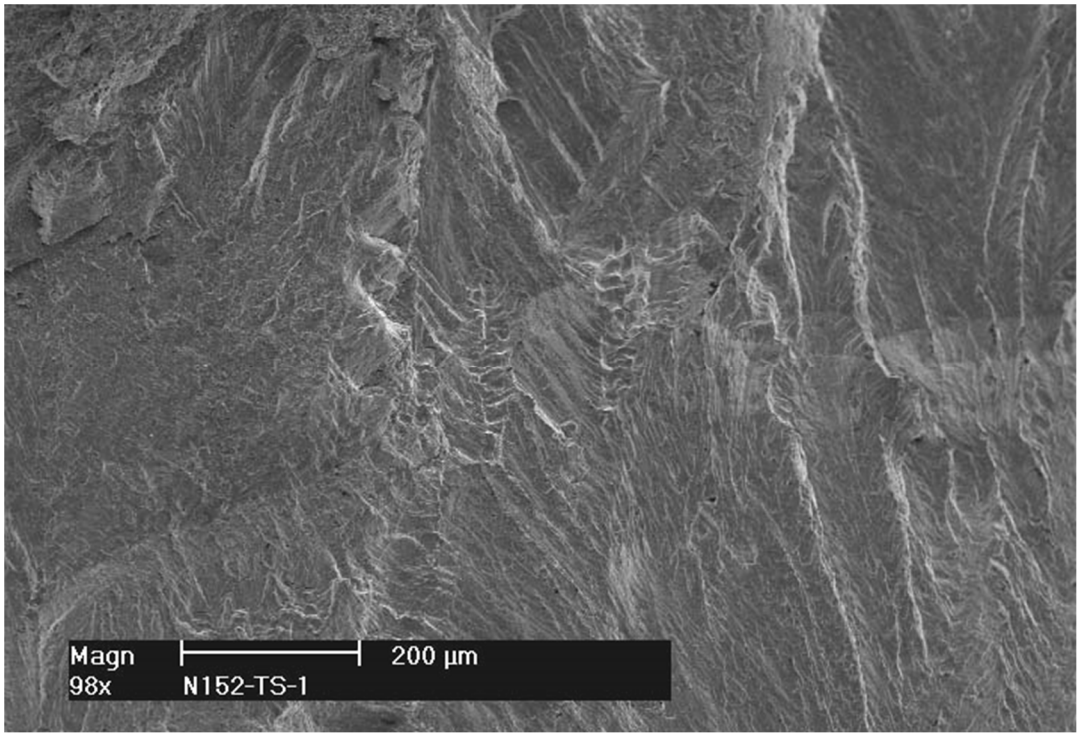

(a)

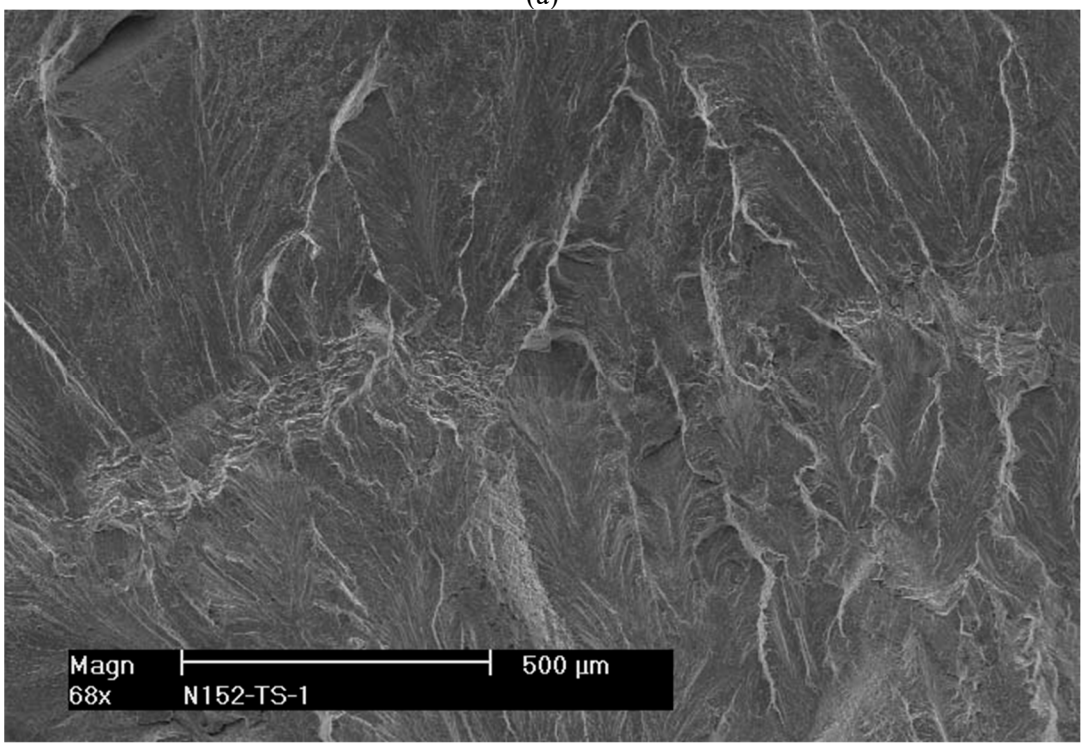

(b)

Figure 45 Fracture surface of specimen N152-TS-1: locations 1 and 3 in Fig. Figure 44a. Crack advance is from bottom to top.

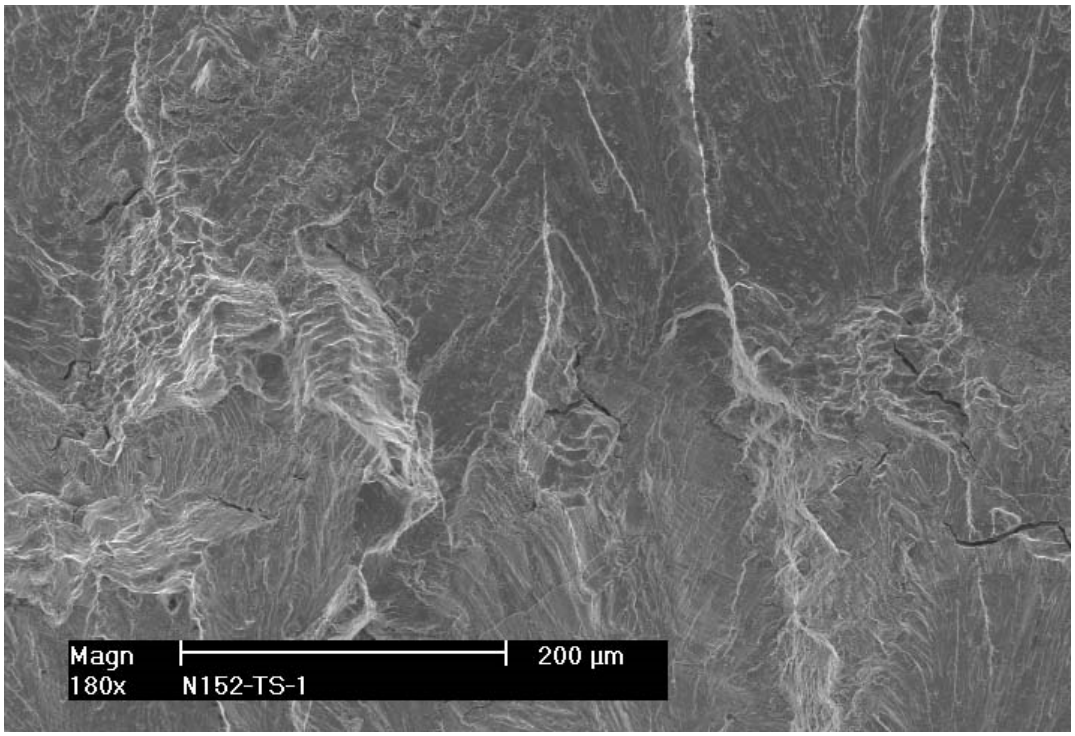

(a)

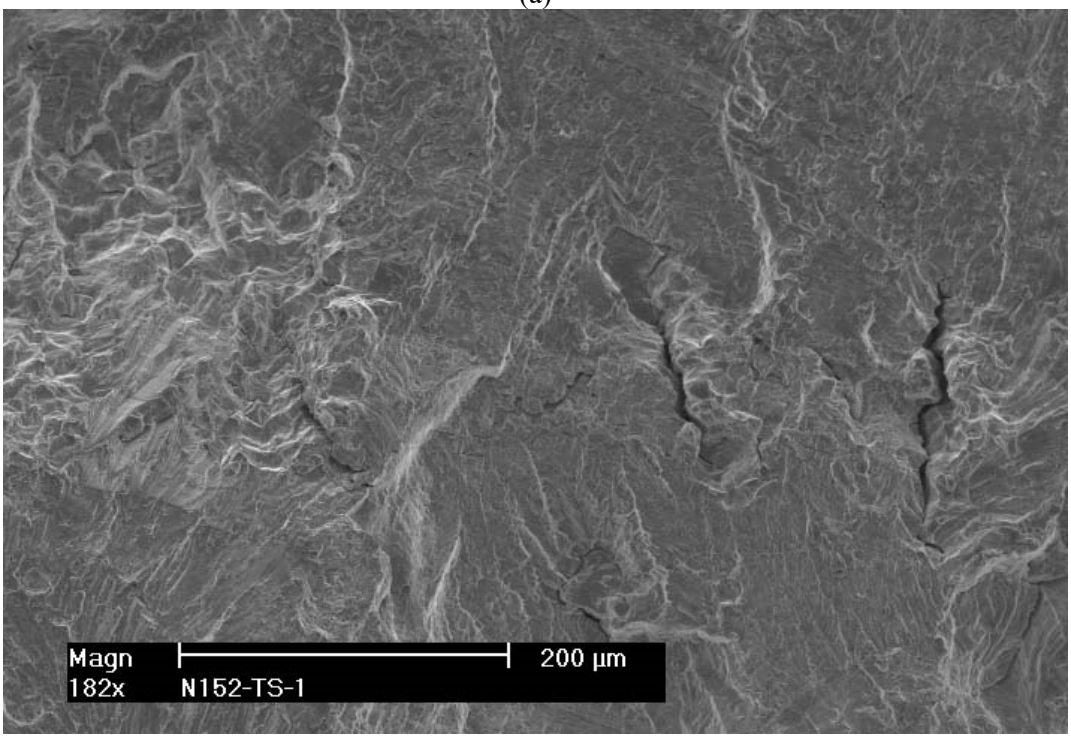

(b)

Figure 46 Fracture surface of specimen N152-TS-1: locations 1 and 4 in Fig. Figure 44b. Crack advance is from bottom to top.

The examination of the fracture surface of specimen N152-TS-1 revealed SCC susceptibility differences between the various locations on the specimen. Specifically, the crack front apparently encountered several microstructures with different dendrite orientations, occasionally

resulting in out of plane cracking along directions other than that of the main crack front. In order to assess the microstructure that was tested, the back of the piece containing the fracture surface was polished and etched. The fracture surface and the etched back are shown in Fig. Figure 47a. Several weld passes are visible on the polished/etched back as well as several grain orientations, most of which are not the elongated weld grains expected in the TS orientation. Indeed, Figure 47b shows that for specimen N152-TS-1 the plane of the crack was oriented at an angle with respect to the weld passes. That is, the testing plane was not oriented along the most SCC-susceptible direction, i.e., along the dendrites, but intersected them at an angle. Figure 47c – obtained from the back of the piece containing the fracture surface - shows such a microstructure, with the dendrites apparently intersecting the plane of the figure. This type of microstructure in the test plane likely explains the lack of the visible secondary cracks, and the apparently different preferred orientations for SCC cracking. Of particular interest at the time was the fracture mode normal to the dendritic microstructure, Figure 48. Later on, this type of fracture would turn out to be the preferred mode of IG SCC propagation in 1st layer weld butter and interface cracking in weldments.

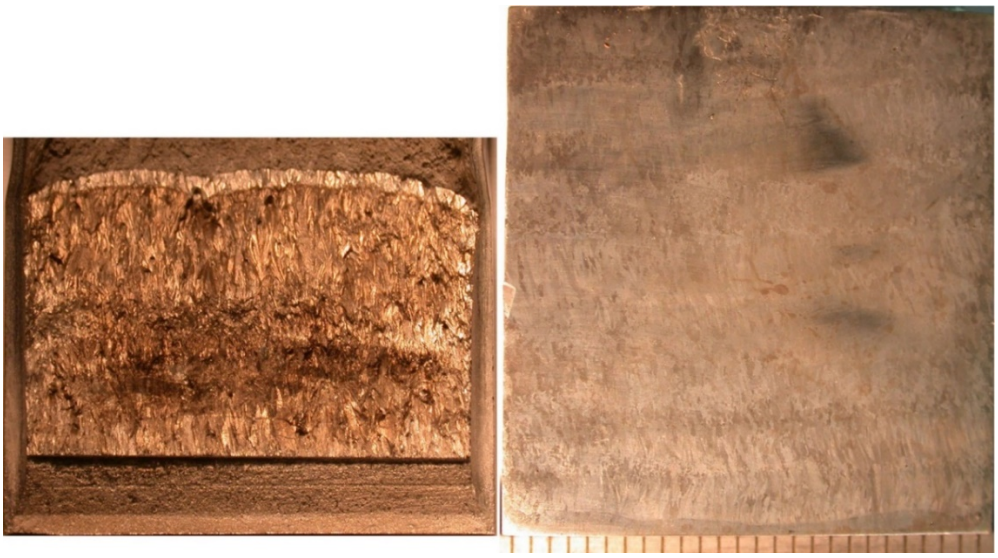

(a)

(b)

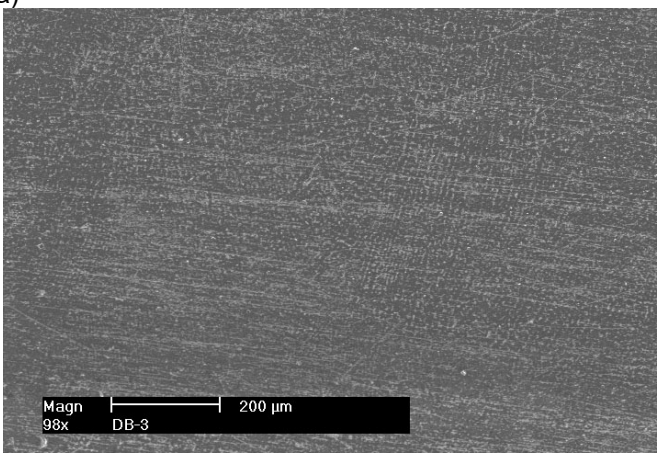

(c)

Figure 47 (a) Fracture surface of specimen N152-TS-1 and the microstructure of the test plane, (b) Specimen notch orientation vs. weld passes (and dendrites), and (c) dendrite microstructure in the test plane.

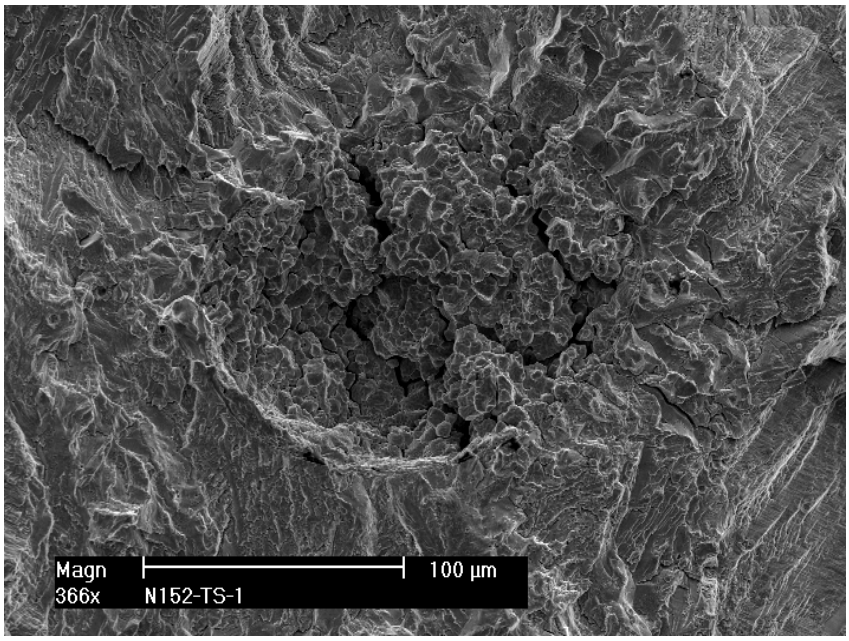

Figure 48 Fracture surface of specimen N152-TS-1: IG SCC propagation in a direction normal to the dendritic grain. Crack advance is from bottom to top.

3.2 SCC CGR Testing of Alloy 152 "Kewaunee" mock-up

The SCC CGR testing of the Alloy 152 "Kewaunee" mock-up prepared by MHI was conducted on two specimens as described in Section 2.3. The first was a 1T CT specimen, and the second was a 1/2T CT machined from one end of the first specimen. The weld wire heat code was 307380.

3.2.1 Specimen MHI152-TS-1

The testing conditions for specimen MHI152-TS-1 are given in Table 13, and the changes in crack length and K_{max} with time are shown in Figure 49. Precracking and transitioning of the test specimen were carried out in the in the PWR environment. Next, a 2h hold was introduced in test period 5 to evaluate the SCC component at this stage in the test. The result is consistent with previous measurements conducted at ANL under this loading condition. The specimen was next set at constant load in test period 6, but growth was negligible. Periodic unloading was reintroduced in test period 7 to reactivate the crack, and growth resumed after approx. 40h in this loading condition. The resulting rate in test period 7 appears consistent with previous ANL measurements conducted under similar conditions. The current test conditions were maintained until approx. 0.1 mm of growth was reached, and then the sample was set at constant load. No growth in test period 8 was followed by cycling in test period 9, then constant load in test period 10. Some growth was observed for the first 60 hours, however, the crack eventually appeared to stall. A new attempt at transitioning was made, and the known cyclic behavior was reproduced in test period 11. A 2h hold was introduced in period 12, and the response (2.6 10^{-11} m/s) suggested that the SCC component is in the low-10^{-12} m/s range; for a SCC component in the 10^{-11} m/s, a response of approx. 4.5 10^{-11} m/s would have been needed (see for example test period 14 for the previous specimen, Table 12). The subsequent test period 13 seems to confirm the low rate. Next, the test continued at higher stress intensity factor (45-50 MPa $m^{1/2}$). This was accomplished in test periods 14-16 by a combination of

increased loading and, in order to protect the pins by limiting the applied load to approx. 5500 lbs, an increased crack length. Next, transitioning steps were undertaken in test periods 17-21 at R=0.8, and an estimate of the SCC CGR component by superposition in test period 21 suggests that this is in the 2 10^{-11} m/s range. Hence, loading was changed to constant load. The SCC CGR in test period 22 (over approx. 600 h) measured very low. Constant load was attempted again in test period 24 and a low rate was measured. Next, transitioning at R=0.5 was undertaken, and this was followed by constant load in test period 27. Again, a low rate was measured; this was followed by transitioning at R=0.3 in test periods 28 and 29. While the environmental enhancement was low, there was little change following the introduction of the 2h hold in test period 29, again suggesting an SCC CGR component is active. Next, the specimen was set at constant load for the final test period (30). This loading condition was maintained for approx. 2,500 h, and the SCC CGR response was very small.

Table 13 Crack growth data for Alloy 152 weld specimen MHI152-TS-1 in PWR water[a].

Test Period	Test Time, h	Temp. °C	Load Ratio R	Rise Time, s	Down Time, s	Hold Time, s	K_{max}, MPa·$m^{1/2}$	ΔK, MPa·$m^{1/2}$	CGR_{env}, m/s	Estimated CGR_{air}, m/s	Crack Length, mm
Pre a	53	318.9	0.3	0.5	0.5		24.7	17.3	7.34E-08	1.20E-07	14.130
Pre b	71	318.9	0.3	50	50		24.8	17.4	1.87E-09	1.23E-09	14.240
Pre c	74	318.8	0.3	0.5	0.5		25.3	17.7	1.00E-07	1.34E-07	14.656
Pre d	78	318.8	0.3	1	1		26.1	18.2	6.47E-08	7.54E-08	15.187
Pre e	95	318.9	0.3	50	50		26.2	18.4	3.37E-09	1.55E-09	15.313
Pre f	100	318.8	0.3	1	1		27.0	18.9	8.27E-08	8.74E-08	15.873
Pre g	167	318.6	0.3	100	100		27.4	19.2	2.01E-09	9.24E-10	16.146
Pre h	174	318.9	0.3	1	1		29.6	20.8	1.22E-07	1.28E-07	17.647
Pre i	191	318.9	0.3	50	50		30.0	21.0	5.05E-09	2.69E-09	17.877
1	198	319.1	0.3	50	12		30.1	21.1	4.89E-09	2.74E-09	17.970
2	263	318.8	0.5	300	12		30.5	15.2	5.75E-10	2.06E-10	18.106
3	336	318.8	0.5	600	12		30.6	15.3	3.23E-10	1.05E-10	18.195
4	432	318.8	0.5	800	12		30.7	15.4	2.53E-10	7.97E-11	18.267
5	769	318.7	0.5	800	12	7,200	30.8	15.4	2.85E-11	8.04E-12	18.312
6	870	321.1	1	0	0		30.8	0.0	negligible	-	18.312
7	2,614	318.9	0.5	12	12	7,200	31.0	15.5	1.69E-11	9.18E-12	18.418
8	2,952	319.9	1	0	0		31.0	0.0	negligible	-	18.414
9	3,046	320.6	0.5	600	12		31.1	15.5	3.15E-10	1.13E-10	18.514
10	3,358	320.6	1	0	0		31.1	0.0	negligible	-	18.520
11	3,453	320.1	0.5	600	12		31.2	15.5	3.13E-10	1.15E-10	18.623
12	4,392	321.0	0.5	600	12		31.5	15.7	2.61E-11	9.28E-12	18.718
13	4,895	320.6	1	0	0		31.5	0.0	1.73E-12	-	18.716
14	4,901	320.8	0.2	1	1		35.4	28.3	2.74E-07	3.72E-07	20.893
15	4,916	320.8	0.2	50	50		36.0	28.8	8.79E-09	7.97E-09	21.197
16	4,922	320.7	0.2	1	1		47.1	37.7	7.41E-07	1.20E-06	25.723
17	4,941	320.6	0.5	50	12		48.9	24.5	7.02E-09	8.79E-09	26.297
18	4,967	320.6	0.5	300	12		49.3	24.7	1.29E-09	1.51E-09	26.417
19	5,085	320.4	0.5	4000	12		49.7	24.8	2.04E-10	1.16E-10	26.512
20	5,205	320.8	0.8	600	12		50.0	10.0	9.90E-11	6.14E-11	26.561
21	5,302	320.7	0.8	600	12	7,200	50.0	10.0	2.26E-11	4.73E-12	26.561
22	5,973	320.5	1	0	0		50.0	0.0	1.97E-12	-	26.564
23	6,142	320.6	0.8	600	12		50.2	10.0	7.37E-11	6.21E-11	26.614
24	6,386	320.6	1	0	0		50.2	0.0	2.87E-12	-	26.614
25	6,596	320.7	0.5	7800	12		50.6	25.3	1.12E-10	6.46E-11	26.713
26	6,813	320.6	0.5	7800	12	7,200	50.8	25.4	5.80E-11	3.41E-11	26.753
27	7,103	320.4	1	0	0		50.8	0.0	7.27E-13	-	26.756
28	7,390	320.5	0.3	18,000	12		51.0	35.7	9.24E-11	6.69E-11	26.830
29	7,972	320.6	0.3	18,000	12	7,200	51.6	36.1	7.16E-11	5.23E-11	26.998
30	10,453	320.2	1	0	0		51.7	0.0	2.43E-13	-	27.006

[a]Simulated PWR water with 2 ppm Li, 1100 ppm B, and 2 ppm. DO<10 ppb. Conductivity was 21±3 μS/cm, and pH 6.4.

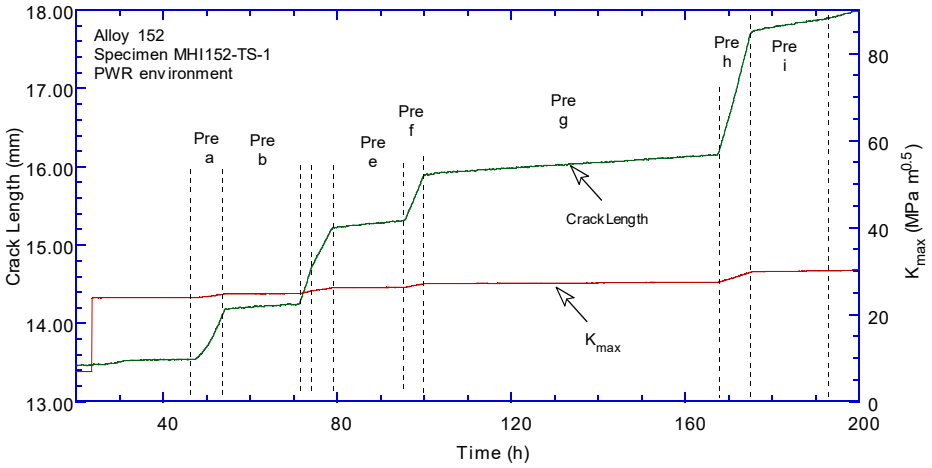

(a)

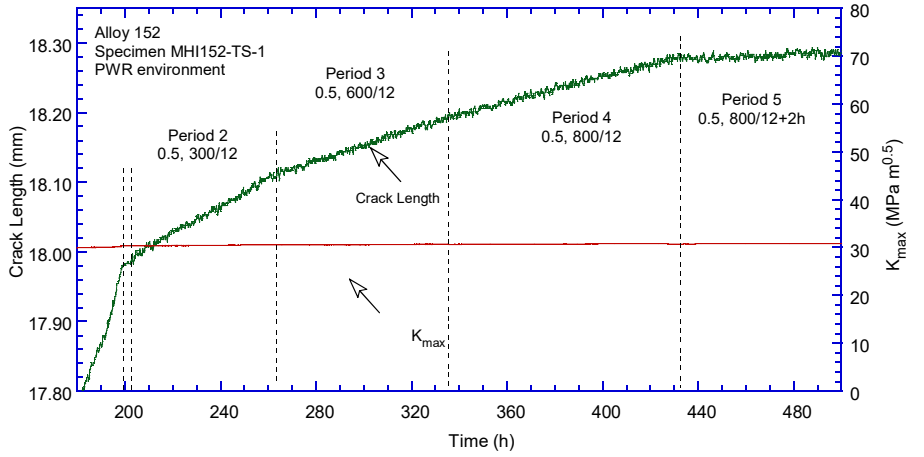

(b)

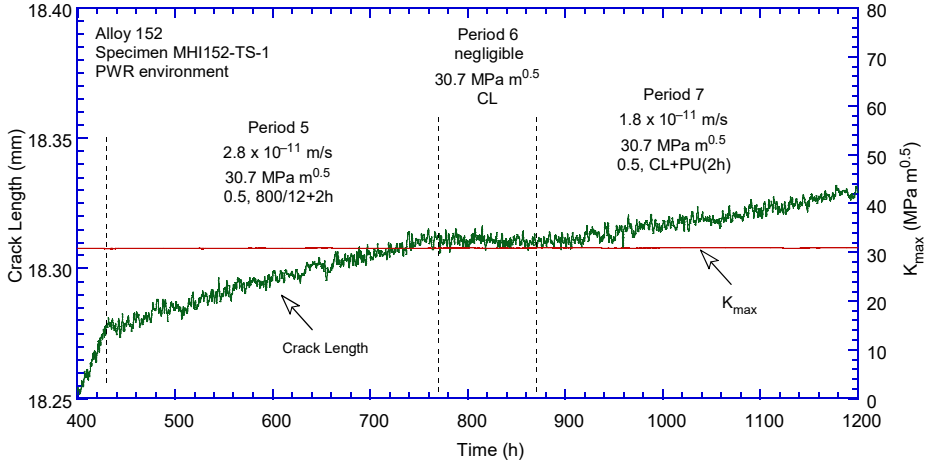

(c)

Figure 49 Crack–length–vs.–time for Alloy 152 weld specimen MHI152-TS-1 in simulated PWR environment during test periods (a) precracking, (b) 1-4, (c) 5-6, (d) 7-8, (e) 9-11, (f) 12-14, (g) 14-18, (h) 19-22, (i) 23-26, (j) 27-29, and (k) 30.

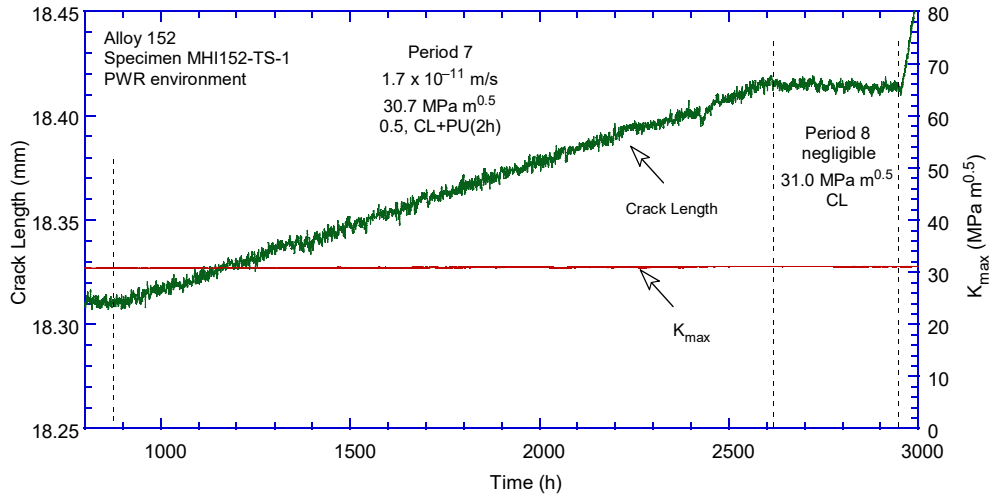

(d)

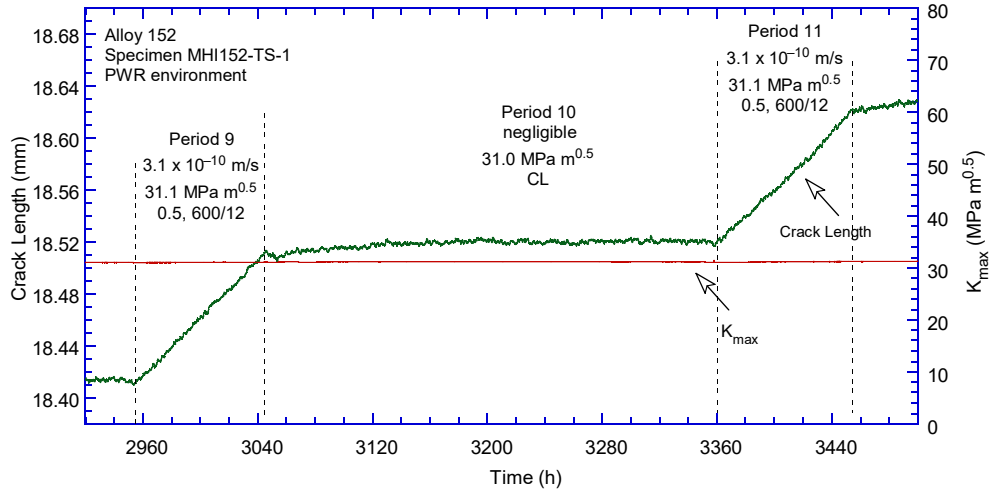

(e)

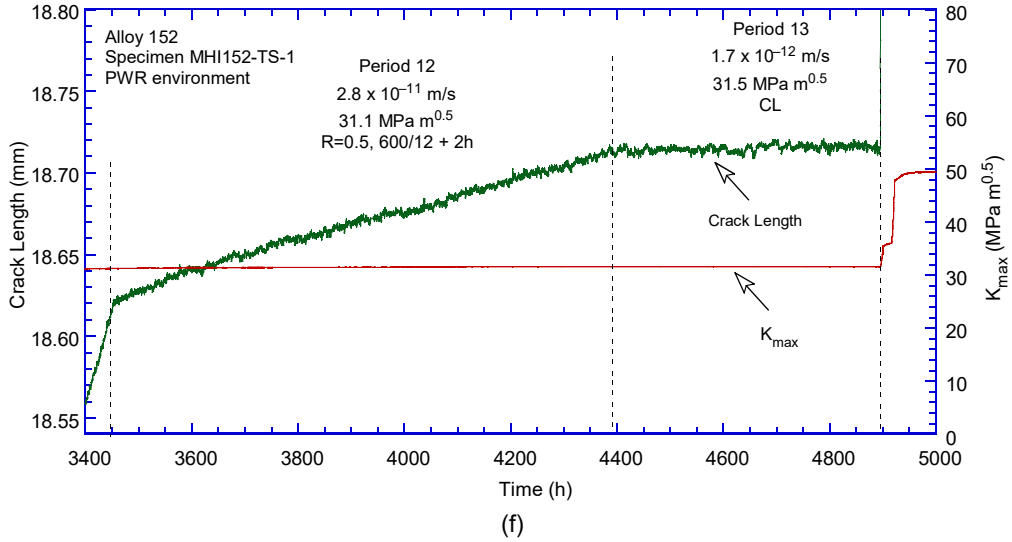

(f)

Figure 49 (Cont.)

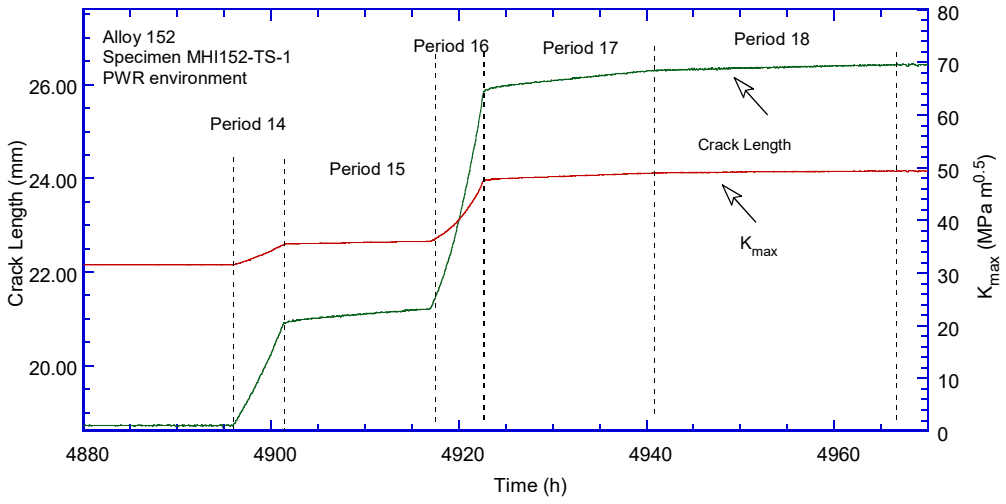

(g)

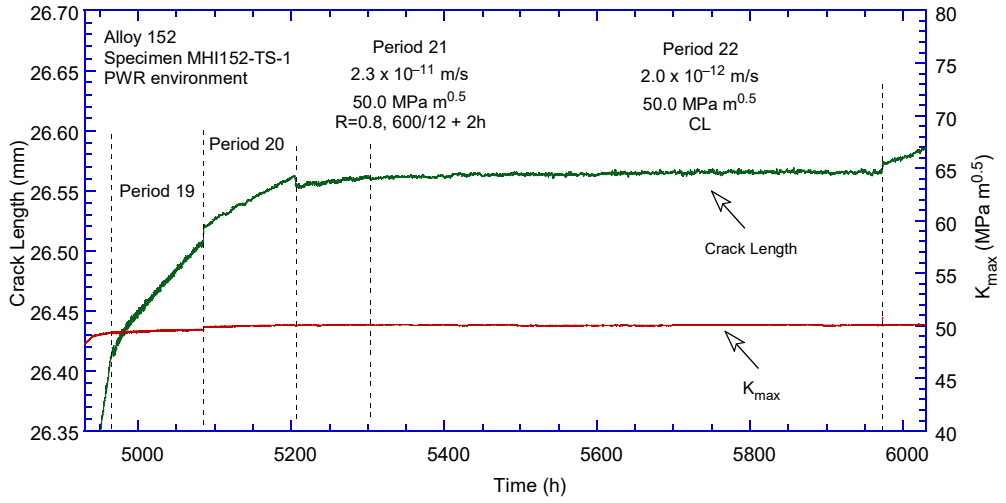

(h)

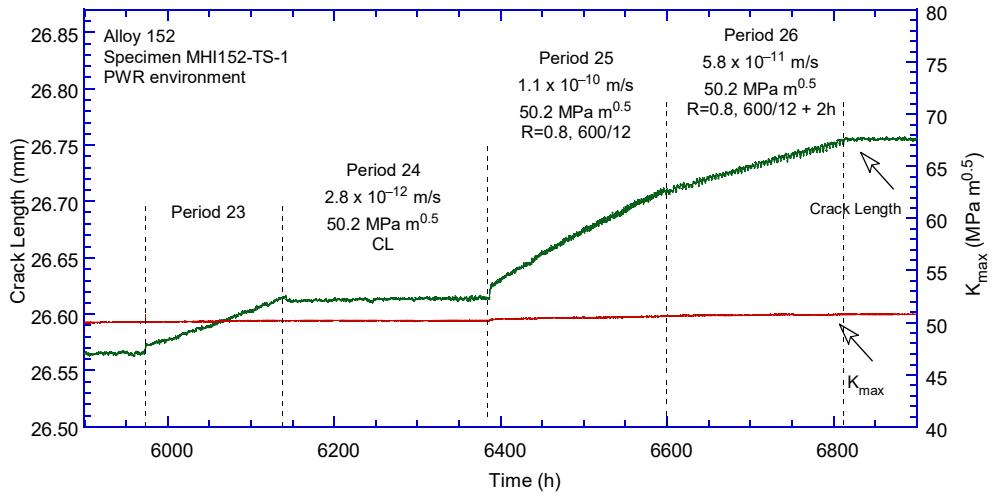

(i)

Figure 49 (Cont.)

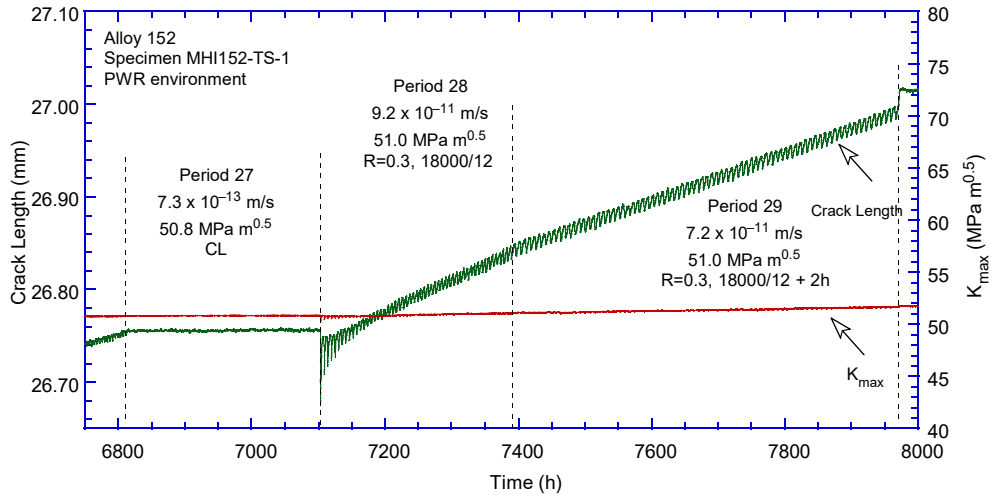

(j)

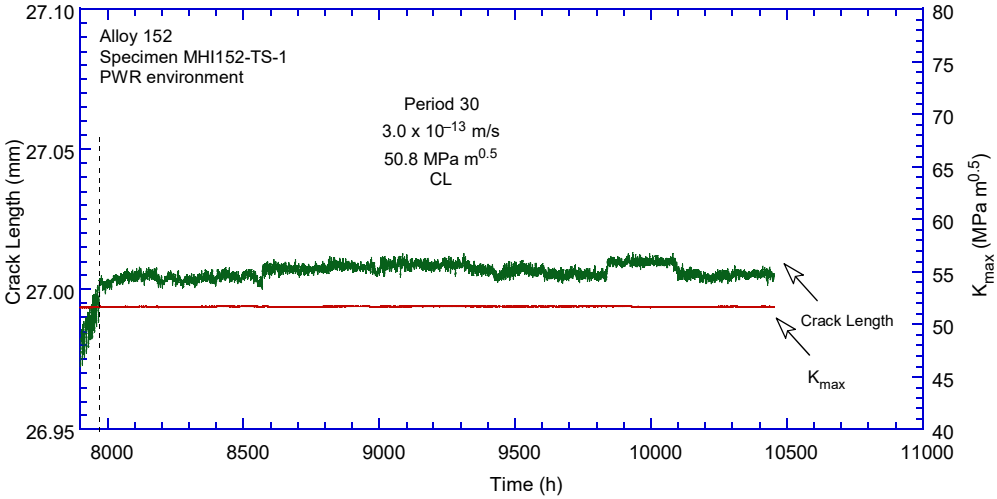

(k)

Figure 49 (Cont.)

Figure 50 shows the cyclic CGR data obtained for the MHI152-TS-1 specimen, and for comparison, data from a previous Alloy 152 specimen that was tested at ANL (N152-TS-1, Section 3.1.2), and the corrosion fatigue curve for Alloy 182 were included. Figure 50a shows that the data for the MHI152 specimen agrees well with that for the previous N152-TS-1 specimen tested. Figure 50b shows that in the second part of the test (starting with test period 14) less environmental enhancement was observed. The reason for the difference is unclear. Nevertheless, cycling at R=0.5 only slightly improved environmental enhancement over cycling at R=0.8, and cyclic at R=0.3 shows even less than the prior two conditions. The difference is further explored in Figure 51. As noted previously, the initial transitioning at a moderate stress intensity factor showed a level of environmental enhancement comparable with the previous specimens. At the high stress intensity factor, the environmental enhancement is about half of the expected value. Nevertheless, the CGR response under cyclic conditions at R=0.5 seems to produce the highest environmental enhancement, and that is consistent with the previous experience.

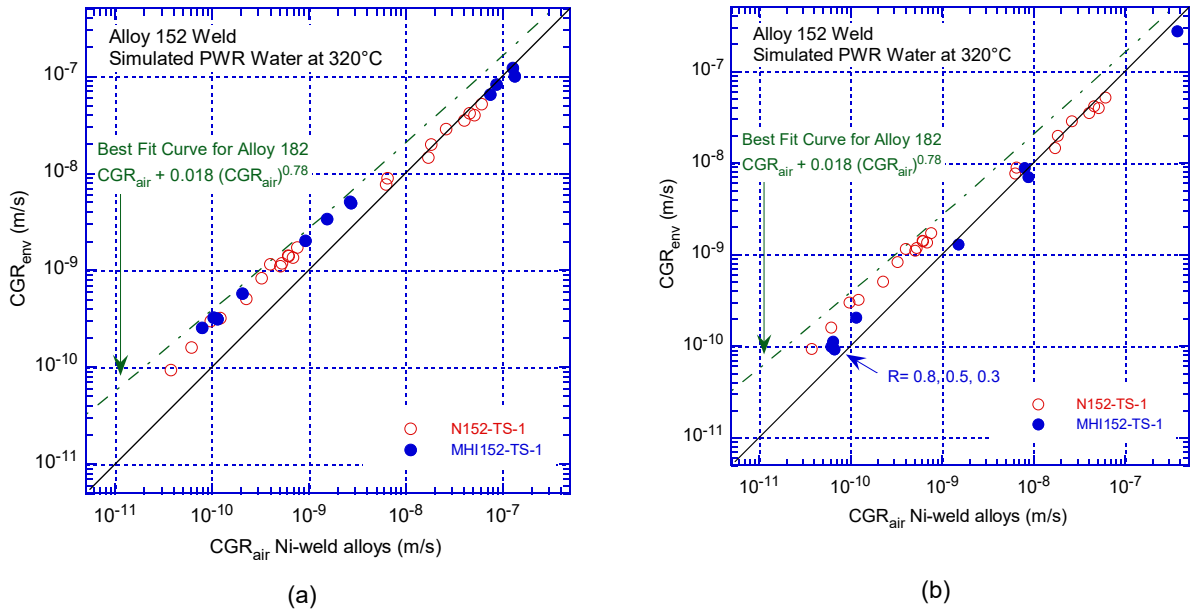

Figure 50 Cyclic CGR data for Alloy 152 specimen MHI152-TS-1 in simulated PWR environment: (a) first part of the test, and (b) second part of the test.

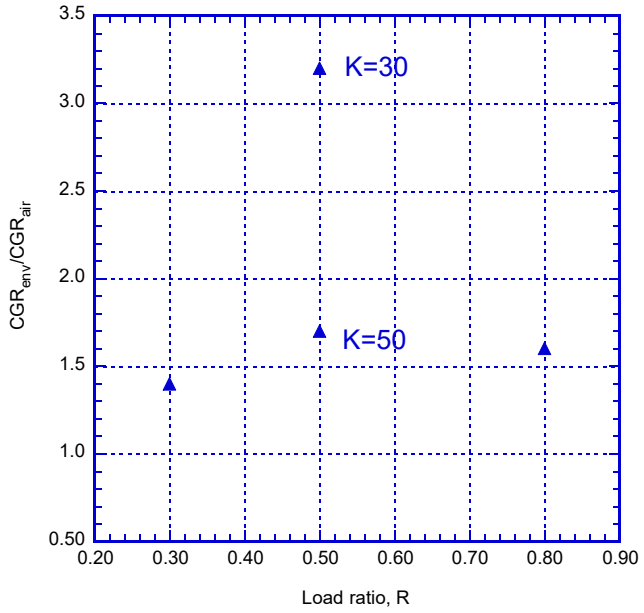

Figure 51 Environmental enhancement as a function of load ratio, R, in two stress intensity regimes.

Figure 52 shows the environmental enhancement for select conditions as well as the resulting SCC CGRs for test specimen MHI152-TS-1 as a function of the distance from the specimen notch. The response from fatigue test periods is also included, and the expected outcome for these conditions is “1”, i.e., the CGR response matches expected fatigue response for this alloy.

Overall, the environmental enhancement (see red symbols) appears to decrease with crack advance, and this effect was also captured in Figure 50. While SCC CGRs measured under constant load have been small, the large discrepancy between PPU (open green) and constant load (solid green) SCC CGRs in the latter part of the test is of concern, Figure 52b. As such, the two 10^{-11} m/s SCC CGRs calculated from cyclic data in test periods 21 and 29 predicted very well the approx. 0.5 mm SCC crack advance that was eventually measured on the fracture surface.

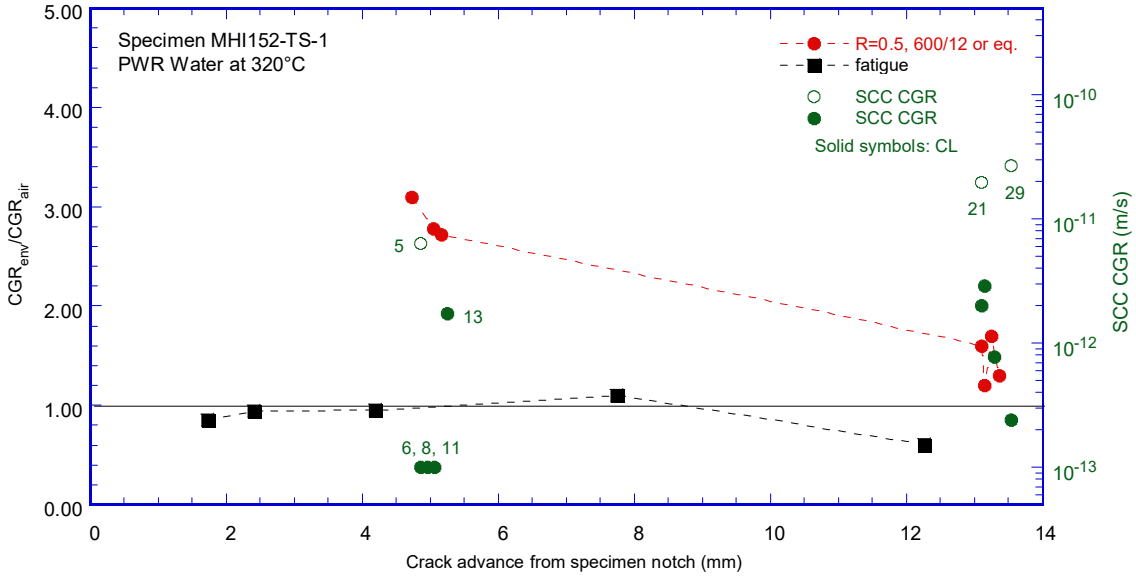

(a)

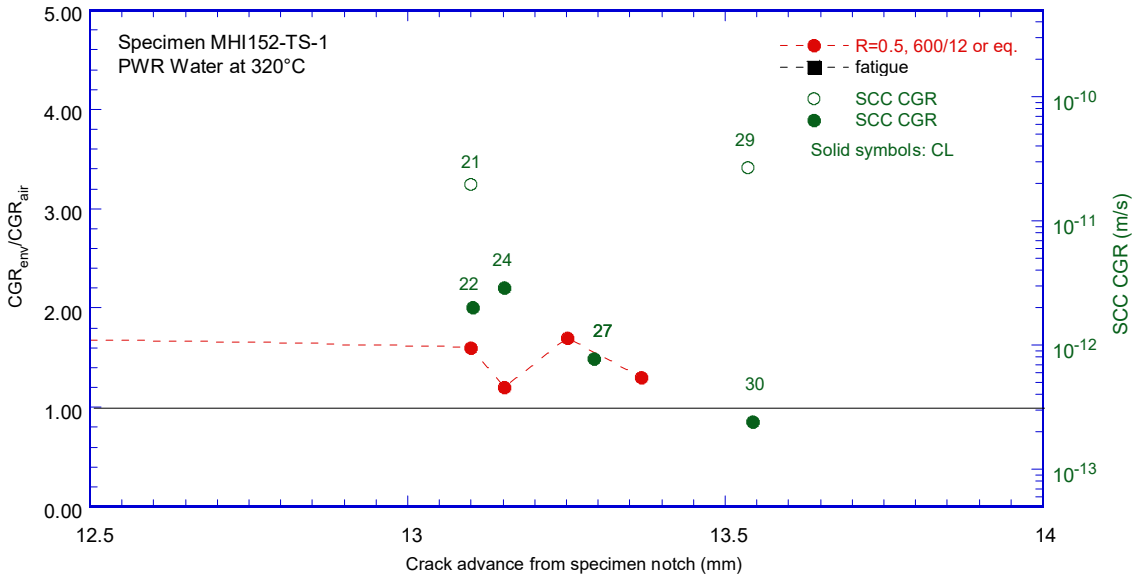

(b)

Figure 52 Environmental enhancement and SCC CGRs for Alloy 152 test specimen MHI152-TS-1 as a function of the distance from the specimen notch: (a) complete data set, and (b) last part of the test.

The post-test examination of specimen MHI152-TS-1 involved both the sides and the fracture surface.

The side surfaces were ground to remove the side grooves, polished and etched, Figure 53. Both images show that the crack propagated in a straight line, along the side grooves of the specimen. Based on these images, the average total growth was 13.11 mm, 3.2% from the DC potential measured total crack advance, hence a fairly straight fracture surface is expected. Of note is the crack branching that occurred on surface CS-2 (indicated by a blue arrow in Fig. Figure 53b, and shown at higher magnification in Figure 54). Crack branching – with a morphology that seems to be IG - starts approx. 4.8 mm from the notch (test periods 3-4, Table 13) and ends 5.95 mm from the notch. Assuming that the SCC-friendly (constant load or gentle cycling meant to preserve the IG fracture mode) conditions ended with fast cycling in test period 14, Table 13, then the end of branching should correspond to the end of test period 13. The end of test period 13, Table 13, is 5.25 mm away from the notch, hence, crack branching – as expected - had an significant impact (0.7 mm on this specimen side) on the DC potential measurements. In order to have the option to further examine this area, an approx. 2 mm – thick slice was cut from this side of the specimen prior to breaking it open.

After the 2 mm –thick cross section was cut to preserve side CS-2, the remaining test specimen was broken open to expose the fracture surface, Figure 55. The total crack advance measured of these images was 13.90 mm, in excellent agreement (2.5%) with the DC potential measurement of 13.54 mm. This level of agreement is not surprising given that the crack was advanced for the most part by fatigue or a cycling component was almost always present. Nevertheless, as described previously, crack branching and the resulting ligaments can have a profound effect on the DC potential measurements locally, especially during constant load and gentle cycling conditions.

Figure 55 also indicates the two regions of IG/interdendritic cracking obtained during testing at moderate K, IG-1 (test periods 3-13, Table 13) and relatively high K, IG-2 (test periods 19-30, Table 13). The vertical arrows indicate the extent of IG/intergranular cracking for each region.

During testing at moderate K (approx. 30 MPa $m^{1/2}$, test periods 3-13, Table 13), only approx. half of the specimen width was engaged, Figure 56. The SCC response was small, from negligible growth to approx. 2 x 10^{-12} m/s. This response was confirmed by cycle + hold testing in test periods 5 and 12. It is not clear why only half of the specimen was engaged and what role, if any, did the previously-described branching play by pinning the crack front during this stage of the test.

During testing at high K (approx. 50 MPa $m^{1/2}$, test periods 19-30, Table 13), the IG engagement was 78%, Figure 57 . The appearance was finger-like, which is not surprising given that this test ended with a long test period at constant load. The comparison of IG and non-IG crack extensions (Figure 58) reveals that the IG fracture mode initiated approx. 0.42 mm before the end of the test, which corresponds to test period 19, Table 13. Unlike region IG-1 where cracking was confined to only one half of the specimen, the distribution of cracking in this region seems uniform.

The cyclic and SCC response during testing at high K was contradictory. One the one hand the environmental enhancement was minimal and the response at constant load was very small and or/negligible. On the other hand, the SCC CGR component calculated by superposition from

cycle + hold testing was much larger, i.e., 2.7 x 10^{-11} m/s in test period 29. Given the amount of IG engagement and the presence of fingered-growth, the SCC rate obtained from the test period with some cycling appear more likely to be the correct one.

In summary, this test consisted of two stages at moderate and relatively high stress intensity factors. Testing at moderate K resulted in a relatively lower IG engagement that was confined to one half of the fracture surface. The reason is unclear. The resulting SCC CGRs at constant load were small, and in agreement with the rates obtained in test periods that involved some cycling. Testing at relatively high K resulted in a relatively high IG engagement that was spread uniformly across the specimen width. The resulting SCC CGRs at constant load were small, and contradictory to the moderate CGRs obtained during test periods that involved some cycling. This is not entirely surprising given the amount of finger-like growth. In retrospect, additional effort should have been made to try to understand and resolve these differences.

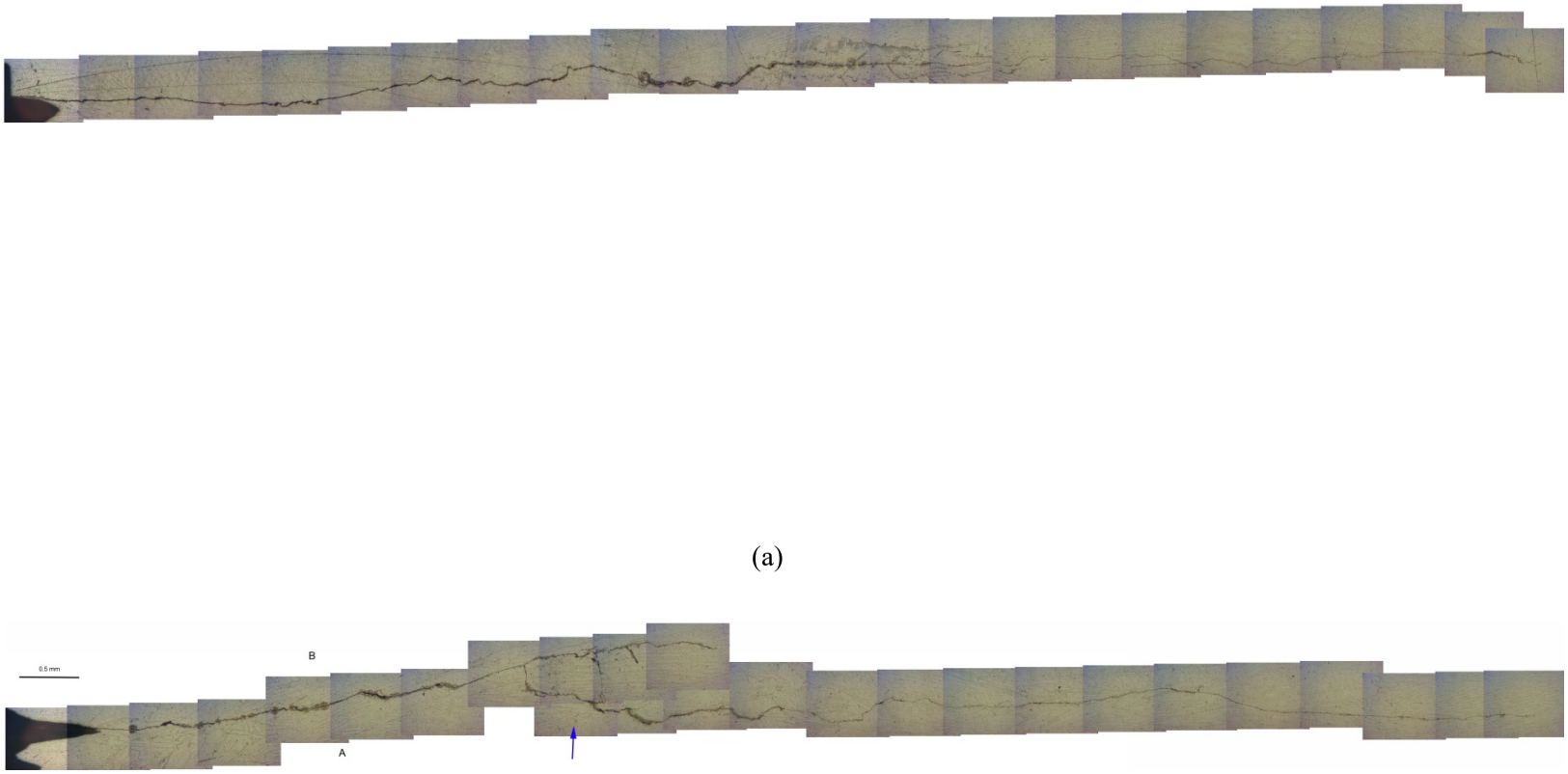

(a)

(b)

Figure 53 Cross sections of specimen MHI152-TS-1: (a) side 1, CS-1, and (b) side 2, CS-2. The blue arrow indicates significant crack branching on CS-2. Crack advance is from left to right.

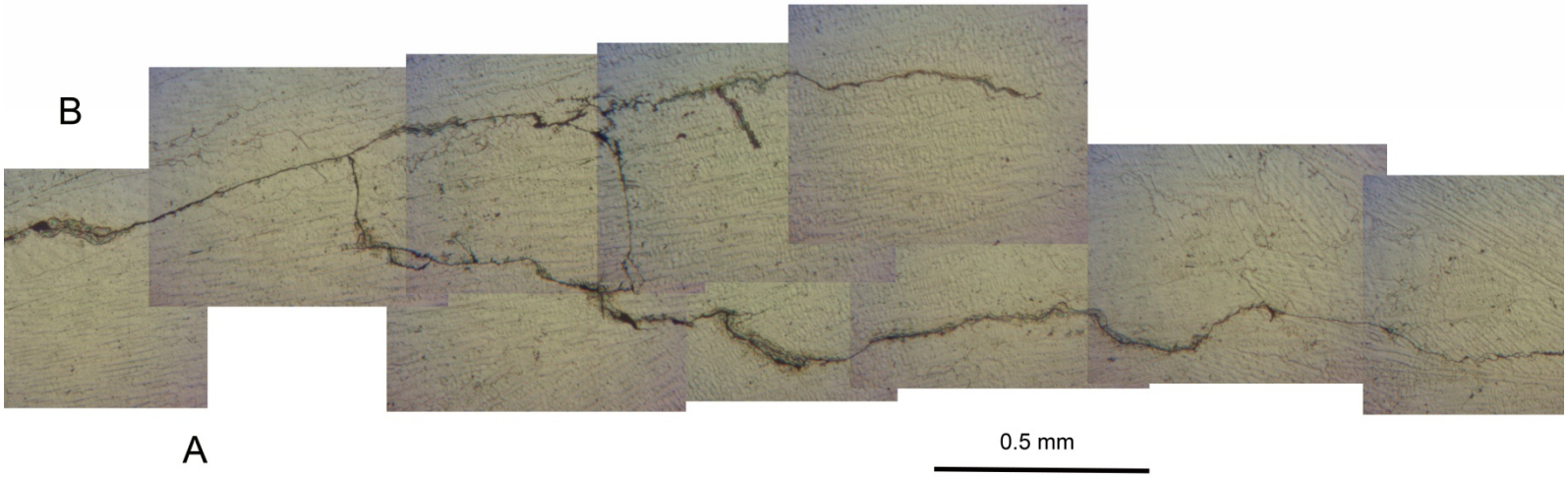

Figure 54 **Crack branching on side surface CS-2 of specimen MHI152-TS-1 at location indicated by the blue arrow in Figure 53b. Crack advance is from left to right.**

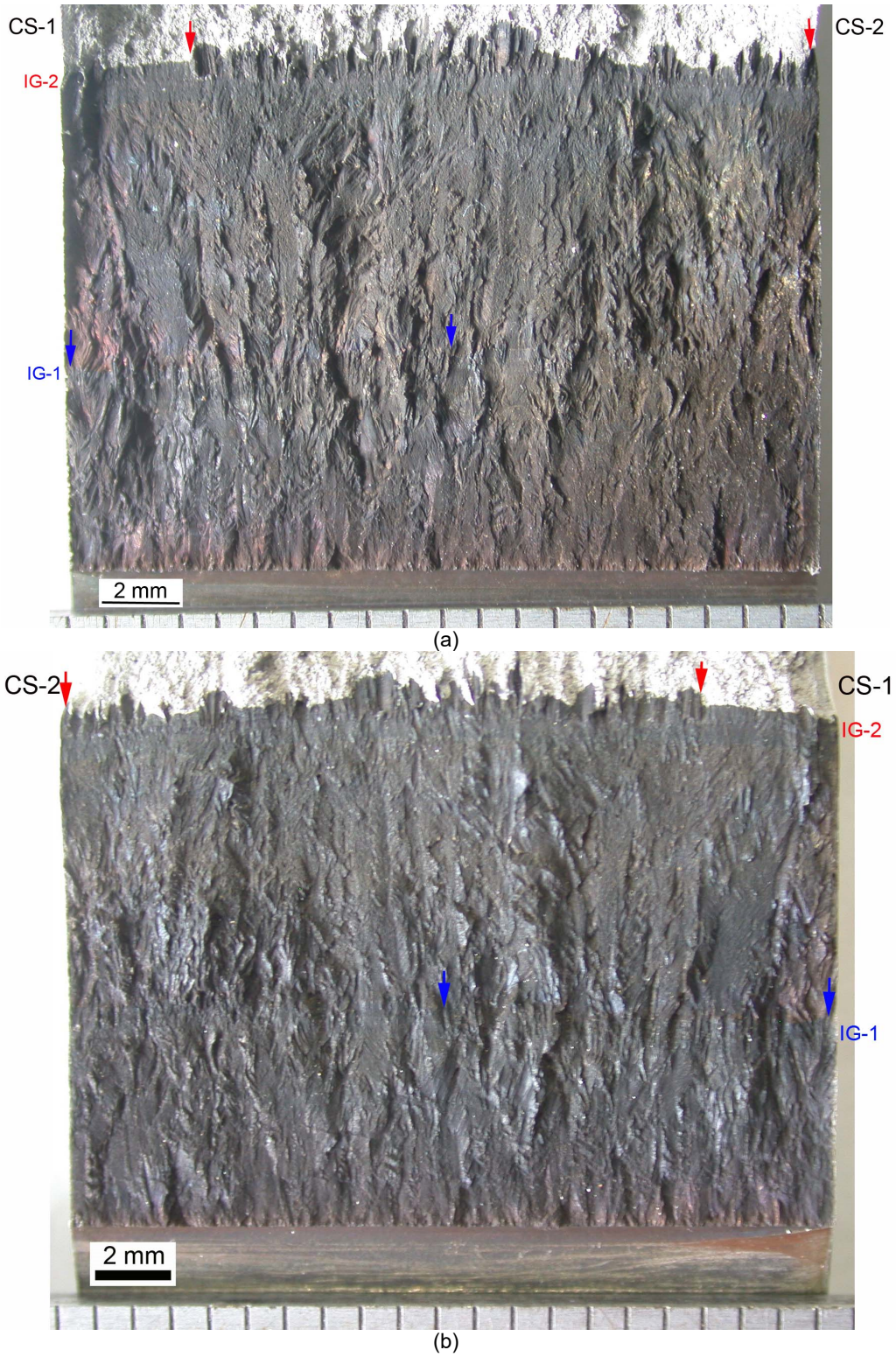

Figure 55 **Fracture surface of Specimen MHI152-TS-1 (a) surface A, and (b) surface B. The relationship to the side surfaces CS-1 and CS-2 is indicated. Blue/red arrows mark the extent of IG/interdendritic cracking. Crack propagation is from bottom to top.**

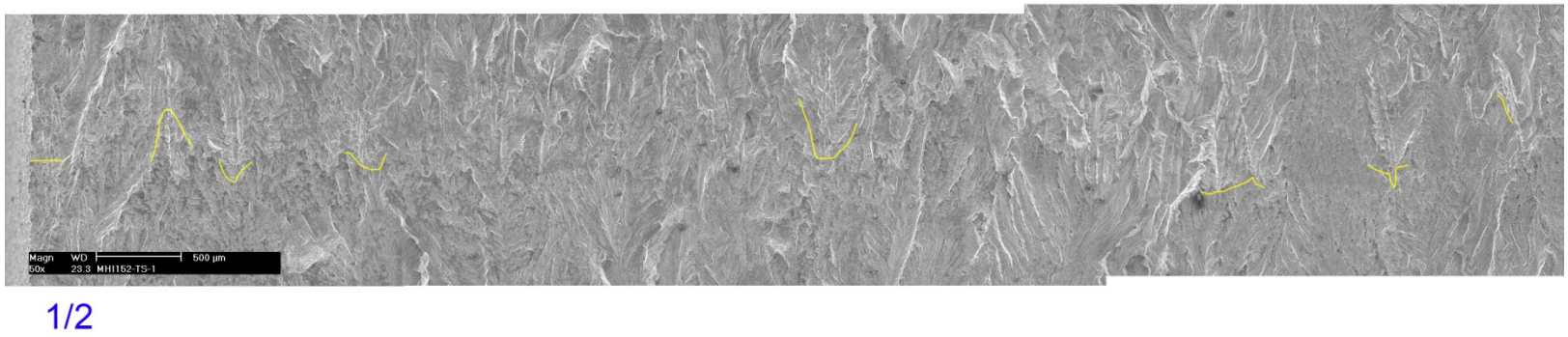

(a)

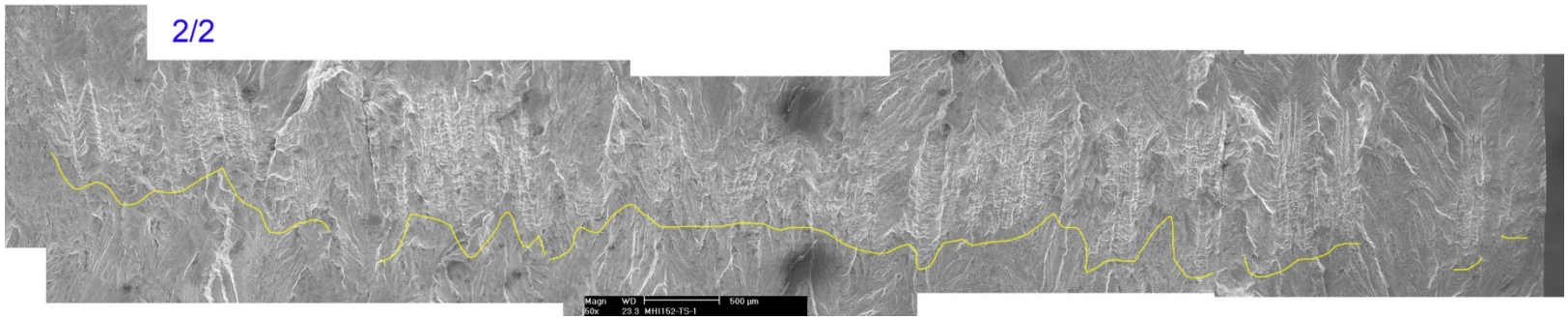

(b)

Figure 56 **Fracture surface of specimen MHI152-TS-1, region IG-1 in Figure 55b: (a) first half, and (b) second half. The yellow line indicated IG/interdendritic cracking. The blue arrow indicates significant crack branching on CS-2. Crack advance is from left to right.**

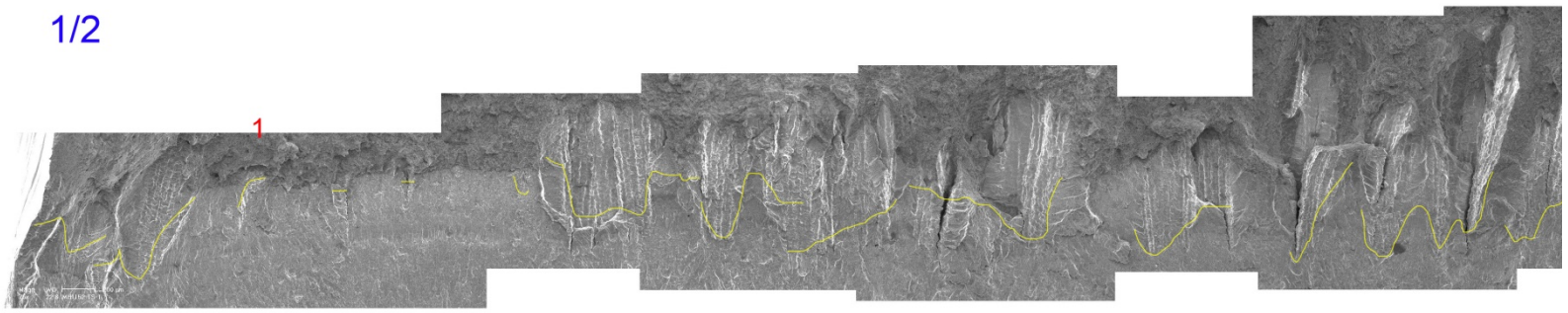

(a)

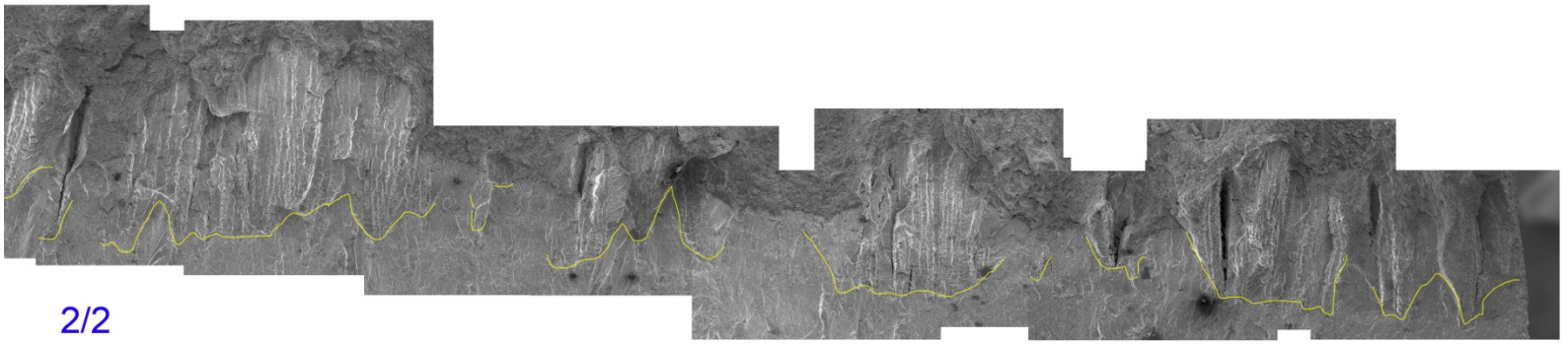

(b)

Figure 57 **Fracture surface of specimen MHI152-TS-1, region IG-2 in Figure 55b: (a) first half, and (b) second half. The yellow line indicated IG/interdendritic cracking. The blue arrow indicates significant crack branching on CS-2. Crack advance is from left to right.**

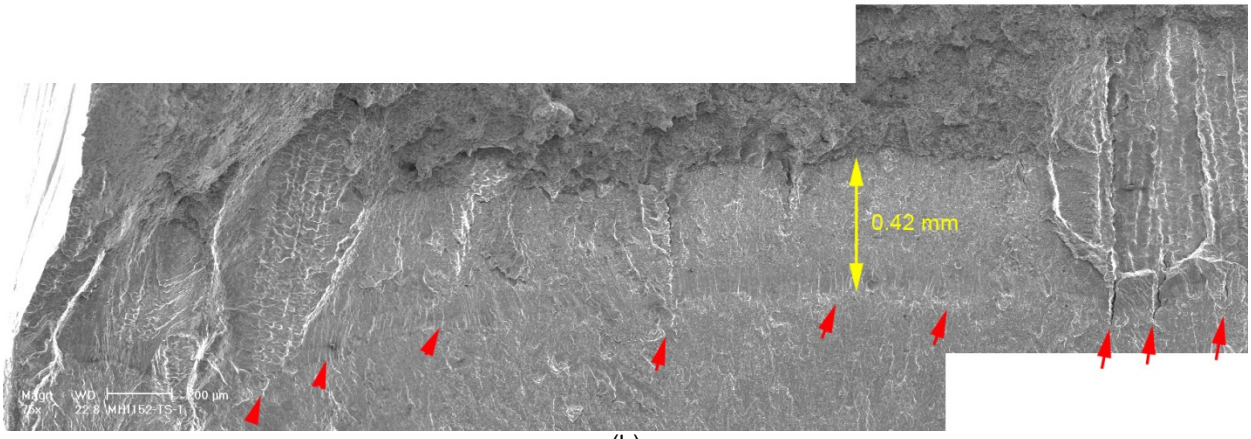

(b)

Figure 58 Fracture at location 1 in Fig. Figure 57a. on the surface of Specimen MHI152-TS-1. The red arrows mark the beginning of transitioning test periods. Crack propagation is from bottom to top.

3.2.2 Specimen MHI152-TS-11

The testing conditions are given in Table 14, and the changes in crack length and K_{max} with time are shown in Figure 59.

After three test periods of precracking in which the fatigue behavior of this alloy was confirmed, the next test period, 1, was a loading condition typically used to advance a crack under PPU. As expected, the resulting rate also confirmed the fatigue behavior of this alloy. Period 2 produced an environmental enhancement according to expectations, while period 3 showed less environmental enhancement. A 2-h hold introduced in test period 4 enabled the SCC CGR component to be calculated at 3 x 10^{-12} m/s. The subsequent test period at constant load showed the SCC CGR to be negligible.

One issue that was not understood at this point in the test was why the environmental enhancement decreased between test periods 2 and 3. The level of environmental enhancement observed in test period 3 (2.4) is slightly smaller than that observed previously in the N152-TS-1 (see section 3.1.2) specimen where the crack direction was not along the dendrites. Hence, branching seems to be able to occur along the more favorable directions and, as was observed in the prior test on the MHI152 weld, essentially pins the crack front. That test demonstrated that the gentle cycling used was ineffective at keeping the crack in plane. Also, in the second part of that test (see Figure 50), the specimen produced low environmental enhancement, however, it is unclear why. SCC CGR results from cycle + hold and constant load did not match, however, a large amount of IG cracking was observed on the fracture surface. Hence, based on the experience with the first specimen, test conditions 2 and 3 were repeated, and the environmental enhancement in test periods 6-8 was lower than expected, thus, test condition 1 (fatigue) was repeated in test period 9. Next, the transitioning test periods were repeated in test periods 10-11, and the environmental enhancement was still low (see also Figure 61). Next, a 2-h hold was introduced in test period 12. The rate evolution in test period 12 (Figure 59f) is interesting: initially the rate was 2.1 x 10^{-11} m/s (SCC CGR component 1.1 x 10^{-11} m/s); at the end of the test period, the rate was 1.2 x 10^{-11} m/s (SCC CGR component 1.0 x 10^{-12} m/s). In other words, the rate evolution in test period 12 demonstrates

once more that a 2-h unload/reload period is ineffective at breaking the ligaments that form in this weld. As such, the unload/reload period was reduced to 1 h in test period 13. Despite the increased frequency, the SCC CGR component in test period 13 was essentially zero, and the subsequent test period 14 at constant load resulted in a “no growth” measurement. The environmental enhancement was probed next in test period 15, and the rate was found to be essentially at the “air” line. Then the loading was returned to fatigue to advance the crack to a different microstructure, then it was observed that the “expected” environmental enhancement was obtained in test period 18 (see also see Figure 61). The specimen was then set at constant load. Initially, the SCC CGR was the highest measured to date on this specimen, 3.4×10^{-12} m/s, however, after several hundreds of hours, the rate diminished by a factor 6 to approximately a “no growth” state. The behavior shown in Figure 59j suggests that ligaments impede the crack advance measurement by DC potential. Cycling loading in test period 20 did not produce a “jump”, however, the environmental enhancement was much lower. Suspecting branching, loading was reverted to fatigue in test period 21 to straighten the fracture surface, and this was followed by re-transitioning at a more aggressive R, but maintaining the same fatigue component as before. Environmental enhancement was also comparable (see also Figure 59). Next, a 2-h hold was introduced in test period 23, and the SCC CGR component was calculated by superposition to be 7.3×10^{-12} m/s. The specimen was set at constant load in subsequent test period 24, and the measured SCC CGR was somewhat lower. The environmental enhancement of the subsequent test period was again lower than prior to the constant load test period. This effect – a drop in environmental enhancement after a test period at constant load - was observed several times during this test (see for example, 3-6, 11-15, 18-20, 22-25 in Figure 61), and the reason is unclear. One plausible explanation would be a case where the most susceptible direction is oriented differently than the main crack front. Hence, the decision was made to advance the crack and look for a favorable orientation (producing an environmental enhancement of 3 or more) and set the specimen at constant load one more time. This is accomplished by alternating slow and fast cycling schemes as well as an occasional fatigue test period such as that in test period 40.

During test period 46, a power failure occurred. After the test pressure and temperature were re-established, loading was changed to fatigue in test period 47 at a lower K_{max} than in the previous test period in attempt to fatigue through the plastic zone that may have formed. Restoring the known fatigue behavior took test periods 47-58 (Figure 59p-q), and the known rate was reproduced only in test period 15 (Figure 59q). The evolution of the fatigue response is summarized in Figure 60b.

After the known fatigue behavior was restored ensuring that the CGR data is not affected by the plastic tip zone that may have formed during shutdown, the test was returned to the original schedule. As such, in test period 60, loading was changed to the typical R=0.5, 600/12. Next, a 2h-hold was introduced in test period 61 to evaluate the SCC CGR, and while the average rate was consistent with IG SCC growth, it is interesting to note that the rate under this condition decreases from 3.6×10^{-11} m/s to 2.2×10^{-11} m/s over a growth increment of approx. 20 microns. Assuming that the corrosion fatigue stays constant over that growth increment, the rate drop reflects a SCC CGR component drop from 2×10^{-11} m/s to 6×10^{-12} m/s. Consistent with the prior observations, it is believed that the drop reflects growth on a direction other than the main front. The subsequent test period at constant load shows the lower, 10^{-12} m/s rate. As such, the crack was allowed to grow for approx. 1,700 hours, and that was followed by cycling similar to that of preceding test period 61. The resulting rate in test period 63 was a factor 2 smaller suggesting that the crack is advancing off-plane. This was followed by another test period at constant load (64).

Next, cyclic loading (R=0.5, 600/12) was reintroduced n test period 65 in an attempt to straighten the fracture surface. This was followed by cycle + hold test periods 66 and 67. In test period 66, the hold was introduced at K_{min}. Under such loading, the growth rate is only due to corrosion fatigue due to cyclic loading; during the hold time, the specimen is practically unloaded. By contrast, in test period 67, the hold was introduced at K_{max}, hence, the measured rate consists of a corrosion fatigue component plus an SCC component during the 2h hold time at K_{max}. In this framework, SCC growth will be the simple subtraction of CGRs measured in test periods 66 and 67. If no SCC occurs, then the rate in test period 67 should equal that in test period 66. Since the CGRs in test periods 66 and 67 were nearly identical, it suggests that no SCC occurred in test period 67. The observation was repeated. The CGR response in test period 68 is about half of test of test 66, and corresponds to the expected rate in air. The hold time was switched between K_{min} and K_{max} several more times, effectively turning the SCC off and on. Difference between CGRs in test periods 67, 69, 71 and 68, 70 is about 1.0 10^{-11} m/s. At this SCC rate, the fracture mode is most likely IG and the engagement is expected to be significant. However, the responses seem to gradually decrease (see for example 71 vs. 67) to the point where the rate measured in 71 was similar to that measured previously in test period 63 (no measurable SCC component). The reason for the gradual decrease is unclear, but perhaps suggests that cracking is occurring off-plane.

The current situation appears to be similar to that observed in the prior test: the fracture mode is IG and cyclic measurements suggest that the SCC CGR is in the 10^{-11} m/s range. Indications are that the preferred crack path is off-plane. With no solution for off-plane cracking, the loading was changed to fast/fast fatigue cyclic and 2h hold for the final test period (73) of this test. Under this loading condition, it will be the fracture surface that will determine whether the advance occurred under cyclic (TG) or hold (IG). The test ended with two test periods of fatigue in ambient air, re-confirming the known fatigue response for this weld alloy.

Table 14 Crack growth data for Alloy 152 weld specimen MHI152-TS-11 in PWR water[a].

Test Period	Test Time, h	Temp. °C	Load Ratio R	Rise Time, s	Down Time, s	Hold Time, s	K_{max}, MPa·m$^{1/2}$	ΔK, MPa·m$^{1/2}$	CGR_{env}, m/s	Estimated CGR_{air}, m/s	Crack Length, mm
Pre a	72	319.1	0.30	1	1		24.4	17.1	5.85E-08	5.76E-08	12.179
Pre b	90	319.2	0.30	50	50		24.7	17.3	2.90E-09	1.21E-09	12.276
Pre c	92	318.7	0.30	1	1		25.5	17.9	6.96E-08	6.90E-08	12.528
1	96	318.8	0.50	12	12		25.8	12.9	3.36E-09	2.59E-09	12.575
2	139	318.6	0.50	300	12		25.9	13.0	3.04E-10	1.05E-10	12.617
3	330	318.5	0.50	600	12		26.3	13.1	1.38E-10	5.59E-11	12.711
4	763	318.6	0.50	600	12	7,200	26.4	13.2	1.14E-11	4.39E-12	12.732
5	1,146	318.6	1.00	0	0		26.3	0.0	no growth	-	12.732
6	1,266	318.5	0.50	600	12		26.6	13.3	1.22E-10	5.86E-11	12.780
7	1,345	318.6	0.50	300	12		26.9	13.4	2.19E-10	1.22E-10	12.839
8	1,458	317.9	0.50	600	12		27.0	13.5	1.15E-10	6.18E-11	12.885
9	1,465	318.4	0.50	12	12		27.1	13.6	3.08E-09	3.17E-09	12.922
10	1,512	318.2	0.50	300	12		27.3	13.6	2.40E-10	1.29E-10	12.961
11	1,581	317.8	0.50	600	12		27.3	13.6	1.39E-10	6.46E-11	12.996
12	1,967	318.5	0.49	600	12	7,200	27.5	14.0	1.26E-11	5.44E-12	13.016
13	2,995	317.9	0.49	600	12	3,600	27.7	14.1	1.89E-11	1.04E-11	13.083
14	3,428	317.8	1.00	0	0		27.7	0.0	no growth	-	13.086
15	3,477	318.0	0.49	600	12		27.7	14.1	9.51E-11	7.30E-11	13.100
16	3,480	318.0	0.30	1	1		25.7	18.0	6.87E-08	7.07E-08	13.294
17	3,482	318.0	0.49	50	12		25.7	13.1	1.20E-09	6.44E-10	13.314
18	3,523	318.0	0.49	600	12		25.8	13.2	1.74E-10	5.42E-11	13.339
19	4,699	318.1	1.00	0	0		25.6	0.0	1.38E-12	-	13.342
20	4,771	318.2	0.48	600	12		25.5	13.3	1.06E-10	5.45E-11	13.369
21	4,777	318.3	0.49	12	12		25.7	13.1	2.56E-09	2.66E-09	13.393
22	4,943	318.1	0.29	1400	12		26.0	18.4	1.42E-10	5.44E-11	13.477
23	5,324	318.3	0.29	1400	12	7,200	26.1	18.5	2.83E-11	9.01E-12	13.517
24	6,074	318.3	1.00	0	0		26.2	0.0	4.37E-12	-	13.532
25	6,218	318.0	0.28	1400	12		26.2	18.9	1.26E-10	5.84E-11	13.593
26	6,223	318.1	0.29	12	12		26.5	18.8	7.11E-09	6.86E-09	13.651
26	6,242	318.1	0.47	50	12		26.7	14.2	9.63E-10	8.30E-10	13.708
28	6,266	318.2	0.48	600	12		26.7	13.9	1.37E-10	6.58E-11	13.719
29	6,272	318.2	0.47	50	12		26.7	14.1	1.04E-09	8.21E-10	13.735
30	6,338	318.1	0.47	600	12		26.8	14.2	1.27E-10	7.00E-11	13.765
31	6,345	318.2	0.48	50	12		26.9	14.0	1.03E-09	8.18E-10	13.785
32	6,386	318.2	0.48	600	12		27.1	14.1	1.31E-10	6.97E-11	13.806
33	6,394	318.0	0.48	50	12		27.2	14.1	1.04E-09	8.50E-10	13.827
34	6,410	318.1	0.48	600	12		27.2	14.2	1.19E-10	7.12E-11	13.834
35	6,417	318.1	0.48	12	12		27.4	14.3	3.15E-09	3.67E-09	13.874
36	6,433	318.1	0.48	50	12		27.7	14.4	1.09E-09	9.13E-10	13.925
37	6,506	318.1	0.48	600	12		27.8	14.5	1.43E-10	7.79E-11	13.961
38	6,512	318.1	0.48	50	12		27.9	14.5	1.02E-09	9.37E-10	13.980
39	6,531	318.0	0.48	600	12		27.9	14.5	1.33E-10	7.88E-11	13.990
40	6,534	318.1	0.30	1	1		27.9	19.5	8.70E-08	9.86E-08	14.306
41	6,537	318.0	0.48	50	12		27.5	14.3	1.38E-09	8.90E-10	14.334
42	6,743	318.1	0.48	600	12		28.3	14.7	1.76E-10	8.37E-11	14.462
43	6,752	318.2	0.48	50	12		28.3	14.7	1.11E-09	1.00E-09	14.483
44	6,767	318.2	0.48	600	12		28.4	14.8	1.82E-10	8.48E-11	14.495
45	6,776	318.1	0.48	50	12		28.6	14.9	1.05E-09	1.04E-09	14.519
46	6,836	318.1	0.48	600	12		28.8	15.0	1.68E-10	8.97E-11	14.558
47	6,841	320.3	0.28	1	1		24.9	17.9	3.75E-09	6.77E-08	14.604
48	6,858	319.6	0.28	50	50		24.8	17.9	3.56E-10	1.34E-09	14.614
49	6,865	319.5	0.28	1	1		25.0	18.0	1.12E-09	6.83E-08	14.630
50	6,881	319.2	0.28	50	50		25.1	18.1	2.03E-10	1.39E-09	14.635
51	6,889	319.6	0.28	1	1		25.2	18.2	9.28E-10	7.12E-08	14.648
52	6,977	319.4	0.28	100	100		25.1	18.1	1.02E-10	6.93E-10	14.637
53	6,986	319.4	0.28	1	1		25.3	18.2	3.09E-09	7.13E-08	14.678
54	7,003	319.4	0.28	50	50		25.3	18.2	4.23E-10	1.44E-09	14.692
55	7,010	319.6	0.28	0.5	0.5		25.9	18.6	1.83E-08	1.58E-07	14.875

Table 14 (cont.)

Test Period	Test Time, h	Temp. °C	Load Ratio R	Rise Time, s	Down Time, s	Hold Time, s	K_{max}, MPa·m$^{1/2}$	ΔK, MPa·m$^{1/2}$	CGR_{env}, m/s	Estimated CGR_{air}, m/s	Crack Length, mm
56	7,026	319.0	0.28	50	50		26.2	18.9	1.23E-09	1.66E-09	14.928
57	7,030	319.6	0.28	0.5	0.5		28.2	20.3	1.21E-07	2.25E-07	15.335
58	7,031	319.8	0.28	1	1		29.2	21.0	1.16E-07	1.30E-07	15.524
59	7,034	320.0	0.48	50	12		29.4	15.3	1.79E-09	1.19E-09	15.571
60	7,178	319.2	0.48	600	12		29.5	15.4	2.42E-10	1.01E-10	15.665
61	7,369	319.4	0.48	600	12	7,200	29.9	15.6	2.88E-11	8.17E-12	15.686
62	9,044	319.1	1.00	0	0.00		29.9	0.0	no growth	-	15.686
63	9,238	319.8	0.49	600	12	7,200	30.5	15.6	1.88E-11	8.50E-12	15.699
64	9,667	319.7	1.00	0	0	0	30.5	0.0	no growth	-	15.700
65	9,742	319.2	0.49	600	12	0	30.7	15.6	1.74E-10	1.12E-10	15.738
66	9,812	319.7	0.49	600	12	7,200 at K_{min}	30.6	15.6	2.26E-11	8.58E-12	15.741
67	10,152	319.9	0.49	600	12	7,200	30.8	15.7	2.21E-11	8.81E-12	15.773
68	10,248	319.9	0.49	600	12	7,200 at Kmin	30.6	15.6	9.36E-12	8.56E-12	15.772
69	10,486	319.8	0.49	600	12	7,200	30.8	15.7	2.01E-11	8.80E-12	15.794
70	10,578	319.8	0.49	600	12	7,200 at Kmin	30.5	15.6	8.56E-12	8.44E-12	15.793
71	10,822	319.8	0.49	600	12	7,200	30.9	15.8	1.95E-11	8.91E-12	15.817
72	11,440	319.2	0.49	600	12	72,000	31.3	15.9	2.98E-12	9.93E-13	15.822
73	15,155	319.2	0.49	12	12	7,200	32.4	16.5	1.66E-11	1.16E-11	16.035
74	15,158	25.9	0.50	12	12		32.6	16.3	2.80E-09	2.14E-09	16.063
75	15,160	26.0	0.30	1	1		33.7	23.6	6.52E-08	6.81E-08	16.225

[a]Simulated PWR water with 2 ppm Li, 1000 ppm B, and 2 ppm. DO<10 ppb. Conductivity was 21±3 µS/cm, and pH 6.4.

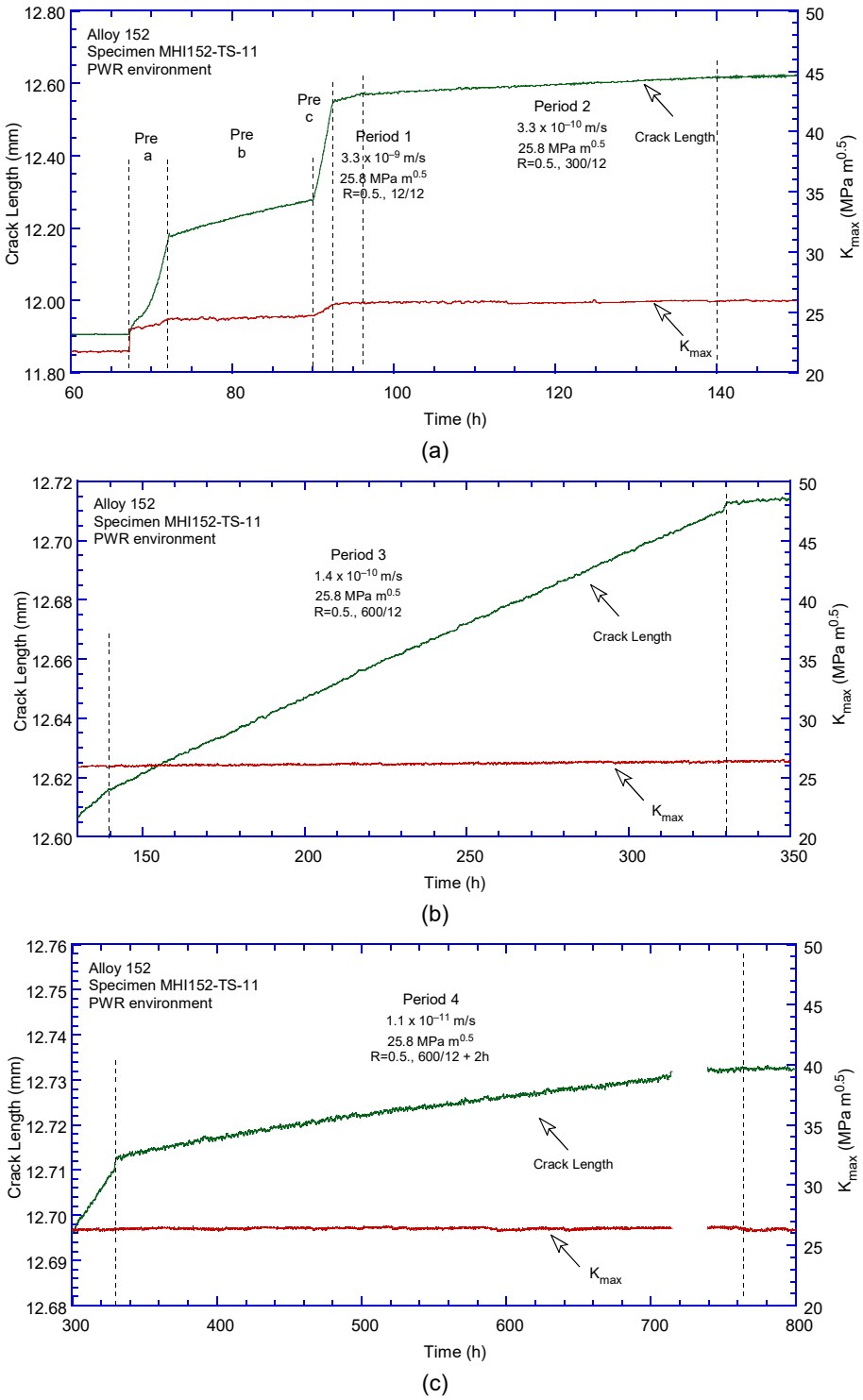

Figure 59 Crack–length–vs.–time for Alloy 152 weld specimen MHI152-TS-11 in simulated PWR environment during test periods (a) precracking-2, (b) 3, (c) 4, (d) 5, (e) 6-11, (f) 12, (g) 13 (h) 14-15, (i) 15-18, (j) 19, (k) 20-23, (l) 24, (m) 25-39, (n) 40. (o) 41-46, (p) 47-58, (q) 57-58, (r) 60, (s) 61-63, (t) 64, (u) 65-71, (v) 72-73, and (x) 73.

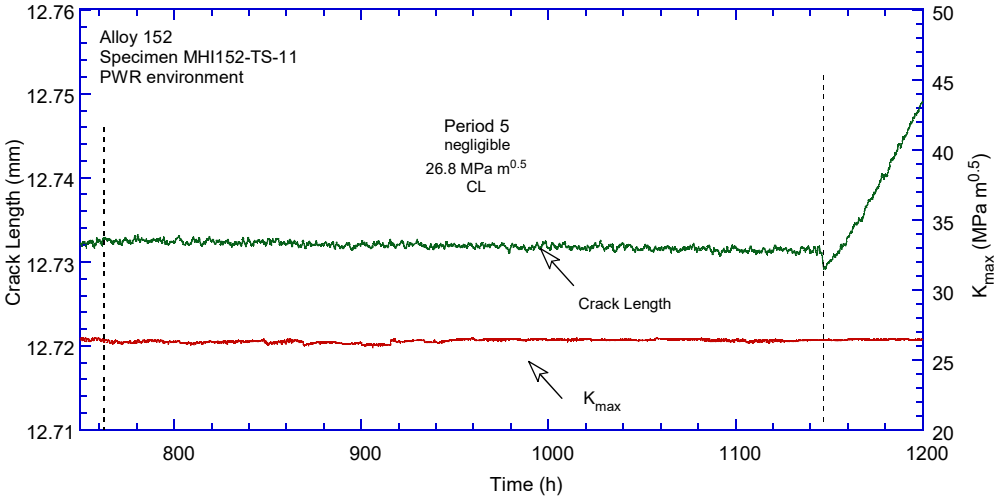

(d)

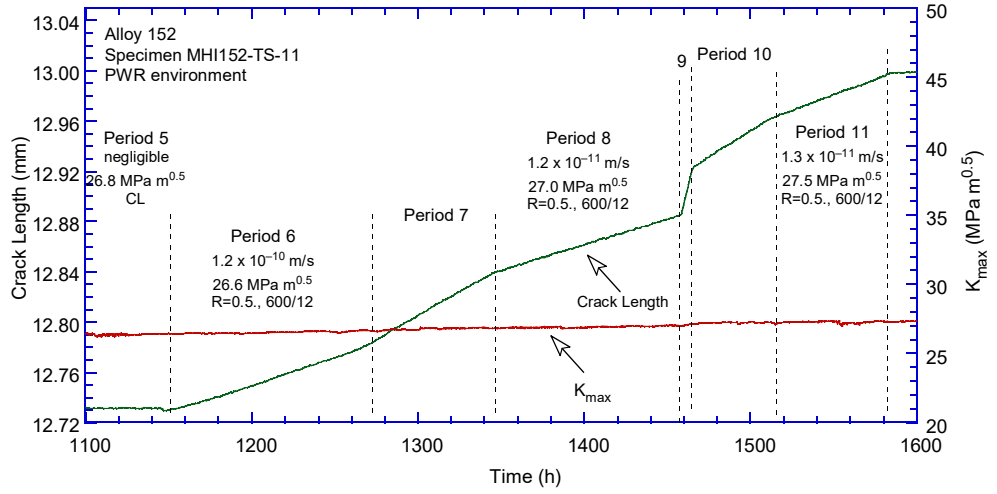

(e)

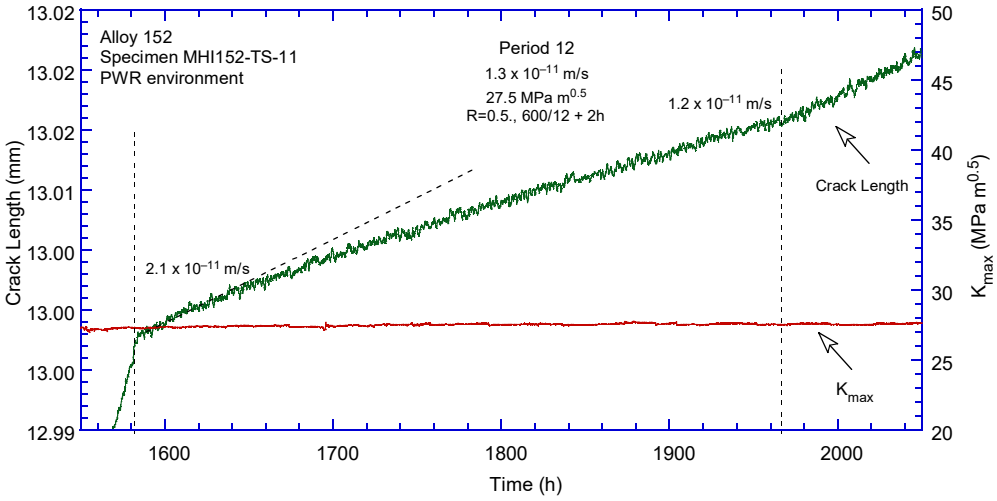

(f)

Figure 59 (cont.)

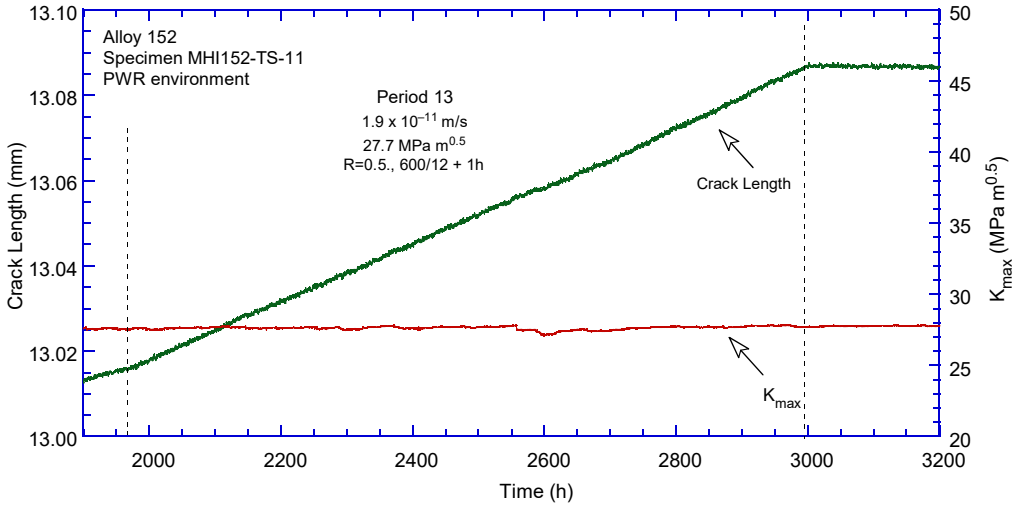

(g)

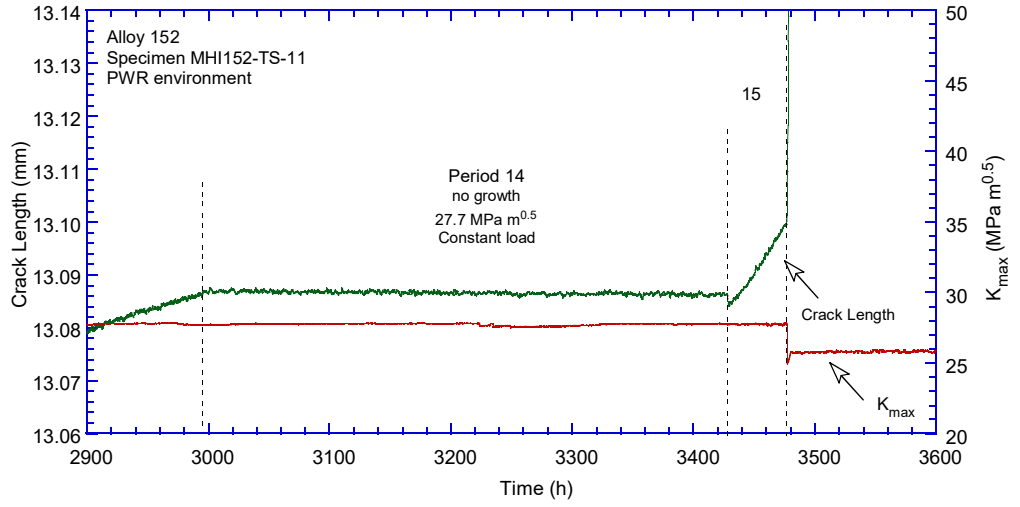

(h)

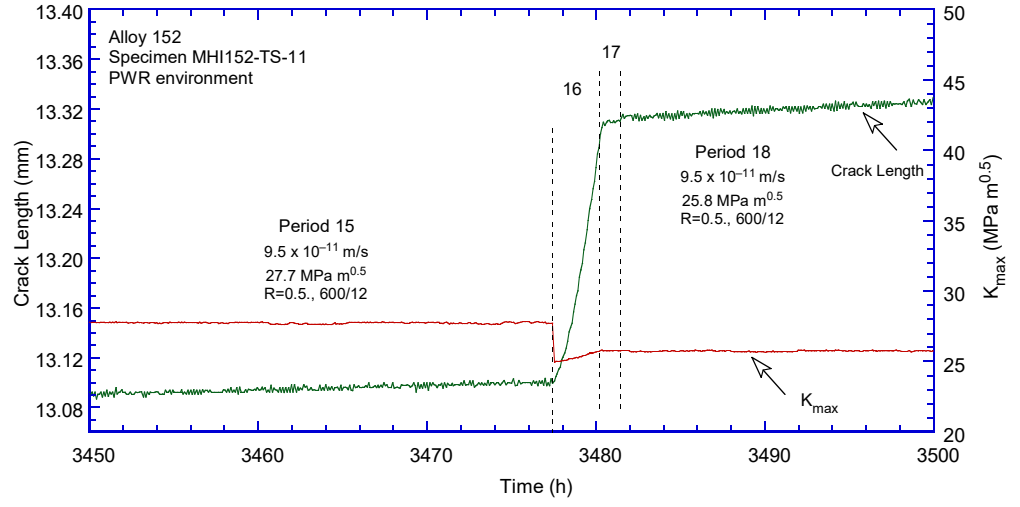

(i)

Figure 59 (cont.)

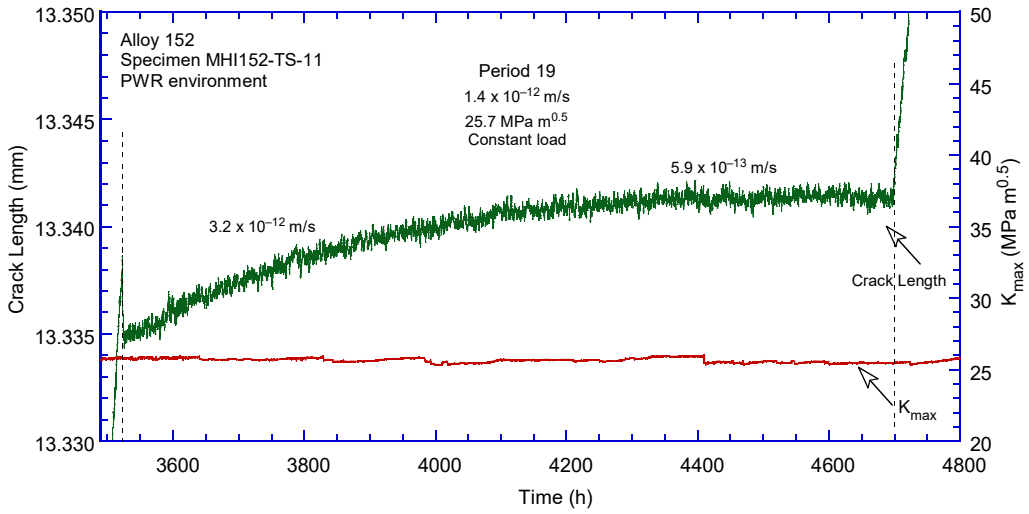

(j)

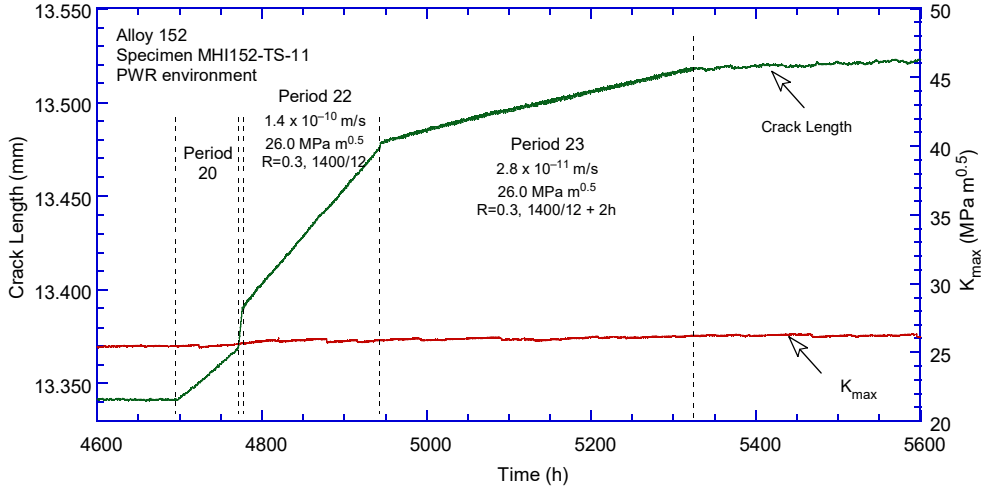

(k)

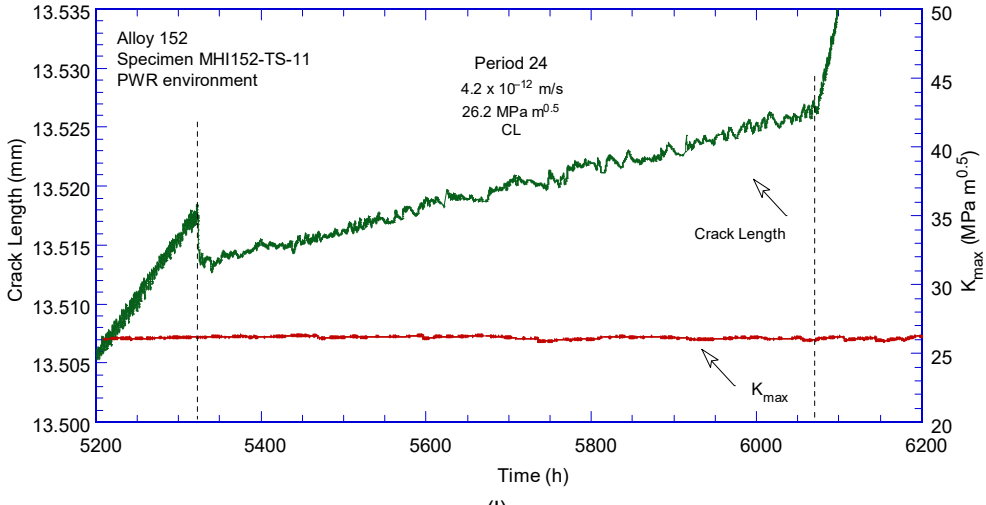

(l)

Figure 59 (cont.)

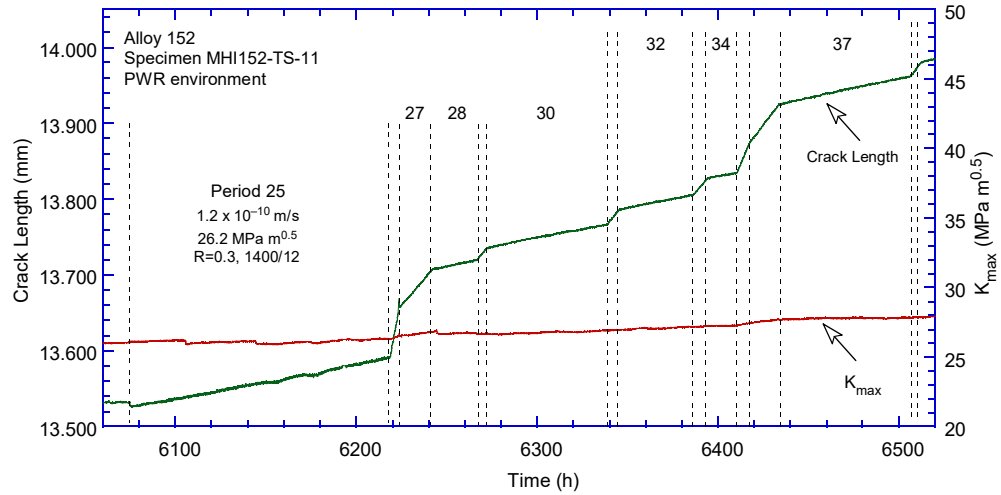

(m)

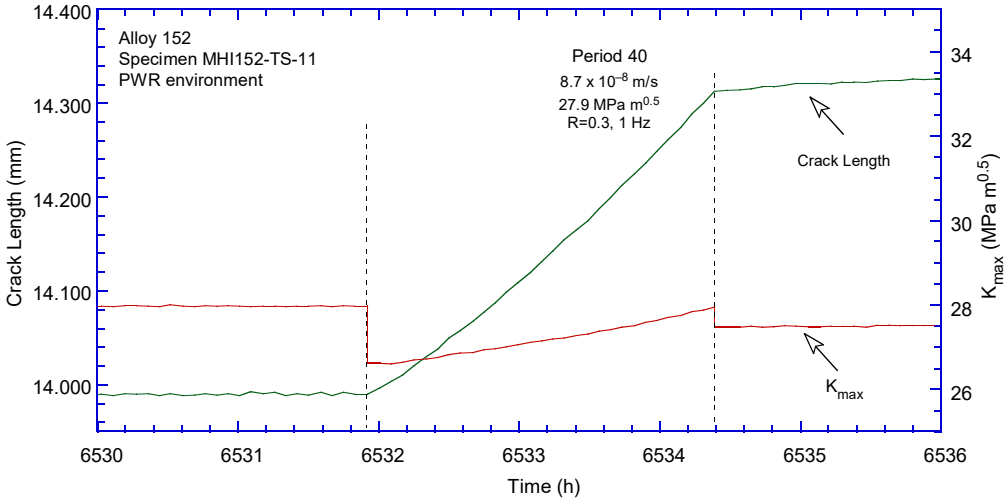

(n)

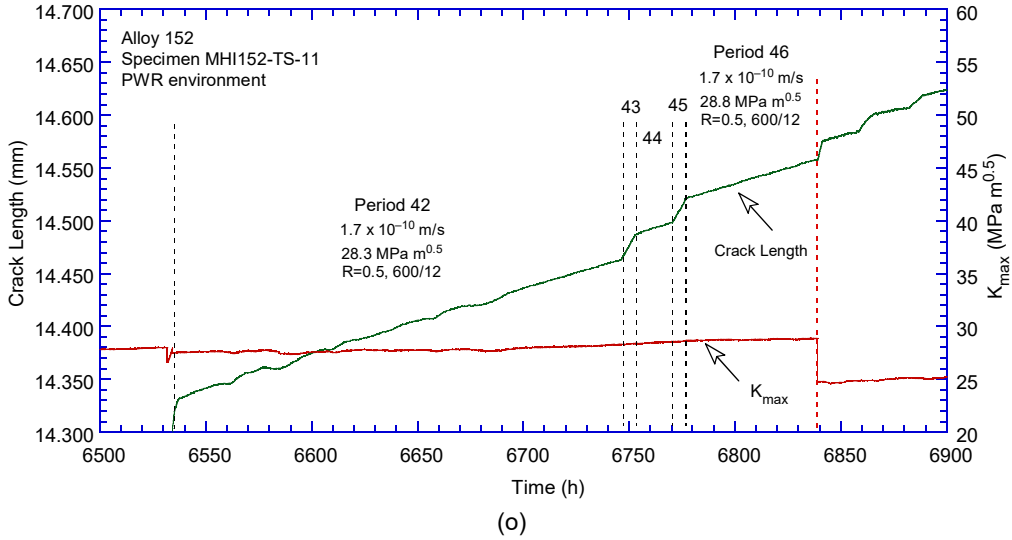

(o)

Figure 59 (cont.)

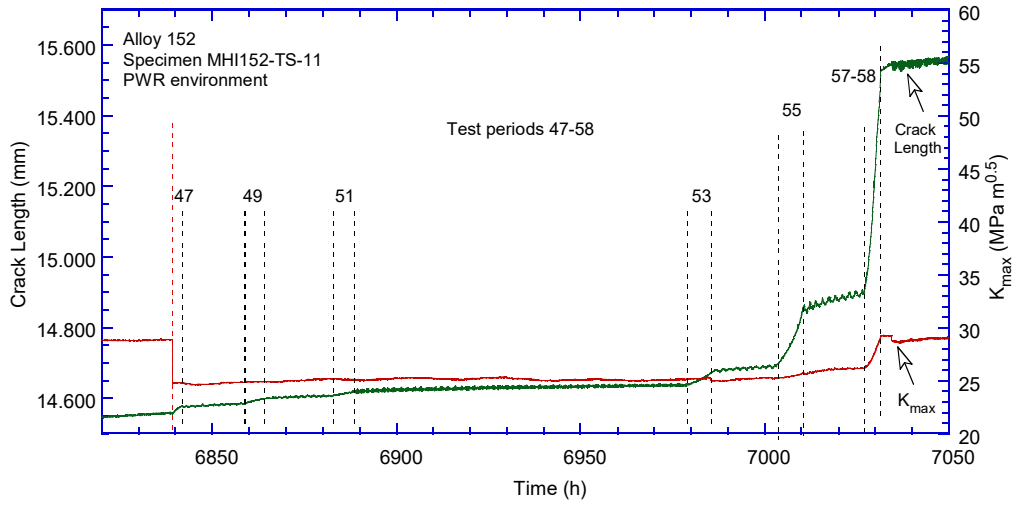

(p)

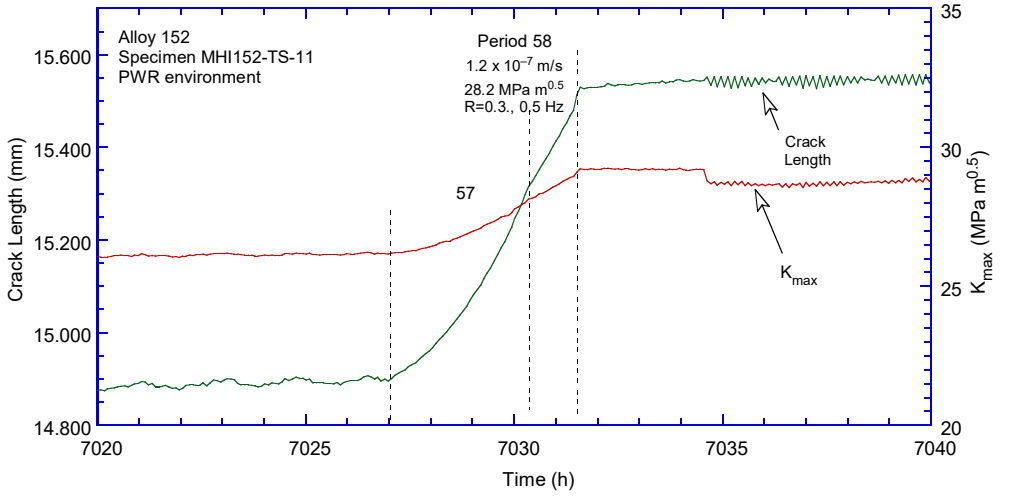

(q)

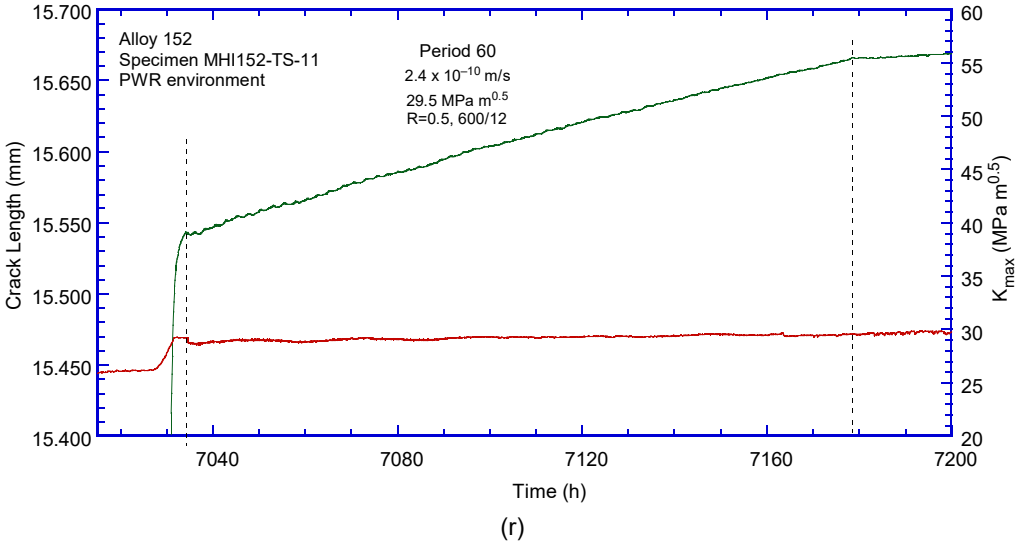

(r)

Figure 59 (cont.)

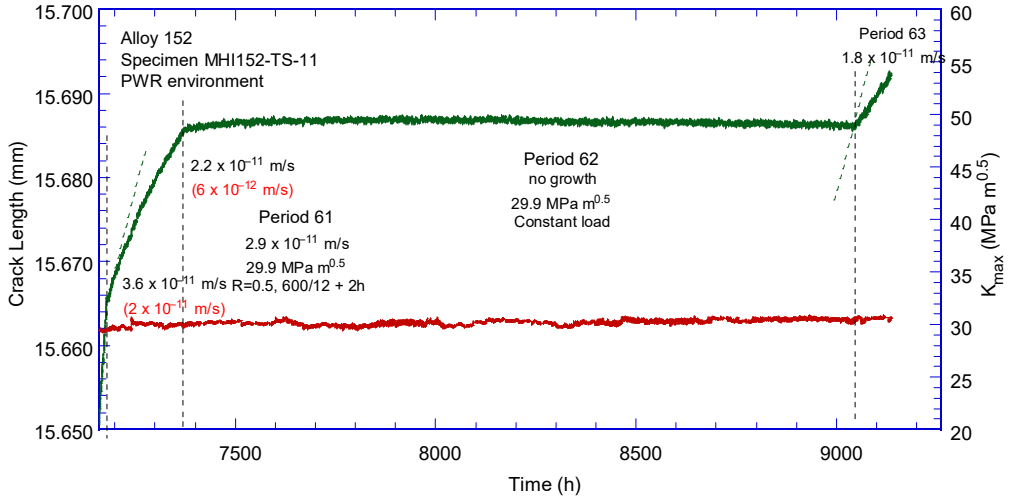

(s)

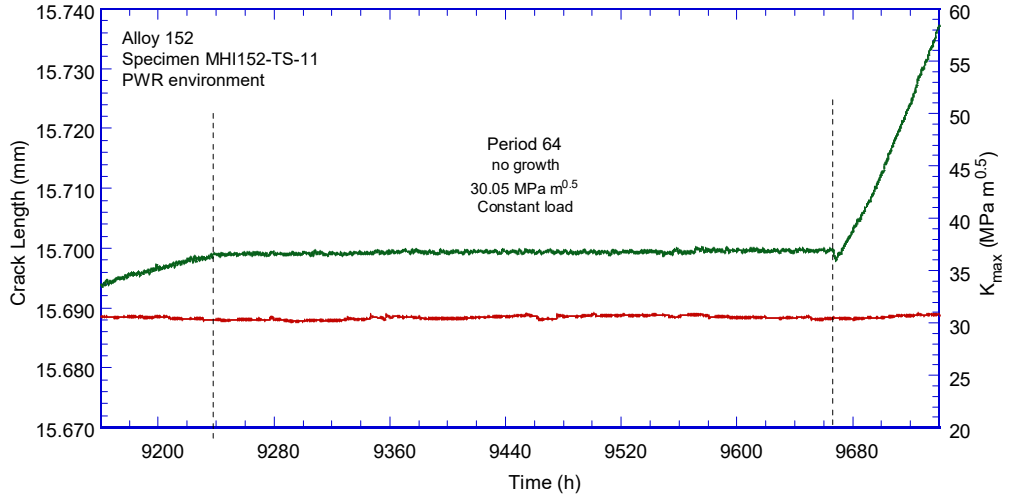

(t)

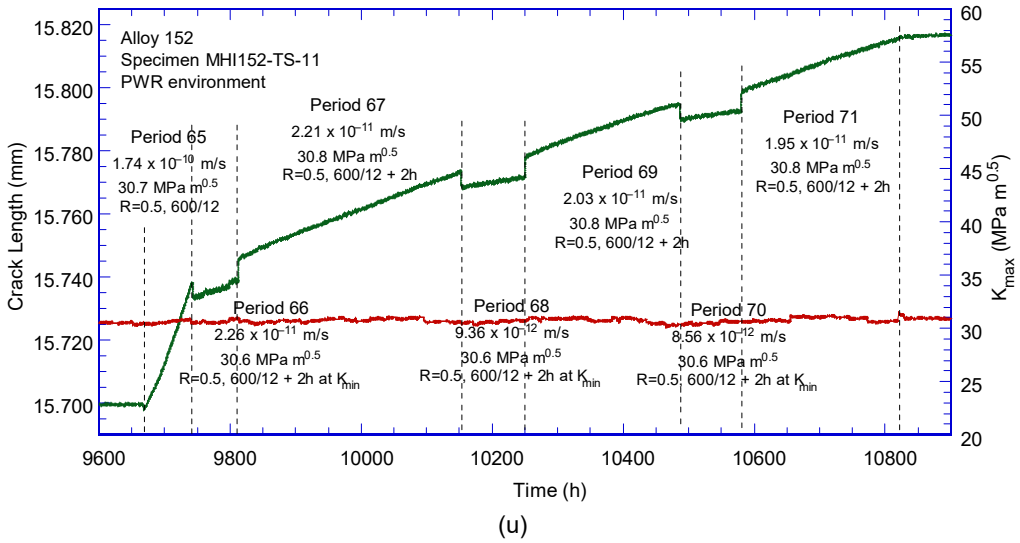

(u)

Figure 59 (cont.)

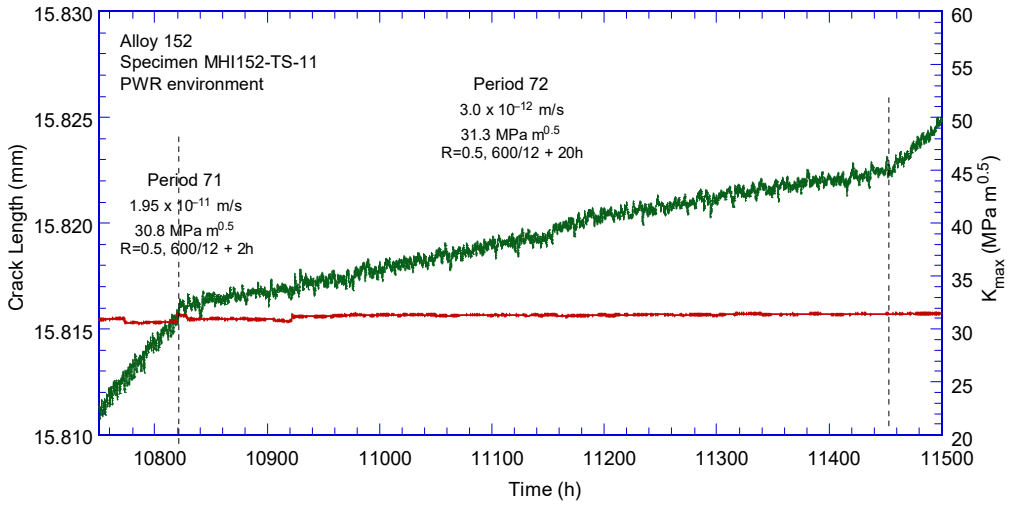

(v)

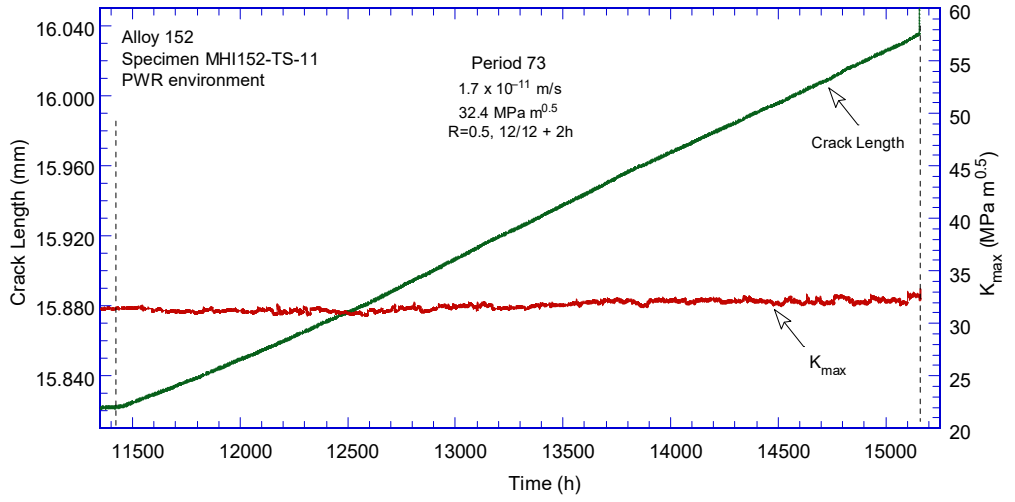

(x)

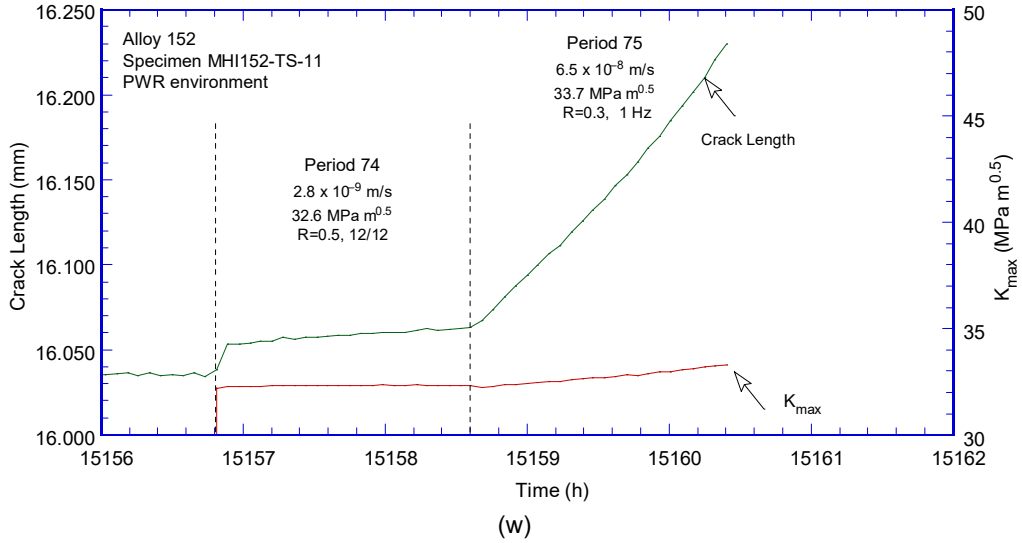

(w)

Figure 59 (cont.)

Figure 60 shows the cyclic CGR data obtained for the current MHI152-TS-11 specimen. In Figure 60a, for comparison, the data obtained on the previous MHI152-TS-1 specimen, and the corrosion fatigue curve for Alloy 182 was included. The data sets are initially in excellent agreement, then, the environmental enhancement in the current specimen appears to decrease. The reason for the decrease is unclear, but was observed in the previous specimen in the second part of the test. Figure 60b shows the evolution of the fatigue response after the power failure in test period 47; the known rate was reproduced only in test period 58, suggesting that that the crack left the plastic zone that occurred due to the power failure.

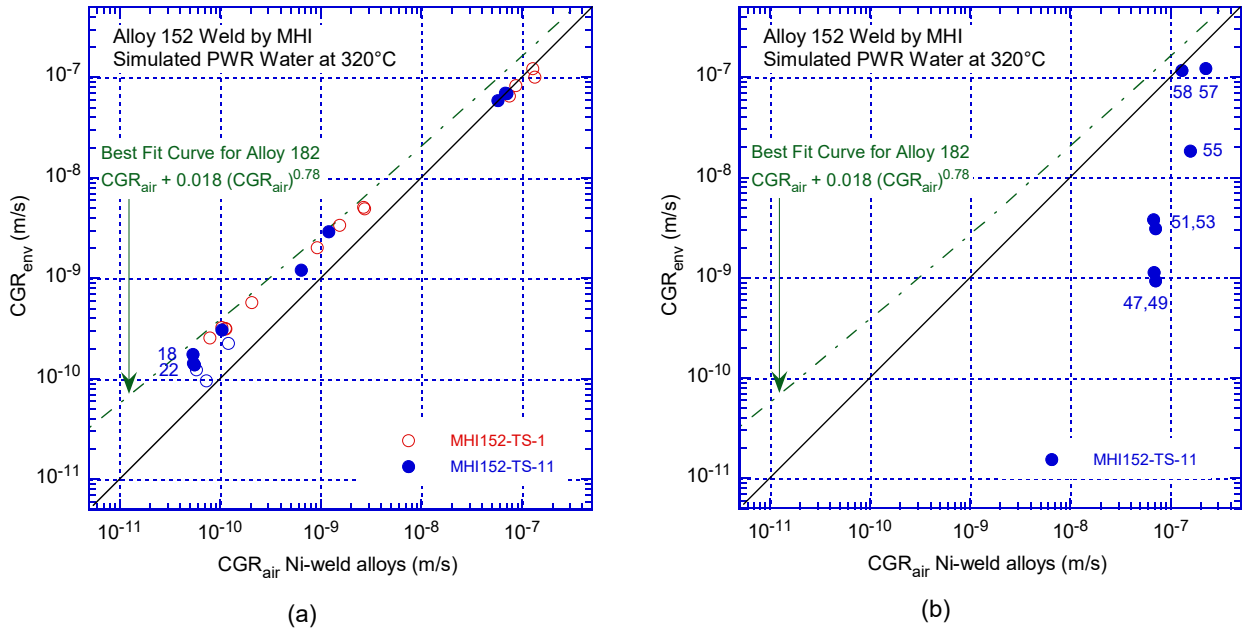

Figure 60 (a) Cyclic CGR data in simulated PWR environment for Alloy 152 weld produced by MHI for the Kewaunee reactor, and (b) Evolution of the fatigue behavior after the power shutdown in test period 46; the expected response was obtained only in test period 58.

Figure 61 shows the environmental enhancement for select conditions as well as the resulting SCC CGRs for test specimen MHI152-TS-11 as a function of the distance from the specimen notch. The response from fatigue test periods (black symbols) is also included, and the expected outcome for these conditions is "1". Initially, the environmental enhancement appears to decrease with crack advance, and this effect was also observed in the second part of the test on previous specimen MHI152-TS-1. Later on, a higher environmental enhancement was obtained in test period 18 and a measurable SCC CGR was measured in test period 19. The observation was repeated in test period 22 under cycling at a more aggressive load ratio. Overall, there seems that the environmental enhancement drops after a test period at constant load (see for example, 3-6, 11-15, 18-20, 22-25 in Figure 61), and the reason is unclear. One plausible explanation would be a case where the most susceptible direction is oriented differently than the main crack front. Currently there is no experimental solution to overcome off-plane cracking. Observations at the end of the test seem to indicate that there is a discrepancy between cyclic and constant load SCC CGRs.

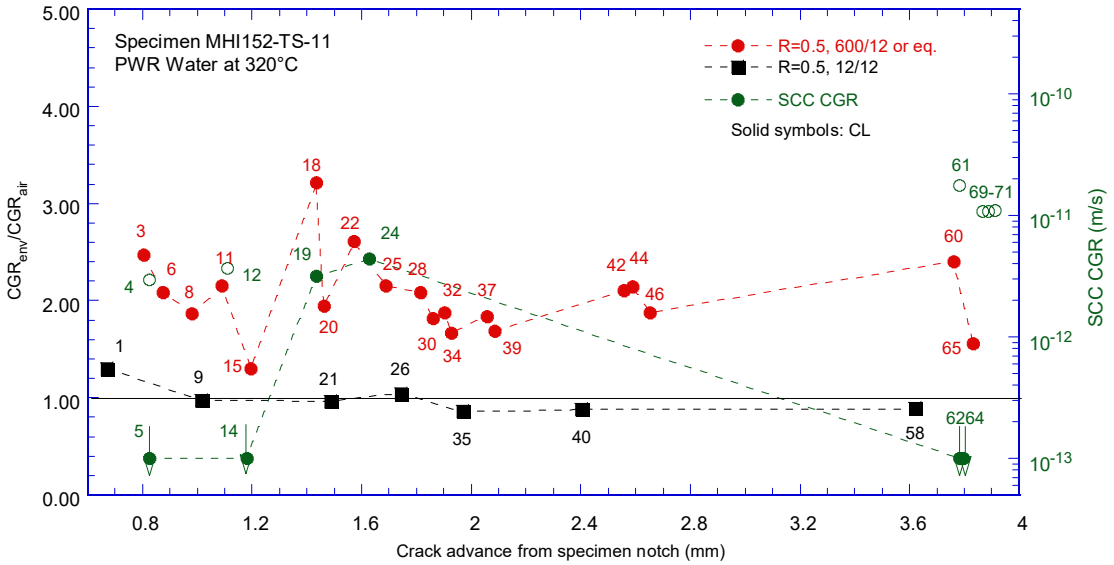

Figure 61 Environmental enhancement and SCC CGRs for Alloy 152 test specimen MHI152-TS-11 as a function of the distance from the specimen notch

The post-test examination involved both the side surfaces and the fracture surface. The two side surfaces are shown in Figure 62.

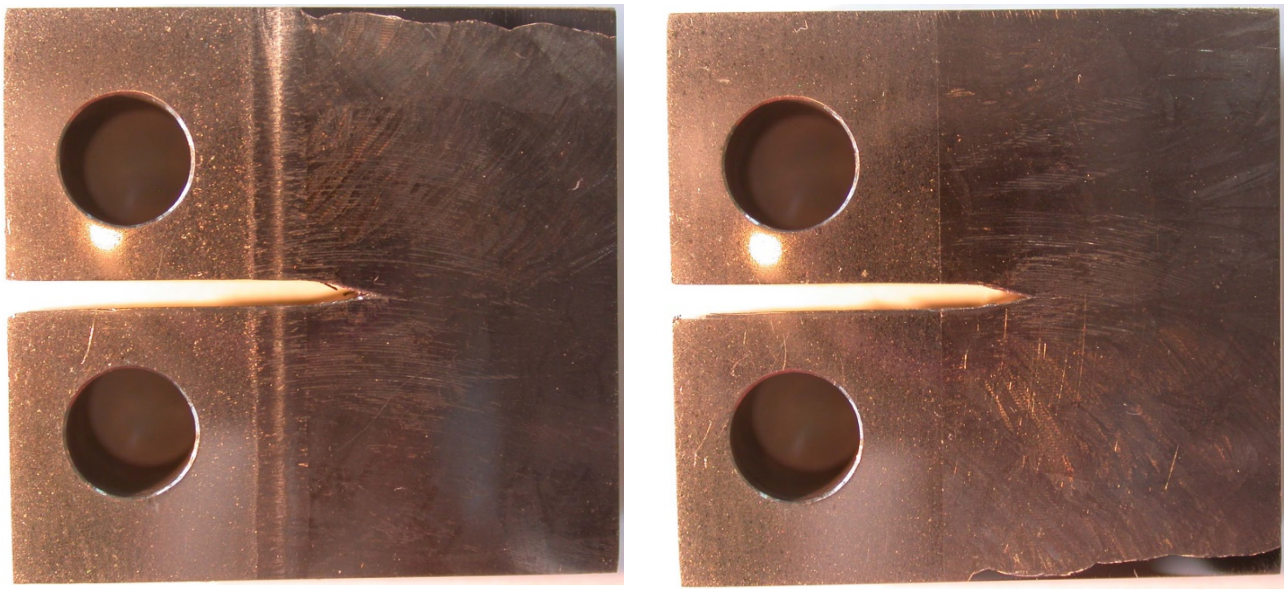

(a) (b)

Figure 62 Side surfaces of specimen MHI152-TS-11. This specimen was cut from the 1T CT specimen MHI152-TS-1that was previously tested in primary water. In order to accommodate the dimensions (ears), a piece of Alloy 690 had to be EB-welded (left side of each picture).

The side surfaces were further examined in the SEM, Figure 63 (side 1) and Figure 64 - Figure 65 (side 2). Both side surfaces show evidence of crack branching (Figure 63a, Figure 64b,c),

and off-plane cracking and branching at the end of the test (Fig. Figure 64b and Figure 65b). The latter was especially surprising given that this test ended with PPU.

The fracture surface is shown in Figure 66, and several locations of interest were subjected to further examination. Figure 67 is an image taken at location 1 in Figure 66 and shows a mixed IG-TG fracture mode. The TG occurred most likely due to the aggressive loading at R=0.5, 12/12 (see Figure 61, fast test periods 1-40 are shown with black symbols). The IG fraction in this region is initially large, 82%, and decreases to 66%.

Additional transitioning attempts were made later on in the test (see locations 2,3 in Figure 66), but the resulting IG does not appear extensive. Figure 68b shows evidence of off-plane cracking.

Figure 69 shows the end of the test. The darker band corresponds to the last fatigue test period in room temperature air, and on occasion, IG fracture was observed to extend in it. However, the IG fracture observed in this last part of the test is only 62%, hence, the “jump” observed in test period 74 (Figure 59w) was small.

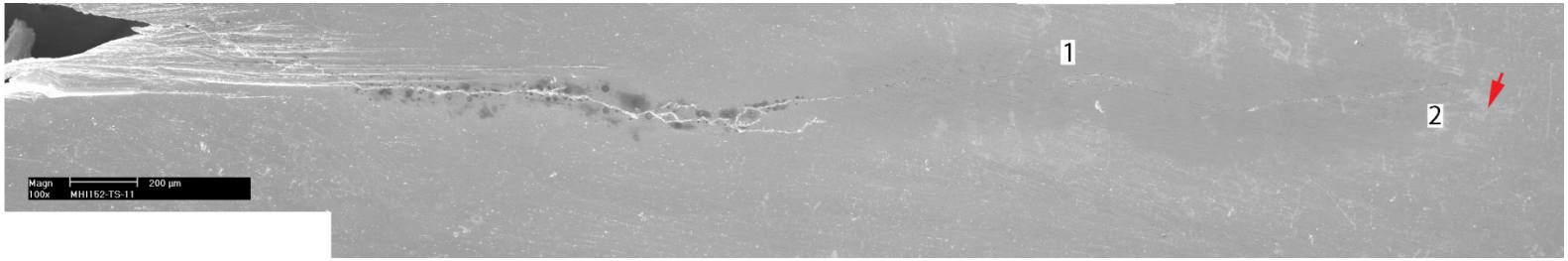

(a)

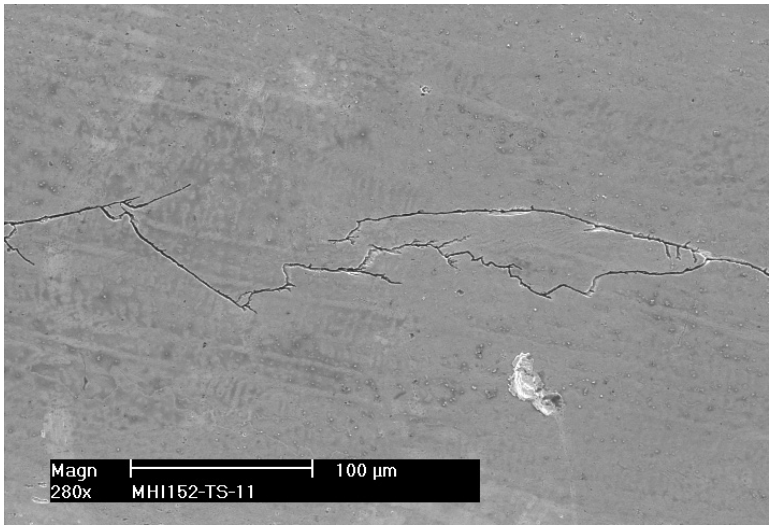

(b)

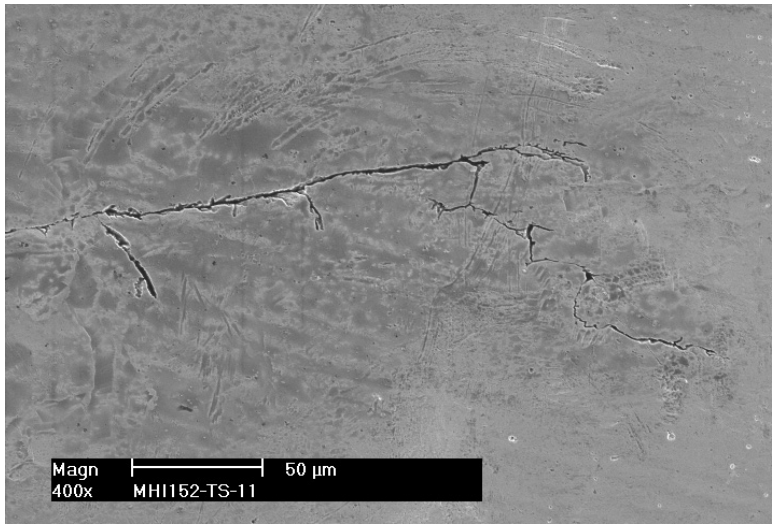

(c)

Figure 63 (a) Cross section 1 of Specimen MHI152-TS-11: (a) (b) detail at location 1, and (c) detail at location 2. Crack advance is from left to right.

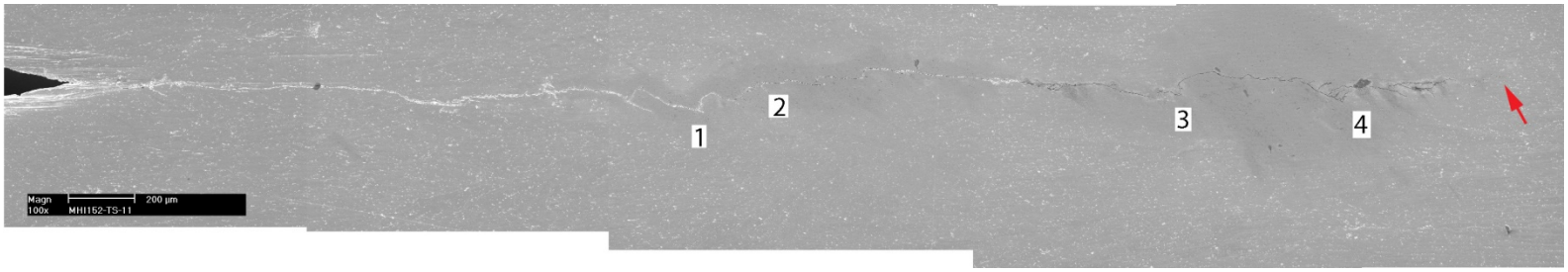

(a)

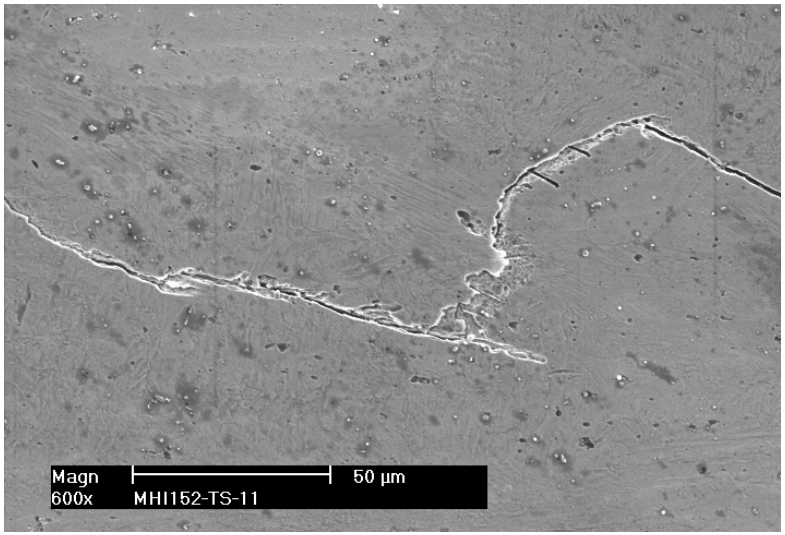

(b)

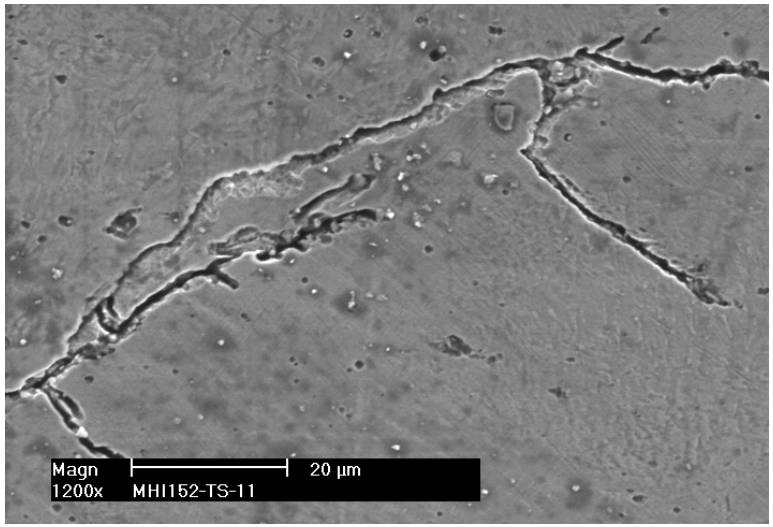

(c)

Figure 64 **(a) Cross section 2 of Specimen MHI152-TS-11: (a) (b) detail at location 1, and (c) detail at location 2. Crack advance is from left to right.**

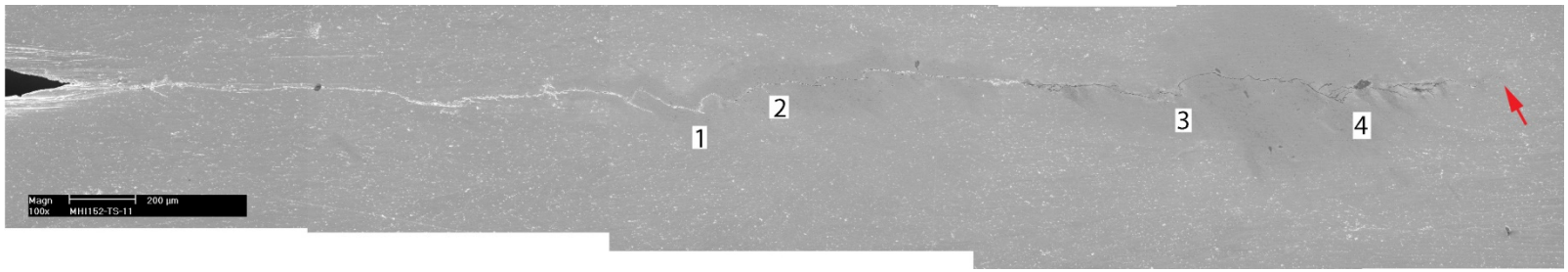

(a)

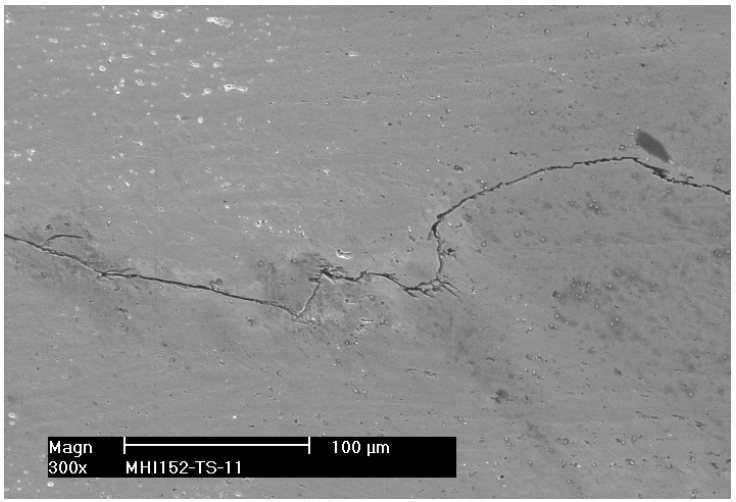

(b)

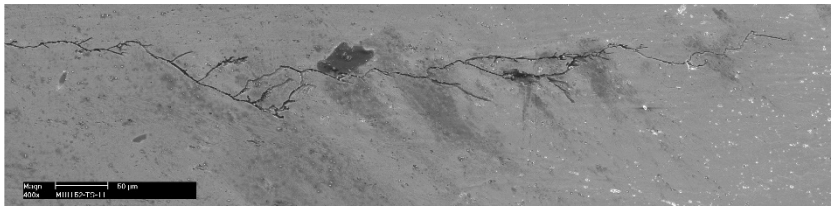

(c)

Figure 65 **(a) Cross section 2 of Specimen MHI152-TS-11: (a) (b) detail at location 3, and (c) detail at location 4. Crack advance is from left to right.**

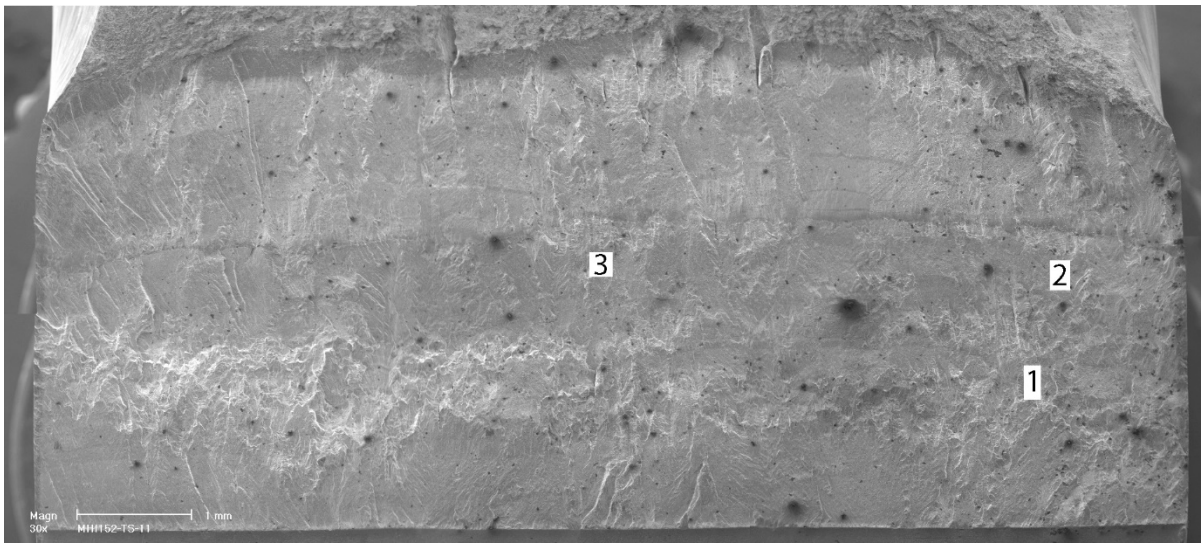

Figure 66 Fracture surface time of Alloy 152 weld specimen MHI152-TS-11 tested in simulated PWR environment. Crack advance is from bottom to top.

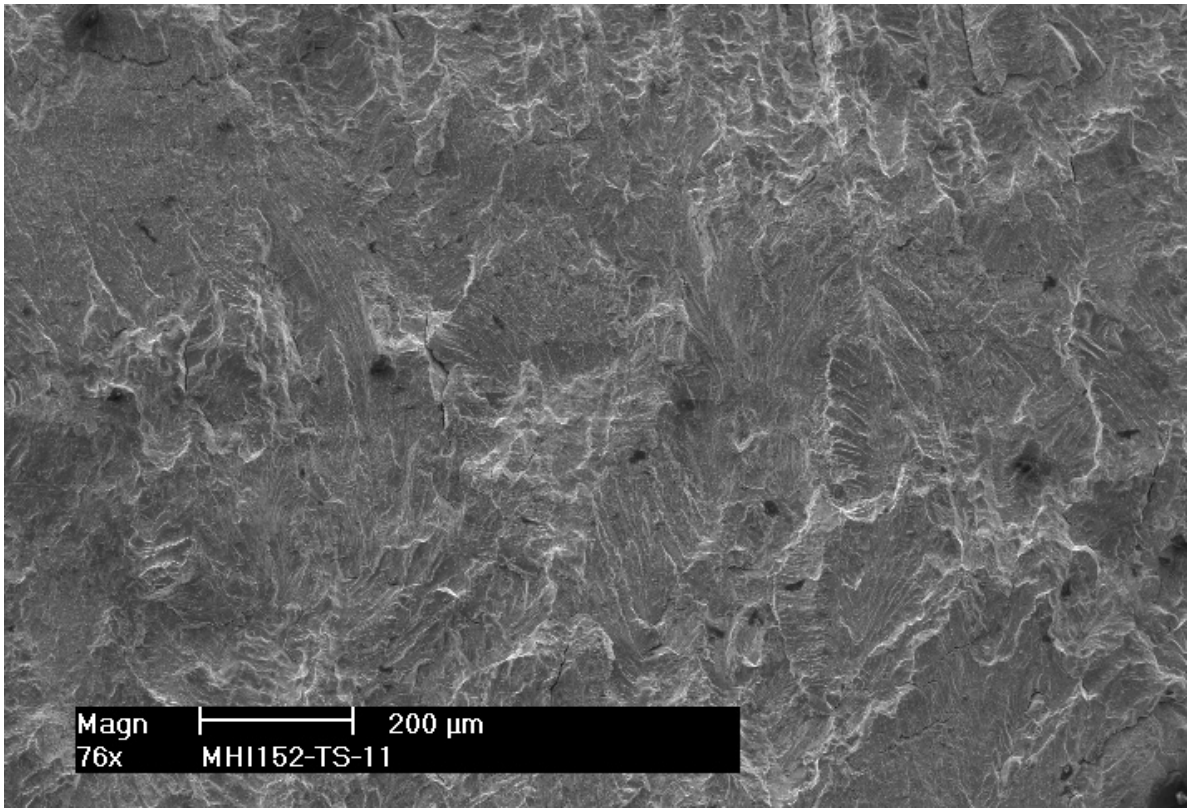

Figure 67 Fracture surface time of Alloy 152 weld specimen MHI152-TS-11 tested in simulated PWR environment, location 1 in Figure 66. Crack advance is from bottom to top.

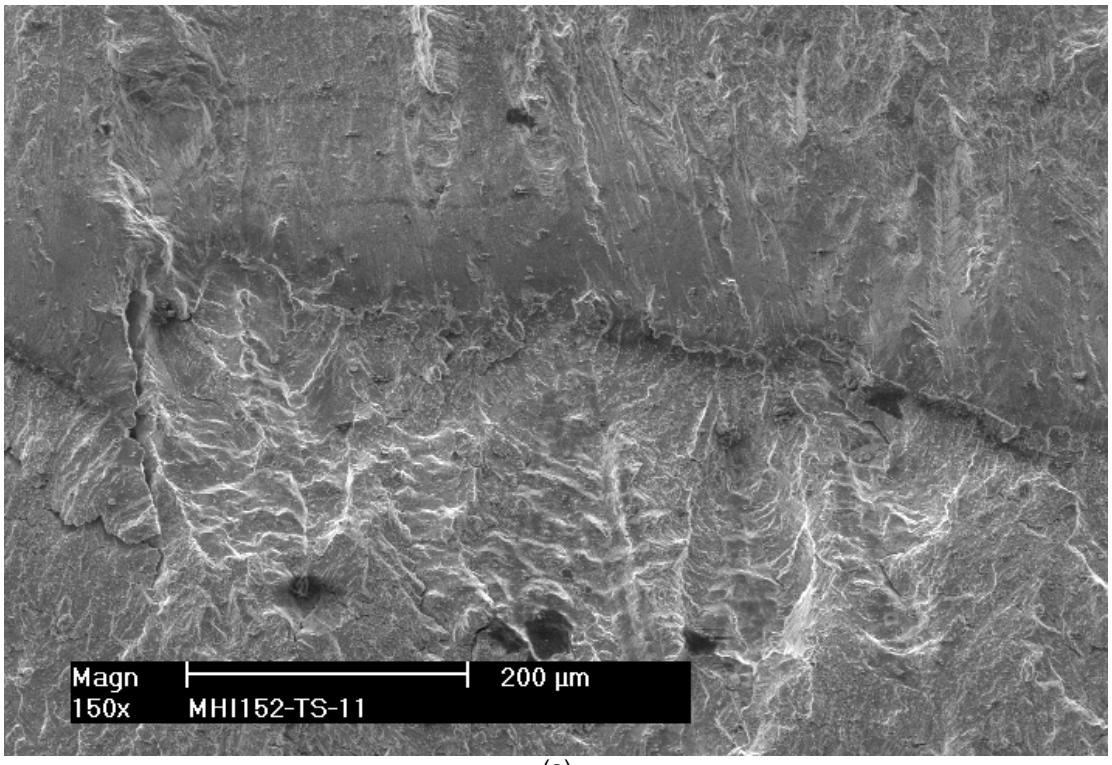

(a)

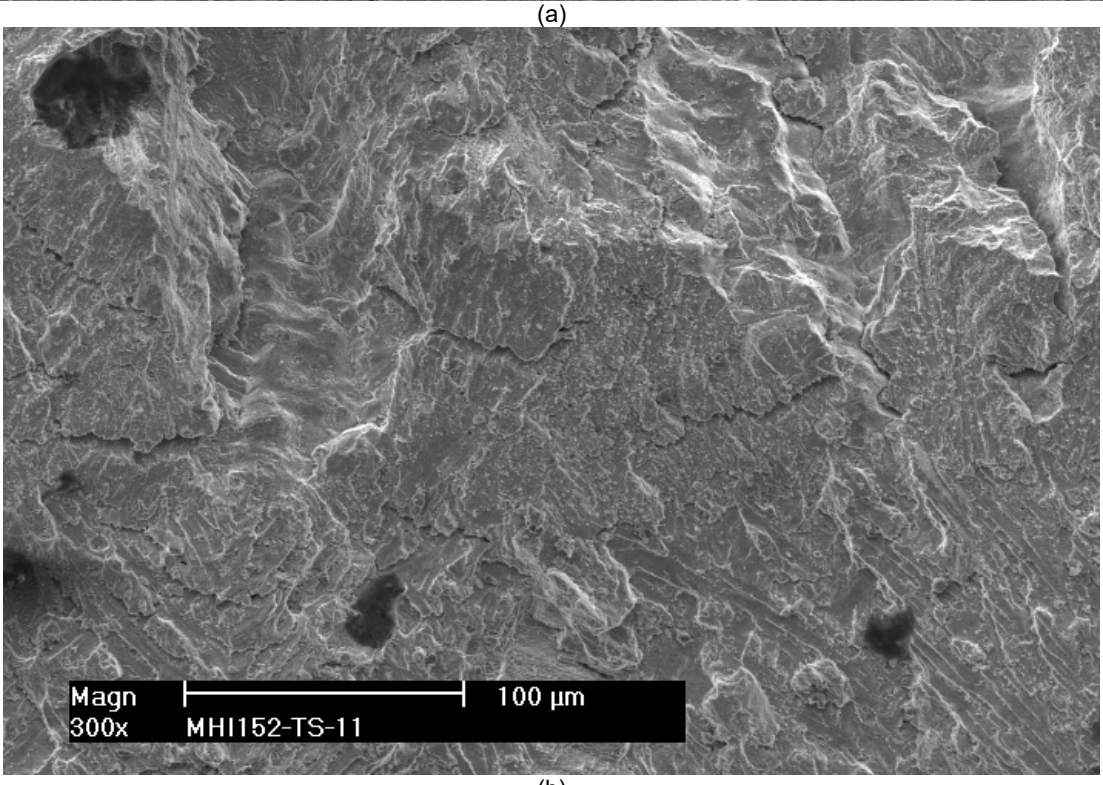

(b)

Figure 68 Fracture surface time of Alloy 152 weld specimen MHI152-TS-11 tested in simulated PWR environment, locations (a) 2, and (b) 3 in Figure 66. Crack advance is from bottom to top.

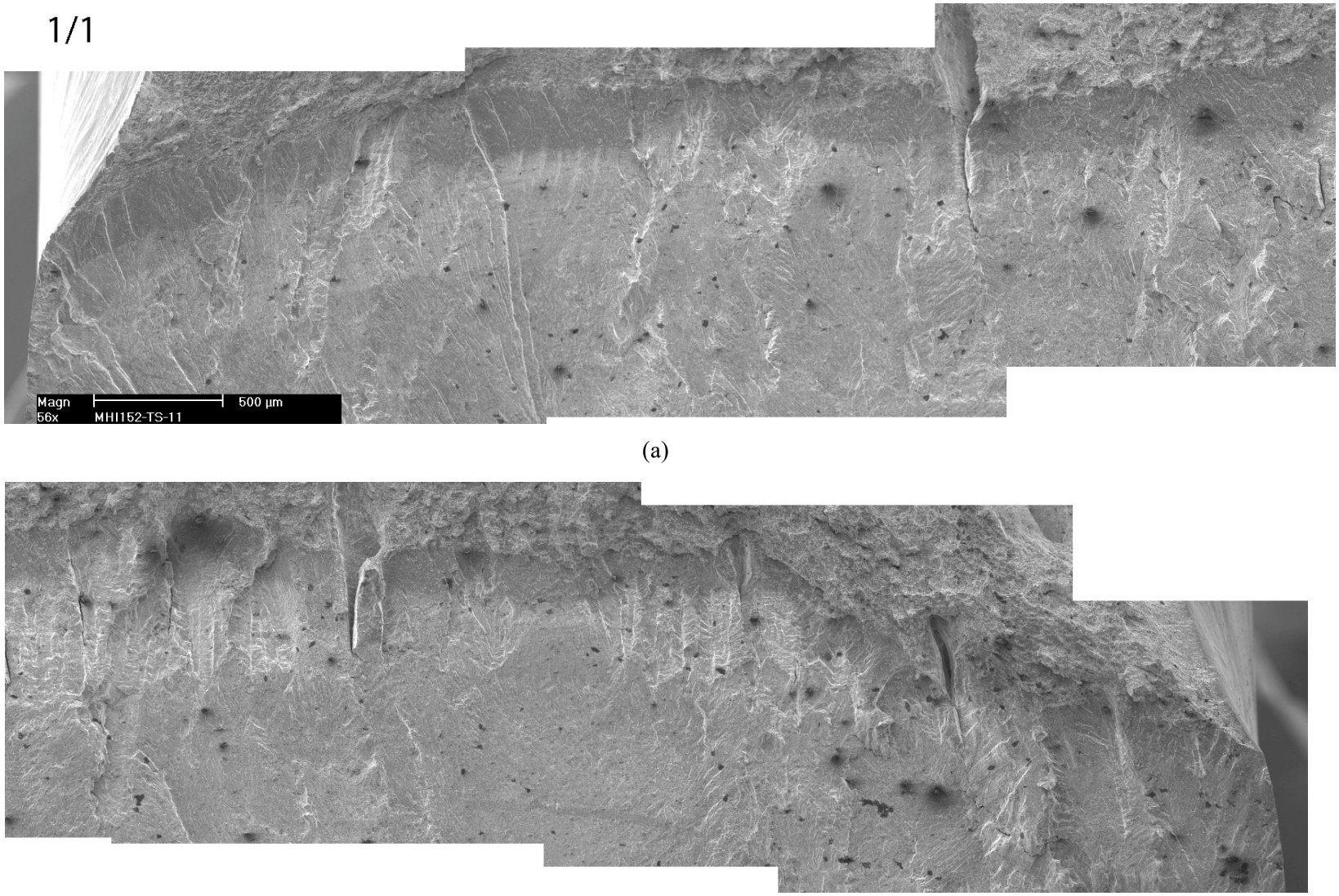

Figure 69 **Fracture surface of Specimen MHI152-TS-11 during the final stages of the test: (a) first half, and (b) second half. Crack advance is from left to right.**

3.3 The effect of Welding Parameters on SCC CGR response

In order to study the effect of the welding parameters on the SCC CGRs of Ni-base Alloy 52/152 welds, CGR testing was carried out on three Alloy 152 weldments produced at ANL with varying parameters, two Alloy 52M welds produced by EPRI with a high heat input, and an Alloy 152M weldment produced by IHI. The tests are presented in the order they were completed. For the ANL-produced welds, the order was "high current" weld, "normal" weld, and the "high heat input" weld.

3.3.1 Specimen HC152-CR-1, "high current" weld produced by ANL

The test specimen HC152-CR-1 was machined from the Alloy 152 weldment produced at ANL using typical welding parameters (joint B in Figure 7). The testing conditions for specimen HC152-CR-1 are given in Table 15, and the changes in crack length and K_{max} with time are shown in Figure 70. The specimen was precracked and transitioned in the simulated primary water environment. The SCC CGR component calculated by superposition in test period 4 was 1.4×10^{-11} m/s, hence the specimen was set at constant load in test period 5. The initial SCC CGR was $6.0\ 10^{-12}$ m/s and decreased to 3.0×10^{-12} m/s over approx. 1,500 h. The test continued with additional transitioning, and the SCC CGR component was calculated by superposition again in test period 7, and was 1.3×10^{-11} m/s. The specimen was set at constant load in test period 8, and SCC CGR measured over approx. 1,000 h was 3.0×10^{-12} m/s.

From the above observations, there appears to be a factor 2-4 discrepancy between the SCC CGRs measured at constant load and the SCC CGR components calculated by superposition using cycle + hold loading conditions. The magnitude of the discrepancy seems consistent with the correction factor one typically applies to weld SCC CGR data obtained at constant load based on post-test measurements on the fracture surface that account for the formation of ligaments. In order to test whether it is the formation of ligaments that cause the decreased SCC CGR response under constant load, constant load with periodic unloading (2h) was introduced in test period 9. The response seemed consistent with the ligament-breaking hypothesis as it matches fairly well the rates calculated by superposition. In summary, the SCC CGR for this weld specimen seems to be 1.3×10^{-11} m/s at K = 27 MPa $m^{1/2}$. Constant load with periodic unloading was maintained for a total of approx. 1,700h and approx. 80 microns of growth. Next, the specimen was set at constant load in test period 10. It was observed that the rate measured in test period 9 only lasted for approx. 5h into test period 10 (see Figure 70h). Hence, in order to provide a minimum of "help" to keep the crack moving along, the test condition was changed to constant load with periodic unloading every 5 h. The effect is shown in Figure 70i, where the time of change was adjusted to "0" and each dotted line corresponds to an 12s/12s unload/reload. The first 5h period saw no growth, while the rate for the subsequent two was approx. 1.1×10^{-11} m/s. The average rate for the subsequent 600h was approx. 8.0×10^{-12} m/s, however, the apparent growth was less well-behaved. For example, Figure 70j shows that the rate dropped substantially around 5,200h, then rebounded immediately after that to a rate close to 1.0×10^{-11} m/s. As such, it appears that the current unload/reload frequency is not effective at breaking the ligaments in this specimen. Thus, the unload period was reduced to 2h to reproduce the previous condition, then set at constant load in test period 13. As the crack appeared to stall at approx. 5,730 h, cycling was reintroduced in an attempt to reactivate the crack, then set at constant load in test period 15. The SCC CGR response was low (consistent with the end of test period 13), and the overall behavior is less well-behaved than observed previously.

Next, the crack was advanced for approx. 1 mm to a different microstructure with the goal of continuing testing at a similar K = 29 MPa $m^{1/2}$ as before, and transitioned to SCC. The fatigue and corrosion fatigue measured initially have essentially been duplicated in this process (see also Figure 71c). Next, the specimen was set at constant load in test period 24. The initial response of approx. 4.0 x 10^{-12} m/s diminished over time, concomitant with some technical problems with the water pressure pump. The test was stopped, the pump was fixed, and cyclic resumed in test period 25. A 2-h hold was introduced in test period 26 at K_{min}, then at K_{max} as usual in test period 27. By alternating the hold times between K_{max} and K_{min} in otherwise identical loading waveforms, it is anticipated that an additional estimate of the SCC CGR can be made. As such, in the first scenario with the hold time at K_{max}, the measured CGR consists of a corrosion fatigue component plus an SCC component during the 2h hold time at K_{max}. In the subsequent test period, with the hold at K_{min}, the CGR is only due to corrosion fatigue due to cyclic loading; during the hold time, the specimen is practically unloaded, so no SCC growth is expected. The SCC CGR is a simple subtraction between the CGRs measured under the two loading schemes. One observes that da/dN in test period 26 was similar to that in test period 25, and the calculation of the SCC CGR component showed no SCC growth in test period 26. Next, test period 27 produced a similar rate as test period 26 initially, followed by a higher rate as perhaps the SCC fracture mode took hold. Since test periods 26 and 27 have a very similar loading, and no SCC growth occurred during hold at K_{min} in test period 26, the difference between the total rates in test periods 27 and 26 is expected to provide a good estimate of the SCC CGR. As such, based on the rates measured in test periods 27 and 26, the SCC CGR appears to be approx. 1 x 10^{-12} m/s. This rate was measured directly at constant load in test period 28 for the first approx. 600h, then the rate appeared to diminish by approx. a factor 3. The test was stopped after approx. 1,400 hrs at constant load. Next, the autoclave system was cooled down and drained of water. The final test period (29) consisted of fatigue in air, Figure 70r, and was conducted with the purpose of determining whether ligaments has formed during the previous test period at constant load. Some accelerated growth was observed initially, suggesting that some ligaments had developed, masking the true crack advance. If these are taken into account, a conservative estimate for the SCC CGR in test period 28 is approx. 3 x 10^{-12} m/s. Next, the specimen was broken open and the fracture surface was examined.

Table 15 Crack growth data for Alloy 152 specimen HC152-CR-1 in PWR water[a].

Test Period	Test Time, h	Temp. °C	Load Ratio R	Rise Time, s	Down Time, s	Hold Time, s	K_{max}, MPa·$m^{1/2}$	ΔK, MPa·$m^{1/2}$	CGR_{env}, m/s	Estimated CGR_{air}, m/s	Crack Length, mm
Pre a	26	320.3	0.30	1	1		25.3	17.7	4.84E-08	6.76E-08	12.133
Pre b	44	320.2	0.30	50	50		25.6	17.9	2.27E-09	1.41E-09	12.216
Pre c	45	320.3	0.30	1	1		25.9	18.1	5.92E-08	7.46E-08	12.324
Pre d	49	320.3	0.30	5	5		26.3	18.4	1.63E-08	1.60E-08	12.457
1	73	320.3	0.50	120	12		26.6	13.3	5.38E-10	2.98E-10	12.508
2	115	320.4	0.50	300	12		26.7	13.4	2.40E-10	1.22E-10	12.544
3	212	320.5	0.50	600	12		26.9	13.4	1.49E-10	6.27E-11	12.596
4	405	320.5	0.50	600	12	7,200	26.9	13.5	2.12E-11	4.85E-12	12.613
5	1,892	320.4	1.00	0	0		27.0	0.0	4.11E-12	-	12.636
6	1,964	320.9	0.50	600	12		27.2	13.6	1.76E-10	6.58E-11	12.677
7	2,065	320.8	0.50	600	12	7,200	27.2	13.6	1.62E-11	5.10E-12	12.686
8	3,067	321.0	1.00	0	0		27.3	0.0	2.78E-12	-	12.696
9	4,745	320.3	0.50	12	120	7,200	27.5	13.7	1.23E-11	5.68E-12	12.770
10	4,817	320.3	1.00	0	0		27.5	0.0	1.81E-12	-	12.772

Table 15 (cont.)

Test Period	Test Time, h	Temp. °C	Load Ratio R	Rise Time, s	Down Time, s	Hold Time, s	K_{max}, MPa·m$^{1/2}$	ΔK, MPa·m$^{1/2}$	CGR_{env}, m/s	Estimated CGR_{air}, m/s	Crack Length, mm
11	5,494	321.8	0.50	12	12	18,000	27.5	13.8	7.90E-12	2.33E-12	12.790
12	5,568	321.5	0.50	12	12	7,200	27.5	13.7	1.43E-11	5.77E-12	12.793
13	5,761	321.3	1.00	0	0		27.5	0.0	2.84E-12	-	12.796
14	5,782	320.1	0.50	600	12		27.5	13.8	1.79E-10	6.87E-11	12.805
15	6,766	319.7	1	0	0		28.5	0.0	3.17E-12	-	12.816
16	6,769	319.8	0.30	1	1		29.3	20.5	8.96E-08	1.23E-07	13.270
17	6,772	320.5	0.30	1	1		26.3	18.4	5.75E-08	7.91E-08	13.520
18	6,791	320.4	0.30	50	50		26.5	18.6	2.69E-09	1.65E-09	13.597
19	6,791	320.1	0.30	1	1		27.9	19.5	7.51E-08	1.01E-07	13.927
20	6,795	319.9	0.50	12	12		28.1	14.1	4.50E-09	3.74E-09	13.980
21	6,814	320.1	0.50	120	12		28.3	14.2	7.48E-10	3.87E-10	14.028
22	6,843	319.5	0.50	300	12		28.5	14.2	3.76E-10	1.57E-10	14.056
23	7,006	319.4	0.50	600	12		29.1	14.6	2.05E-10	8.59E-11	14.187
24	7,658	319.0	1.00	0	0		29.1	0.0	8.18E-13	-	14.180
25	7,804	320.2	0.50	600	12		29.8	14.9	2.28E-10	9.58E-11	14.291
26	7,945	320.2	0.50	600	12	7,200 K_{min}	29.9	15.0	1.89E-11	7.48E-12	14.300
27	8,239	320.1	0.50	600	12	7,200 K_{max}	30.1	15.0	1.97E-11	7.59E-12	13.324
28	9,676	320.0	1.00	0	0		30.1	0.0	1.40E-12	-	14.329
29	9,705	23.7	0.25	5	5		28.1	21.1	4.96E-09	7.64E-09	14.388

[a]Simulated PWR water with 2 ppm Li, 1100 ppm B, and 2 ppm. DO<10 ppb. Conductivity was 21±3 μS/cm, and pH 6.4.

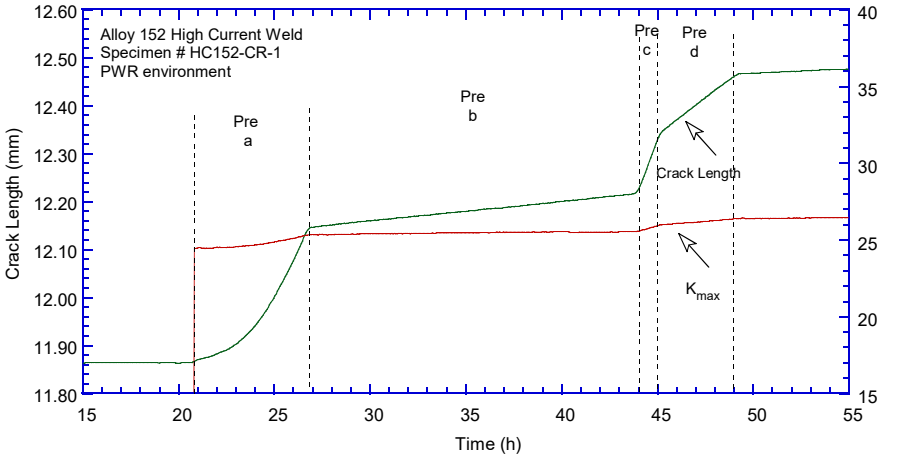

(a)

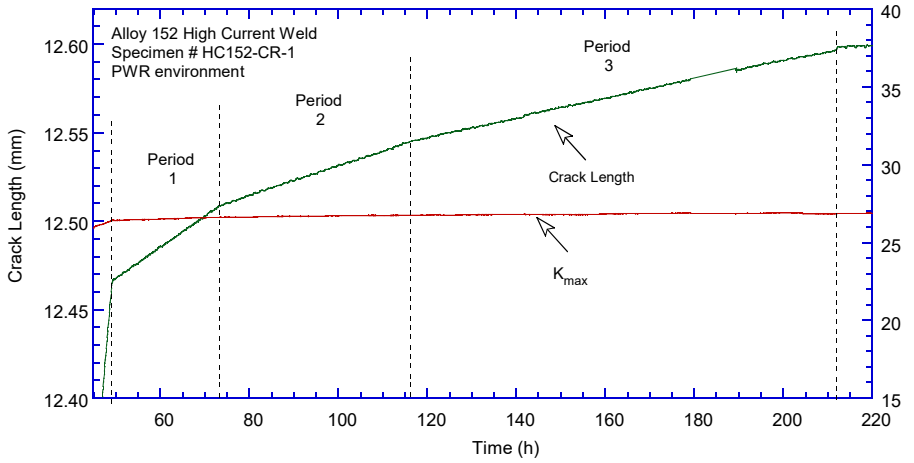

(b)

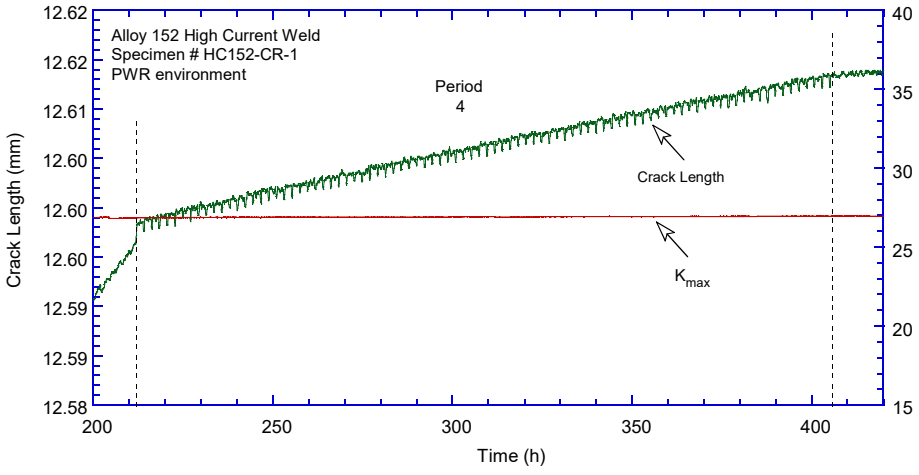

(c)

Figure 70 Crack–length–vs.–time for specimen Alloy 152 weld specimen HC152-CR-1 in simulated PWR environment during test periods (a) precracking, (b)1-3, (c) 4, (d) 5, (e) 6-7, (f) 8, (g) 9, (h) transition 9-10, (i) transition 10-11, (j) 11, (k) 11-13, (l) 14-15,(m) 16-20, (n) 21-23, (o) 24, (p) 25-27, (q) 28, and (r) 29.

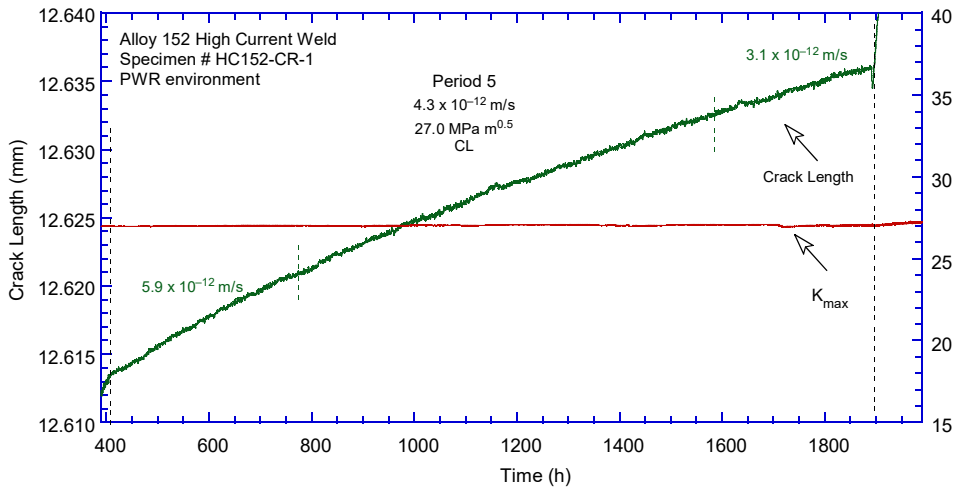

(d)

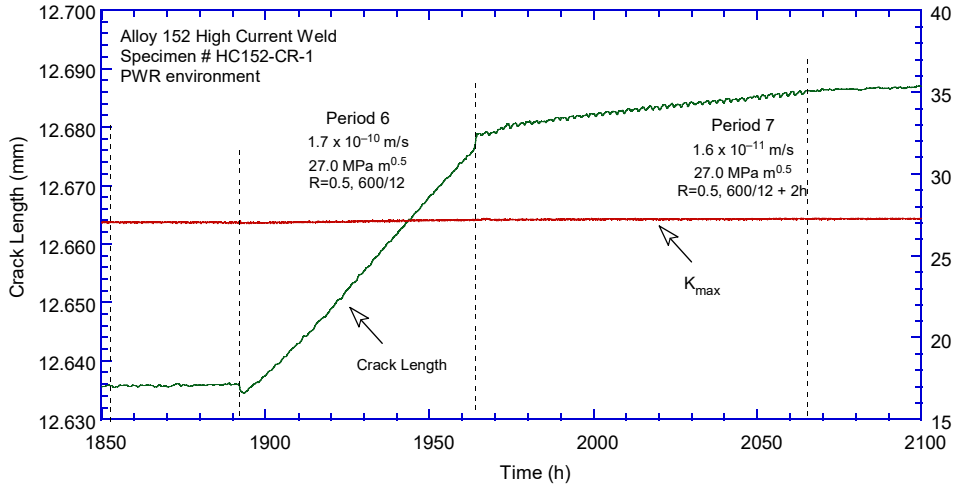

(e)

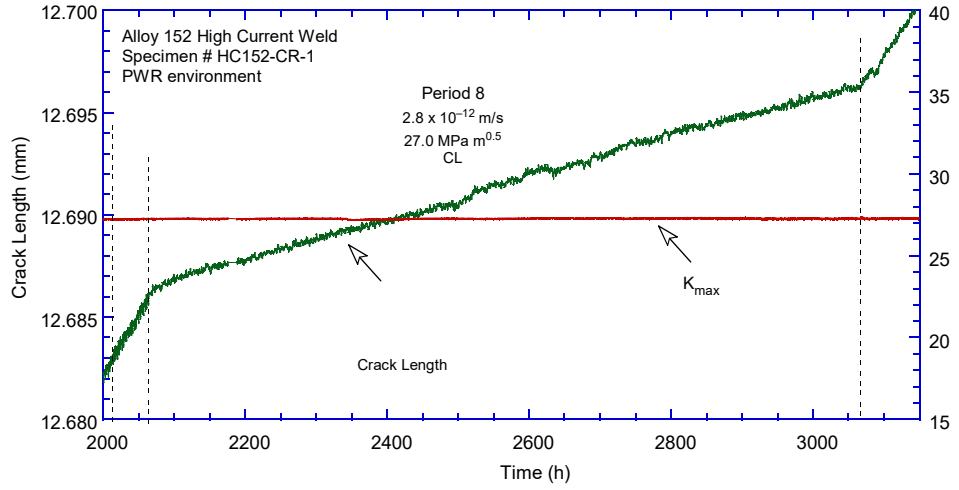

(f)

Figure 70 (cont.)

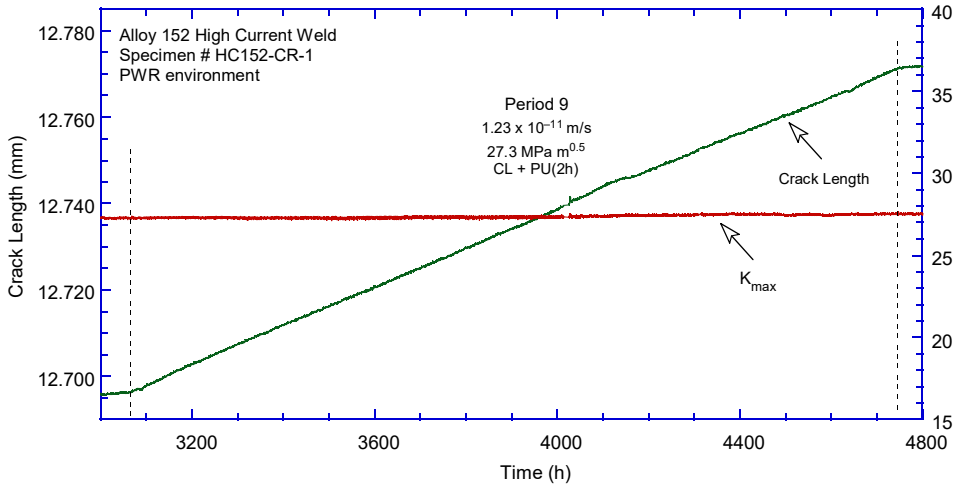

(g)

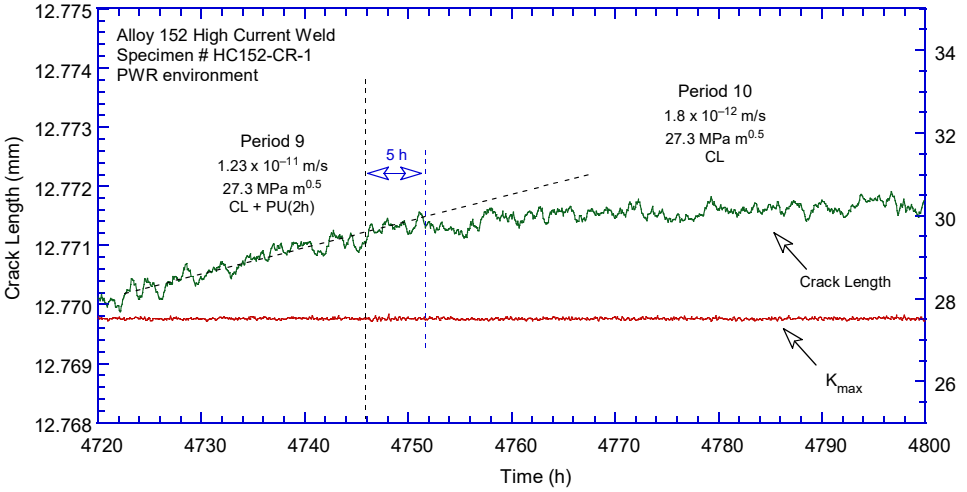

(h)

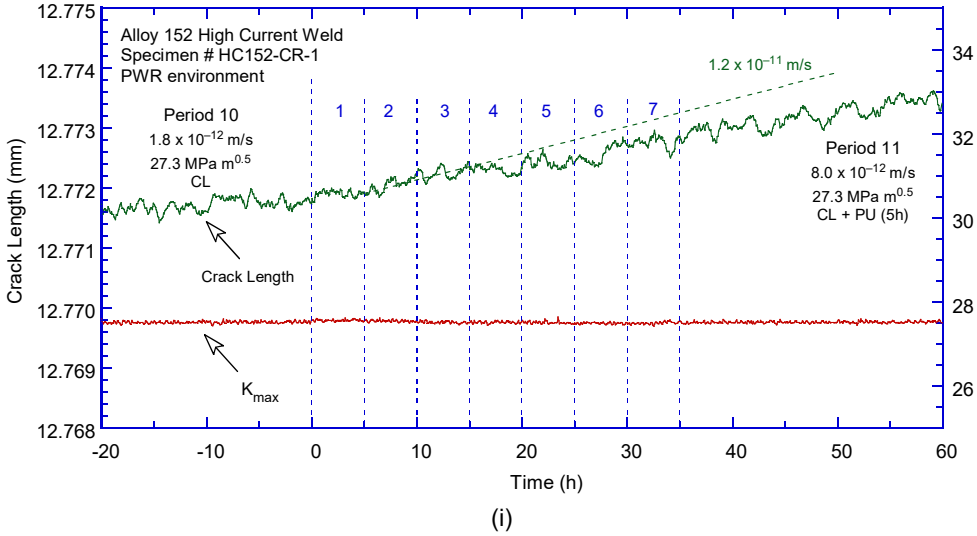

(i)

Figure 70 (cont.)

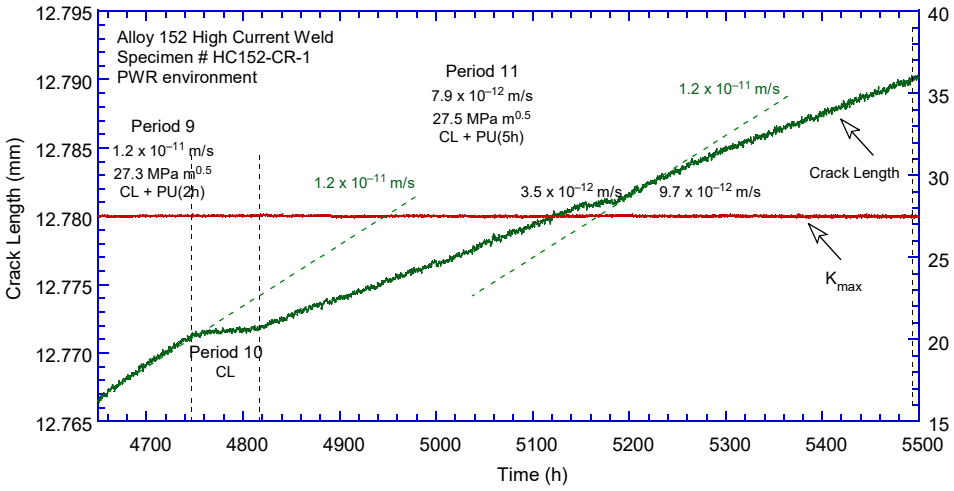

(j)

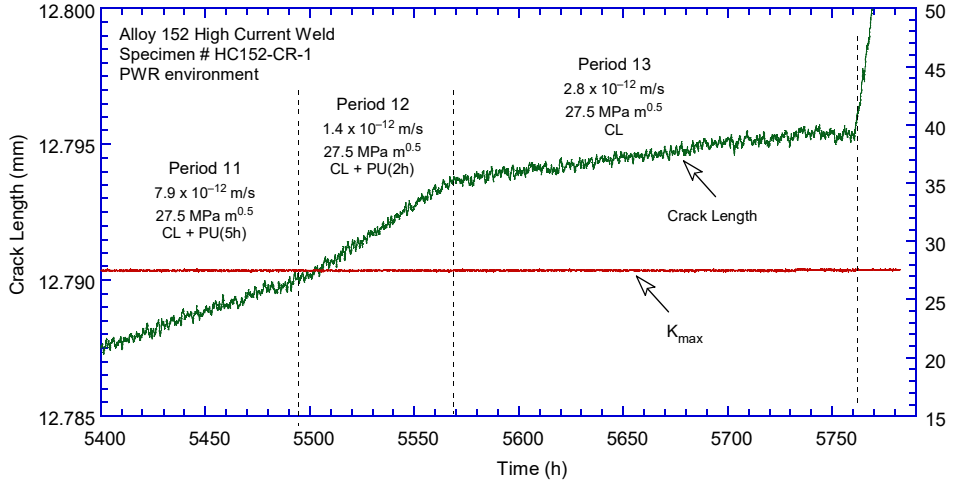

(k)

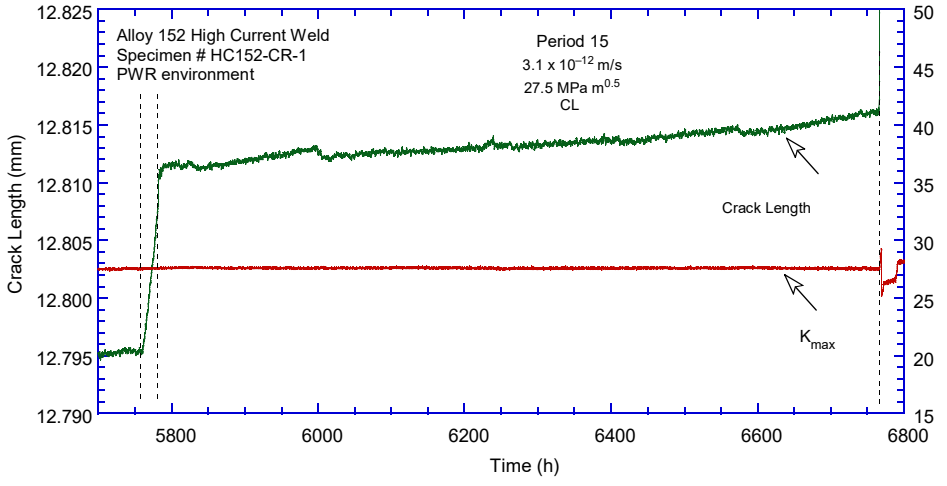

(l)

Figure 70 (cont.)

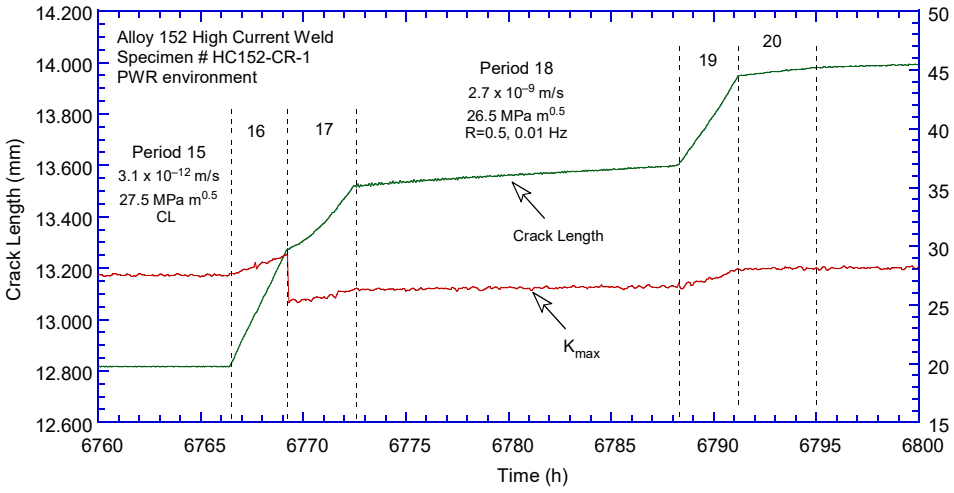

(m)

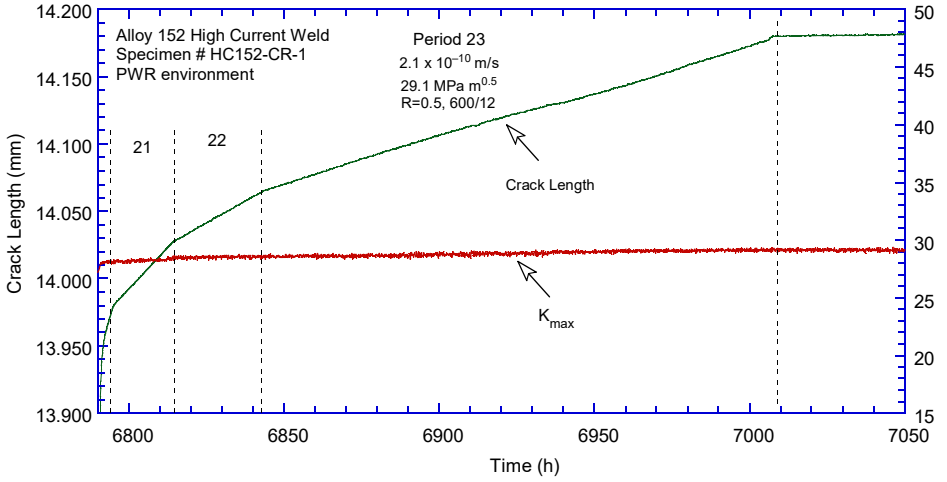

(n)

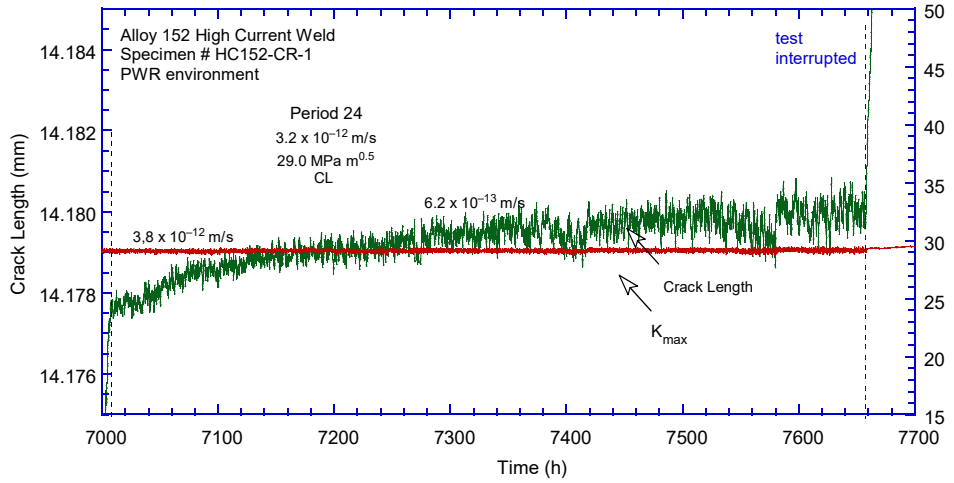

(o)

Figure 70 (cont.)

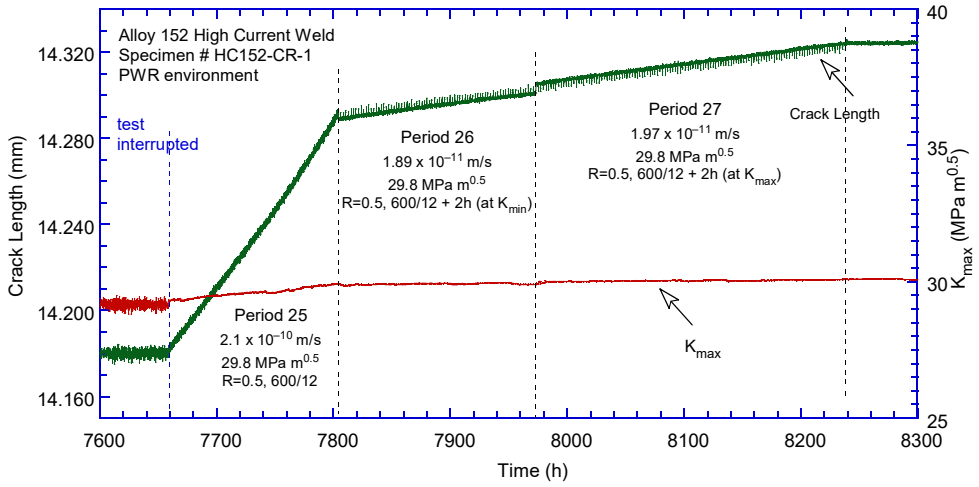

(p)

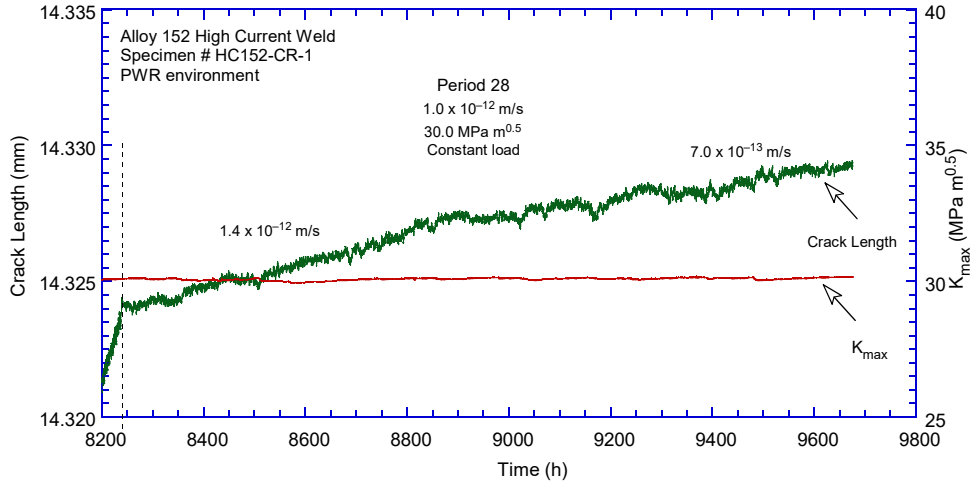

(q)

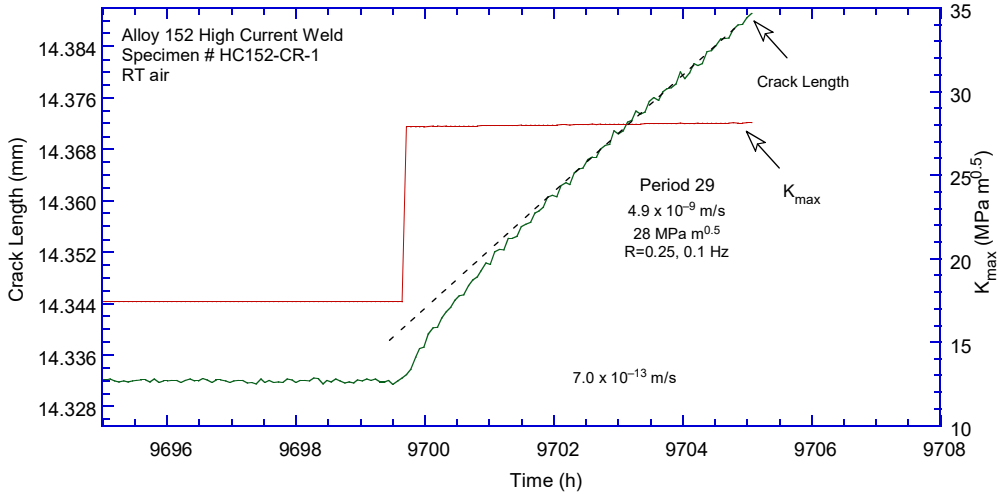

(r)

Figure 70 (cont.)

Figure 71 summarizes the cyclic CGRs for the “high current” Alloy 152 weld specimen HC152-CR-1 in simulated primary water. Similar data for specimens N152-TS-1 and A152-TS-5 produced using “normal” parameters but with a different Alloy 152 heat are included for comparison. Figure 71a shows that the response of specimen HC152-CR-1 appears to be slightly higher than that of N152-TS-1, however, the “high current” weld specimen is oriented in a more favorable direction vs. the weld dendrites than specimen N152-TS-1. Thus, the comparison with the A152-TS-5 is more appropriate, and in this case, Figure 71b shows that the response of the “high current” weld is clearly lower than that of the A152 series weld. Specifically, the environmental enhancement for the R=0.5, 600/12 condition measured in test periods 3 and 6 was 2.4 and 2.7, respectively – a little lower than expected for a weld specimen oriented along the dendrites. A second set of fatigue and corrosion fatigue data obtained on HC152-CR-1 specimen confirmed the previous observations Figure 71c. Overall, the fatigue behavior seems consistent with that of the previous welds, however, the environmental enhancement for the “high current” weld seems a little lower than expected.

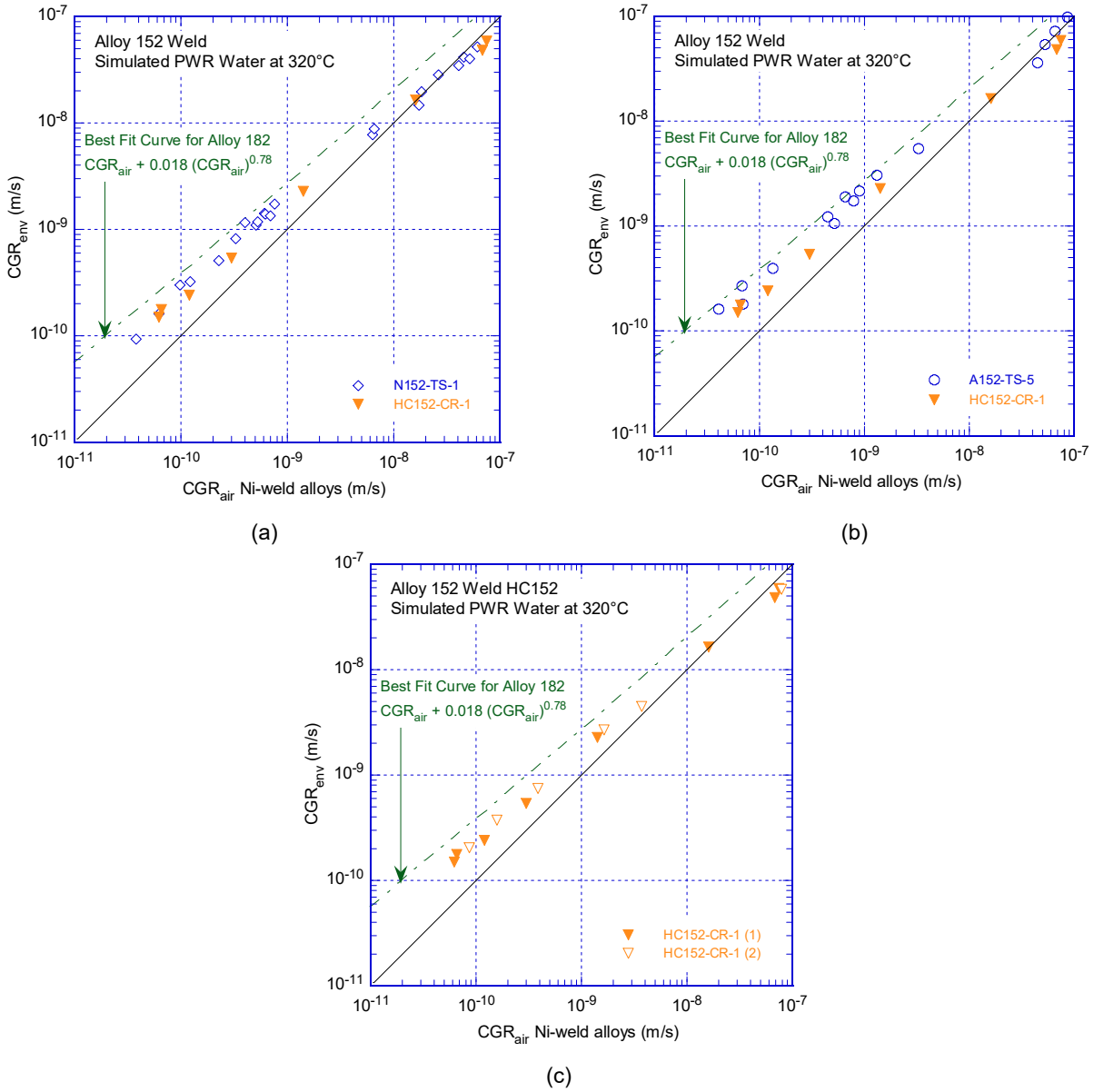

Figure 71 Cyclic CGRs for high current Alloy 152 weld specimen HC152-CR-1 in simulated primary water. Comparisons with (a) specimen N152-TS-1, (b) specimen A152-TS-5 produced using "normal" welding parameters, and (c) second part of the test are included.

Figure 72 summarizes the SCC CGRs for from the weld specimen HC152-CR-1, and includes data from the Alloy 152 (normal parameters) specimens that were tested previously. The SCC CGR data obtained under constant load (CL) is shown with solid symbols and the SCC CGR data obtained under constant load with periodic unloading is shown with open symbols. Unlike the data resulting from the specimens tested previously, in the current set of results the data obtained under constant load and the data obtained from cycle+hold never overlap. As expressed previously, concern is with the fact that the CGR response under cycle+hold is somewhat proportional with the hold time (2h vs. 5h) suggesting that fatigue is in fact the driving force for growth. Nevertheless, this aspect will be largely elucidated when the fracture surface will be examined. Overall, the SCC CGR data obtained from the "high current" weld appears to

be lower than those for the welds produced with “normal” parameters. However, in order to isolate the effect of the welding parameters, the best comparison will be provided by a test on the weld made using the same heat and same weld geometry as the current “high current” weld but made using the “normal” parameters.

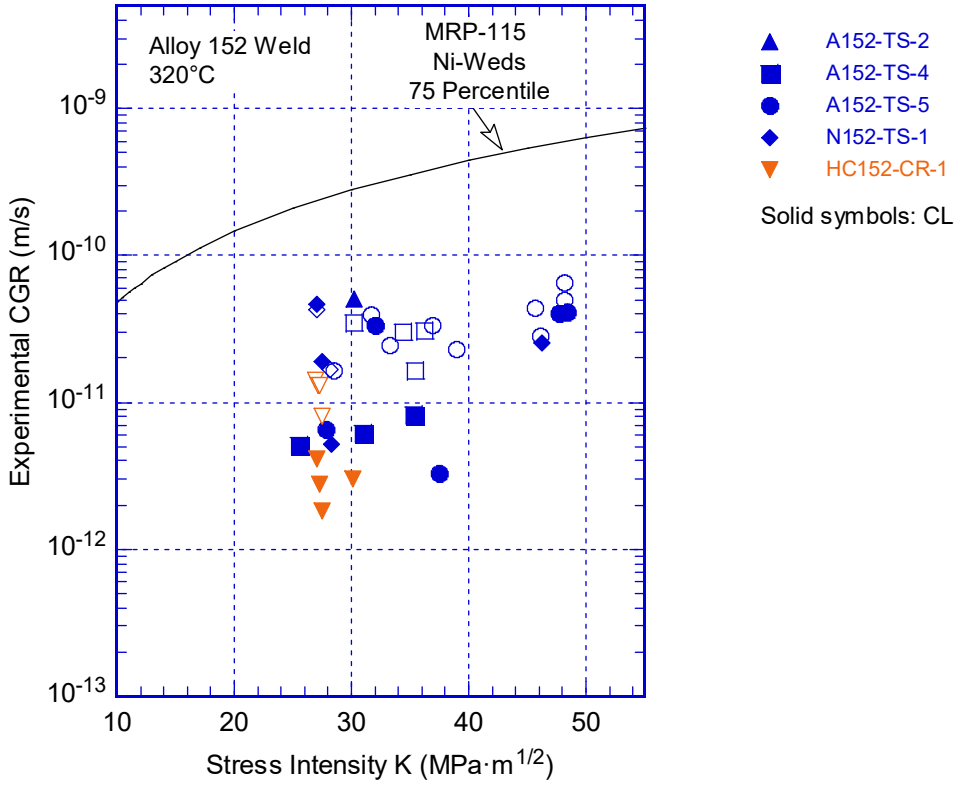

Figure 72 SCC CGRs vs. stress intensity factors for high current Alloy 152 weld specimen HC152-CR-1 in simulated primary water. Also included are data from Alloy 152 A152 and N152 welds produced using “normal” welding parameters.

Following the test, the specimen was broken open to expose the fracture surface, Figure 73. Transitioning to an IG SCC fracture mode and the subsequent SCC CGR evaluations were attempted in two distinct regions in the specimen: IG-1 (test periods 3-15, Table 15) and IG-2 (test periods 22-28, Table 15). The total crack advance was measured to be 2.81 mm, in very good agreement (12%) with the DC potential measurement of 2.46 mm, hence no correction of the DC potential data was needed.

Figure 74 shows the first part of the test and region IG-1. The dark band seen in the figure corresponds to the 0.220 mm crack advance in test periods 3-15, Table 15. Engagement is low, 20%. More significantly, the additional micrographs shown in Figure 75 do not show the secondary IG cracks that usually precede the full-blown IG engagement as was the case with A152, N152, and MHI152 series of welds. This outcome suggests that the transitioning scheme used (5-6 x 10^{-11} m/s in air) was not successful for this weld. In other words, the HC152 microstructure does not seem to “support” an IG fracture at a rate in the 10^{-11} m/s range. The

limited IG fracture that was observed occurred most likely under constant load, and was partially maintained under constant load with periodic unloading or cycle + hold as these have 2-5 x 10^{-12} m/s components in air, as no interruptions were observed in the IG fracture mode once that was initiated. This suggests that these rates are closer to the rates that would result/maintain the IG SCC fracture mode.

Figure 76 focuses on region IG-2. As with IG-1, the engagement was low, 35%. Similarly, the additional micrographs shown in Figure 77 do not appear to show the secondary cracks that usually precede the full-blown IG engagement, reinforcing the previous finding that the transitioning scheme was unsuccessful. Some tiny fissures were observed instead, Figure 77a.

In summary, the HC152 weld seems fairly SCC resistant. This finding is consistent with the reduced environmental enhancement reported previously, Figure 71. Loading conditions with 10^{-11} m/s air components that routinely produced IG fracture in the A152, N152, and MHI152 welds resulted in TG fracture in this weld. The limited amount of IG cracking suggests that this developed under constant load and was maintained under loading conditions with air components approximately one order of magnitude lower, 10^{-12} m/s. Nevertheless, the lack of substantial IG growth under constant load with periodic unloading or cycle + hold conditions, prevent those rates to be reported as SCC CGRs. Overall, the fractography observations are only consistent with the 10^{-12} m/s rates measured under constant load for this specimen, i.e. the solid symbols in Figure 72. It is not clear at this stage whether it is the weld geometry, heat or welding procedure that was responsible for the increased SCC resistance.

Figure 73 Fracture surface of specimen HC152-CR-1. Crack advance is from bottom to top.

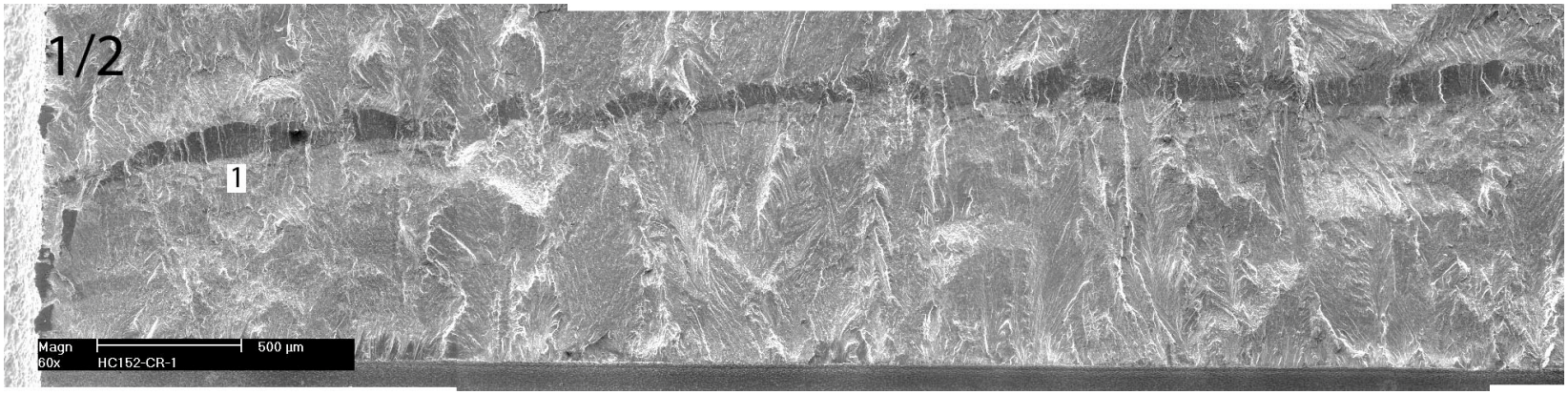

(a)

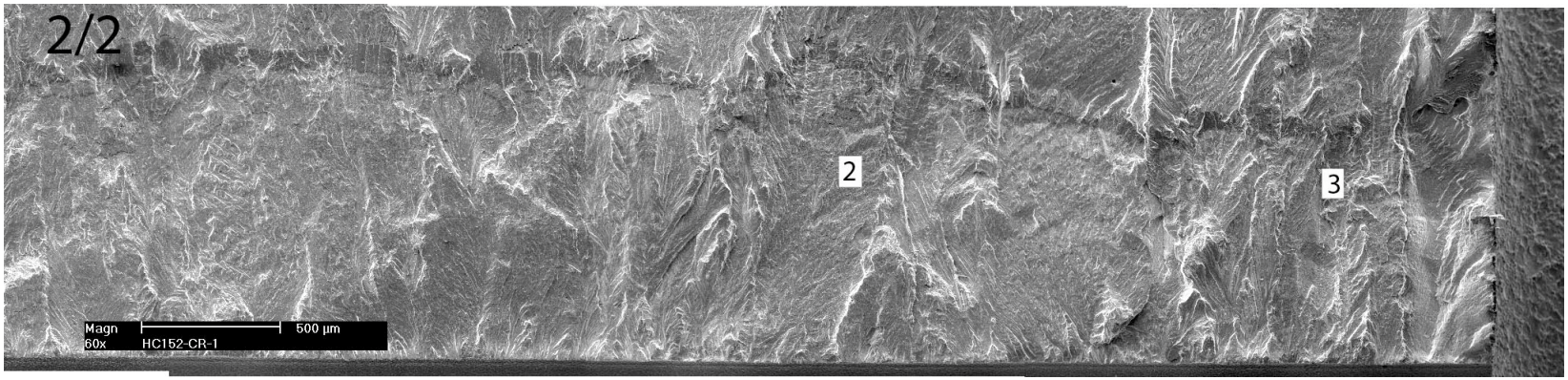

(b)

Figure 74 The fracture surface of specimen HC152-CR-1, region IG-1: (a) first half, and (b) second half. Crack propagation in is from bottom to top.

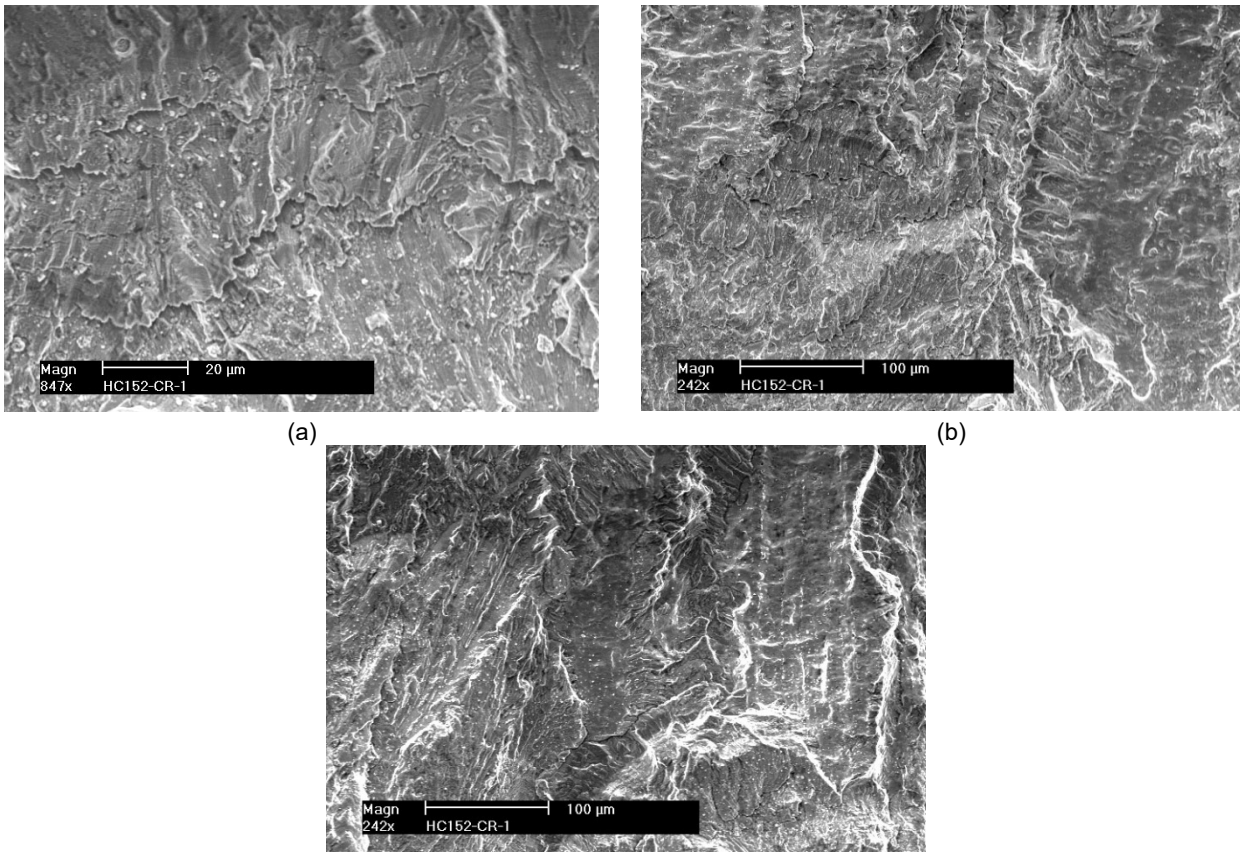

(a) (b)

(c)

Figure 75 Fracture surface of specimen HC152-CR-1, region IG-1 at location: (a) 1, (b) 2, and (c) 3 in Figure 74. Crack advance is from bottom to top.

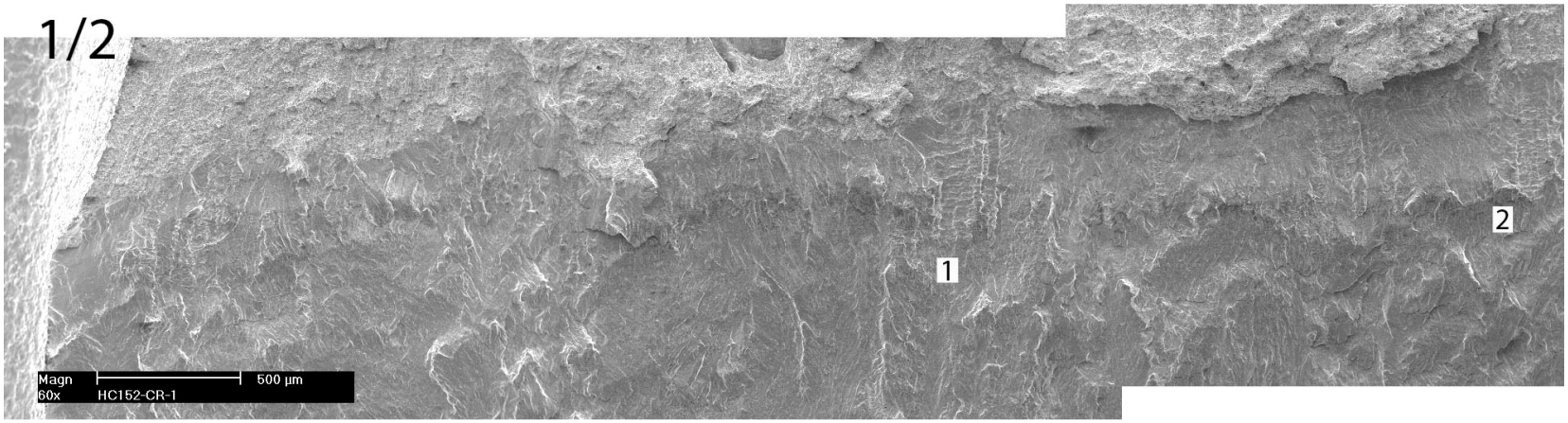

(a)

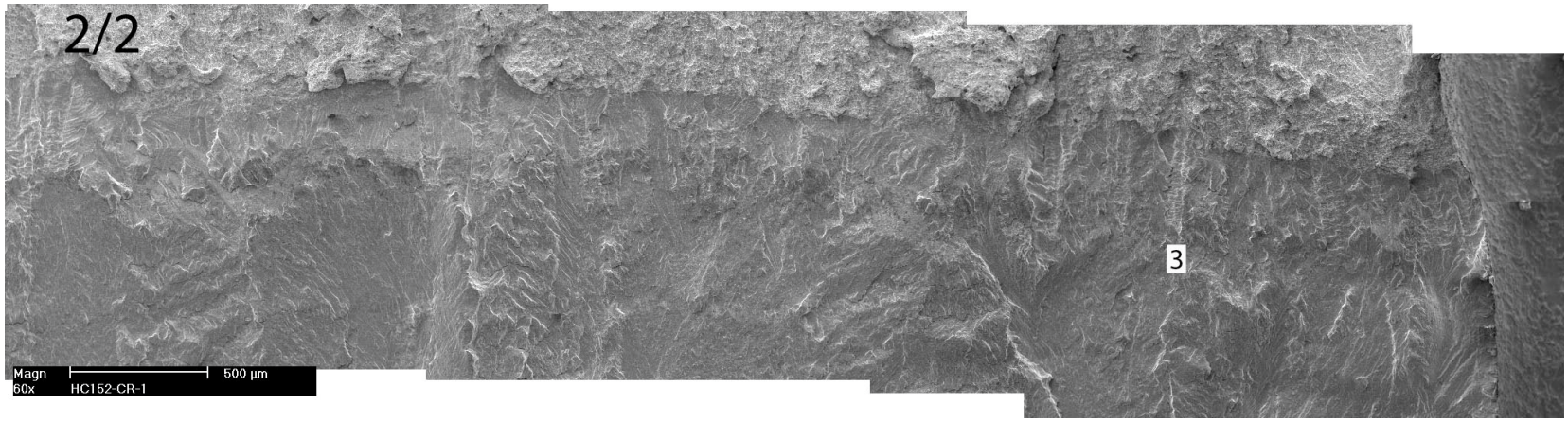

(b)

Figure 76 The fracture surface of specimen HC152-CR-1, region IG-2: (a) first half, and (b) second half. Crack propagation in is from bottom to top.

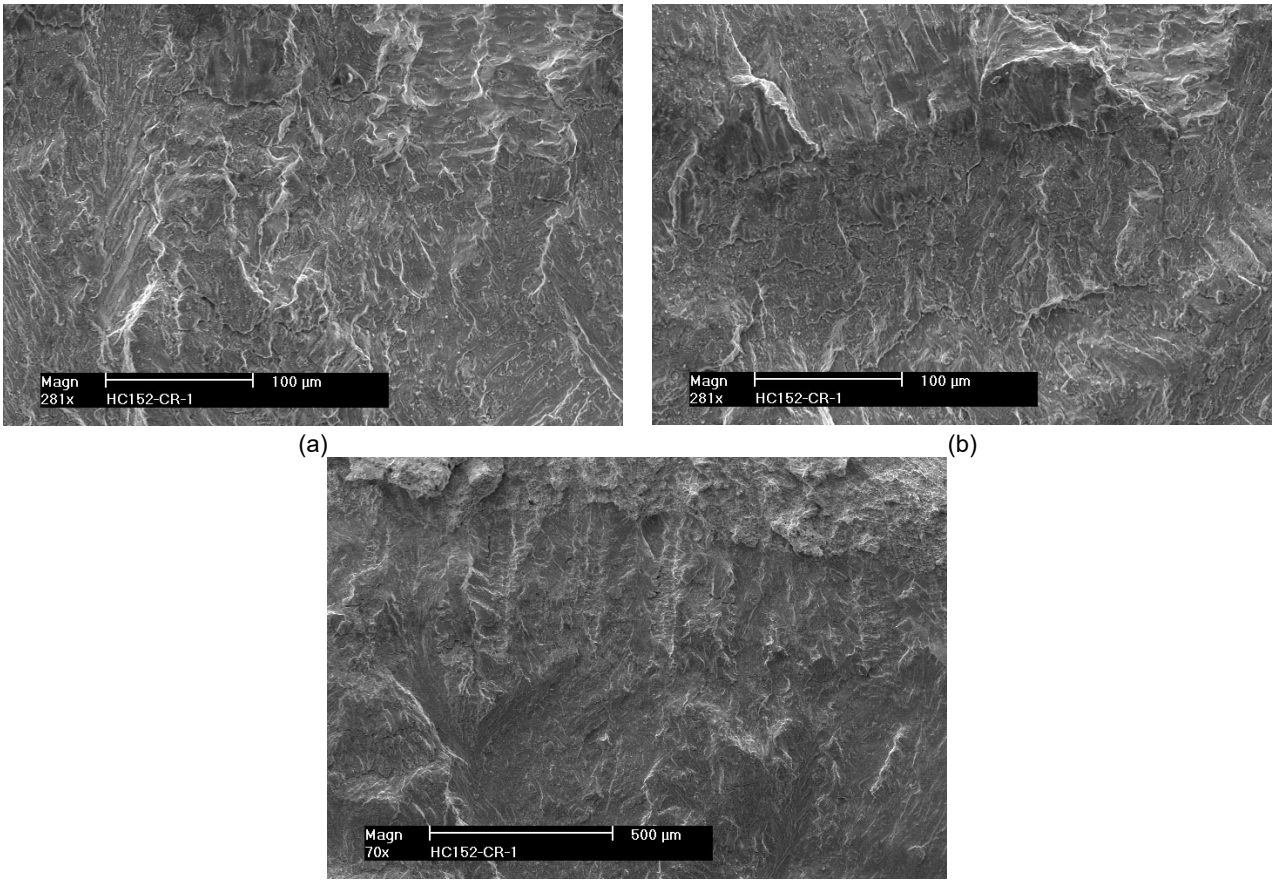

Figure 77 Fracture surface of specimen HC152-CR-1, region IG-2 at location: (a) 1, (b) 2, and (c) 3 in Figure 76. Crack advance is from bottom to top.

3.3.2 Specimen NC152-CR-1, "normal" parameters weld produced by ANL

The test specimen NC152-CR-1 was machined from the Alloy 152 weldment produced at ANL using typical welding parameters (joint A in Figure 7) The testing conditions are given in Table 16, and the changes in crack length and K_{max} with time are shown in Figure 78. As usual, the test started with fatigue precracking and transitioning in the primary water environment. Since the purpose of this test is to provide a comparison to the data obtained on the weld produced with high current (joint B in Figure 6) described in the previous section, the testing conditions for the current test were chosen to match precisely those used in the previous. As with the previous test, transitioning was followed by a test period with 2-h hold, and constant load in test period 5. After the crack was allowed to grow for approx. 1,300 hours, cycling similar to that of preceding test period 4 was introduced in test period 6 to check for ligaments or off-plane cracking. After a rate similar to that measured in test period 4 was measured, constant load conditions resumed. After approx. 1,000h at constant load, the SCC CGR was comparable to that measured previously in test period 5. Next, after briefly advancing the crack in test period 8, the same approach used in the other tests based on alternating the hold between K_{min} and K_{max} was undertaken here with the purpose of confirming the low SCC CGRs measured at constant load. Initial measurements in test periods 9 and 10 seem to confirm that finding, however, the observations were repeated in test periods 11-12. Overall, the SCC CGR seems to be small. This was next confirmed under constant load in test period 13. Next, the "usual" R=0.5, 600/12 (and 2h hold) conditions were repeated in test periods 14 and 15, and the responses were higher than observed previously in both cases. It is interesting to note that the response in test periods 15 was approx. $1x10^{-11}$ m/s higher than in any of the prior conditions (see periods 4, 6, and 10 in Table 16).

Next, the specimen was advanced in fatigue in test periods 16 and 17, and transitioning was repeated using loading conditions similar to those used previously. The response was nearly identical to prior observations. Again, the response under cycle + hold in test period 22 was approx. $1x10^{-11}$ m/s higher than most prior conditions suggesting that an IG fracture mode may have developed. As the SCC CGR estimated by superposition was indeed $1x10^{-11}$ m/s, the specimen was set at constant load in test period 23. The test was left at constant load for approx. 2,100h and resulted in approx. 10 microns of growth. Since the resulting SCC CGR under constant load was consistent with the prior ones (and actually, slightly lower), the test was stopped.

Table 16 Crack growth data for Alloy 152 specimen NC152-CR-1 in PWR water[a].

Test Period	Test Time, h	Temp. °C	Load Ratio R	Rise Time, s	Down Time, s	Hold Time, s	K_{max}, MPa·m$^{1/2}$	ΔK, MPa·m$^{1/2}$	CGR_{env}, m/s	Estimated CGR_{air}, m/s	Crack Length, mm
Pre a	79	319.7	0.30	1	1		24.7	17.3	4.24E-08	6.05E-08	11.979
Pre b	95	319.6	0.30	50	50		24.9	17.4	2.36E-09	1.25E-09	12.045
Pre c	97	319.7	0.30	1	1		25.8	18.0	8.08E-08	7.27E-08	12.330
Pre d	98	319.7	0.30	2	2		26.1	18.3	5.02E-08	3.85E-08	12.435
Pre e	100	319.7	0.30	5	5		26.4	18.5	2.47E-08	1.61E-08	12.514
1	103	319.7	0.50	120	12		26.4	13.2	7.08E-10	2.90E-10	12.525
2	120	319.6	0.50	300	12		26.6	13.3	3.81E-10	1.19E-10	12.548
3	168	319.6	0.50	600	12		26.7	13.4	2.10E-10	6.07E-11	12.584
4	413	319.7	0.50	600	12	7,200	26.8	13.4	1.50E-11	6.07E-11	12.600
5	1,776	319.7	1.00	0	0		27.1	0.0	4.13E-12	-	12.621
6	1,849	320.1	0.50	600	12	7,200	26.8	13.4	1.69E-11	5.19E-12	12.625
7	2,837	320.1	1.00	0	0		27.0	0.0	2.54E-12	-	12.634
8	2,861	320.4	0.50	600	12	0	27.0	13.5	1.95E-10	6.43E-11	12.656
9	3,191	320.3	0.50	600	12	7,200 at K_{min}	27.1	13.5	1.75E-11	4.96E-12	12.675
10	3,772	320.5	0.50	600	12	7,200	27.2	13.6	1.51E-11	5.08E-12	12.711
11	3,964	320.6	0.50	600	12	7,200 at K_{min}	27.2	13.6	1.55E-11	5.10E-12	12.716
12	4,609	320.7	0.50	600	12		27.4	13.7	1.53E-11	5.23E-12	12.758
13	5,762	320.4	1.00	0	0		27.4	0.0	1.62E-12	-	12.763
14	5,858	319.6	0.50	600	12		27.6	13.8	2.11E-10	6.93E-11	12.835
15	5,927	319.6	0.50	600	12	7,200	27.8	13.9	2.53E-11	5.44E-12	12.844
16	5,931	319.5	0.30	1	1		27.0	18.9	1.08E-07	8.83E-08	13.404
17	5,932	319.6	0.30	2	2		27.8	19.5	6.01E-08	4.96E-08	13.594
18	5,949	319.5	0.50	120	12		28.1	14.0	8.84E-10	3.72E-10	13.656
19	5,958	319.6	0.50	300	12		28.1	14.1	4.35E-10	1.50E-10	13.670
20	6,026	319.5	0.50	600	12		28.4	14.2	2.45E-10	7.74E-11	13.729
21	6,454	320.0	0.50	1000	12		29.6	14.8	1.87E-10	5.58E-11	14.018
22	6,670	320.2	0.50	1000	12	7,200	29.7	14.8	3.08E-11	6.84E-12	14.043
23	8,768	392.2	1.00	0	0		29.8	0.0	1.36E-12	-	14.053

[a]Simulated PWR water with 2 ppm Li, 1000 ppm B, and 2 ppm. DO<10 ppb. Conductivity was 21±3 μS/cm, and pH 6.4.

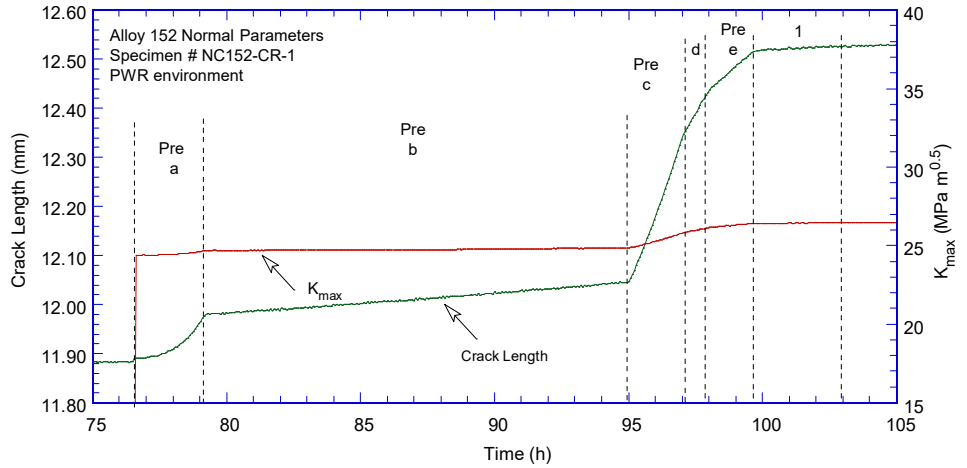

(a)

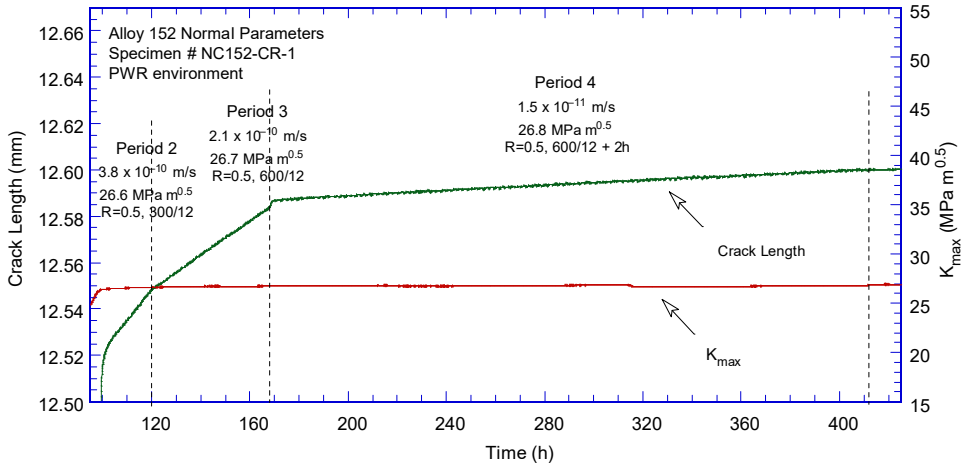

(b)

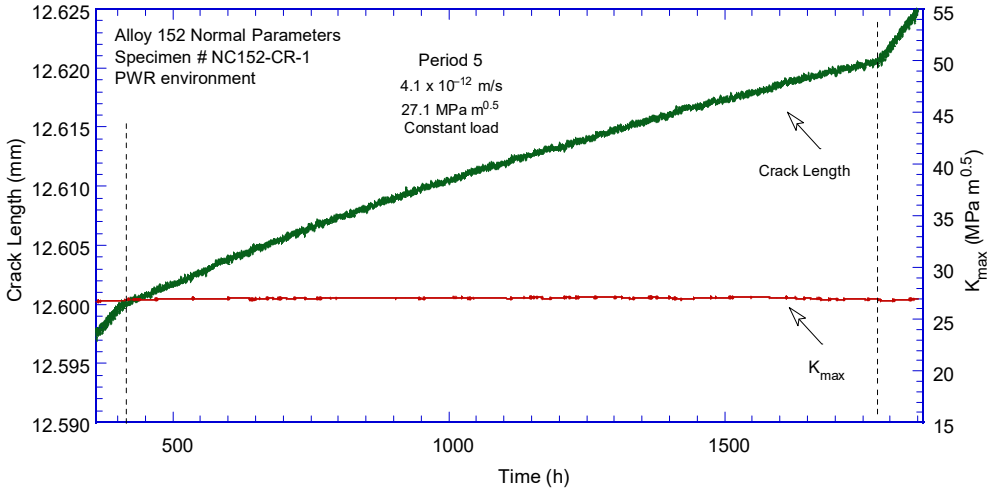

(c)

Figure 78 Crack–length–vs.–time for Alloy 152 weld specimen NC152-CR-1 in simulated PWR environment during test periods (a) precracking-1, (b) 2-4, (c) 5, (d) 6, (e) 7, (f) 8-12, (g) 13, (h) 14-15, (i) 16-17, (j) 18-22, and (k) 23.

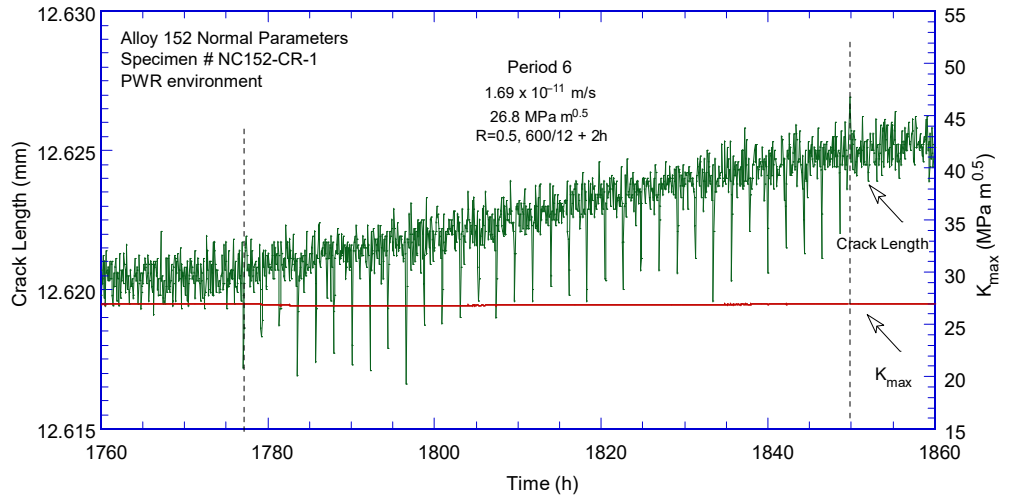

(d)

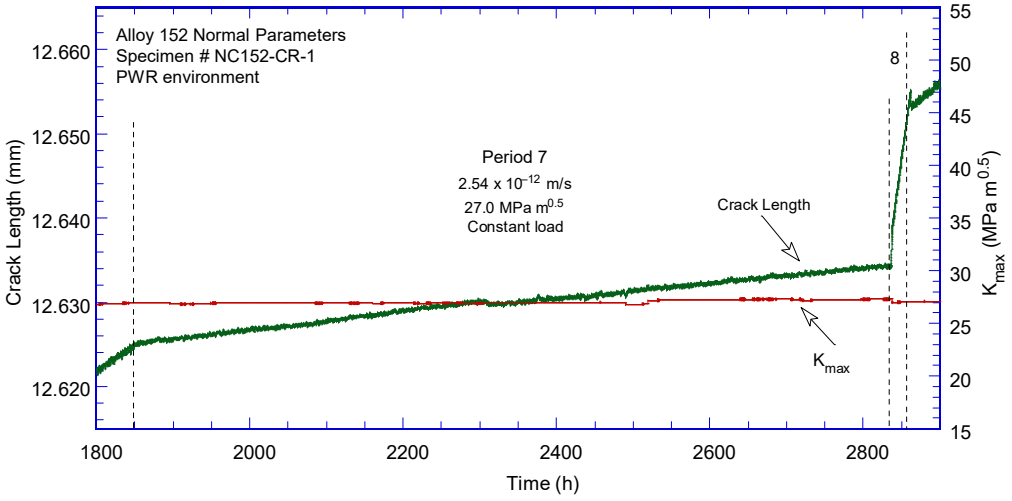

(e)

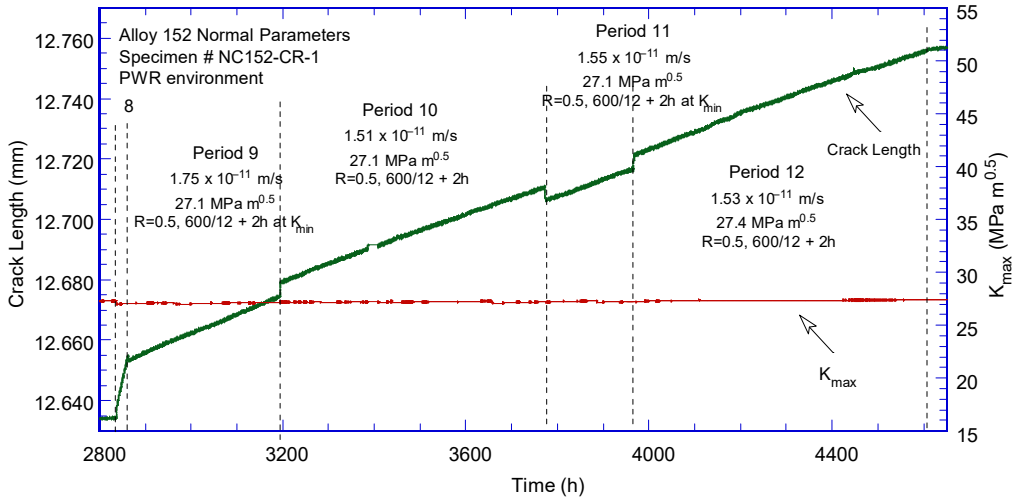

(f)

Figure 78 (cont.)

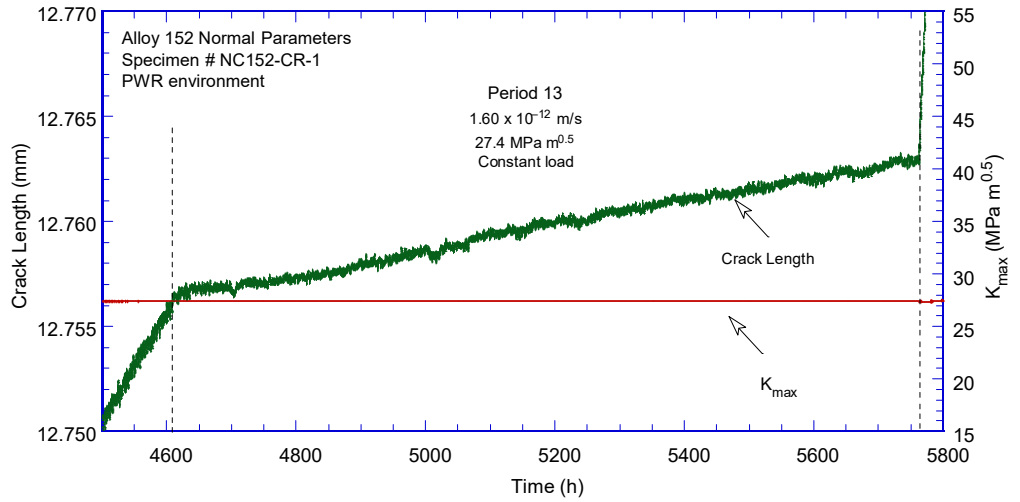

(g)

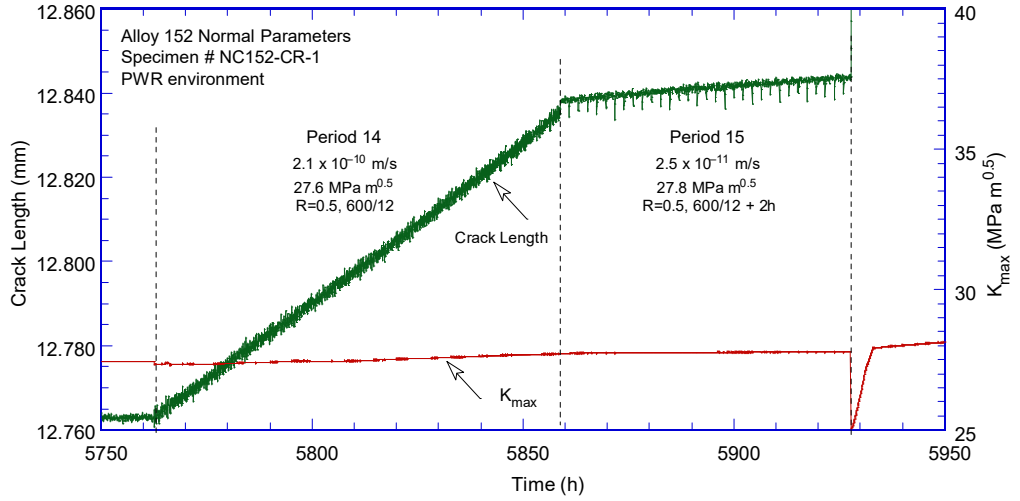

(h)

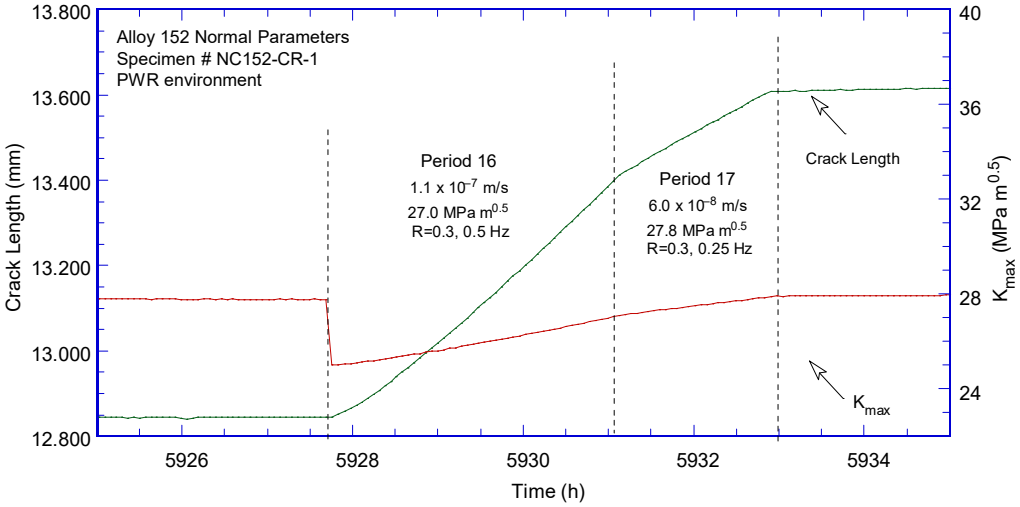

(i)

Figure 78 (cont.)

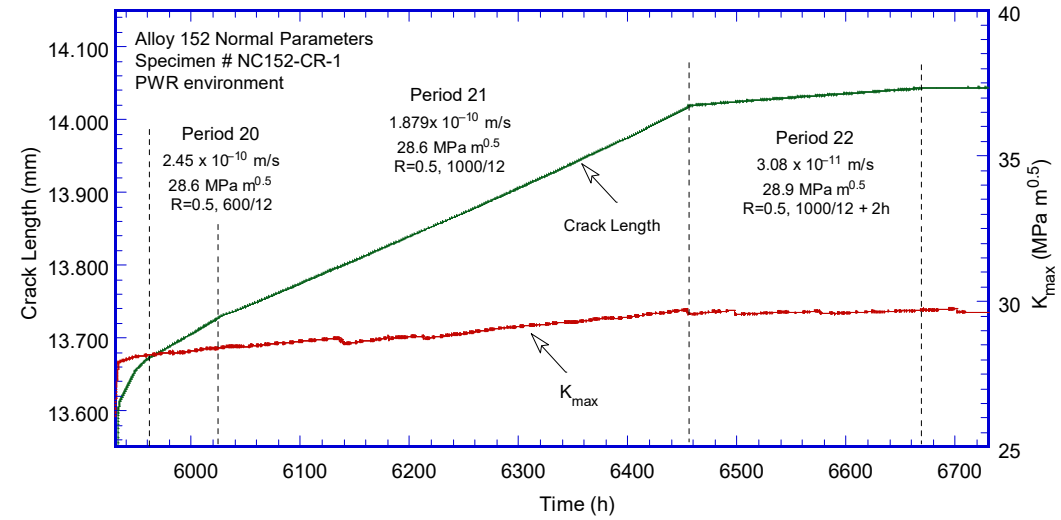

(j)

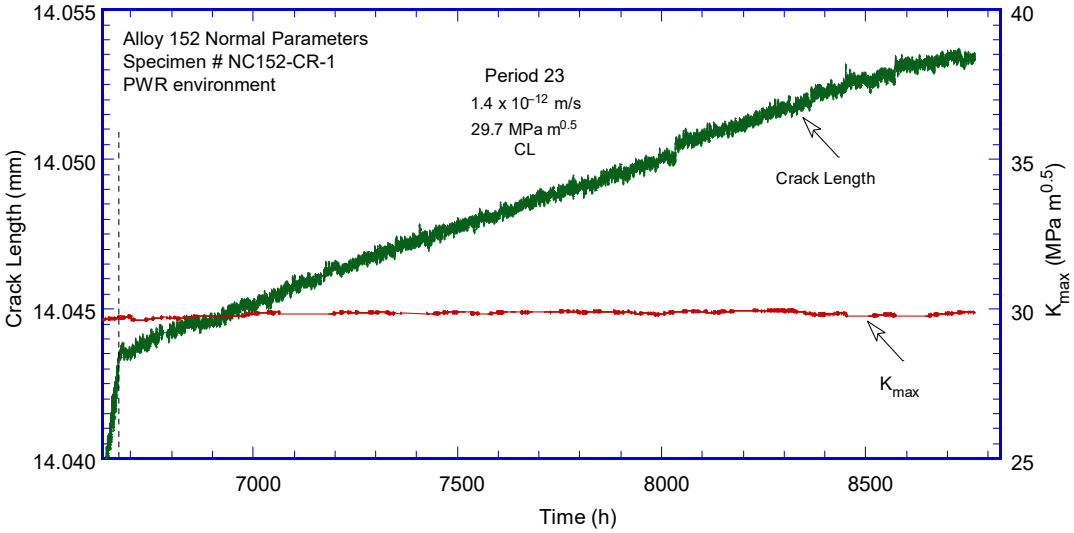

(k)

Figure 78 (cont.)

Figure 79 shows the cyclic CGR data obtained for the current NC152-CR-1 weld specimen (normal parameters), and for comparison, data from previous tests on another weld produced with "normal" parameters (A152-TS-5) as well as the weld produced with high current (HC152-CR-1). The corrosion fatigue curve for Ni-base welds was included in the plots for comparison. The comparisons suggest that the data resulting from the weld produced with normal parameters is consistent with that from previous welds produced with similar parameters (Figure 79a), while the weld produced with a high current appears to be slightly more resistant to fatigue than the "normal" weld (Figure 79b).

Figure 80 shows the SCC CGR data obtained for the current NC152-CR-1 weld specimen (normal parameters), and for comparison, data from the previous test on HC152-CR-1 (high current). Also included are data obtained from the A152 series. Overall, the data from the A152 series appears more susceptible to SCC than the welds produced for the study of the welding parameters. The welding parameters tested do not seem to affect the SCC CGR response.

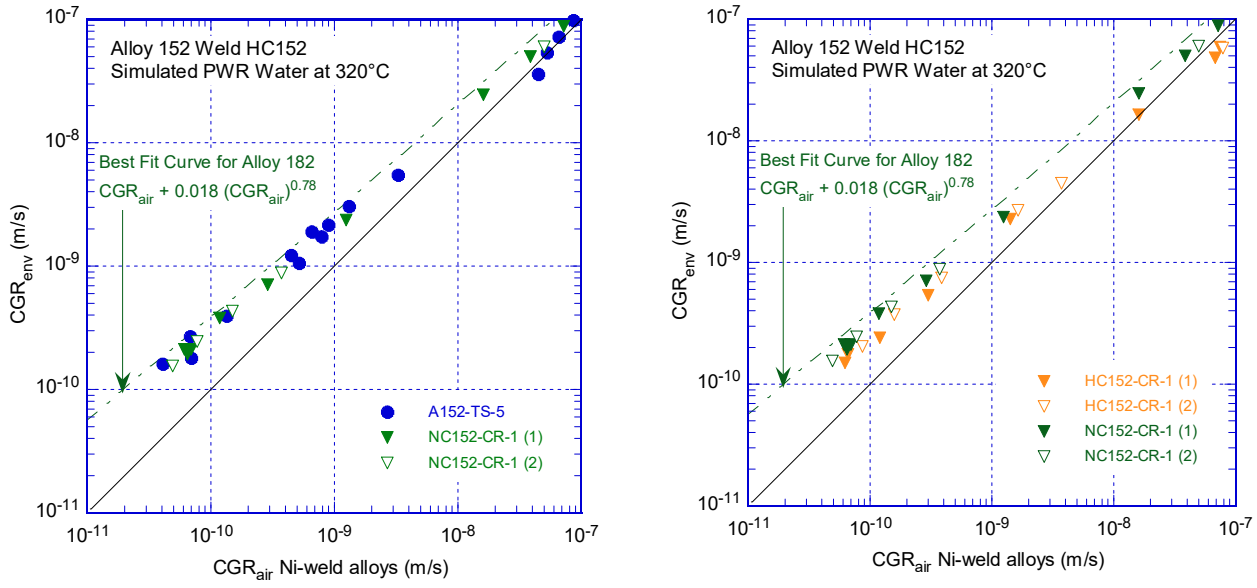

Figure 79 **Cyclic CGR data for Alloy 152 weld specimen NC152-CR-1 simulated primary water. Comparisons with (a) specimen A152-TS-5 produced using "normal" welding parameters, and (b) specimen HC152-CR-1 produced with high current.**

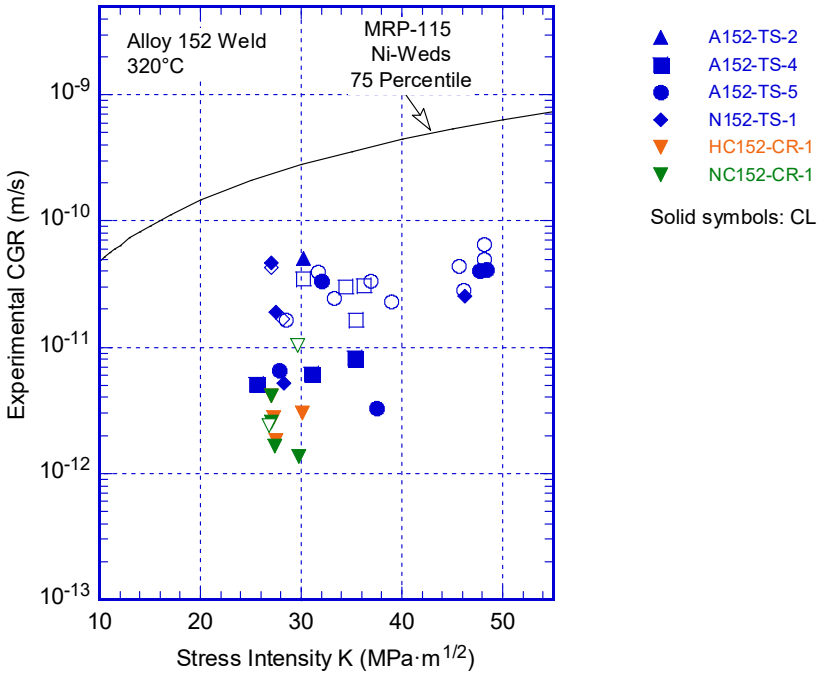

Figure 80 **SCC CGRs vs. stress intensity factors for high current Alloy 152 weld specimens NC152-CR-1 ("normal") and HC152-CR-1 ("high current") in simulated primary water. Also included are data from Alloy 152 A152 and N152 welds produced using "normal" welding parameters.**

The resulting fracture surface is shown in Figure 81 (macro) and Figure 82 (SEM). The IG fraction for the most part of the test was small (16%) with the exception of the last part of the test where the IG fraction (81%) was the largest measured for this and the previous ("high current") specimen. The SCC response under constant load was consistently small for both specimens, however, the cycle+hold response was seen to increase in the current specimen (see the test periods marked with yellow in Table 16). As such, one noes that the total response nearly doubles in test period 22 vs. the earlier ones conducted under similar loading conditions (period 22 has a rise time of 1000s, hence, is actually gentler). As mentioned previously, the SCC CGR component in test period 22 is $1x10^{-11}$ m/s, hence, in the prior test periods was smaller than that. Likely (based on the "high current" specimen response), the total rate of 1.5E-11 m/s under cycle+hold conditions reflect corrosion fatigue growth in a region with modest (20-40%) IG engagement. On the other hand, the $3x10^{-11}$ m/s rate under cycle+hold is consistent with the response measured in other Alloy 152 welds where 10^{-11} m/s SCC CGRs were confirmed at constant load. Overall, there appears that the response under cycle+hold conditions is strongly dependent on the fracture mode, and in specimens with high IG, is perhaps a better descriptor for the SCC CGR response.

Figure 81 **Fracture surface of specimen NC152-CR-1. Crack advance is from bottom to top.**

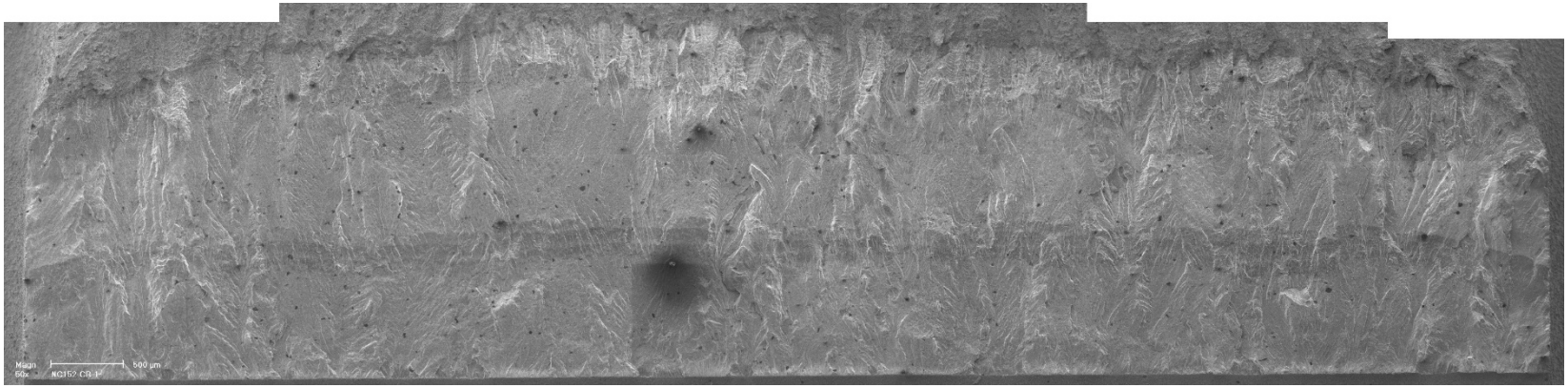

Figure 82 Fracture surface of Specimen NC152-CR-1. Crack advance is from bottom to top.

3.3.3 Specimen HH152-CR-1, "high heat input" weld produced by ANL

The test specimen HH152-CR-1 was machined from the Alloy 152 weldment produced at ANL using "high heat input" welding parameters (joint C in Figure 6). The "high heat input" weld C is 20% higher heat input that "normal" weld A or "high current" weld B. A common requirement for both welds B and C was that they "pass" inspection. The 20% increase in heat input in weld C is similar to that of the EPRI-produced weld vs. a survey of several procedures used in the field.

The SCC CGR test was initiated with precracking in water followed by transitioning. The testing conditions are given in Table 17, and the changes in crack length and K_{max} with time are shown in Figure 83. The first SCC CGR determination in test period 6 suggests the weld in resistant to SCC. Next, the crack was advanced by 0.5 mm and re-transitioned. The second SCC CGR determination in test period 11 suggests the weld in resistant to SCC. Finally, the crack was advanced for a third time, and re-transitioned. The third SCC CGR determination suggests that this weldment is resistant to SCC.

Table 17 Crack growth data for Alloy 152 high heat input weld Specimen HH152-CR-1 in PWR water[a].

Test Period	Test Time, h	Temp. °C	Load Ratio R	Rise Time, s	Down Time, s	Hold Time, s	K_{max}, MPa·m$^{1/2}$	ΔK, MPa·m$^{1/2}$	CGR_{env}, m/s	Estimated CGR_{air}, m/s	Crack Length, mm
Pre a	25	321.0	0.3	1	1		23.5	16.5	5.23E-08	5.09E-08	11.971
Pre b	27	321.2	0.3	5	5		23.7	16.6	9.98E-09	1.06E-08	12.019
Pre c	45	320.9	0.3	50	50		23.9	16.7	1.90E-09	1.08E-09	12.078
Pre d	49	320.5	0.3	1	1		25.1	17.6	6.90E-08	6.58E-08	12.491
1	52	320.4	0.5	120	12		27.8	13.9	7.10E-10	3.62E-10	12.512
2	68	320.6	0.5	300	12		28.0	14.0	3.90E-10	1.49E-10	12.540
3	95	320.3	0.5	600	12		28.1	14.0	2.19E-10	7.50E-11	12.559
4	238	319.8	0.50	600	12	7,200	27.9	14.0	1.89E-11	5.59E-12	12.572
5	314	320.3	0.50	600	12	14,400	28.1	14.0	1.80E-11	2.99E-12	12.575
6	720	321.0	1.00	0	0		28.3	0.0	2.20E-12		12.579
7	744	320.5	0.30	1	1		27.0	18.9	7.83E-08	8.87E-08	13.003
8	762	318.9	0.50	120	12		29.8	14.9	9.20E-10	4.67E-10	13.102
9	792	320.4	0.50	600	12		30.4	15.2	2.63E-10	1.03E-10	13.126
10	931	320.7	0.50	600	12	7,200	30.6	15.3	2.79E-11	8.20E-12	13.139
11	1,411	320.1	1.00	0	0	0	30.5	0.0	1.72E-12	-	13.141
12	1,534	320.4	0.50	600	12	7,200	30.6	15.3	2.16E-11	8.17E-12	13.151
13	1,554	319.8	0.50	600	12	0	30.3	15.2	2.41E-10	1.02E-10	13.167
14	1,600	320.4	0.50	120	12	0	31.2	15.6	1.03E-09	5.80E-10	13.320
15	1,625	320.7	0.50	600	12	0	31.5	15.7	3.26E-10	1.20E-10	13.348
16	1,666	320.1	0.50	600	12	7,200	31.1	15.5	5.61E-11	8.69E-12	13.357
17	1,759	320.6	0.50	600	12	14,400	31.5	15.8	1.89E-11	4.82E-12	13.362
18	1,867	320.8	1.00	0	0	0	31.5	0.0	2.00E-12	-	13.363

[a]Simulated PWR water with 2 ppm Li, 1000 ppm B, and 2 ppm. DO<10 ppb. Conductivity was 21±3 µS/cm, and pH 6.4.

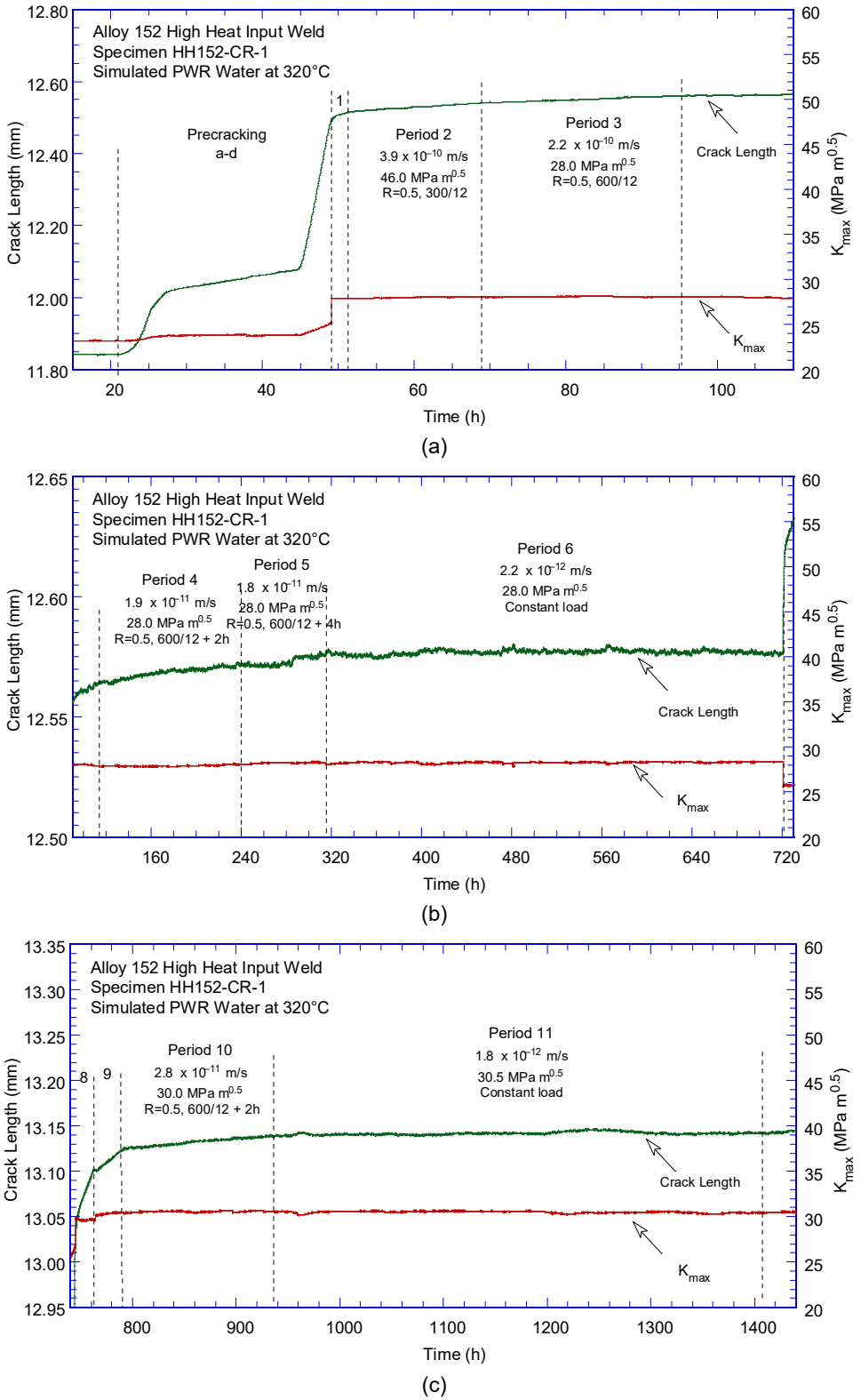

Figure 83 Crack–length–vs.–time for Alloy 52M high heat input weld Specimen HH152-TS-2 in simulated PWR environment during test periods (a) precracking-3, (b) 4-6, (c) 8-11, and (d) 12-18.

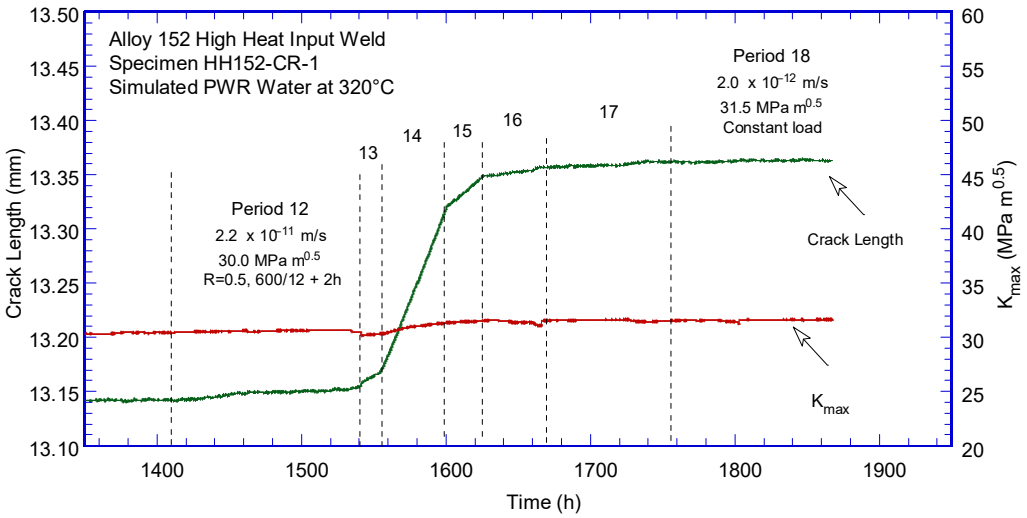

(d)

Figure 83 (cont.)

Figure 84 shows the cyclic CGR data obtained for the current HH152-CR-1 specimen and provides comparisons with data obtained in this program on other relevant specimens. As such, Figure 84a provides a comparison with the previously-tested NC152-CR-1 ("normal" parameters) and HC152-CR-1 ("high current") specimens made in the same geometry and using the same heat of material. Figure 84b provides a comparison with the data obtained on the high heat input Alloy 52M produced by EPRI. Overall, the data seems to be in good agreement with all of these data sets, with no clear trend visible.

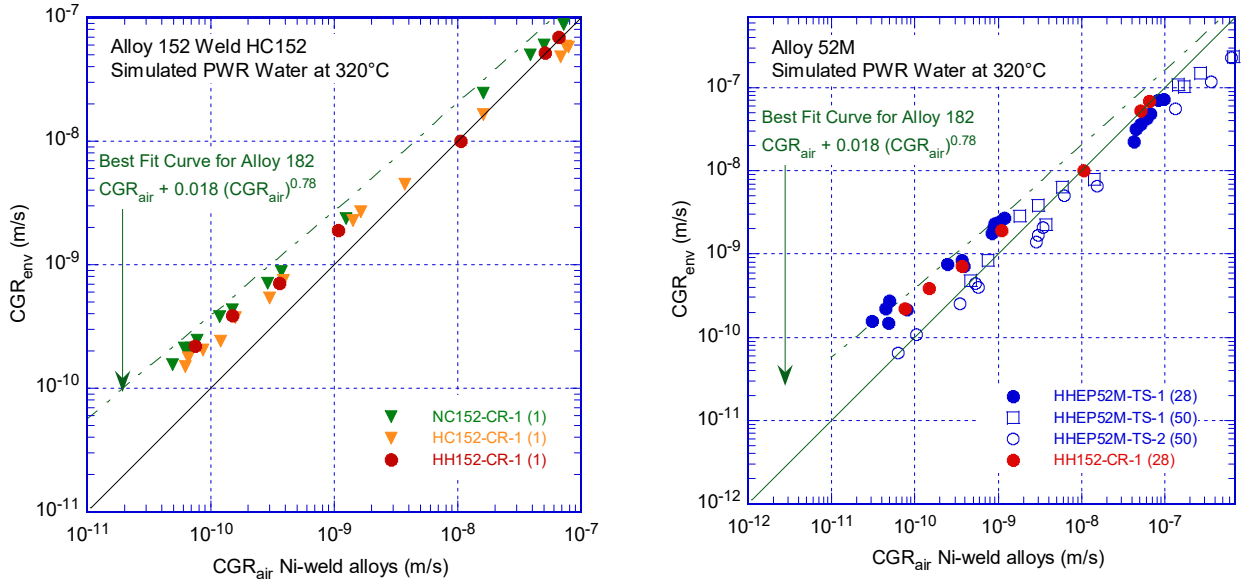

(a) (b)

Figure 84 Cyclic CGR data for high heat input Alloy 152 Specimen HH152-CR-1 compared with (a) NC152-CR-1 ("normal" parameters) and HC152-CR-1 ("high current") weld specimens of the same Alloy 152 heat, and (b) high heat input Alloy 52M produced by EPRI.

Figure 85 shows the SCC CGR data obtained for the current HH152-CR-1 weld specimen (high heat input parameters), and for comparison, data from the previous tests on HC152-CR-1 (high current) and NC152-CR-1 ("normal" parameters) are included. Also included are data obtained from the A152 series. Overall, the data from the A152 series appears more susceptible to SCC than the welds produced for the study of the welding parameters. The welding parameters tested do not seem to affect the SCC CGR response.

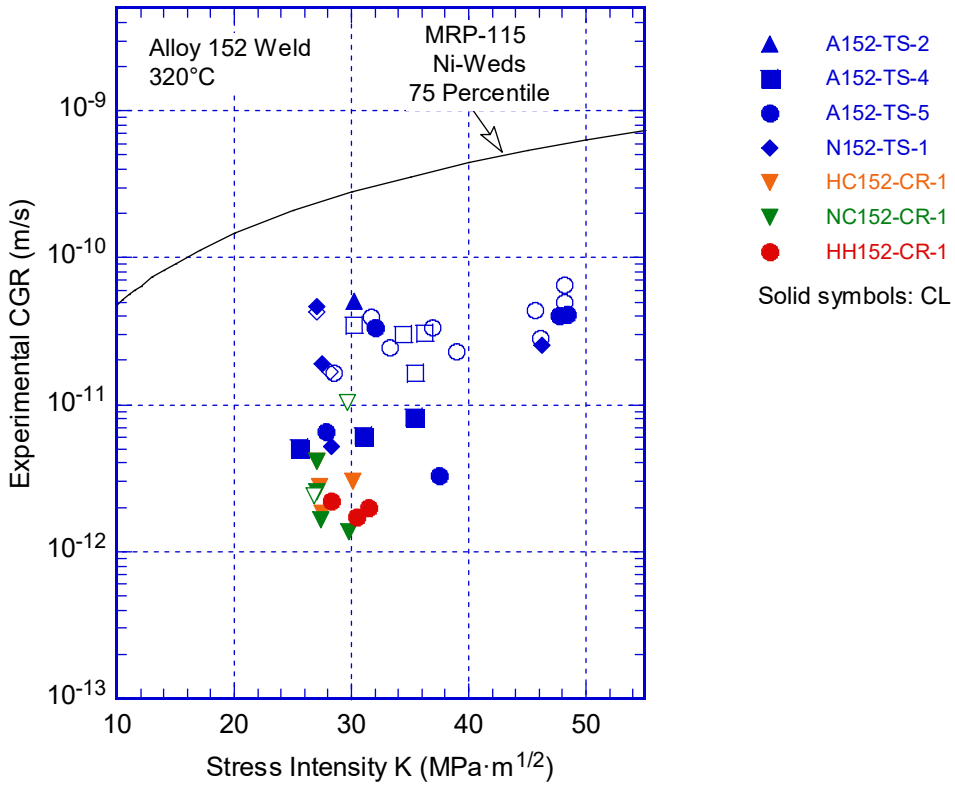

Figure 85 SCC CGRs vs. stress intensity factors for high current Alloy 152 weld specimens NC152-CR-1 ("normal") and HC152-CR-1 ("high current") in simulated primary water. Also included are data from Alloy 152 A152 and N152 welds produced using "normal" welding parameters.

3.3.4 Specimen HHEP52M-TS-1, “high heat input” weld produced by EPRI

Figure 86 shows Specimen HHEP52M-TS-1 fabricated in the TS orientation.

Figure 86 Specimen HHEP52M-TS-1 machined from the high heat input Alloy 52M weld produced by EPRI.

The test was initiated with precracking and transitioning in the primary water environment. The testing conditions are given in Table 18, and the changes in crack length and K_{max} with time are shown in Figure 87. Given the apparently large environmental enhancement observed, the specimen was set at constant load early in the test (period 4), however, no growth was measured. Next, the crack was further advanced by approx. 1 mm, was re-transitioned at a higher K and set at constant load. Next, the crack was moved to a different microstructure and transitioning was repeated. Upon measuring almost “no growth” under cycle + hold in test period 16 for an extended period of time, cycling was reintroduced in test period 17, then hold was reintroduced in test period 18. The CGR response is approx. 2x lower than measured previously in test period 11, but so are the most recent cyclic CGRs. The “no growth” condition was substantiated next under constant load in test period 19.

Next, it was decided to evaluate the SCC CGR response at a higher K (50 MPa $m^{1/2}$). In order to facilitate this, the crack was advanced in fatigue in test periods 20-28, and re-transitioning at the higher K was begun. These continued with a cycle + hold sequence with increasing hold times, followed by constant load. Unlike the previous constant load test periods at moderate stress intensity factor, the test period appeared to show some growth despite clear evidence from the previous test period that the two sample surfaces are touching. At approximately 4,800h, the hydraulics tripped, unloading the specimen. Upon re-applying the load, the crack started at rate approx. 3x faster than before. It is not clear at this stage whether the crack truly advances or appears to advance in a region that was previously cracked, and in either case the two touching surfaces are likely masking the true advance. Next, in order to probe whether the crack advances or not, the specimen was unloaded. Surprisingly, the apparent crack length

was higher rather than lower, however, growth eventually stalled. Upon reloading, growth resumed at least initially at a rate comparable to the previous one. The effect of unloading/reloading on the crack response is significant. When the specimen is unloaded, if the surfaces are simply touching, the measured crack advance should decrease as the surfaces would touch even more than before. Instead, there appears that “disturbances” expose that the crack advance is actually larger, similar to the effect of a PPU cycle, i.e., exposing the real crack length. In essence, concern is that the overall response and the effects of unloading/reloading are not consistent with a “no growth” case where the surfaces are touching simply because of the length of the crack. As such, it was decided that an additional specimen will be produced and tested directly at the higher K to avoid the long crack advance and touching surfaces, and verify that the previously-described observations are artifacts of the long crack advance. Nevertheless, the crack in this system was re-transitioned and set at constant load for a final time in test period 40. A low SCC CGR was measured.

Table 18 Crack growth data for high heat input weld Alloy 52M Specimen HHEP52M-TS-1 in PWR water[a].

Test Period	Test Time, h	Temp. °C	Load Ratio R	Rise Time, s	Down Time, s	Hold Time, s	K_{max}, MPa·m$^{1/2}$	ΔK, MPa·m$^{1/2}$	CGR_{env}, m/s	Estimated CGR_{air}, m/s	Crack Length, mm
Pre a	152	321.7	0.3	1	1		22.5	15.7	2.26E-08	4.23E-08	13.353
Pre b	168	321.7	0.3	50	50		22.4	15.7	1.77E-09	8.39E-10	13.401
Pre c	175	321.4	0.3	1	1		22.9	16.0	3.14E-08	4.53E-08	13.770
Pre d	191	320.6	0.3	50	50		22.9	16.1	2.31E-09	9.12E-10	13.841
Pre e	199	320.3	0.3	1	1		23.6	16.5	3.66E-08	5.12E-08	14.363
Pre f	215	321.4	0.3	50	50		23.7	16.6	2.43E-09	1.05E-09	14.435
Pre g	223	320.4	0.3	1	1		24.5	17.1	4.27E-08	5.93E-08	15.046
Pre h	239	319.8	0.3	50	50		24.5	17.2	2.70E-09	1.19E-09	15.115
Pre i	245	320.6	0.3	1	1		25.2	17.6	4.85E-08	6.68E-08	15.637
1	273	320.7	0.5	120	12		25.3	12.7	7.50E-10	2.47E-10	15.740
2	311	320.5	0.5	600	12		25.4	12.7	2.74E-10	4.95E-11	15.763
3	359	322.0	0.5	1000	12		25.4	12.7	1.56E-10	3.05E-11	15.790
4	497	319.9	1				25.4	0.0	no growth	-	15.790
5	504	320.9	0.3	1	1		26.5	18.5	7.04E-08	8.22E-08	16.588
6	569	321.5	0.3	100	100		26.9	18.9	2.06E-09	8.89E-10	16.867
7	572	322.2	0.3	1	1		27.5	19.2	7.23E-08	9.69E-08	17.250
8	646	322.3	0.5	120	12		27.8	13.9	8.27E-10	3.67E-10	17.452
9	665	322.0	0.5	600	12		27.8	13.9	6.81E-10	7.35E-11	17.480
10	738	321.0	0.5	1000	12		27.9	13.9	2.20E-10	4.39E-11	17.521
11	816	321.0	0.5	1000	12	7,200	27.9	13.9	4.96E-11	5.36E-12	17.525
12	1,263	321.0	1	0	0		27.9	0.0	no growth	-	17.525
13	1,338	321.9	0.5	120	12		28.2	14.1	7.06E-10	3.89E-10	17.762
14	1,602	321.5	0.5	600	12		28.4	14.2	2.16E-10	7.92E-11	17.873
15	1,817	321.4	0.5	1000	12		28.5	14.3	1.47E-10	4.86E-11	17.986
16	2,349	318.6	0.5	1000	12	7,200	28.6	14.3	9.72E-13	5.77E-12	17.986
17	2,512	318.7	0.5	1000	12		28.6	14.3	1.00E-10	4.77E-11	18.042
18	2,683	318.7	0.5	1000	12	7,200	28.6	14.3	1.73E-11	5.84E-12	18.055
19	2,992	318.7	1	0	0		28.6	0.0	no growth		18.055
20	3,000	320.3	0.3	1	1		30.5	21.3	1.08E-07	1.45E-07	19.339
21	3,017	321.2	0.3	50	50		30.7	21.5	3.88E-09	3.03E-09	19.480
22	3,021	320.4	0.3	1	1		31.6	22.1	1.02E-07	1.69E-07	20.027
23	3,088	320.6	0.3	100	100		32.2	22.6	2.83E-09	1.83E-09	20.395
24	3,096	319.4	0.3	1	1		35.4	24.8	1.49E-07	2.67E-07	22.174
25	3,112	320.2	0.3	50	50		36.1	25.3	6.39E-09	5.81E-09	22.516
25	3,121	320.6	0.3	1	1		44.1	30.9	2.37E-07	6.64E-07	25.963
27	3,136	321.6	0.3	50	50		44.7	31.3	7.90E-09	1.42E-08	26.205
28	3,139	320.0	0.3	1	1		48.5	33.9	2.78E-07	9.72E-07	27.454
29	3,160	319.9	0.5	120	12		49.2	24.6	2.26E-09	3.72E-09	27.669
30	3,190	319.5	0.5	600	12		49.6	24.8	8.49E-10	7.61E-10	27.759
31	3,259	319.2	0.5	1000	12		50.0	25.0	4.75E-10	4.71E-10	27.883
32	3,359	320.2	0.5	1000	12	7200	49.8	24.9	1.49E-10	5.74E-11	27.840
33	3,424	319.6	0.5	1000	12	14400	49.9	25.0	8.40E-11	3.07E-11	27.867
34	3,691	318.1	0.5	1000	12	28800	49.9	25.0	3.42E-11	1.55E-11	27.862
35	6,766	319.9	1	0	0		50.3	0.0	1.00E-11		28.015
36	6,797	322.5	0.5	1000	12		50.3	25.2	3.70E-10	5.04E-10	28.015
37	6,983	321.7	0.5	1000	12	7200	50.4	25.2	4.50E-11	6.11E-11	28.029
38	7,147	321.5	0.5	1000	12	14400	50.5	25.2	2.54E-11	3.27E-11	28.042
39	7,320	321.5	0.5	1000	12	28800	50.5	25.2	1.54E-11	6.04E-12	24.052
40	8,215	322.5	1	0	0		50.5	0.0	2.00E-12	-	28.064

[a]Simulated PWR water with 2 ppm Li, 1000 ppm B, and 2 ppm. DO<10 ppb. Conductivity was 21±3 μS/cm, and pH 6.4.

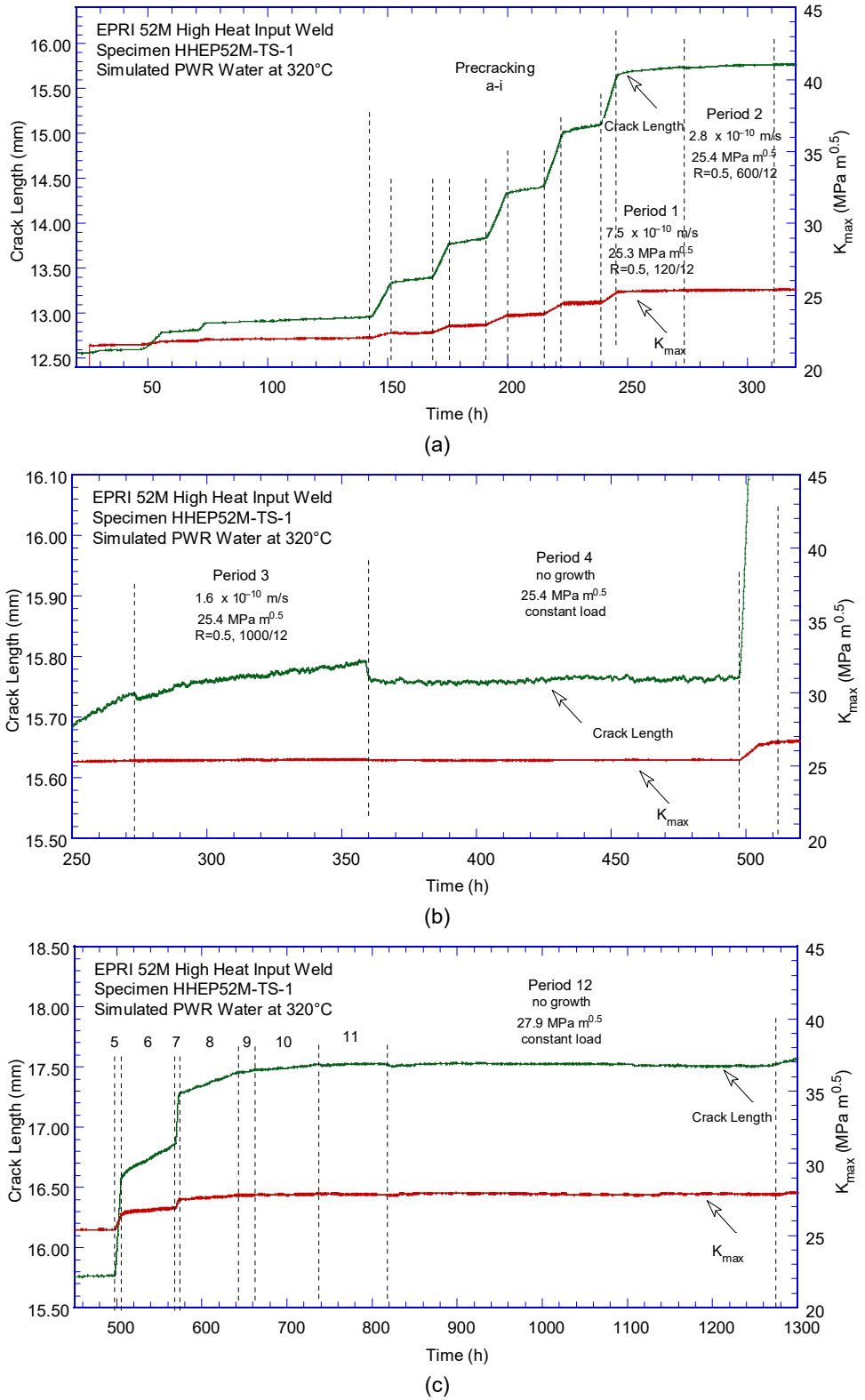

Figure 87 Crack–length–vs.–time for high heat input weld Alloy 52M Specimen HHEP52M-TS-1 in simulated PWR environment during test periods (a) precracking-2, (b) 3-4, (c) 5-12, (d) 13-19, and (e) 20-31, (f) 31-33, and (g) 34.

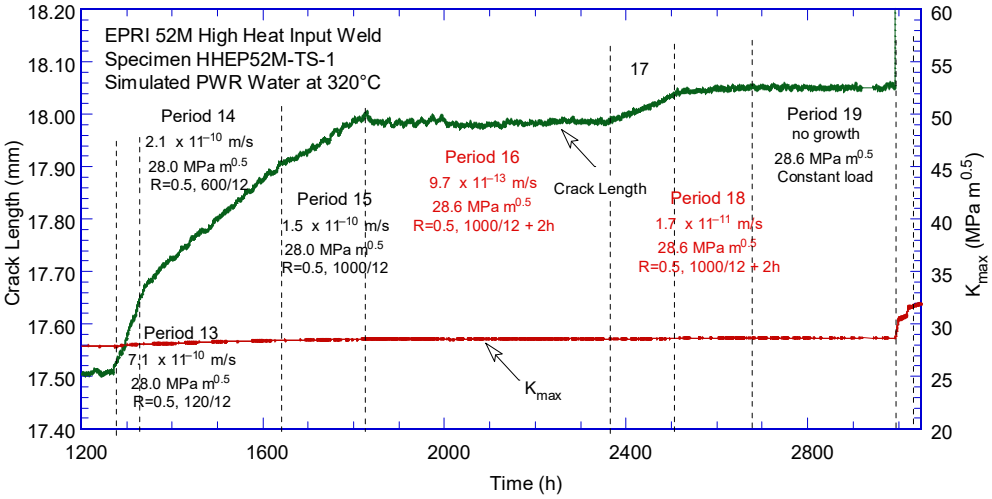

(d)

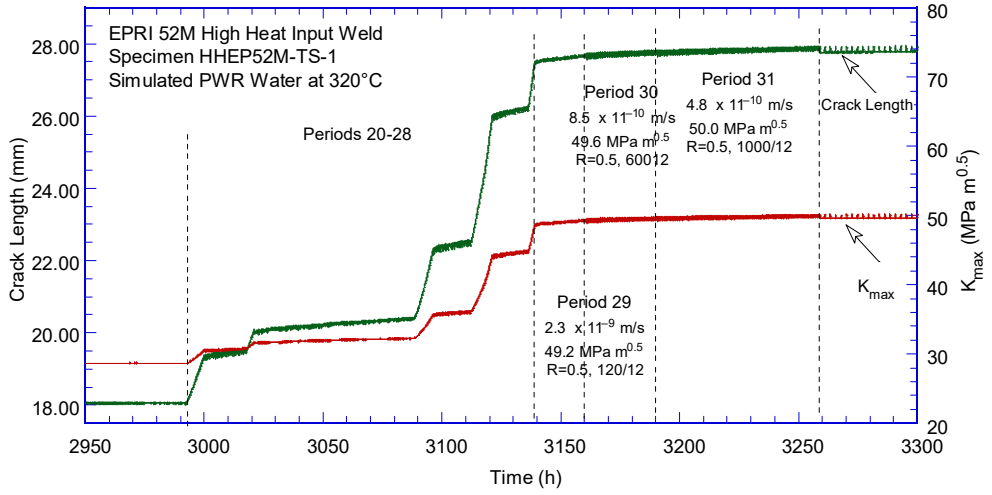

(e)

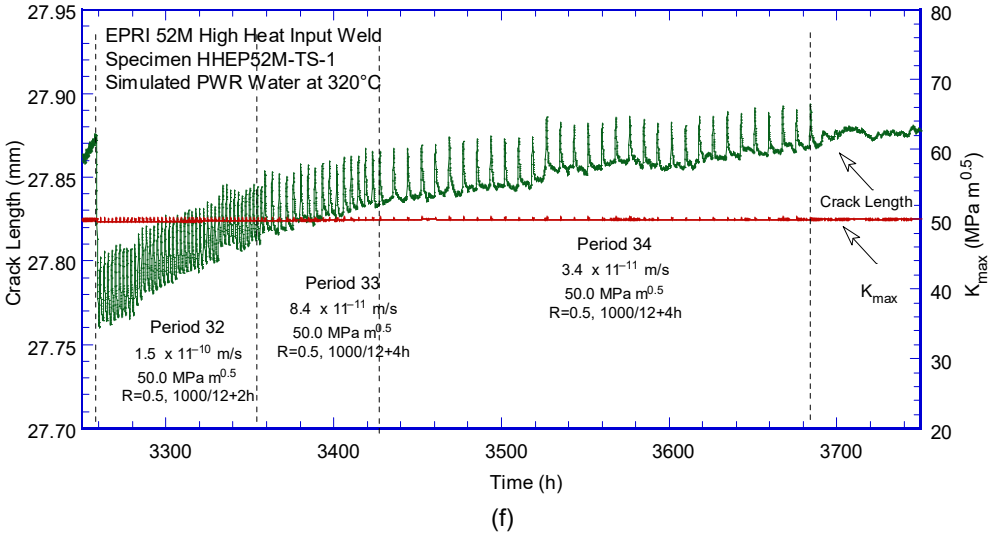

(f)

Figure 87 (cont.)

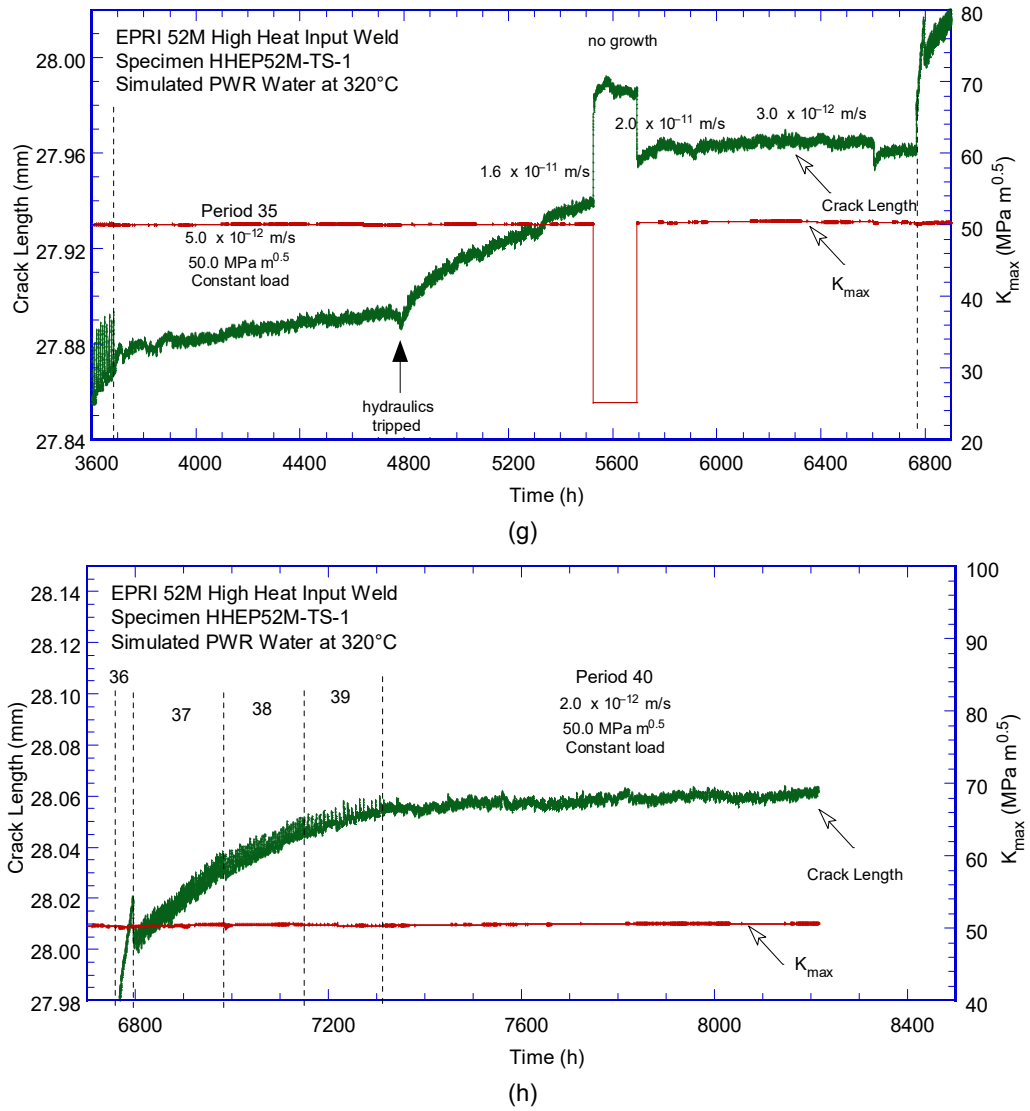

Figure 87 (cont.)

Figure 88 shows the cyclic CGR data obtained for the current HHEP52M-TS-1 specimen. Figure 88a shows that the fatigue response compares well with other Alloy 52M weldments, such as from the EPRI repair weld and the WOL produced at ANL [27]. The environmental enhancement in this high heat input weld is similar to that measured for the unconstrained ANL Alloy 52M WOL, and slightly higher than that for the repair weld produced by EPRI; however, the EPRI repair weld did not show an increase of the cyclic rates vs. the original (un-repaired) weld. In other words, the effects of the presumably increased levels of deformation (leading to an increased K) on the fatigue CGR response in these Alloy 52M weldments are absent. Figure 88b shows the cyclic response during initial precraking and transitioning at moderate K (25-28 MPa $m^{1/2}$) and subsequent precracking and transitioning at high K (50 MPa $m^{1/2}$). The fatigue response matches the initial response, however, the corrosion fatigue response shows no environmental enhancement at the higher K.

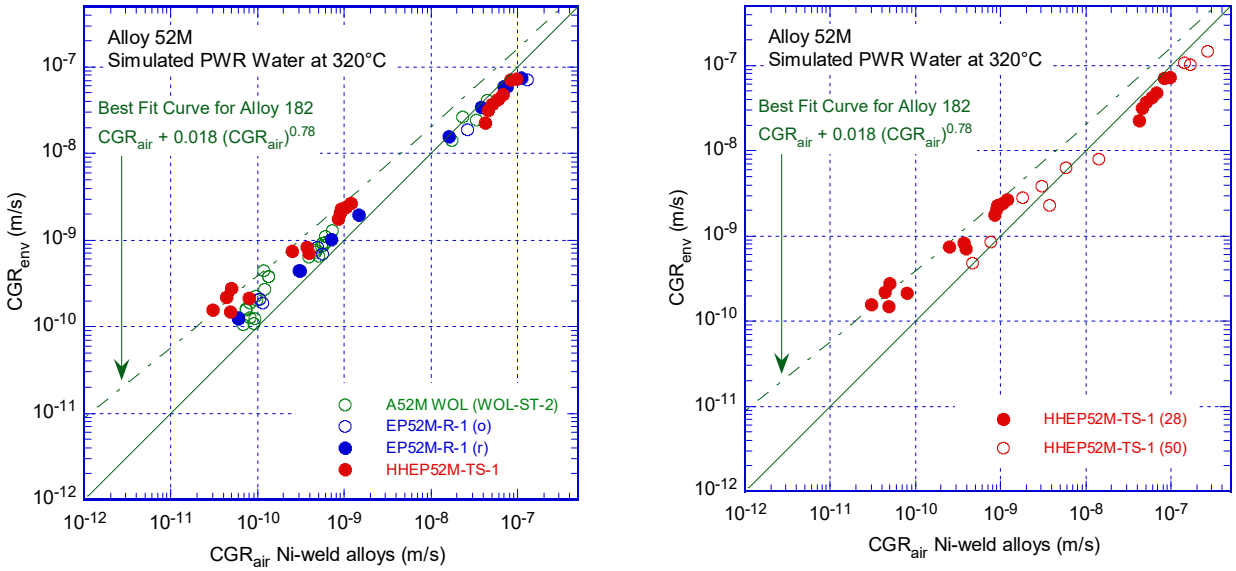

(a) (b)

Figure 88 (a) Cyclic CGR data for Specimen HHEP52M-TS-1 machined from the high heat input Alloy 52M weld produced by EPRI. Similar data for the Alloy 52M repair (r) and original (o) produced by EPRI, as well as an Alloy 52M WOL produced by ANL is included. (b) Cyclic CGR data for Specimen HHEP52M-TS-1 during initial precraking and transitioning at moderate K (25-28 MPa m$^{1/2}$) and subsequent precracking and transitioning at high K (50 MPa m$^{1/2}$).

The entire fracture surface of specimen HHEP52M-TS-1 is shown in Figure 89. The image indicates that the testing procedure resulted in a straight, uniform fracture surface. Measurements made on this image are in an excellent agreement (2%) with the DC potential measurements, hence no correction was performed.

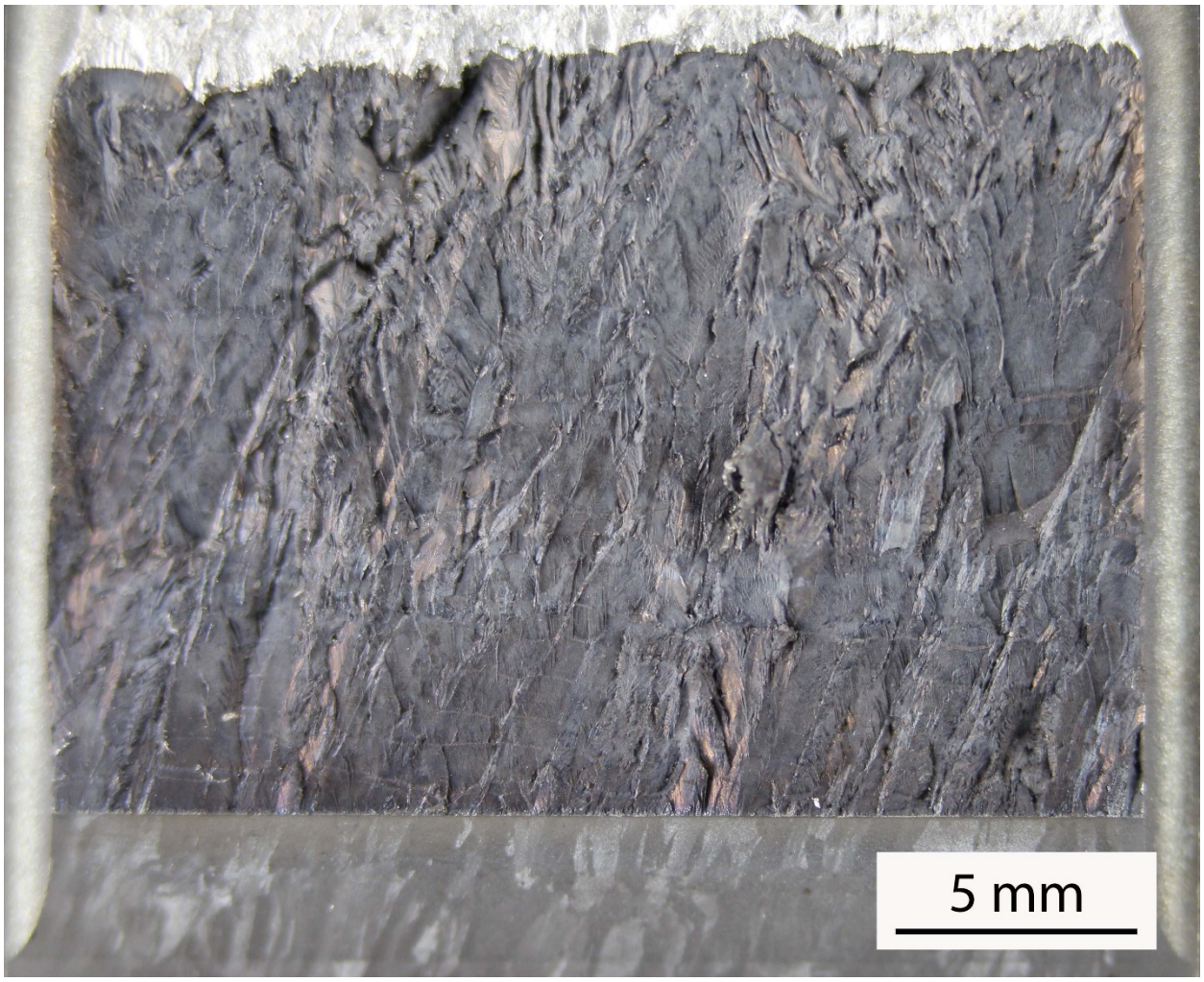

Figure 89 **Fracture surface of specimen HHEP52M-TS-1. Crack advance is from bottom to top.**

3.3.5 Specimen HHEP52M-TS-2, “high heat input” weld produced by EPRI

Specimen HHEP52M-TS-2 (Figure 90) was machined in the same general orientation as the first specimen presented in the previous section, but with a longer initial crack to avoid some of the artifacts observed in that test. Also, the SCC CGR response was only evaluated at a higher K (50 MPa $m^{1/2}$).

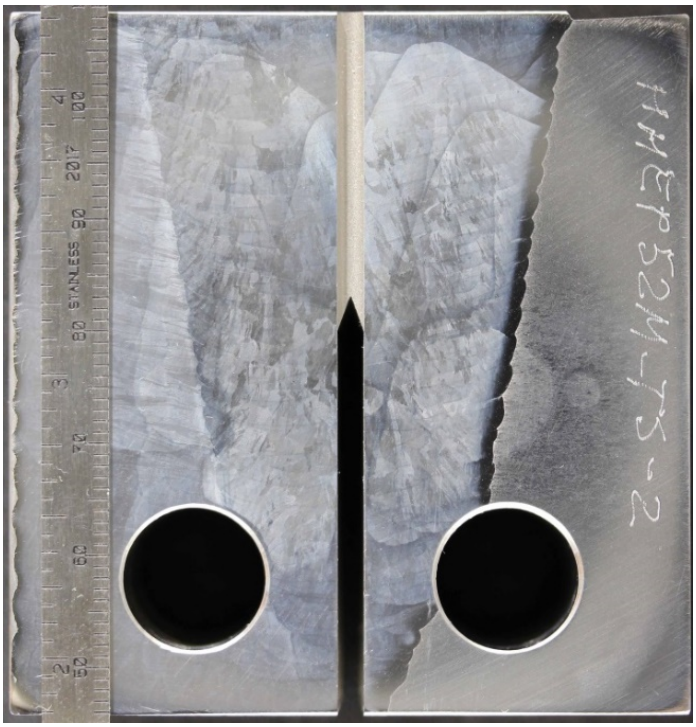

Figure 90 Specimen HHEP52M-TS-2 machined from the high heat input Alloy 52M weld produced by EPRI.

The testing conditions are given in Table 19, and the changes in crack length and K_{max} with time are shown in Figure 91. The test was initiated with precracking and transitioning in the primary water environment, followed by initial transitioning steps. A first, “no growth” determination of the SCC CGR was made in test period 6. Next, the crack was advanced by approx. 0.7 mm to a different microstructure and re-transitioned. Response under constant load in test period 16 was still low. Finally, the crack was advanced by approximately 3 mm to a different microstructure, was re-transitioned, and set at constant load. The SCC CGR was a moderate 2 x 10^{-11} m/s.

Table 19 Crack growth data for Alloy 52M high heat input weld Specimen HHEP52M-TS-2 in PWR water[a].

Test Period	Test Time, h	Temp. °C	Load Ratio R	Rise Time, s	Down Time, s	Hold Time, s	K_{max}, MPa·m$^{1/2}$	ΔK, MPa·m$^{1/2}$	CGR_{env}, m/s	Estimated CGR_{air}, m/s	Crack Length, mm
Pre a	23	320.8	0.3	1	1		43.5	30.5	2.27E-07	6.30E-07	25.712
Pre b	25	321.2	0.3	5	5		44.1	30.9	5.58E-08	1.34E-07	25.937
Pre c	26	321.3	0.3	2	2		45.0	31.5	1.16E-07	3.64E-07	26.281
Pre d	43	321.0	0.3	50	50		45.6	31.9	6.60E-09	1.53E-08	26.477
1	66	321.0	0.5	120	12		46.0	23.0	1.38E-09	2.85E-09	26.601
2	91	320.6	0.5	600	12		46.1	23.0	3.95E-10	5.72E-10	26.634
3	167	320.5	0.5	1000	12		46.3	23.1	2.54E-10	3.50E-10	26.699
4	354	320.8	0.5	1000	12	7,200	46.4	23.2	3.14E-11	4.31E-11	26.721
5	595	320.8	0.5	1000	12	14,400	46.5	23.2	2.09E-11	2.32E-11	26.739
6	1,099	320.2	1	0	0		46.5	0.0	no growth	-	26.739
7	1,243	319.7	0.5	1000	12	14,400	46.4	23.2	1.43E-11	2.28E-11	26.739
8	1,267	319.8	0.5	120	12		46.7	23.4	1.68E-09	3.00E-09	26.845
9	1,338	320.1	0.5	600	12		47.0	23.5	4.98E-10	6.16E-10	26.929
10	1,392	320.3	0.5	120	12		48.2	24.1	2.07E-09	3.44E-09	27.337
11	1,436	321.0	0.75	120	12		48.5	12.1	4.37E-10	5.28E-10	27.405
12	1,507	319.6	0.75	600	1		48.5	12.1	1.07E-10	1.04E-10	27.431
13	1,579	319.8	0.75	1000	12		48.6	12.2	6.52E-11	6.32E-11	27.450
14	1,771	319.9	0.75	1000	12	7,200	48.7	12.2	1.59E-11	7.74E-12	27.454
15	2,010	319.8	0.75	1000	12	14,400	48.6	12.1	9.20E-12	4.09E-12	27.464
16	2,509	320.1	1	0	0		48.7	0.0	no growth	-	27.468
17	2,607	320.2	0.75	120	12		48.9	12.2	3.32E-10	5.43E-10	27.569
18	2,612	321.0	0.3	1	1		59.4	41.6	9.79E-07	2.26E-06	30.285
19	2,628	320.1	0.75	600	12		59.8	14.9	1.52E-09	2.47E-10	30.362
20	2,699	320.2	0.75	1000	12		60.5	15.1	4.64E-10	1.56E-10	30.531
21	2,772	320.2	0.75	1000	12	7,200	60.1	15.0	1.32E-10	1.85E-11	30.443
22	2,965	320.2	0.75	1000	12	14,400	60.3	15.1	8.41E-11	9.97E-12	30.470
23	4,669	319.4	1	0	0		60.7	0.0	1.80E-11	-	30.544

[a]Simulated PWR water with 2 ppm Li, 1000 ppm B, and 2 ppm. DO<10 ppb. Conductivity was 21±3 μS/cm, and pH 6.4.

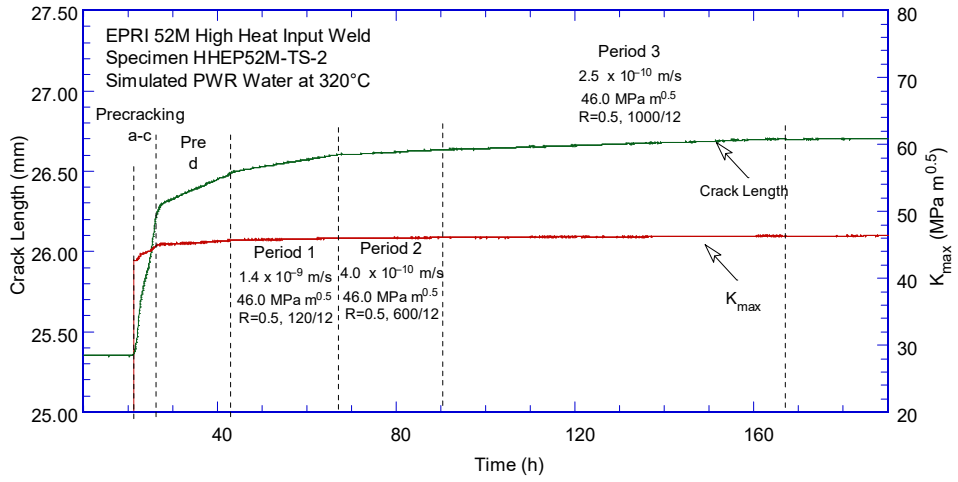

(a)

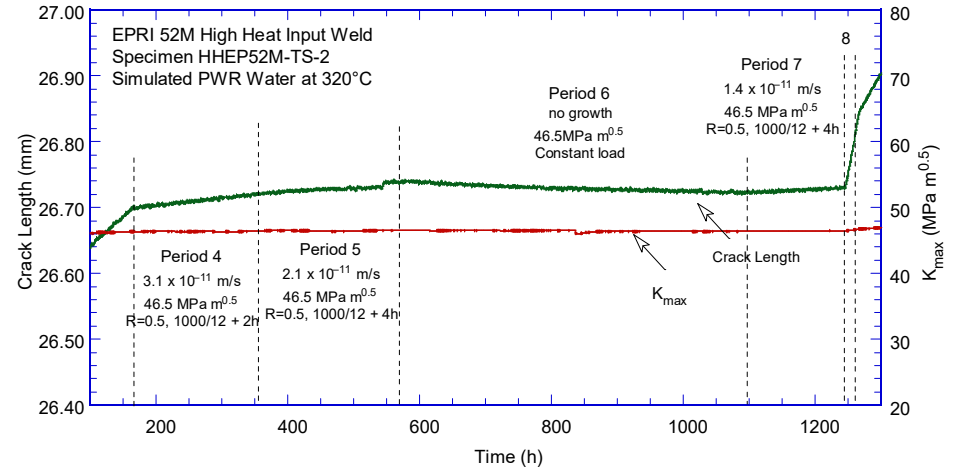

(b)

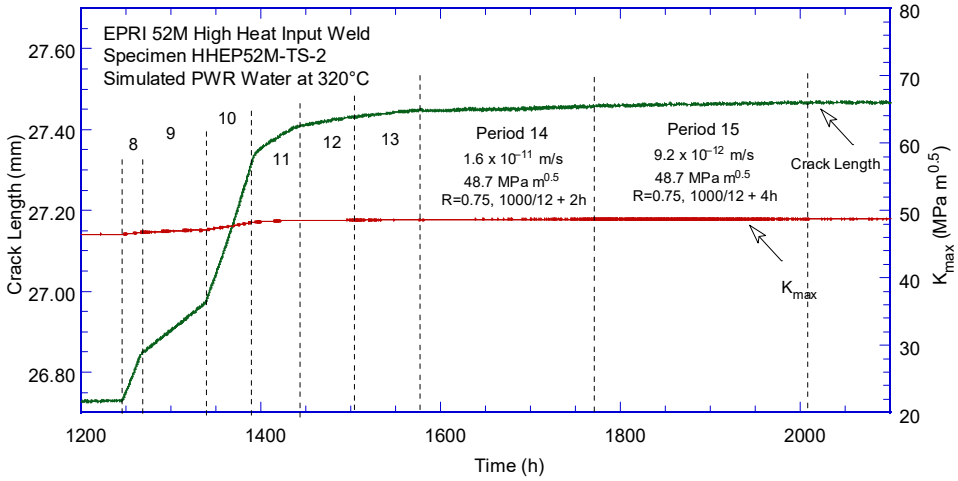

(c)

Figure 91 Crack–length–vs.–time for Alloy 52M high heat input weld Specimen HHEP52M-TS-2 in simulated PWR environment during test periods (a) precracking-3, (b) 4-7, (c) 8-15, (d) 16, (e) 19-22, and (f) 23

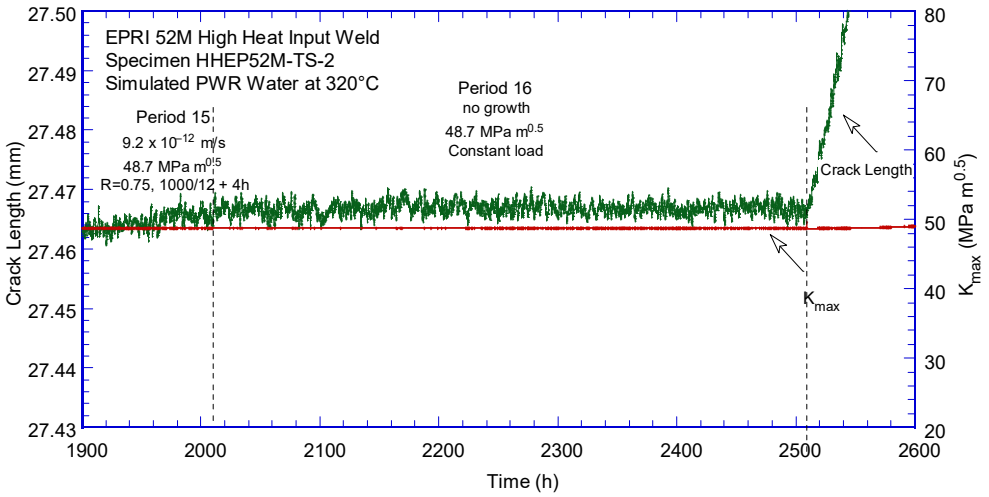

(d)

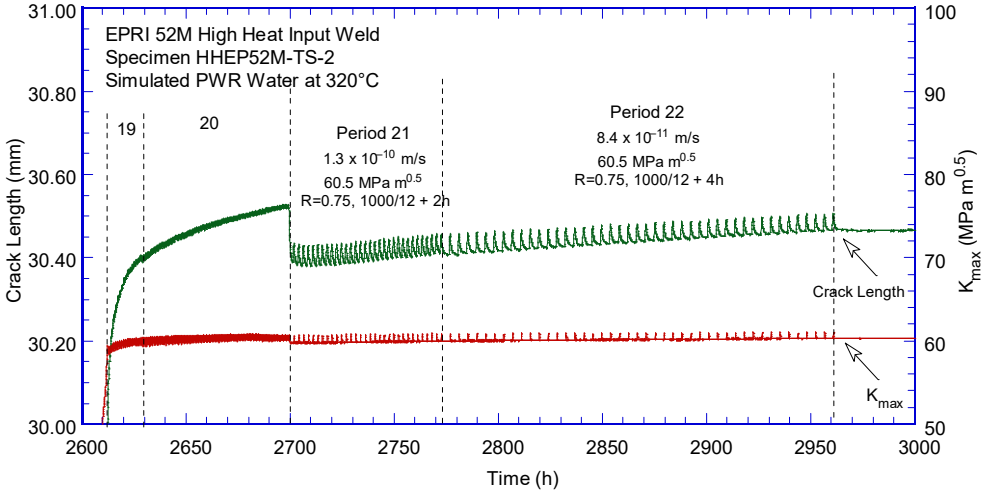

(e)

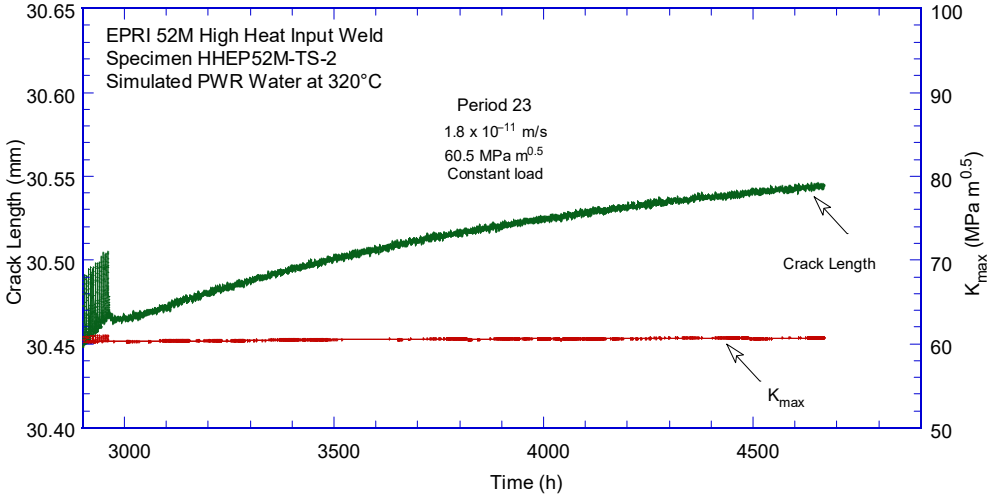

(f)

Figure 91 (cont.)

Figure 92 compares the cyclic CGR response Alloy 52M high heat input weld Specimens HHEP52M-TS-1 and HHEP52M-TS-2 tested under moderate (30 MPa $m^{0.5}$) and high (30 MPa $m^{0.5}$) stress intensity factors. The data for the current specimen appears to be in good agreement with that from the previous specimen tested under similarly high stress intensity factors.

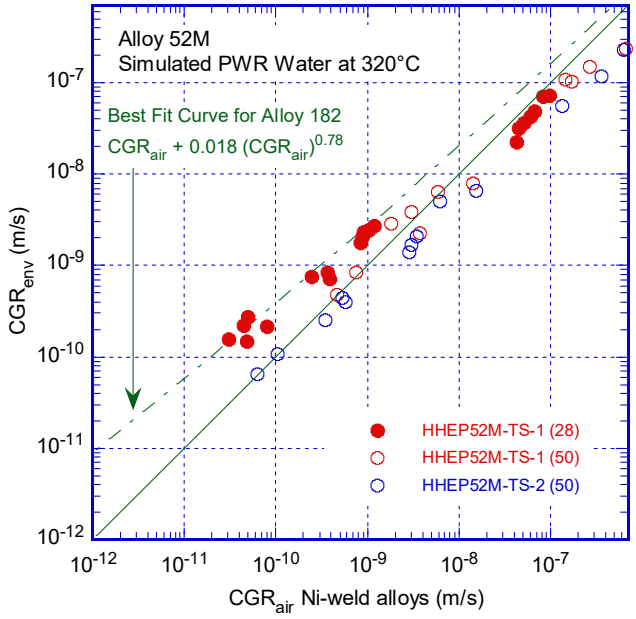

Figure 92 Cyclic CGR data for Alloy 52M high heat input weld Specimens HHEP52M-TS-1 and HHEP52M-TS-2 tested under moderate (30 MPa $m^{0.5}$) and high (30 MPa $m^{0.5}$) stress intensity factors.

3.3.6 Specimen IHI152M-TS-1, weldability issues weld produced by IHI

The Alloy 152M weld Specimen IHI152M-TS-1 (Figure 93) was machined (see red contour) to enable testing of two weld fillers (see dotted black line). According to the WPS, the first filler had weldability issues.

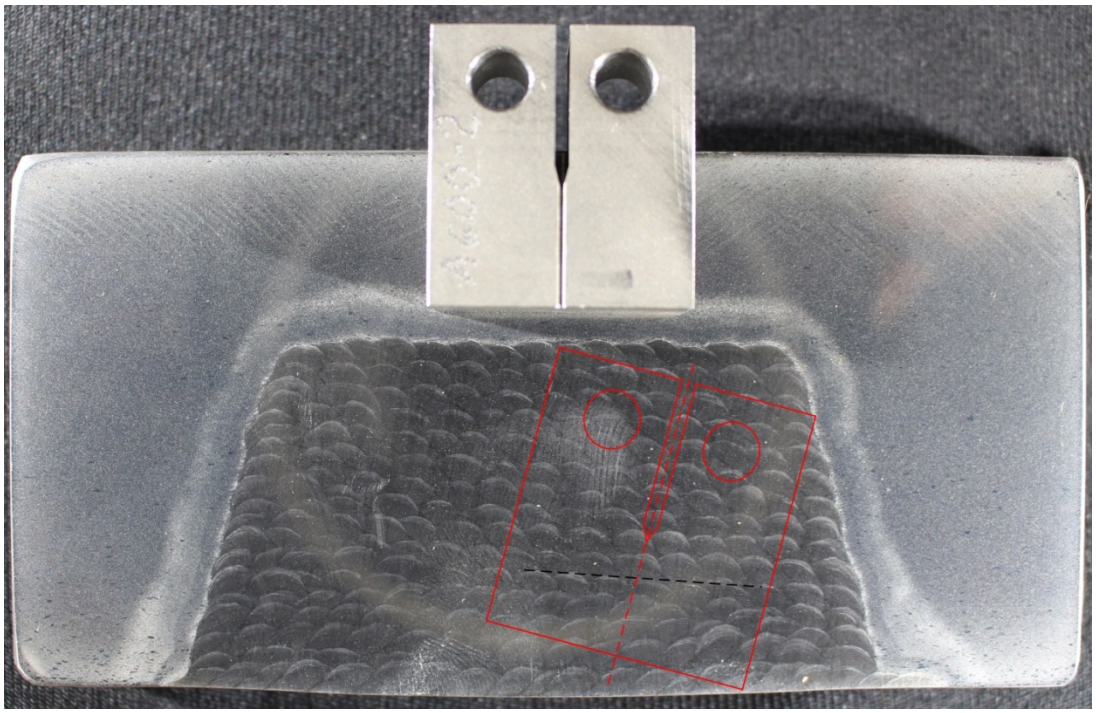

Figure 93 Alloy 152M weld produced by IHI and CT specimen positioning (red). The black dotted line indicates the separation between two filler heats; the first heat was abandoned because according to the WPS it showed "poor weldability and many spatter was generated during welding".

The testing conditions are given in Table 20, and the changes in crack length and K_{max} with time are shown in Figure 94. The test was initiated with precracking and transitioning in the primary water environment. A relatively small response was measured under cycle+hold in test period 5, suggesting that transitioning at IG SCC has not occurred. The subsequent SCC CGR measured under constant load confirmed the "no growth" condition. The same cyclic response with little environmental enhancement was reproduced in test periods 8-10. Next, the crack was advanced to a different microstructure and transitioning was attempted again. The response in test period 14 suggests that transitioning to IG SCC has not occurred, and the "no growth" condition was confirmed at constant load in test period 15.

Next, the crack was advanced by 0.25 mm, and transitioning steps were undertaken. The response was consistent with the previous measurements, and suggested that no transitioning had occurred and that the SCC CGR would be low. The rate was confirmed in test period 20. The latest set of measurements were conducted at approx. 1.5 mm from the specimen notch (the dotted black line in Figure 93 – change to different weld heat – is estimated to be at 4.2 mm from the specimen notch).

Next, in test periods 21-22 the crack was advanced towards the region made with the different Alloy 152 filler to a distance of approx. 2.9 mm from the specimen notch – see dotted line in Figure 93 – was re-transitioned, and a final SCC CGR determination will be made for this weld. One already notes that changing the hold periods between K_{max} (specimen loaded) and K_{min} (specimen unloaded) in test periods 25-26 does not produce a change in CGR. Further, a 2x decrease in loading frequency in test periods 27-28 results in a 2x decrease in CGR, a behavior that suggests that fatigue is the driving force for growth. Hence, SCC CGR at constant load is expected to be small. Next, the specimen was advanced to the region made with the second filler in test periods 30-33 (cyclic CGRs were reproduced), and transitioning steps were undertaken. One observes that a 2x decrease in loading frequency in test periods 36-37 results in a 2x decrease in CGR, a behavior that suggests that fatigue is the driving force for growth. The specimen was set at constant load in test period 38, and indeed no growth is measured.

Next, the loading was changed to cycling to advance the crack to a different microstructure. As the crack advance increased beyond 6 mm, the growth began to accelerate due to increasing K, in steps (see light blue dotted lines in Fig. m and n), eventually breaking the specimen at approx. 6.3 mm crack length. Next, the test was stopped and the specimen was be removed for examination.

Table 20 Crack growth data for repair weld specimen IHI152M-TS-1 in PWR water[a].

Test Period	Test Time, h	Temp. °C	Load Ratio R	Rise Time, s	Down Time, s	Hold Time, s	K_{max}, MPa·m$^{1/2}$	ΔK, MPa·m$^{1/2}$	CGR_{env}, m/s	Estimated CGR_{air}, m/s	Crack Length, mm
Pre a	47	320.0	0.30	1	1		23.9	16.8	4.12E-08	5.40E-08	12.011
Pre b	49	320.3	0.30	2	2		24.2	16.9	2.63E-08	2.82E-08	12.090
Pre c	51	320.0	0.30	5	5		24.3	17.0	1.19E-08	1.15E-08	12.137
Pre d	70	320.0	0.30	50	50		24.5	17.2	1.91E-09	1.19E-09	12.199
1	105	320.4	0.50	120	12		24.8	12.4	3.18E-10	2.24E-10	12.252
2	164	320.3	0.50	600	12		24.8	12.4	1.14E-10	4.52E-11	12.276
3	195	320.3	0.50	120	12		25.0	12.5	4.31E-10	2.31E-10	12.319
4	261	320.6	0.50	600	12		25.1	12.5	1.15E-10	4.74E-11	12.349
5	405	320.5	0.50	600	12	7,200	25.2	12.6	1.20E-11	3.68E-12	12.354
6	887	320.6	1.00	600			25.2	0.0	no growth	-	12.350
7	1,170	320.8	0.50	600	12	7,200	25.2	12.6	8.49E-12	3.74E-12	12.363
8	1,192	320.9	0.50	120	12		25.3	12.6	4.60E-10	2.44E-10	12.395
9	1,358	320.7	0.50	600	12		25.5	12.7	1.30E-10	5.04E-11	12.474
10	1,457	320.5	0.50	600	12	7,200	25.6	12.8	1.40E-11	3.95E-12	12.481
11	1,602	320.7	0.50	600	12		25.7	12.9	1.22E-10	5.25E-11	12.541
12	1,701	320.6	0.50	120	12		26.3	13.2	5.33E-10	2.87E-10	12.714
13	1,939	320.1	0.50	600	12		26.8	13.4	1.40E-10	6.14E-11	12.833
14	2,201	320.4	0.50	600	12	7,200	27.0	13.5	1.50E-11	4.89E-12	12.847
15	2,937	321.0	1.00	0	0		27.1	0.0	no growth	-	12.849
16	3,101	321.5	0.50	120	12		28.1	14.0	6.61E-10	3.80E-10	13.193
17	3,365	322.6	0.50	600	12		28.8	14.4	1.77E-10	8.53E-11	13.358
18	3,538	322.4	0.50	600	12	7,200	28.7	14.3	2.11E-11	6.44E-12	13.371
19	3,919	320.1	0.50	600	12	14,400	29.3	14.6	9.11E-12	3.54E-12	13.386
20	4,219	319.9	1.00	0	0		29.3	0.0	no growth	-	13.386
21	4,521	319.1	0.30	1	1	0	30.1	21.1	1.03E-07	1.37E-07	14.302
22	4,270	318.9	0.30	50	50	0	31.0	21.7	4.43E-09	3.09E-09	14.483
23	4,292	318.7	0.50	120	12	0	31.7	15.8	1.07E-09	6.02E-10	14.598
24	4,460	319.2	0.50	600	12	0	32.5	16.3	2.67E-10	1.35E-10	14.758
25	4,532	319.6	0.50	600	12	7,200	32.6	16.3	3.21E-11	1.05E-11	14.762
26	4,603	319.4	0.50	600	12	7,200 at K_{min}	32.4	16.2	3.30E-11	1.02E-11	14.759
27	4,772	319.6	0.50	600	12	7,200	32.7	16.3	2.34E-11	1.06E-11	14.783
28	4,962	319.5	0.50	600	12	14,400	32.7	16.3	1.25E-11	5.48E-12	14.792
29	5,394	319.2	1.00	0	0		32.5	0.0	5.80E-13	-	14.792

Table 20 (cont.)

Test Period	Test Time, h	Temp. °C	Load Ratio R	Rise Time, s	Down Time, s	Hold Time, s	K_{max}, MPa·m$^{1/2}$	ΔK, MPa·m$^{1/2}$	CGR_{env}, m/s	Estimated CGR_{air}, m/s	Crack Length, mm
30	5,400	319.2	0.30	1	1		36.8	25.7	2.61E-07	3.10E-07	16.134
31	5,401	319.0	0.30	1	1		33.4	23.4	2.21E-07	2.08E-07	16.330
32	5,402	319.0	0.30	1	1		31.2	21.8	1.85E-07	1.57E-07	16.513
33	5,419	318.9	0.30	50	50		32.7	22.9	6.66E-09	3.80E-09	16.735
34	5,441	319.0	0.50	120	12		33.8	16.9	1.42E-09	7.88E-10	16.875
35	5,537	318.9	0.50	600	12		35.0	17.5	4.00E-10	1.81E-10	17.011
36	5,633	319.1	0.49	600	12	7,200	35.0	17.9	5.12E-11	1.48E-11	16.997
37	6,088	319.5	0.49	600	12	14,400	35.5	18.1	2.18E-11	8.16E-12	17.042
38	6,591	319.6	1.00	0	0		35.1	0.0	7.93E-13	-	17.061
39	6,787	319.5	0.49	120	12		46.8	23.4	3.66E-09	3.00E-09	18.200

[a]Simulated PWR water with 2 ppm Li, 1000 ppm B, and 2 ppm. DO<10 ppb. Conductivity was 21±3 μS/cm, and pH 6.4.

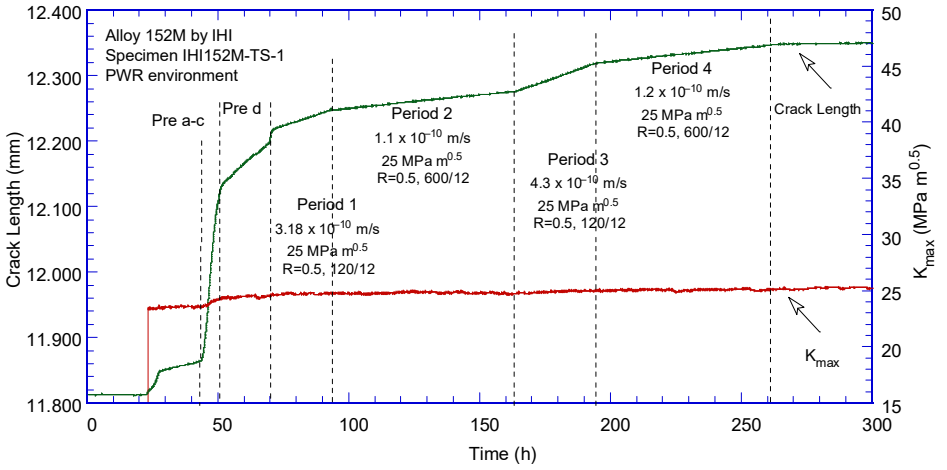

(a)

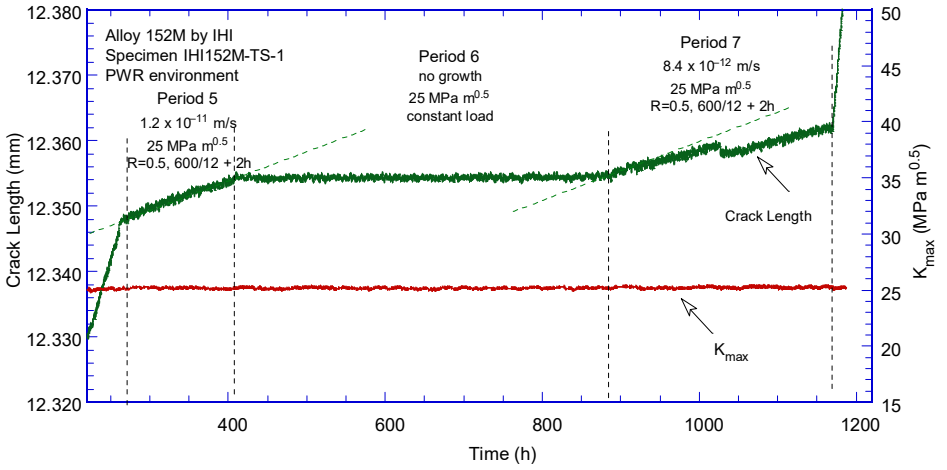

(b)

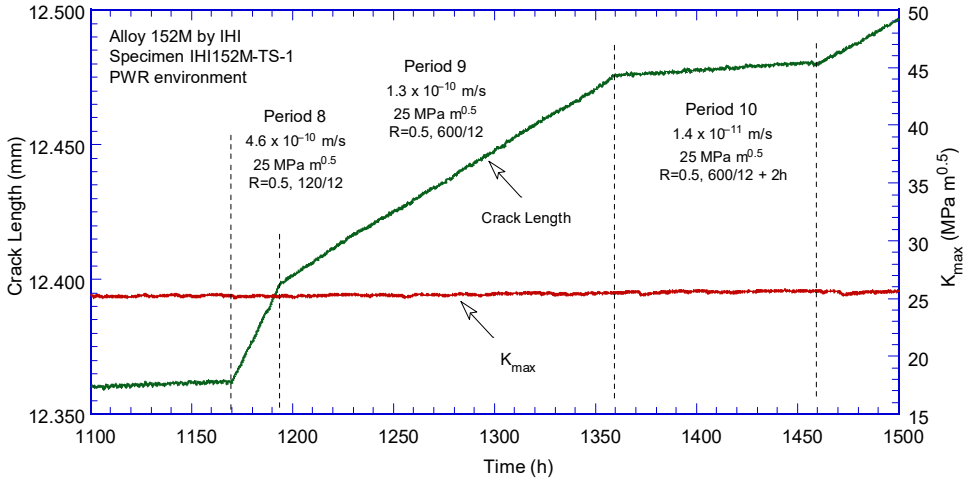

(c)

Figure 94 Crack–length–vs.–time for weld specimen IHI152M-TS-1 in simulated PWR environment during test periods (a) precracking-4, (b) 5-7, (c) 8-10, (d) 11-14, (e) 15, (f) 16-19, (g) 20, (h) 21-24, (i) 25-28, (j) 29, (k) 30-35, (l) 36-38, (m) 39, and (n) end of 39.

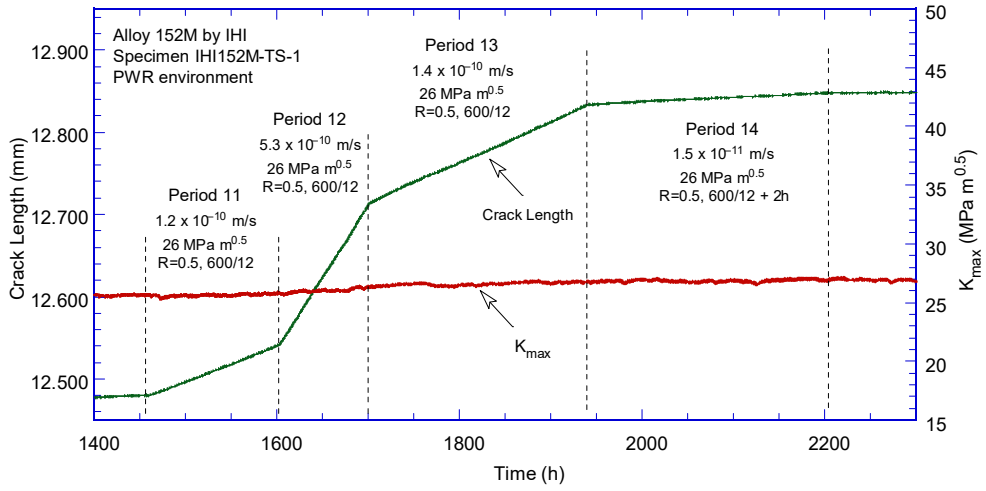

(d)

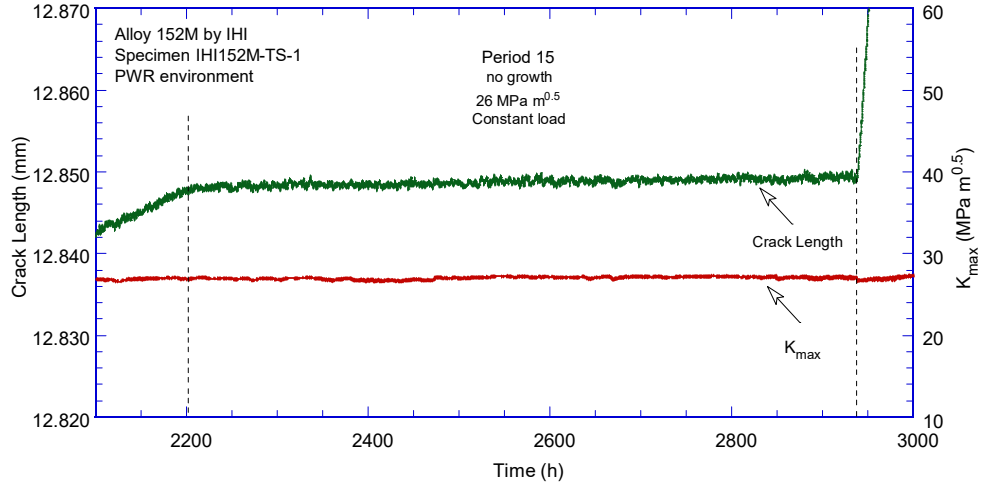

(e)

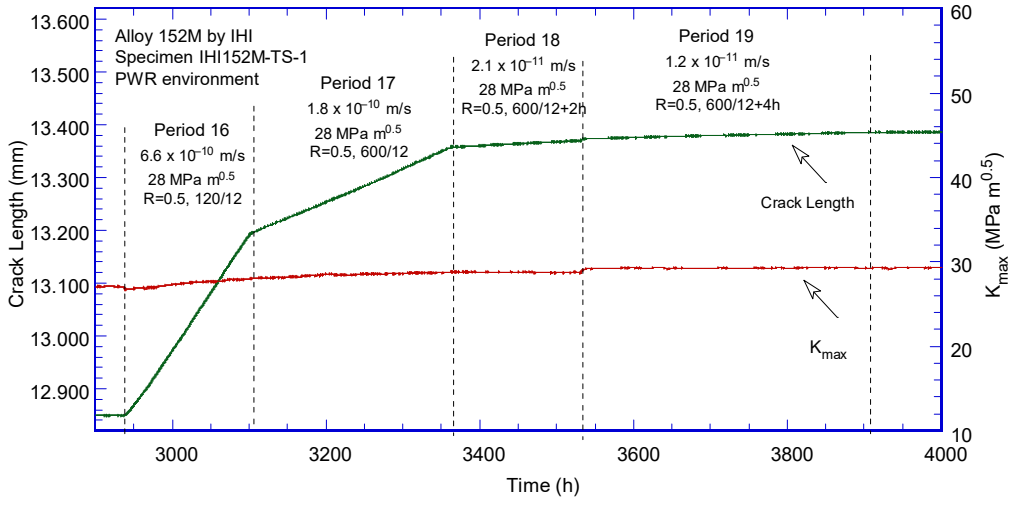

(f)

Figure 94 (cont.)

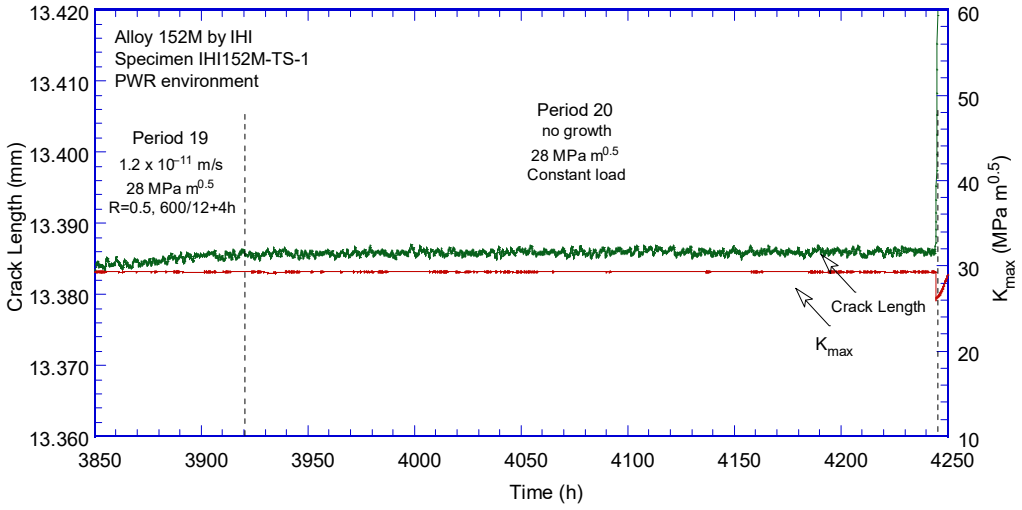

(g)

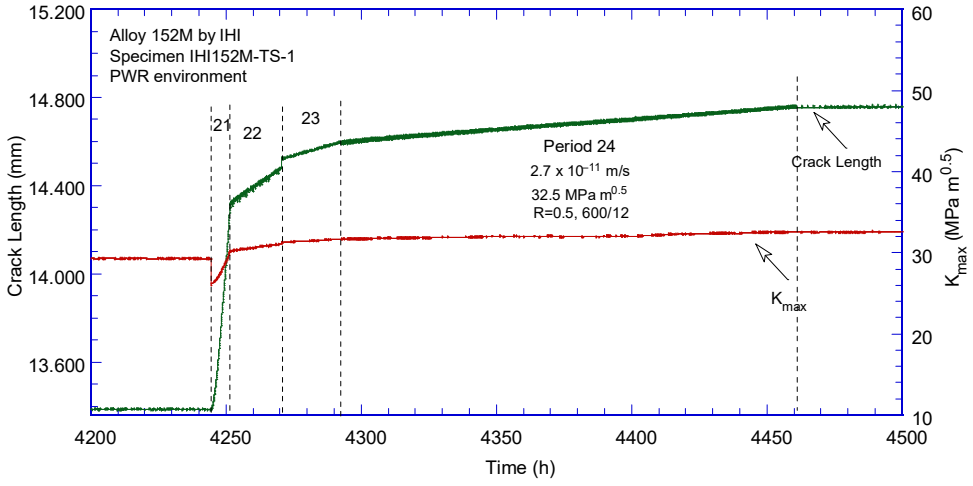

(h)

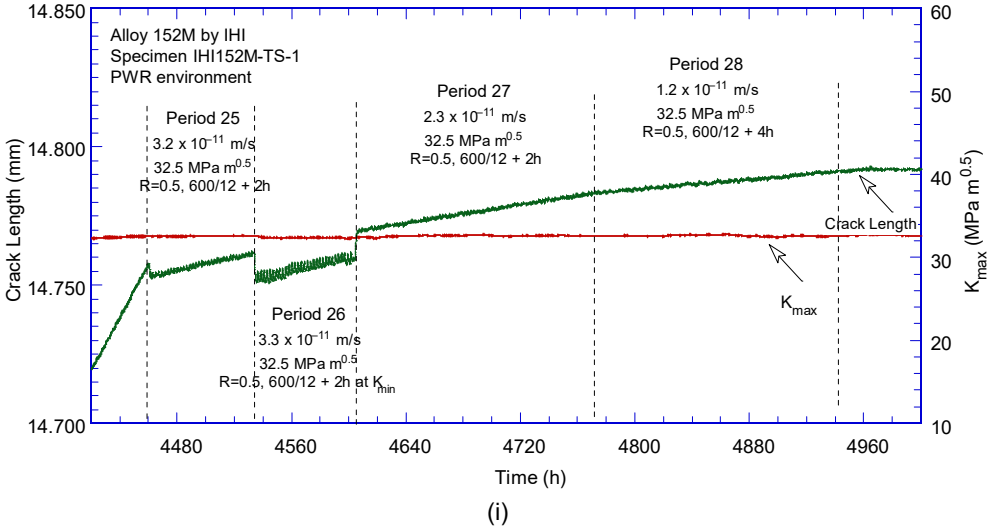

(i)

Figure 94 (cont.)

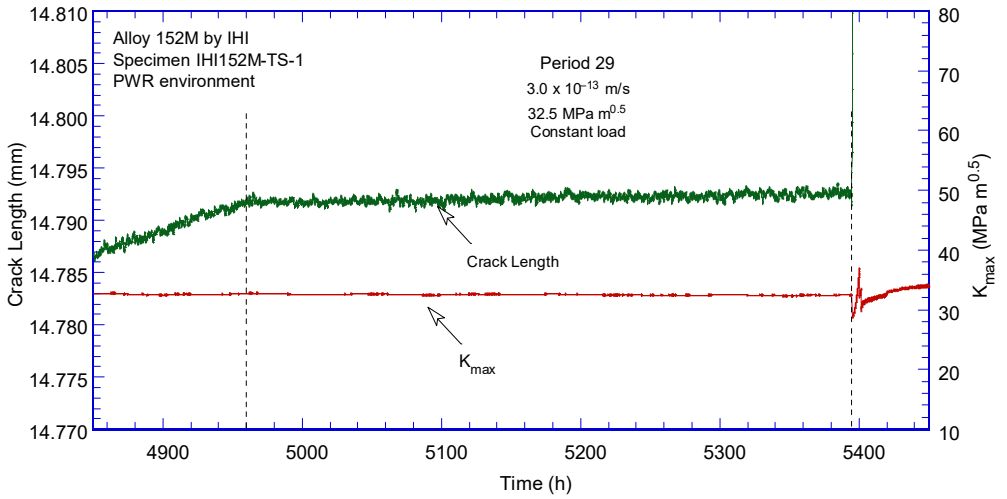

(j)

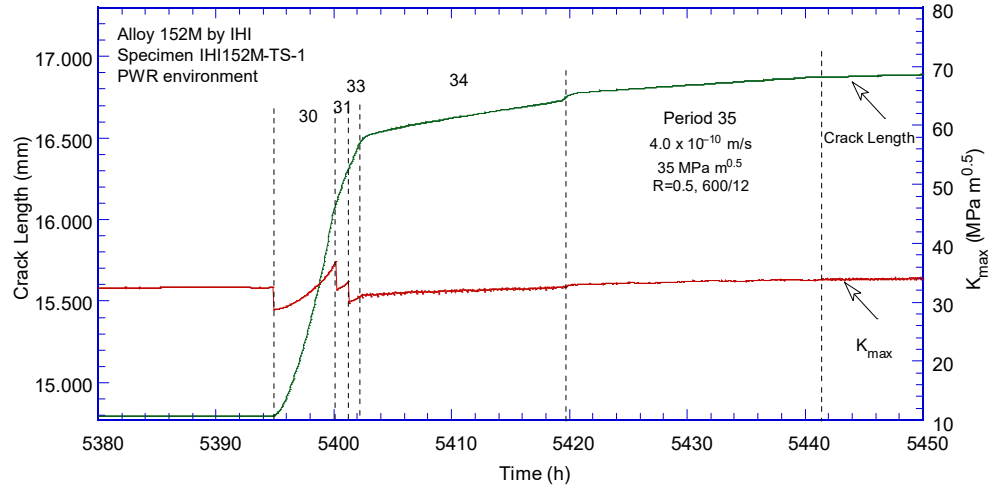

(k)

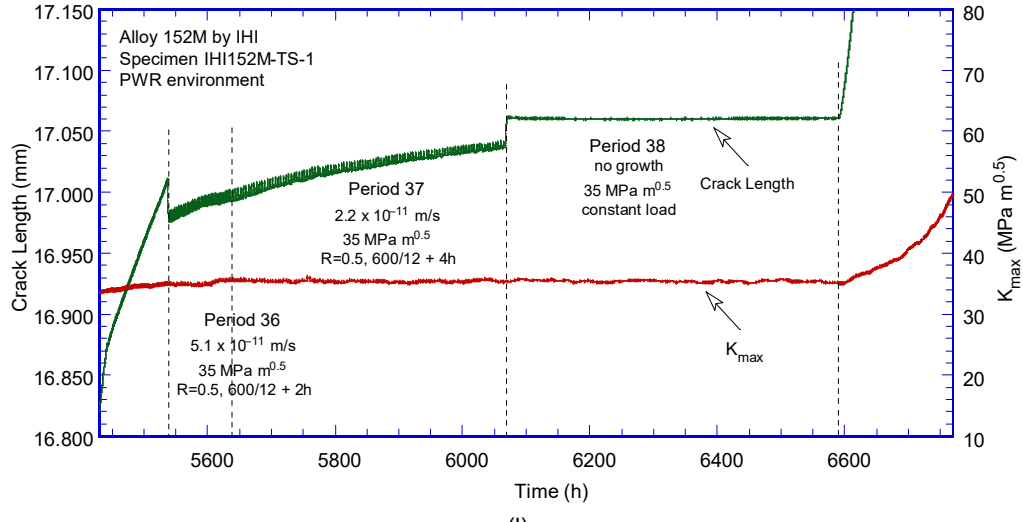

(l)

Figure 94 (cont.)

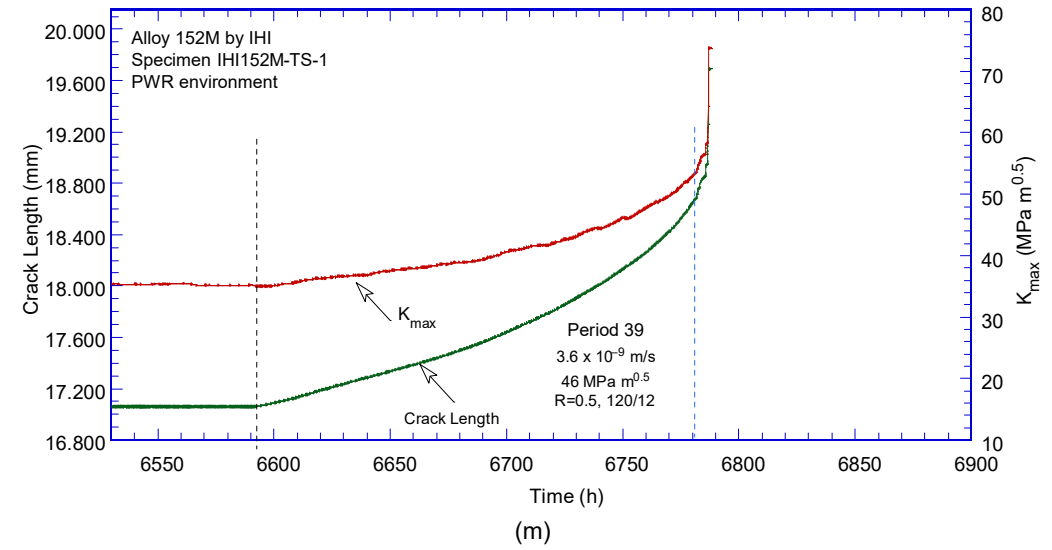

(m)

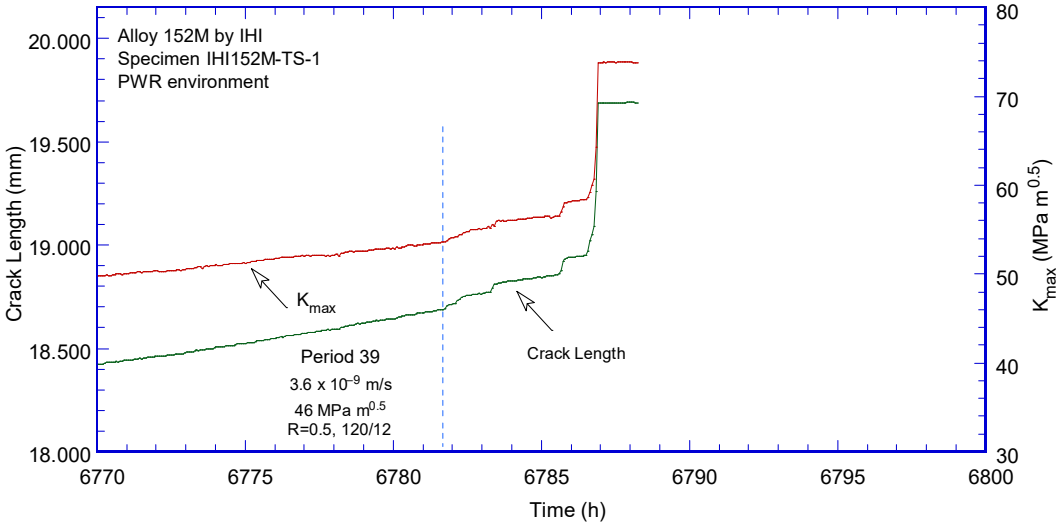

(n)

Figure 94 (cont.)

Figure 95 shows the cyclic CGR data obtained for the IHI Alloy 152M weld. The response is as expected, remarkably consistent, and shows a low environmental enhancement. The cyclic response obtained during the advancement to the weld region made with a different filler code is consistent with the first set.

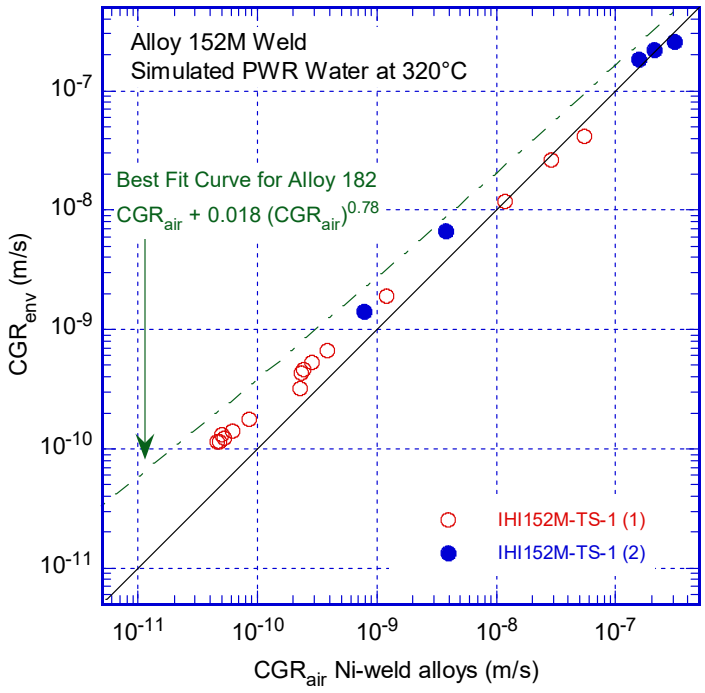

Figure 95 Cyclic CGR data for the IHI Alloy 152M weld in simulated primary environment.

The entire fracture surface of specimen IHI152M-TS-1 is shown in Figure 96. The image indicates that the testing procedure resulted in a straight, uniform fracture surface. Measurements made on this image are in excellent agreement (1%) with the DC potential measurements, hence no correction was performed. The red arrows at 3.3 mm from the specimen notch (through test period 29, Table 20) indicate the regions made with different weld fillers.

The fracture surface was also examined in the SEM, and essentially no IG fracture was found. This outcome is consistent with the low environmental enhancement measured in this specimen and the no SCC growth recorded throughout the test.

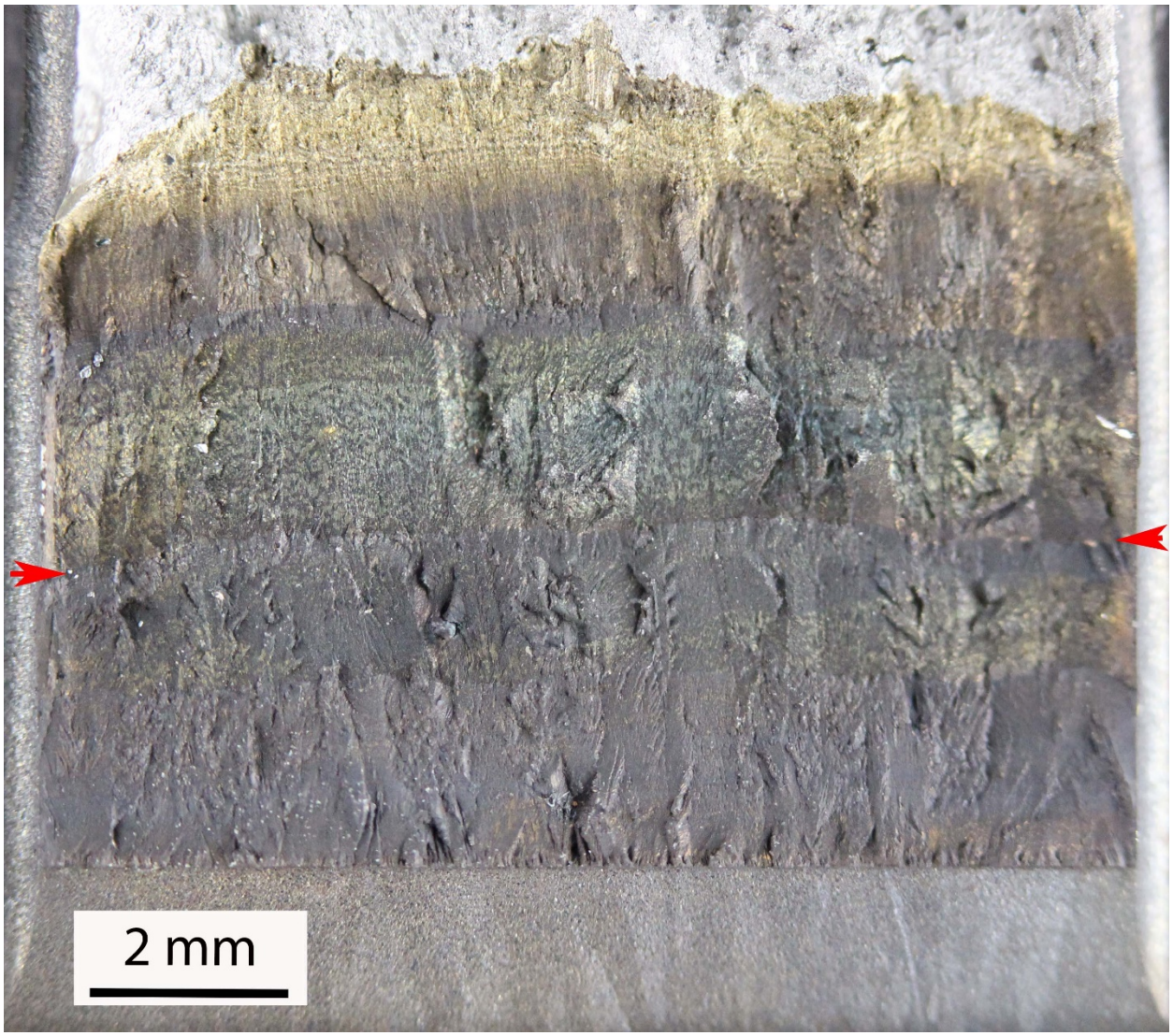

Figure 96 **Fracture surface of specimen IHI152M-TS-1. The red arrows indicate the regions made with different weld fillers. Crack advance is from bottom to top.**

3.4 The Effect of Cold Work on SCC CGR response

For the purpose of investigating the effect of cold work on the SCC CGR response, three tests were conducted on an Alloy 52 weld in the as-welded and 20% cold-forged conditions. The Alloy 52 weld was produced by MHI on a piece of Alloy 690 CRDM tubing, see Section 2.7. The as-welded condition was tested in the CR orientation. The 20% cold-forged condition was tested in the CR orientation (parallel to the direction of forging), and in the LR orientation (normal to direction of forging.

3.4.1 Specimen MC52-CR-1, "as-received" weld produced by MHI

The test on specimen MC52-CR-1 was initiated with precracking in the PWR environment, followed by transitioning. The testing conditions are given in Table 21, and the changes in crack length and K_{max} with time are shown in Figure 97. In test period 4, a 2-h hold was introduced to assess the SCC CGR component, and this was calculated to be 5.9 10^{-12} m/s. The rate measured initially (first 100 h) in the subsequent test period at constant load was close, 3.3 10^{-12} m/s, then diminished to an average 1.6 10^{-12} m/s.

Next, the crack front was straightened by fatigue in test period 6, and re-transitioned. In test period 9, a 2-h hold was introduced to assess the SCC CGR component, and this was calculated to be 2.9 10^{-12} m/s. Thus, instead of constant load, the hold time was increased to 4-h, thus reducing the fatigue component to 3.0 10^{-12} m/s, in an attempt to increase the IG engagement. The SCC CGR component calculated in test period 10 was still small, 2.2 10^{-12} m/s. This step was intended to be followed by constant load, however, the power failure described at the beginning of this report made it necessary to return to fatigue loading in test period 11. Figure 97f shows that after an initially slower growth early in test period 11 (at lower K_{max} than previously), the previous fatigue response was established later in the same test period. This was followed by reproducing the response to the R=0.5, 600/12 cycle in test period 12 (see also Figure 98a. Once the known behavior was re-established, the test continued according to the original plan: the 4-h hold in test period 13 resulted in a higher rate than observed previously in test period 10, however, the SCC CGR component was calculated to be low, in the 10^{-12} m/s range. This rate has been confirmed at constant load in test period 14. Next, gentle cycling identical to that of test period 13 was introduced in test period 15, and the resulting rate was a factor 4 less than measured prior to the constant load test period. This behavior suggests that the preferred cracking direction is off-plane. This was followed by another test period at constant load (16).

Next, cyclic loading (R=0.5, 600/12) was reintroduced in test period 17 in an attempt to straighten the fracture surface. This was followed by cycle + hold in test periods 18 and 19. In test period 18, the hold was introduced at K_{min}. Under such loading, the growth rate is only due to corrosion fatigue due to cyclic loading; during the hold time, the specimen is practically unloaded. By contrast, in test period 19, the hold was introduced at K_{max}, hence, the measured rate consists of a corrosion fatigue component plus an SCC component during the 2h hold time at K_{min}. In this framework, SCC growth will be the simple subtraction of CGRs measured in test periods 19 and 18.

If no SCC occurs, then the rate in test period 19 should equal that in test period 18. The sequence was repeated until test period 23, and several observations become apparent:

1) The resulting CGR in test period 18 (specimen unloaded during hold) was actually larger than measured previously during test periods 4 and 9 when the hold was at K_{max}. It is likely that test period 17 (also higher than measured previously under similar conditions) straightened the crack front.

2) The resulting CGR in test period 19 (2h hold at K_{max}) was actually smaller than that resulting from test period 18 (specimen unloaded during hold) 2h hold at K_{min}). The result seems to suggest that, given the opportunity to propagate, the SCC crack will go off-plane.

3) Subsequent test periods 20 and 22 with hold at K_{min} have the same da/dN as test period 17, and that that is the expected result as it shows that no growth occurs during hold at K_{min}. The resulting rates are the "baseline" for evaluating the effect of the subsequent cycles with hold at K_{max}.

4) Test periods 19, 21, and 23 with hold at K_{max} results are systematically higher than the "baseline" by: $3.4x10^{-12}$, $3.2x10^{-12}$and $2.4x10^{-12}$m/s. The rates represent growth under CL (during hold at K_{max}).

5) There is a decreasing trend in the rates calculated above. There is also a decreasing trend in the rates measured in test periods 18, 20, 22 and in test periods 19, 21, 23. These trends substantiate the earlier observations regarding test periods 13 and 15 (a factor 4 decrease in response after an extended constant load period). All seem to indicate that the preferred cracking direction is off-plane, and it is not clear what the DC potential measured responses under constant load mean under the current circumstances.

Next, a 20h hold time was introduced in test period 24. The response ($3.1x10^{-12}$ m/s) seems to substantiate the findings described at 4) above. Next, the specimen was set at constant load in test period 25. The response was similar ($2.0x10^{-12}$m/s) for the first 100 h, then eventually dropped to zero.

Next, the crack was advanced for approx. 0.35 mm in test periods 26-27, and re-transitioned. The response obtained in test periods 26-31 is very similar to that measured previously on this weld (see also Figure 98b). The specimen was set at constant load in test period 32. The SCC CGR was $1.33x10^{-12}$ m/s.

After the constant load test period 32, the system was brought to room temperature, drained of water and an additional test period in fatigue was conducted (Figure 97n) to determine whether ligaments had formed during the test in water. It is interesting to note that the initial response during this test period was slightly higher than expected, and only settled at an expected rate (see Figure 98b) after approx. 80 μm of growth.

Table 21 Crack growth data for Alloy 52 specimen MC52-CR-1 in PWR water[a].

Test Period	Test Time, h	Temp. °C	Load Ratio R	Rise Time, s	Down Time, s	Hold Time, s	K_{max}, MPa·m$^{1/2}$	ΔK, MPa·m$^{1/2}$	CGR_{env}, m/s	Estimated CGR_{air}, m/s	Crack Length, mm
Pre a	53	318.5	0.29	1	1		23.6	16.8	1.55E-08	5.19E-08	11.851
Pre b	119	318.5	0.29	100	100		23.6	16.8	5.10E-10	5.18E-10	11.911
Pre c	126	318.3	0.29	1	1		25.2	17.9	4.57E-08	6.73E-08	12.368
Pre d	143	318.3	0.29	50	50		25.5	18.1	2.21E-09	1.41E-09	12.443
Pre e	145	318.3	0.29	1	1		26.1	18.5	4.85E-08	7.81E-08	12.616
Pre f	147	318.3	0.29	2	2		26.6	18.9	2.92E-08	4.20E-08	12.736
Pre g	150	318.3	0.29	5	5		26.9	19.1	1.41E-08	1.77E-08	12.819
Pre h	168	318.3	0.29	50	50		27.2	19.3	2.33E-09	1.84E-09	12.892
1	175	318.3	0.49	50	12		27.4	14.0	8.98E-10	8.34E-10	12.918
2	215	318.3	0.49	300	12		27.4	14.0	2.30E-10	1.40E-10	12.950
3	335	318.3	0.49	600	12		27.5	14.0	1.28E-10	7.04E-11	13.004
4	791	318.3	0.49	600	12	7,200	27.7	14.1	1.49E-11	6.61E-12	13.029
5	2,128	318.2	1.00	0	0		27.9	0.0	1.12E-12	-	13.036
6	2,362	318.3	0.49	600	12		28.3	14.4	1.14E-10	7.96E-11	13.123
7	2,364	318.3	0.49	12	12		28.0	14.3	2.45E-09	3.81E-09	13.134
8	2,387	318.3	0.49	600	12		28.1	14.4	1.20E-10	7.77E-11	13.145
9	2,794	318.5	0.49	600	12	7,200	28.6	14.6	1.32E-11	6.39E-12	13.164
10	3,127	318.4	0.49	600	12	14,400	28.5	14.6	7.72E-12	3.30E-12	13.173
11	3,128	319.0	0.29	0.5	0.5		27.3	19.4	9.60E-08	1.89E-07	13.284
12	3,174	318.4	0.49	600	12		27.7	14.1	1.39E-10	7.26E-11	13.313
13	3,361	318.5	0.49	600	12	14,400	27.7	14.1	1.59E-11	2.91E-12	13.321
14	5,015	318.5	1.00	0	0		27.6	0.0	1.30E-12	-	13.328
15	5,230	319.4	0.49	600	12	14,400	28.0	14.3	4.26E-12	3.06E-12	13.333
16	5,659	319.2	1.00	0	0	0	28.0	0.0	1.11E-12	-	13.334
17	5,735	319.4	0.50	600	12	0	28.0	14.0	1.68E-10	7.32E-11	13.371
18	5,804	319.3	0.50	600	12	7,200 at K_{min}	28.0	14.0	1.97E-11	5.63E-12	13.372
19	6,144	319.4	0.50	600	12	7,200	28.0	14.0	1.70E-11	5.65E-12	13.399
20	6,241	319.2	0.50	600	12	7,200 at Kmin	28.0	14.0	1.36E-11	5.63E-12	13.403
21	6,472	319.3	0.50	600	12	7,200	28.3	14.2	1.64E-11	5.90E-12	13.421
22	6,572	319.2	0.50	600	12	7,200 at Kmin	28.3	14.1	1.28E-11	5.86E-12	13.421
23	6,724	319.4	0.50	600	12	7,200	28.4	14.2	1.52E-11	5.97E-12	13.434
24	7,987	318.9	0.50	600	12	72,000	28.2	14.1	3.05E-12	6.17E-13	13.449
25	8,521	318.5	1.00	0	0		28.4	0.0	2.00E-12	-	13.449
26	8,524	319.2	0.30	1	1		25.8	18.1	5.39E-08	7.25E-08	13.636
27	8,539	319.2	0.30	50	50		26.2	18.3	2.31E-09	1.54E-09	13.705
28	8,545	319.2	0.50	50	12		26.1	13.1	9.60E-10	6.61E-10	13.730
29	8,562	319.1	0.50	300	12		26.0	13.0	2.34E-10	1.08E-10	13.744
30	8,591	319.2	0.49	600	12		26.0	13.3	1.27E-10	5.67E-11	13.757
31	8,803	319.3	0.49	600	12	7,200	26.5	13.5	1.78E-11	4.73E-12	13.770
32	9,743	319.3	1.00	0	0		26.9	0.0	1.33E-12	#DIV/0!	13.774
33	9,746	37.4	0.30	1	1		27.4	19.2	2.08E-08	2.92E-08	13.914

[a]Simulated PWR water with 2 ppm Li, 1100 ppm B, and 2 ppm. DO<10 ppb. Conductivity was 21±3 μS/cm, and pH 6.4.

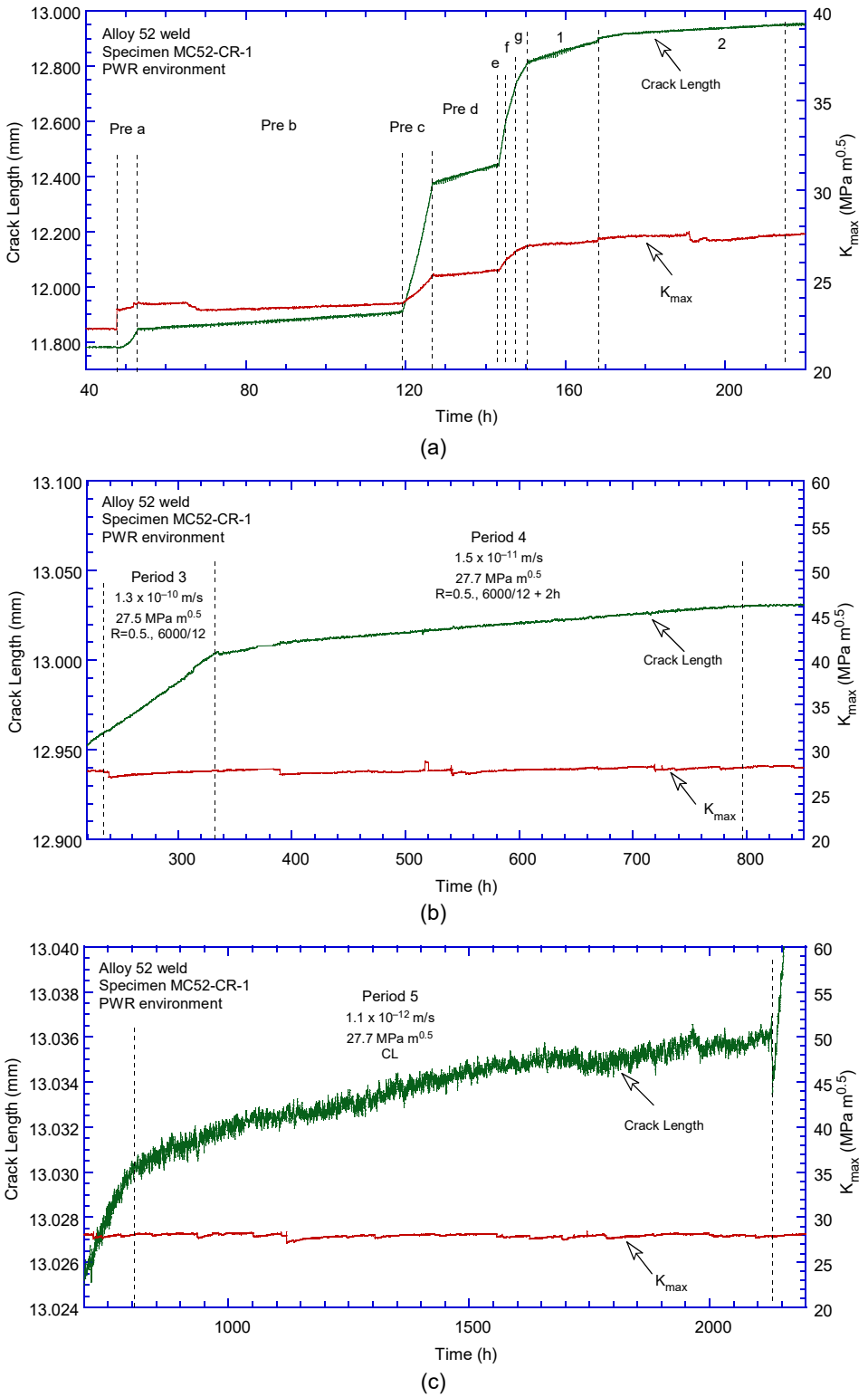

Figure 97 Crack–length–vs.–time for Alloy 52 specimen MC52-CR-1 in simulated PWR environment during test periods (a) precracking-2, (b) 2-4, (c) 5, (d) 6-9, (e) 10, (f) 11, (g) 12-15, (h) 16, (i) 17-23, (j) 24, (k) 25, (l) 26-31, (m) 32, and (n) 33.

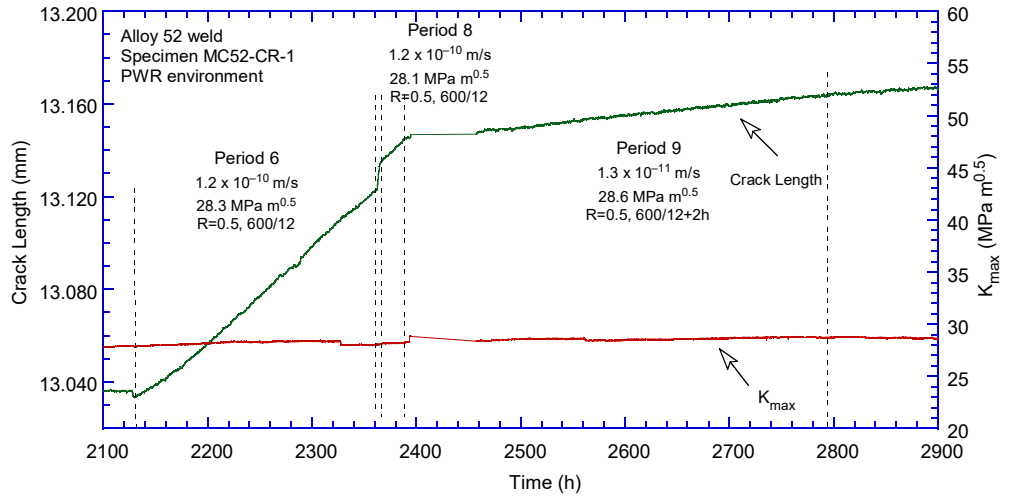

(d)

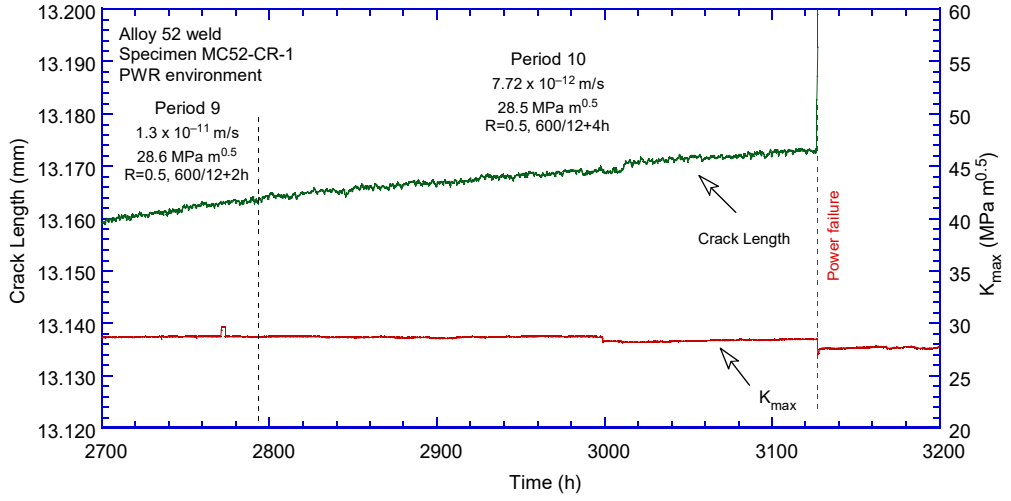

(e)

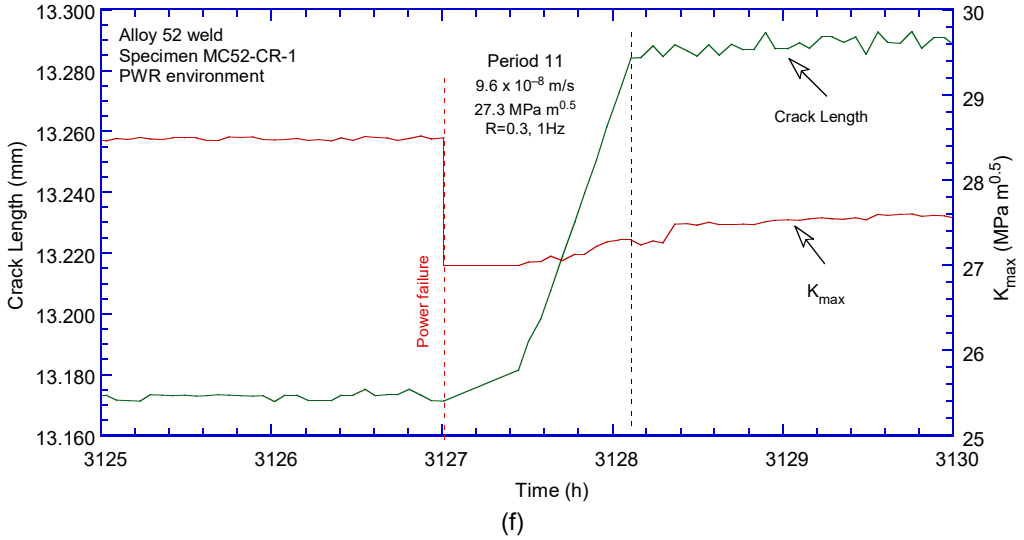

(f)

Figure 97 (cont.)

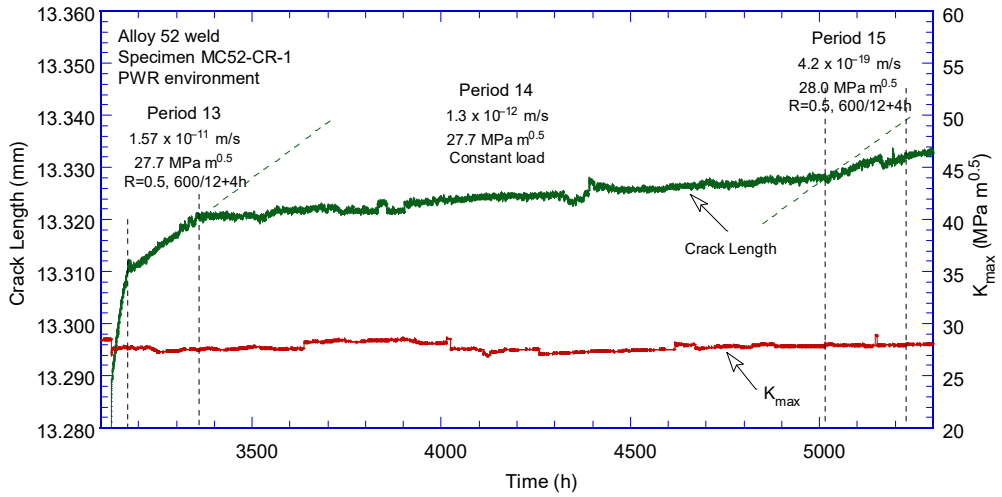

(g)

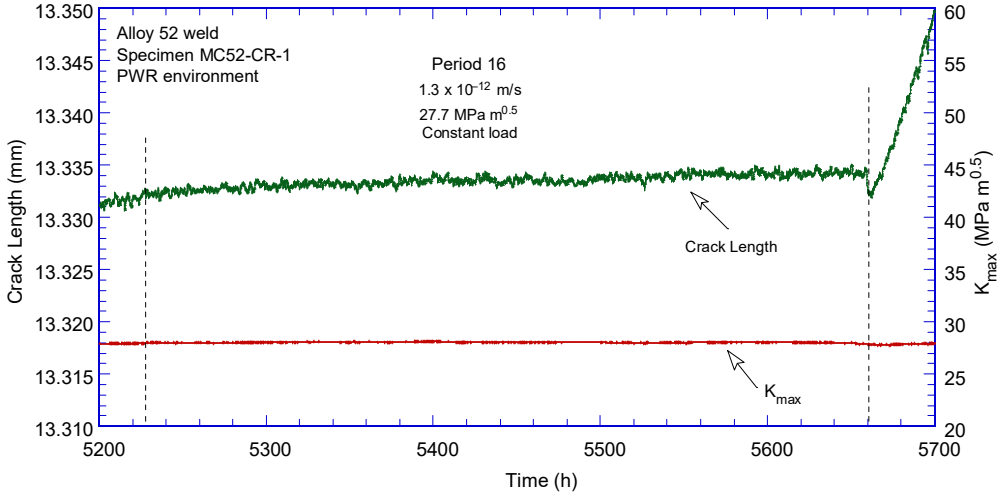

(h)

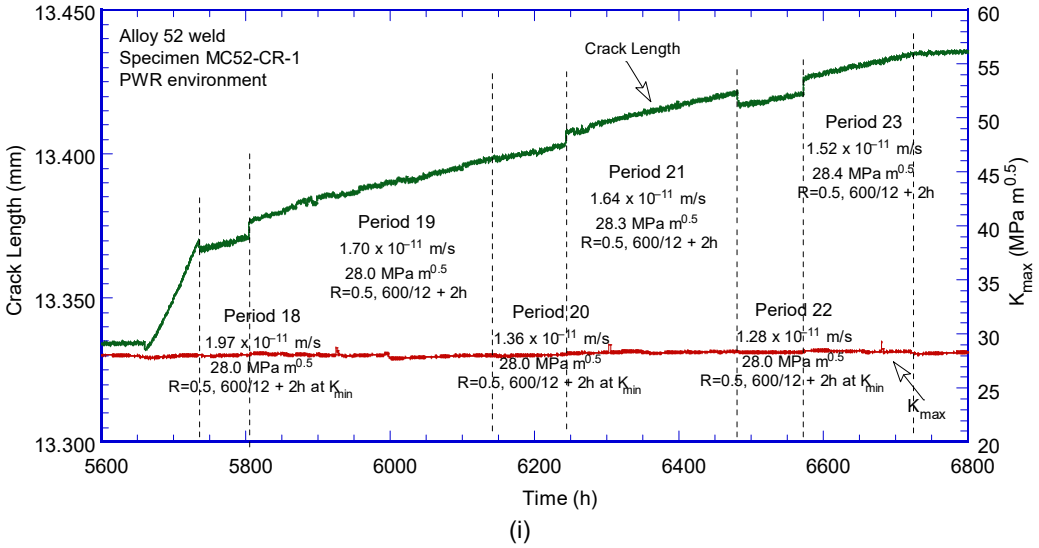

(i)

Figure 97 (cont.)

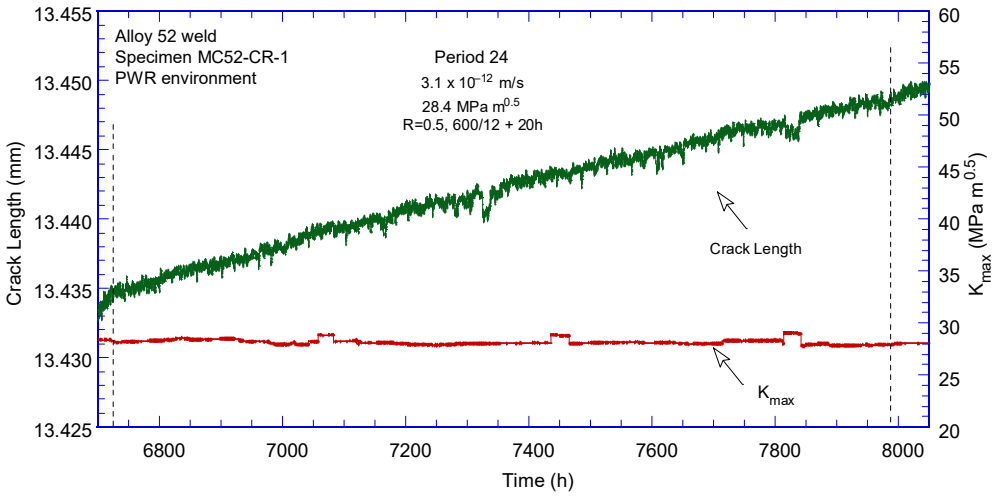

(j)

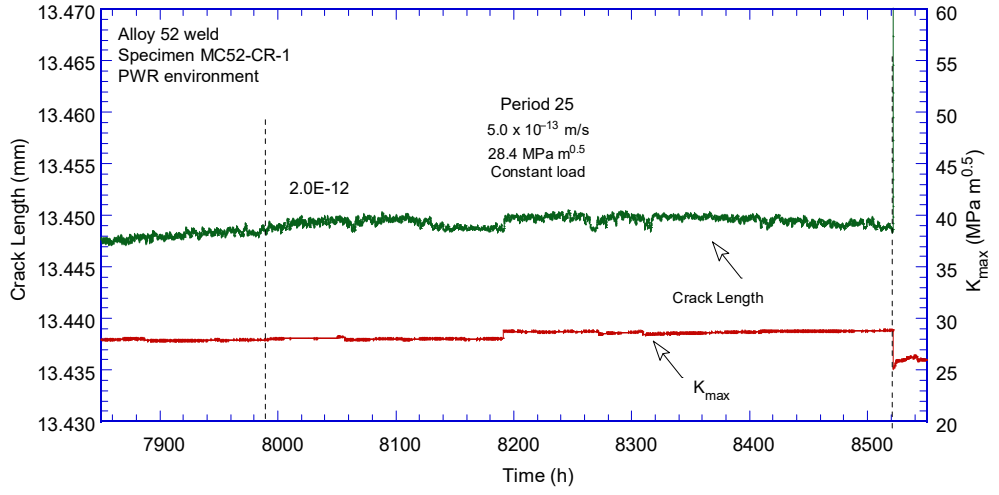

(k)

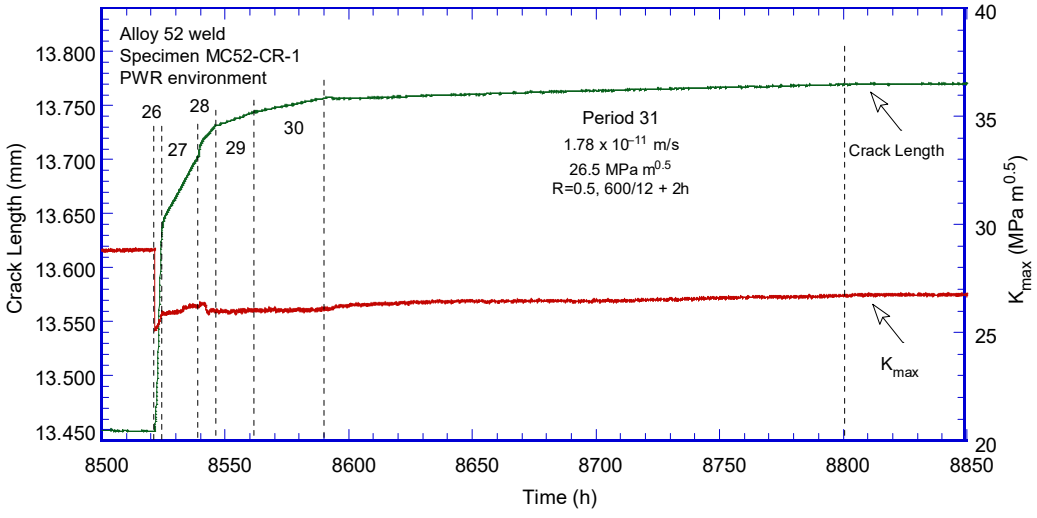

(l)

Figure 97 (cont.)

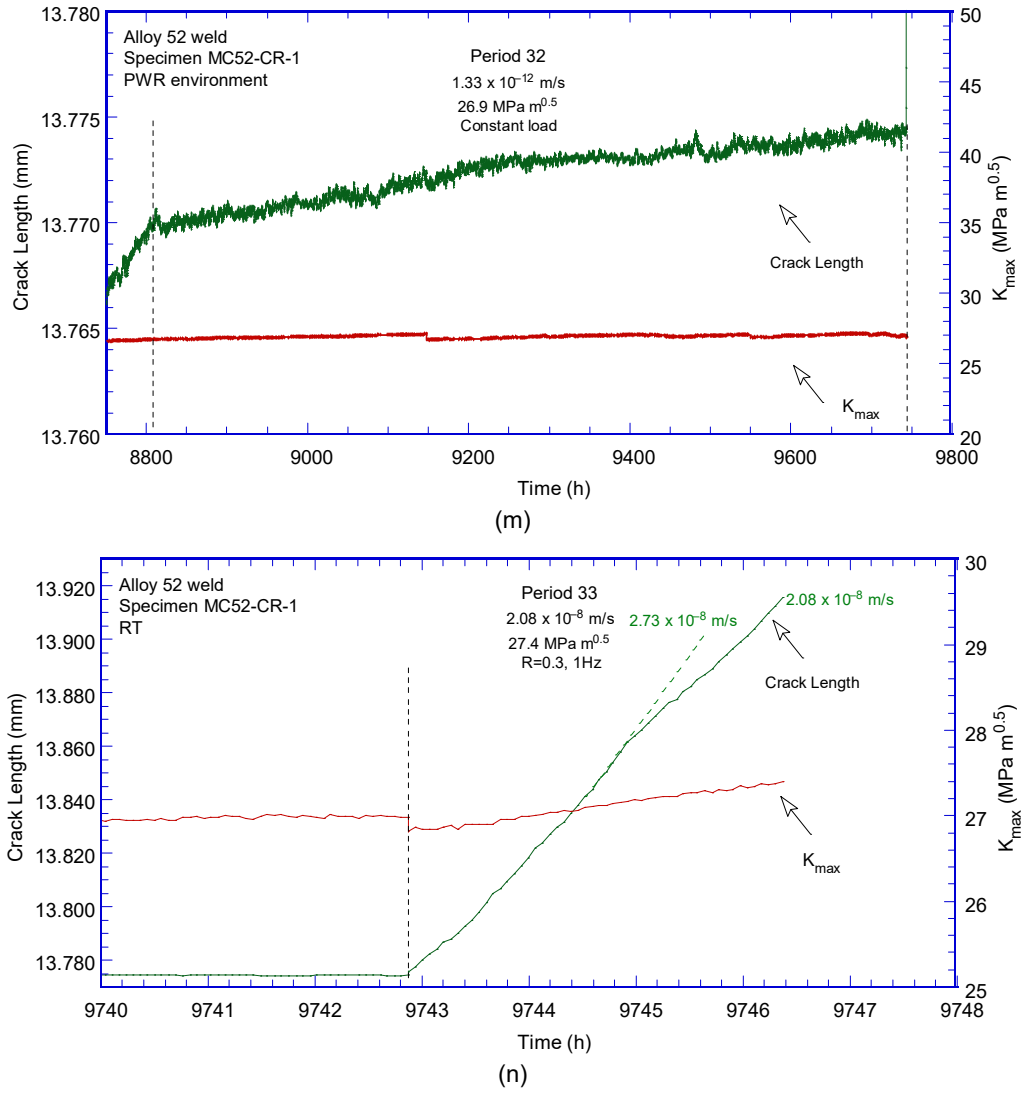

Figure 97 (cont.)

Figure 98 shows the cyclic CGR data obtained to date for the current MC52-CR-1 specimen during the initial precracking and transitioning (Figure 98a), and additional crack advance in fatigue and transitioning (Figure 98b). Both figures include the corrosion fatigue curve for Alloy 182 for comparison. The final test period (33) obtained during fatigue in air is indicated in Figure 98b.

Figure 99 summarizes the SCC CGR data obtained on this Alloy 52 weld produced by MHI. The CGRs obtained from test periods where some cycling was always present (estimate from cycle + hold or the difference between CGRs with the hold time at K_{max} and K_{min}) are shown with open symbols and appear to be slightly higher than those measured at constant load (solid symbols), but overall the SCC CGRs are very small. Several “no growth” results are not included in the plot.

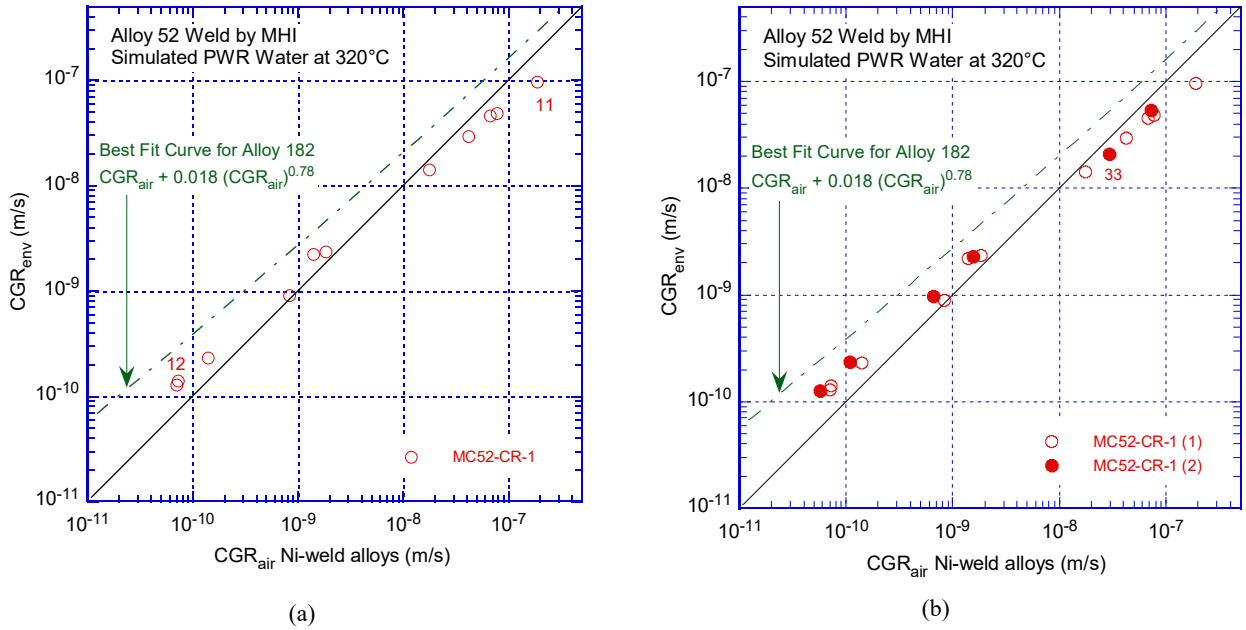

Figure 98 Cyclic CGR data for Alloy 52 specimen MC52-CR-1 during (a) initial precracking and transitioning, and (b) additional crack advance in fatigue and transitioning in simulated PWR environment.

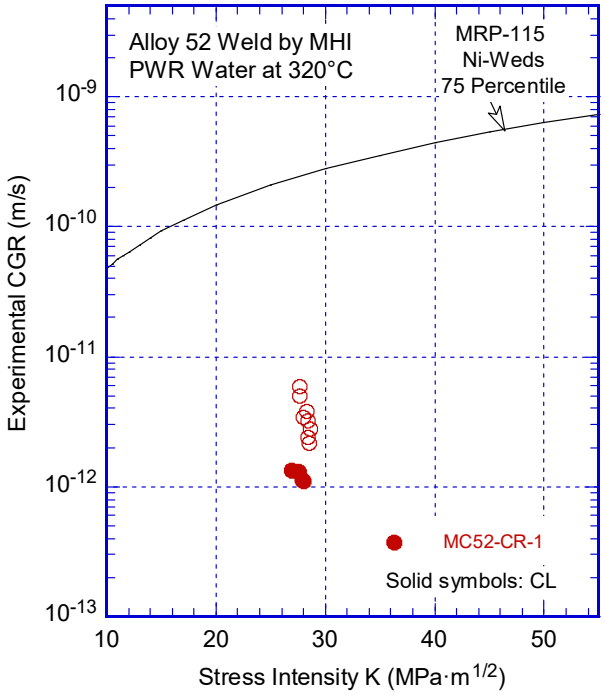

Figure 99 SCC CGR data in simulated PWR environment for Alloy 52 weld produced by MHI.

During the post-test examination of the specimen, two observations/outcomes needed attention:

1) failure to reproduce cyclic data after long test periods at constant load (see for example Figure 97g); it was speculated during the test, that off-plane cracking may be occurring, hence, the cross sections of the test specimen will be examined for evidence of off-plane cracking.

2) Low SCC CGRs were measured irrespective of the method used (constant load, PPU, alternating hold between K_{max} and K_{min}), Figure 99. In light of the low rates, the degree of IG engagement is of special interest.

Given the above, the post-test examination of specimen MC52-CR-1 included both the cross sections and the fracture surface.

After the test ended, the two side surfaces were ground to eliminate the side grooves, polished and etched, Figure 100. While every effort was made to align the specimen along the dendrite growth in the V-shape weld given the size constraints, the images show that the crack direction was about 15º off the dendrite growth direction.

The SEM micrographs of the side surfaces are shown in Figure 101. There is no evidence of IG cracking on these images, hence it cannot be established whether off-plane cracking occurred or not. If it did, it was perhaps a local effect, difficult to establish on what will likely be a fracture surface with limited IG engagement.

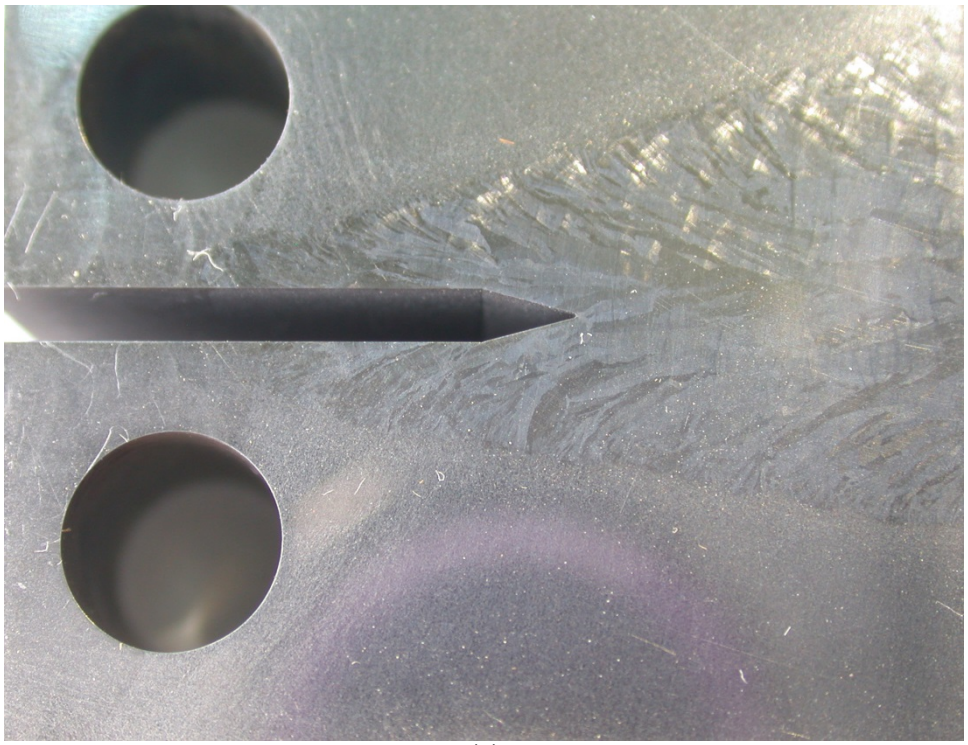

(a)

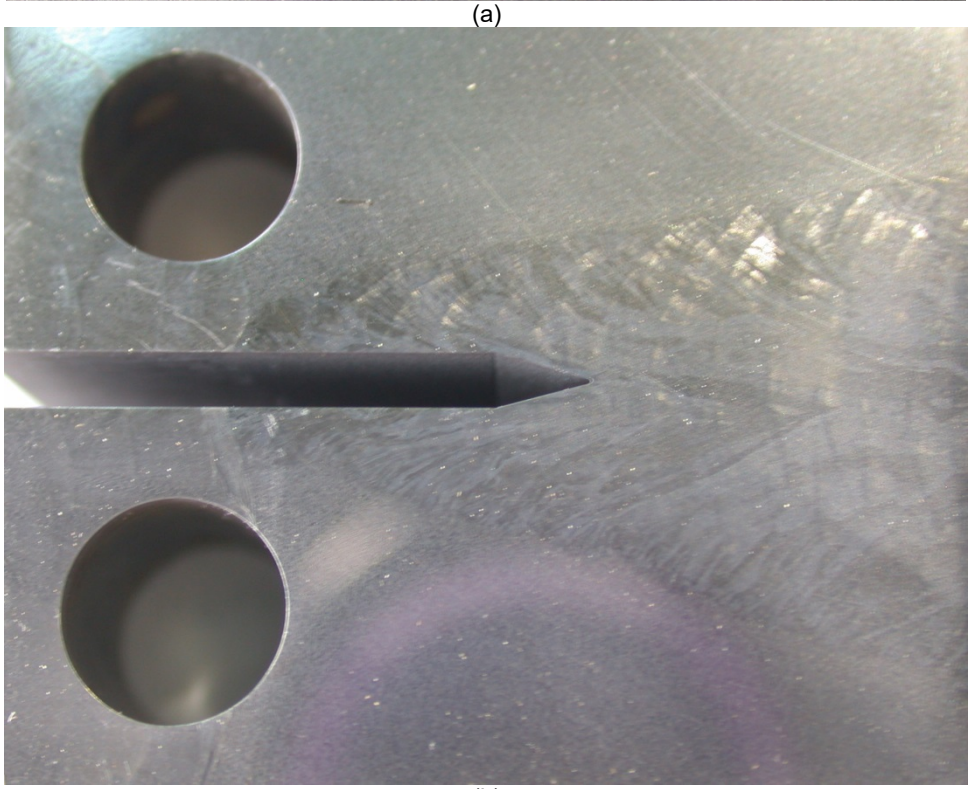

(b)

Figure 100 Side cross sections of Alloy 52 specimen MC52-CR-1 tested in simulated PWR environment: (a) side 1 and (b) side 2.

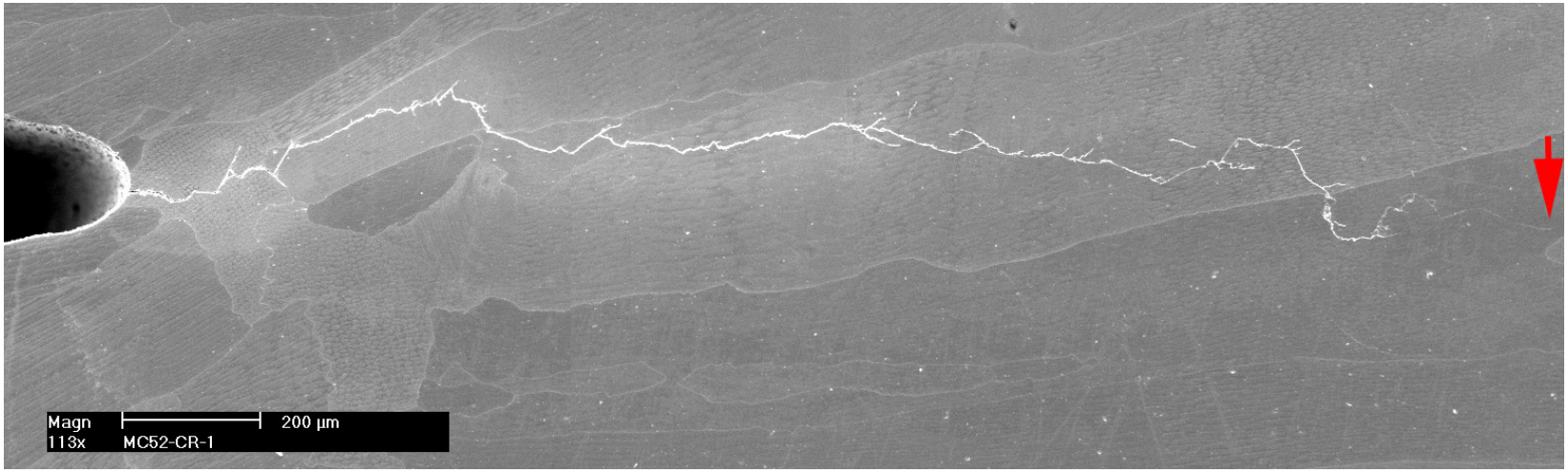

(a)

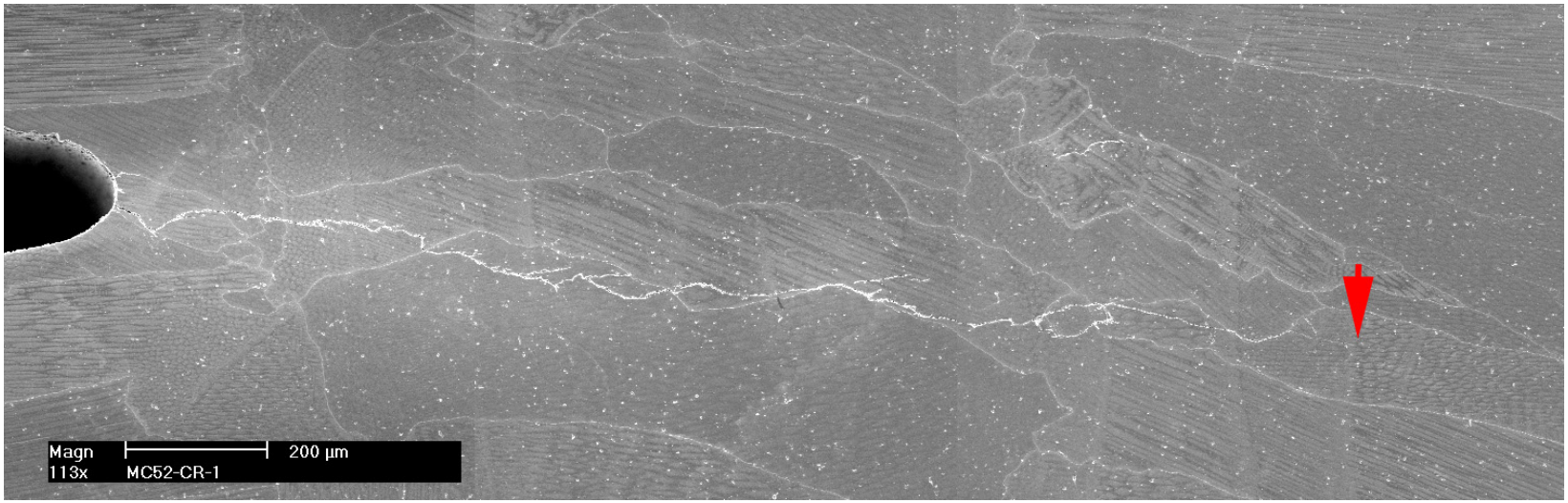

(b)

Figure 101 Cross sections of Alloy 52 specimen MC52-CR-1 tested in simulated primary water. Crack advance is from left to right. The red arrows mark the end on the crack.

The fracture surface of the specimen is shown in Figure 102. The total measured crack extension is 2.31 mm which is 14% larger than the DC-potential measured extension of 1.99 mm. Hence no correction was made to the data shown in Table 21.

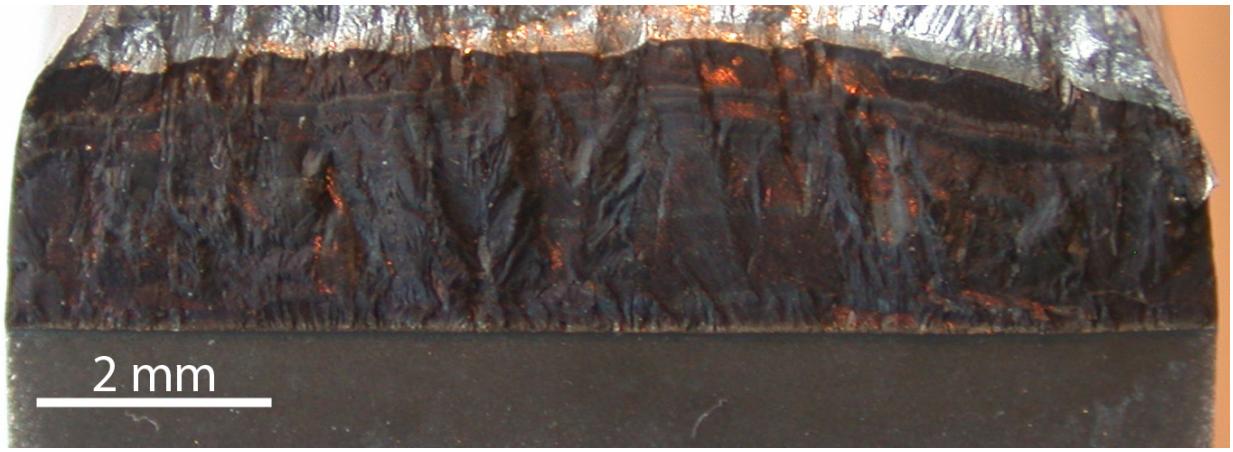

Figure 102 Fracture surface of Alloy 52 specimen MC52-CR-1 tested in simulated PWR environment: Crack advance is from bottom to top.

Figure 103 shows the SEM image of the fracture surface, and the crack morphology at several locations indicated in the picture will be discussed with additional detail.

The fracture morphology of this specimen was primarily TG, and Figure 104 illustrates the main fracture modes. IG fracture (Figure 104a) was extremely limited; for the most part, the crack propagated in a TG manner (Figure 104b), and, on occasion, secondary off-plane cracks have been observed (Figure 104). The white arrows in Figure 104a and Figure 104c indicate some of those cracks.

Figure 105 shows a case where the fracture morphology of the off-plane crack appears interdentritic, however, this case was not the norm for this specimen. In most cases, the off-plane cracks appeared TG, and these are illustrated in Figure 106.

Overall, the Alloy 52 specimen MC52-CR-1 was resistant to fatigue, corrosion fatigue, and SCC. The low SCC CGRs were measured at constant load and confirmed under various other loading conditions. The low IG fracture further confirms the resistance of this specimen to IG SCC.

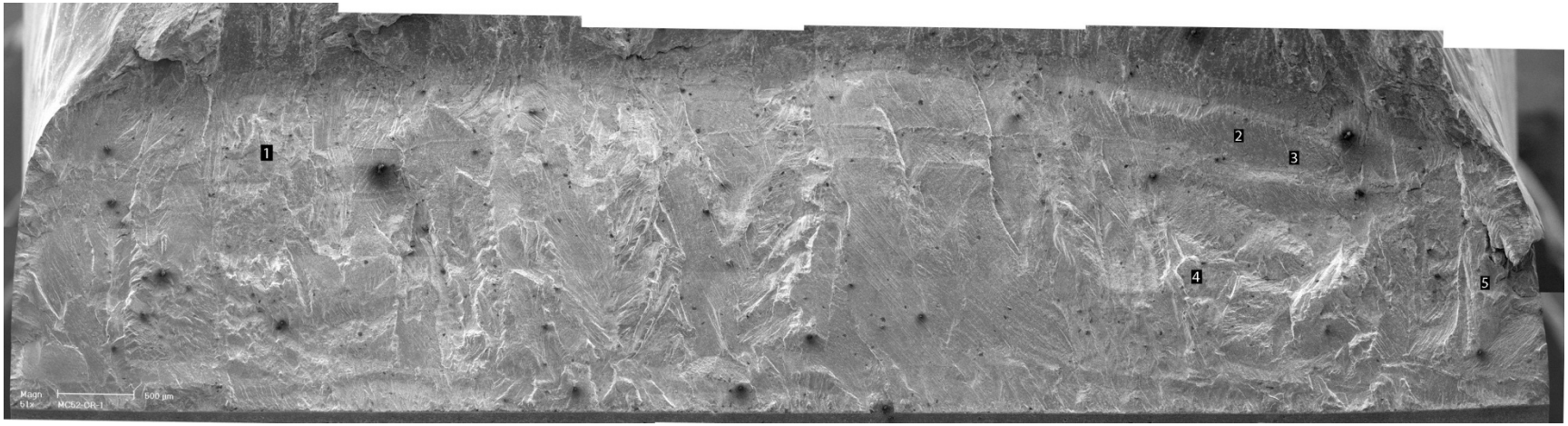

Figure 103 Fracture surface of Alloy 52 specimen MC52-CR-1 tested in simulated primary water. Crack advance is from bottom to top.

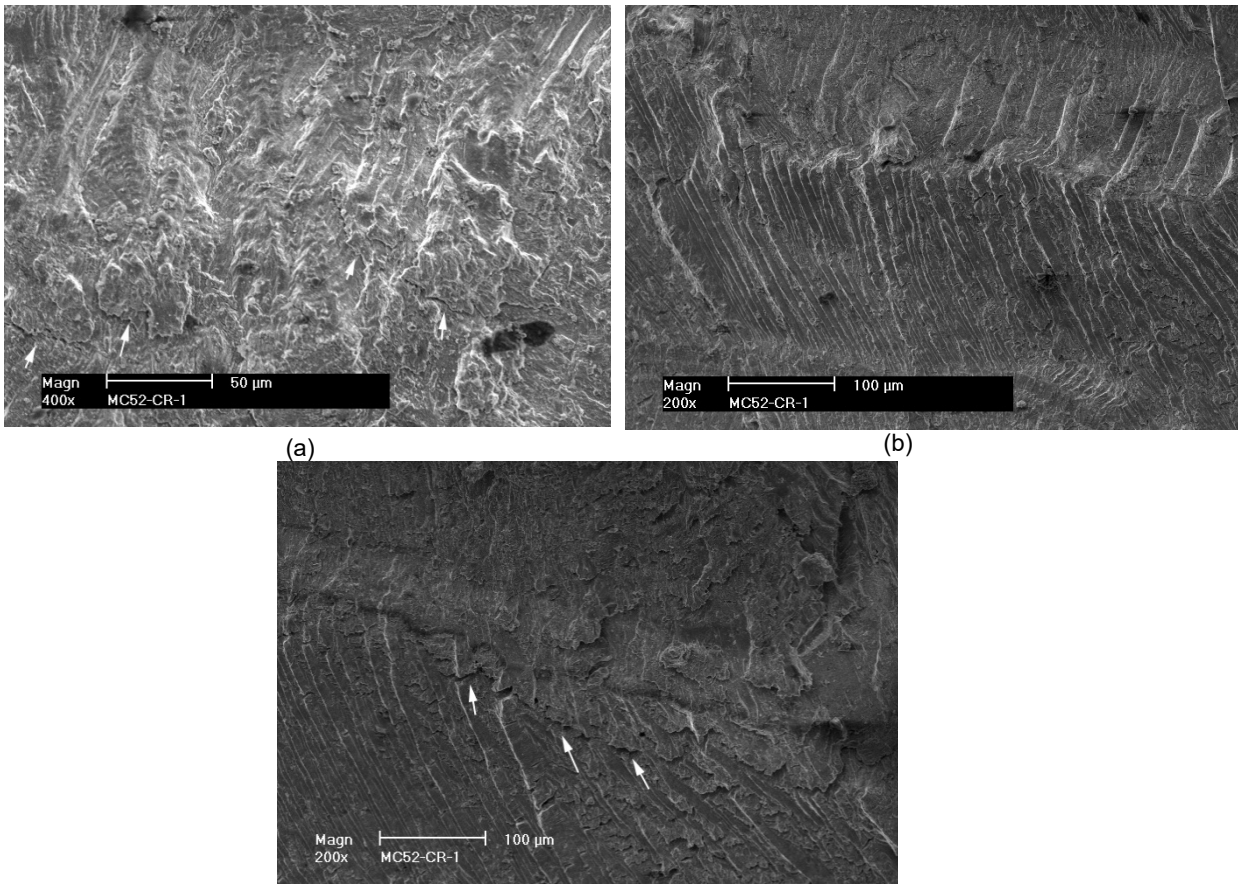

Figure 104 Fracture surface of specimen MC52-CR-1 at location (a) 1, (b) 2, and (c) 3 in Figure 103. Crack advance is from bottom to top.

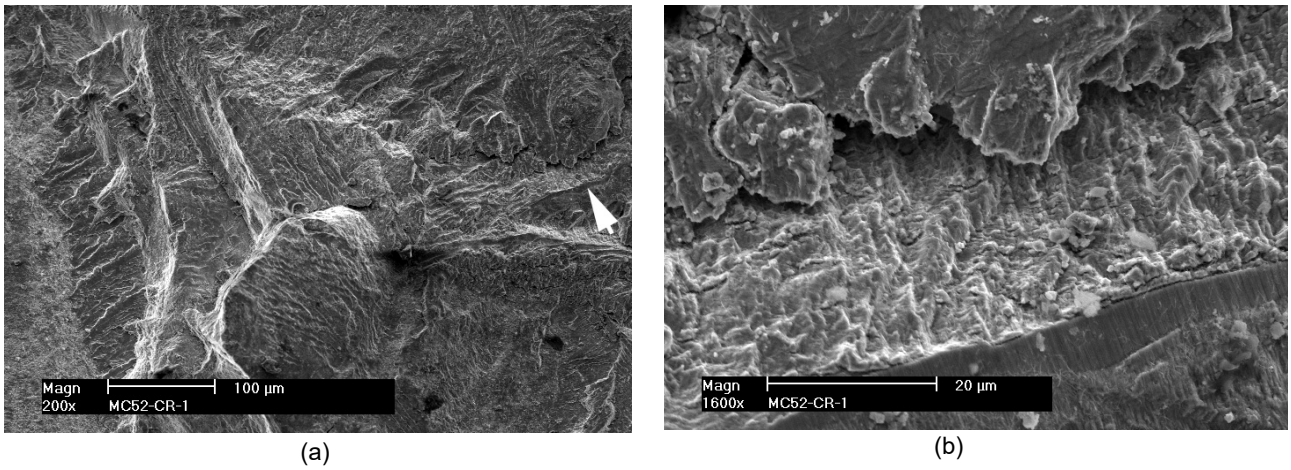

Figure 105 Fracture surface of specimen MC52-CR-1 at (a) location 4 in Figure 103, and (b) morphology of the off-plane crack at the location indicated by the arrow in (a). Crack advance is from bottom to top.

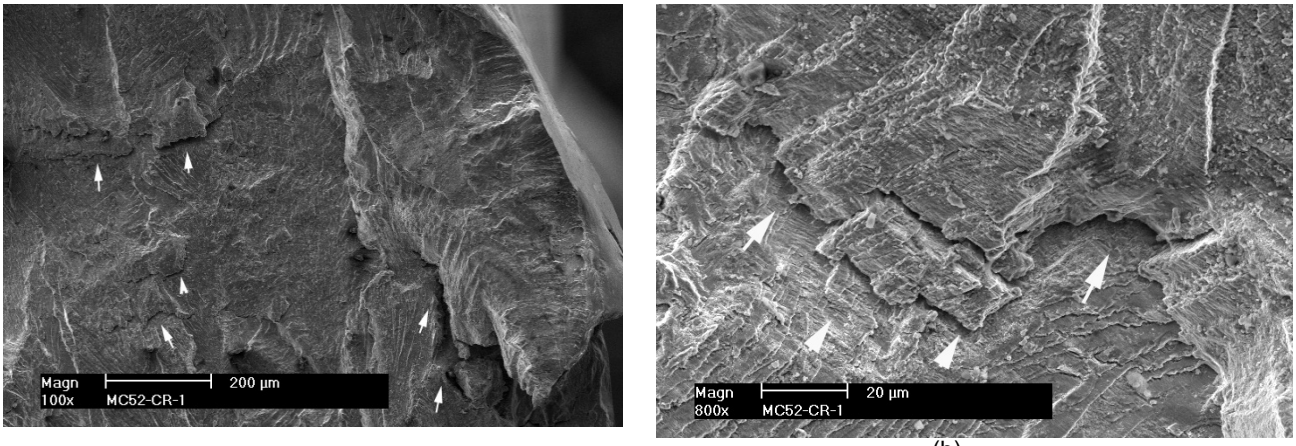

(a) (b)

Figure 106 Fracture surface of specimen MC52-CR-1 at (a) location 5 in Figure 103, and (b) morphology of the off-plane crack. Arrows indicate the off-plane cracks. Crack advance is from bottom to top.

3.4.2 Specimen MC52-20CF-CR-1, 20% cold-forged weld produced by MHI

The testing conditions are given in Table 22, and the changes in crack length and K_{max} with time are shown in Figure 108. The test was initiated with precracking in the PWR environment, followed by transitioning and an initial constant load period (5). Constant load resulted in no growth, hence, cyclic loading similar to those used in test period 4 resumed, and yielded a similar CGR. As such, no ligaments or off-plane cracking seems to have occurred. A 2-h hold was introduced in test period 7, and the SCC CGR component appears to be indeed low.

During test period 7, a sudden leak occurred at the pullrod seal. The loading system was tripped by the low position limit (actuator position) and control had transferred from “load” to “position” control (this is typical to prevent damage to the specimen). The max crack extension measured minutes after the leak was approximately 13.050 mm, substantially larger than the prior DC potential determinations, despite the decreasing load and temperature. The crack extension reading then decayed with the loss of pressure and temperature. The system cooled to room temperature (RT), and then the autoclave was opened up. Next, 700 lbs were applied to the specimen to open up the crack (max load was 990 lbs before the leak), and the DC potential settings were changed to the RT conditions established before the test in water. Crack extension was indeed approximately 13.050 mm. Given the above observations, we were able to determine that a ligament in the specimen broke resulting in a jolt in pullrod/loading system thus tripping the “position” limit. The same jolt caused the pullrod seal failure and subsequent loss of pressure.

After the system was opened up, the pull rod was removed and the seal examined. The rupture appears to be indeed consistent with a “jolt” from the pullrod, Figure 107.

Figure 107 The ruptured of the pullrod seal appears consistent with a “jolt”.

Table 22 Crack growth data for Alloy 52 specimen MC52-20CF-CR-1 in PWR water[a].

Test Period	Test Time, h	Temp. °C	Load Ratio R	Rise Time, s	Down Time, s	Hold Time, s	K_{max}, MPa·m$^{1/2}$	ΔK, MPa·m$^{1/2}$	CGR_{env}, m/s	Estimated CGR_{air}, m/s	Crack Length, mm
Pre a	104	319.6	0.27	1	1		24.6	18.0	2.74E-08	6.64E-08	12.387
Pre b	166	319.7	0.27	100	100		24.9	18.2	6.16E-10	6.98E-10	12.461
Pre c	168	319.6	0.27	1	1		25.3	18.5	3.09E-08	7.49E-08	12.599
Pre d	170	319.6	0.27	2	2		25.5	18.6	1.87E-08	3.85E-08	12.649
Pre e	173	319.7	0.27	5	5		25.7	18.7	8.73E-09	1.58E-08	12.692
Pre f	191	319.7	0.27	50	50		25.8	18.8	1.58E-09	1.62E-09	12.742
1	197	319.7	0.48	50	12		26.1	13.5	6.89E-10	7.26E-10	12.759
2	265	319.8	0.48	300	12		26.2	13.6	1.99E-10	1.24E-10	12.799
3	358	319.7	0.48	600	12		26.4	13.7	7.99E-11	6.38E-11	12.825
4	503	319.7	0.48	1000	12		26.4	13.7	4.67E-11	3.83E-11	12.849
5	1,081	319.6	1.00	0	0		26.9	0.0	no growth	-	12.849
6	1,270	319.8	0.48	1000	12		27.0	14.0	4.75E-11	4.17E-11	12.879
7	2,014	319.9	0.48	1000	12	7,200	27.1	14.1	1.04E-11	5.16E-12	12.905

[a]Simulated PWR water with 2 ppm Li, 1000 ppm B, and 2 ppm. DO<10 ppb. Conductivity was 21±3 μS/cm, and pH 6.4.

In summary, cracking in this this 20% cold forged specimen seems to have left behind some unbroken ligaments, and this hypothesis will be explored during the post-test examination of the specimen. Nevertheless, measurements of the crack advance on the fracture surface will establish whether that is consistent with the length measured just prior to the jolt (extension 0.804 mm) or immediately after the jolt (extension 0.963).

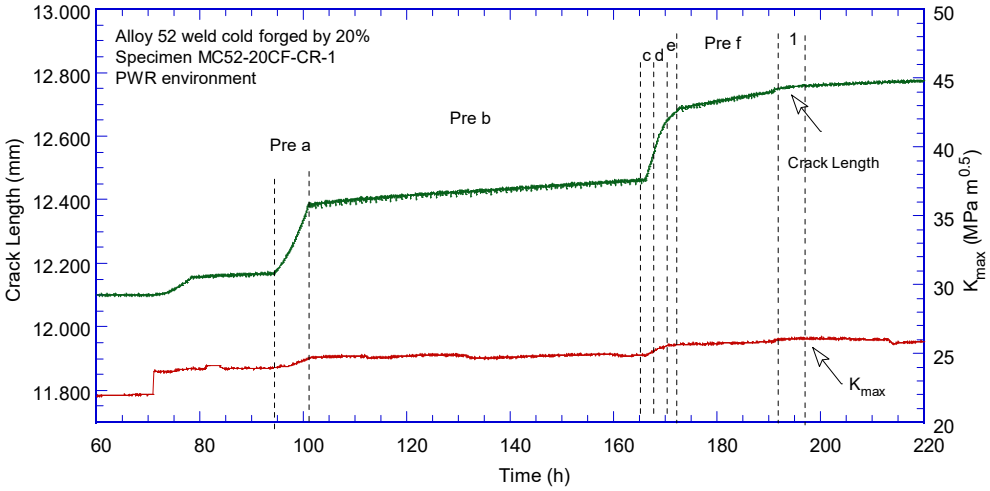

(a)

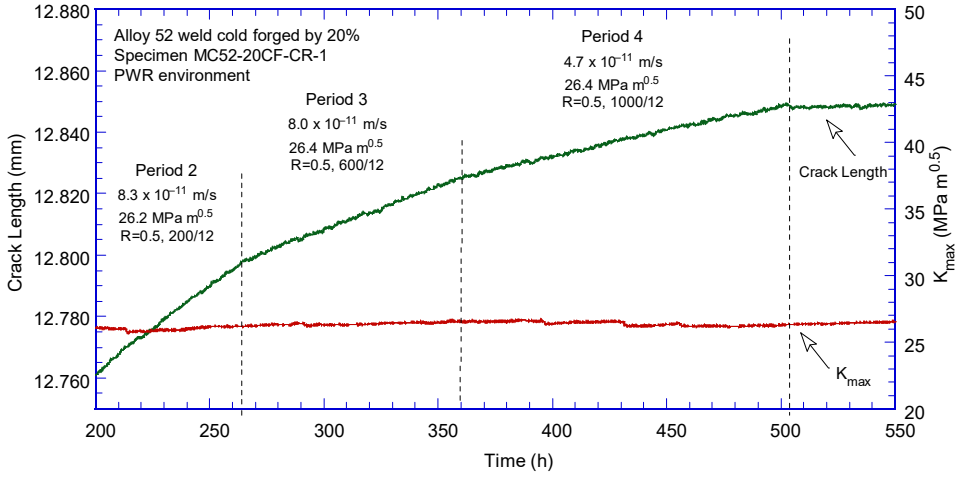

(b)

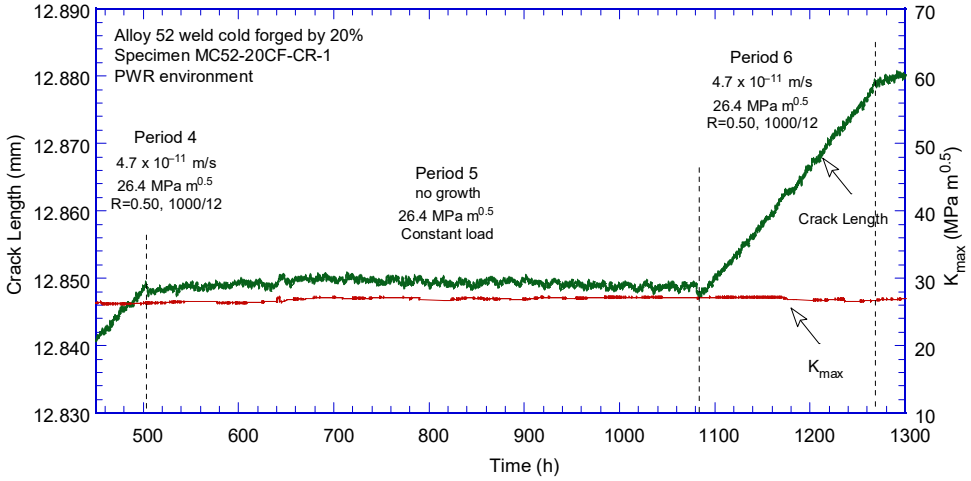

(c)

Figure 108 Crack–length–vs.–time for Alloy 52 specimen MC52-20CF-CR-1 in simulated PWR environment during test periods (a) precracking-1, (b) 2-4, (c) 5-6, and 7.

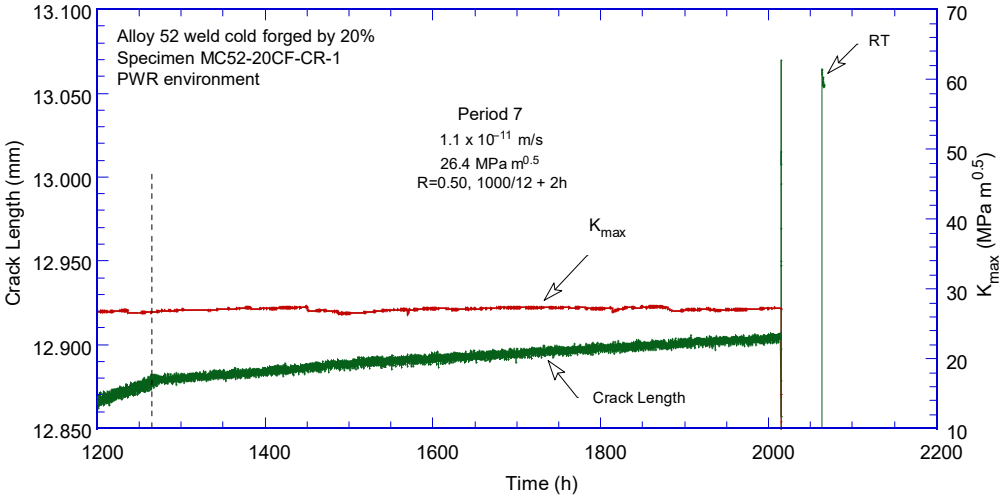

(d)

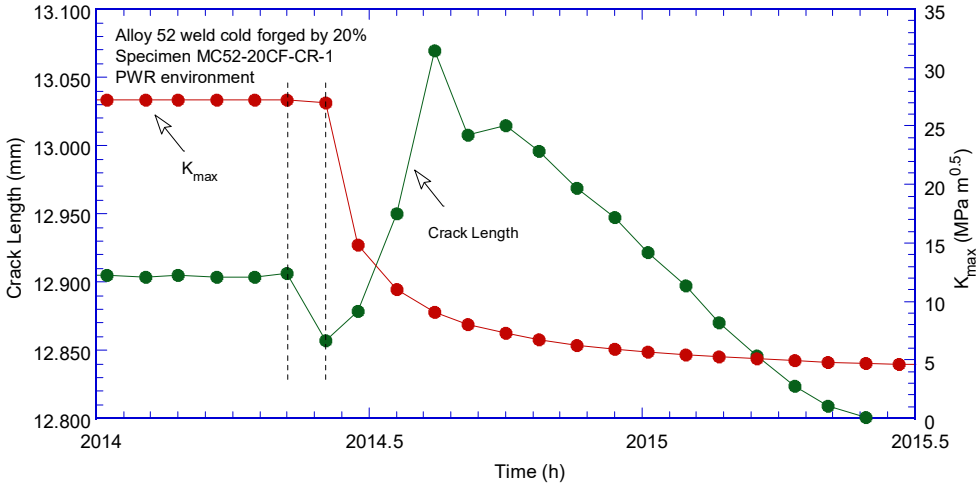

(e)

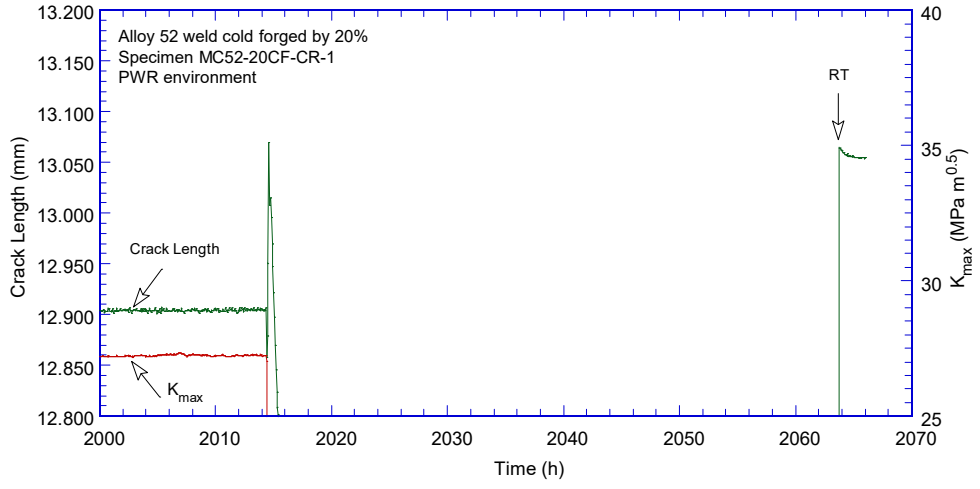

(f)

Figure 108 (cont.)

Figure 109 shows the cyclic CGR data for the current MC52-20CF-CR-1 (20% cold forged) and the previous weld specimen MC52-CR-1 in the as-received condition, and tries to put the data into perspective. Surprisingly, the fatigue response of the cold forged specimen is lower than that of the as-received specimen, Figure 109a. The effect of cold forging appears to be completely opposite from that of cold-rolling; to illustrate, Figure 109b shows the almost 10x effect of 26% cold-rolling on Alloy 690. Nevertheless, unlike rolling which was parallel to the testing plane for the Alloy 690 specimen in the ST orientation, cold-forging was normal to the testing plane in the current test.

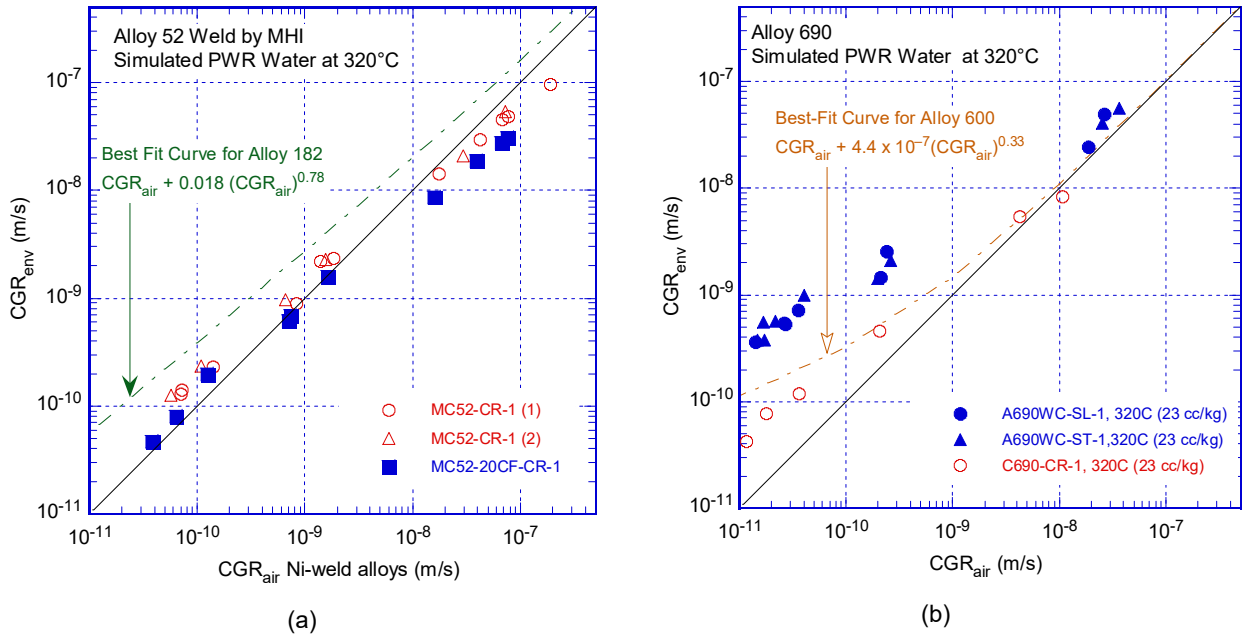

Figure 109 Cyclic CGR data for (a) Alloy 52 specimen MC52-20CF-CR-1 (cold forged by 20%) vs. the same weld in the as-received condition, and (b) Alloy 690 in the as received and 26% cold-rolled condition [5].

Figure 110 summarizes the SCC CGR data obtained on this Alloy 52 weld produced by MHI in the as-welded and 20% cold-forged (CF) conditions. The CGRs obtained from test periods where some cycling was always present (estimate from cycle + hold or the difference between CGRs with the hold time at K_{max} and K_{min}) are shown with open symbols and appear to be slightly higher than those measured at constant load (solid symbols), but overall all the SCC CGRs are very small. From the current test, one data point resulting from cycle+hold in test period 7 was included. The “no growth” data point resulting from test period 5 was not included in the plot.

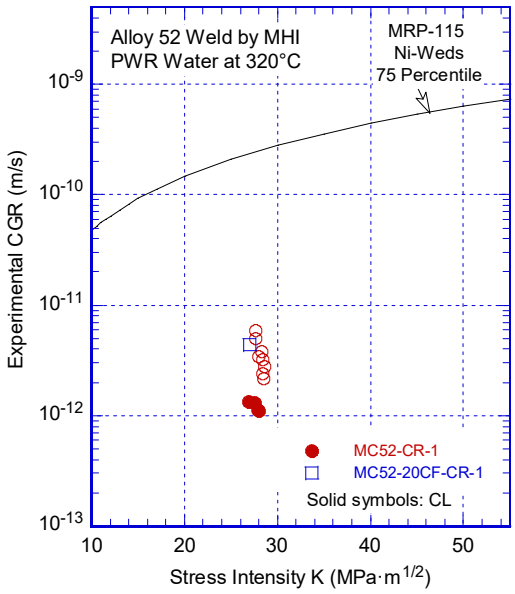

Figure 110 SCC CGR data in simulated PWR environment for Alloy 52 weld produced by MHI in the as-welded and 20% cold-forged (CF) conditions.

The fracture surface of the specimen is shown in Figure 111. The total measured crack is 1.17 mm which is 31% larger than the DC-potential measured extension just prior to the jolt (0.804 mm), and 17% larger than that measured immediately after the jolt (0.963). As such, there appears plausible that one or more ligaments broke suddenly causing a jolt in the load train, thus leading to the leak described previously. Several areas of interest are indicated with white arrows in Figure 112, and those were examined further. While region 1 only shows features consistent with corrosion fatigue (Figure 112b, c), regions 2 and 3 show areas consistent with ductile rupture (Figure 112b). The fracture mode on one such area (3) – spanning several hundred microns – is shown in Figure 113. Nevertheless, no correction was made to the data shown in Table 21.

The fracture morphology of this specimen was primarily TG, hence, the no growth conditions measured at constant load in test period 7 and estimated under cycle + hold in test period 7 appear to be valid.

Figure 111 Fracture surface of Alloy 52 specimen MC52-20CF-CR-1 tested in simulated PWR environment. Crack advance is from bottom to top.

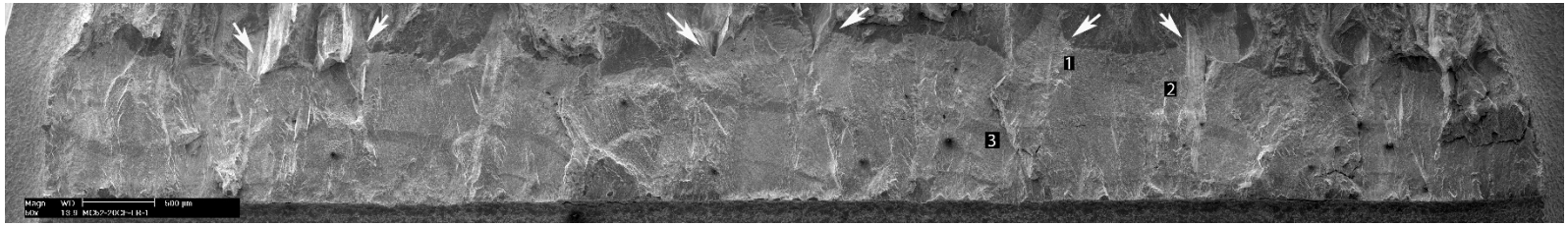

(a)

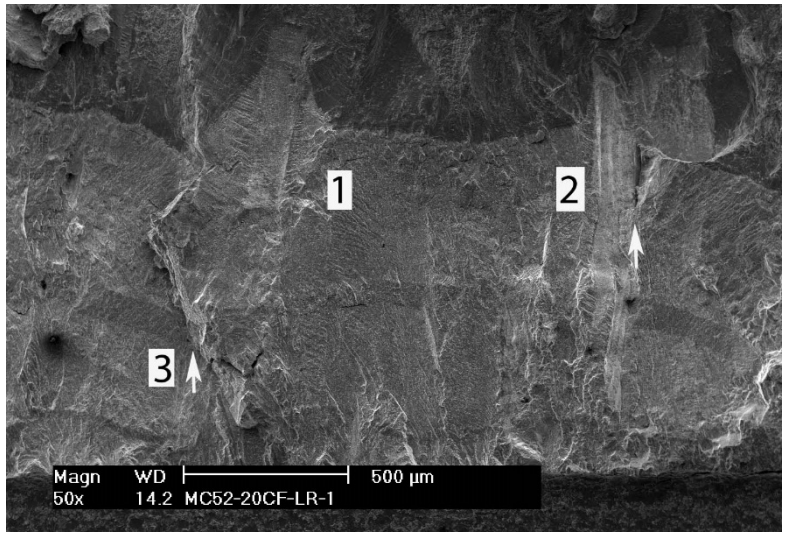

(b)

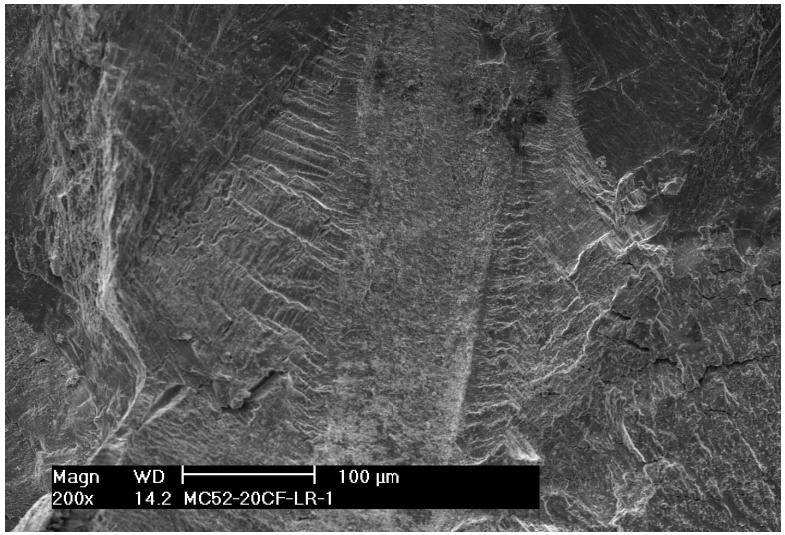

(c)

Figure 112 (a) Fracture surface of Alloy 52 specimen MC52-20CF-CR-1 tested in simulated PWR environment. (b) detail at locations 1-3, and (c) detail at location 1. Crack advance is from bottom to top.

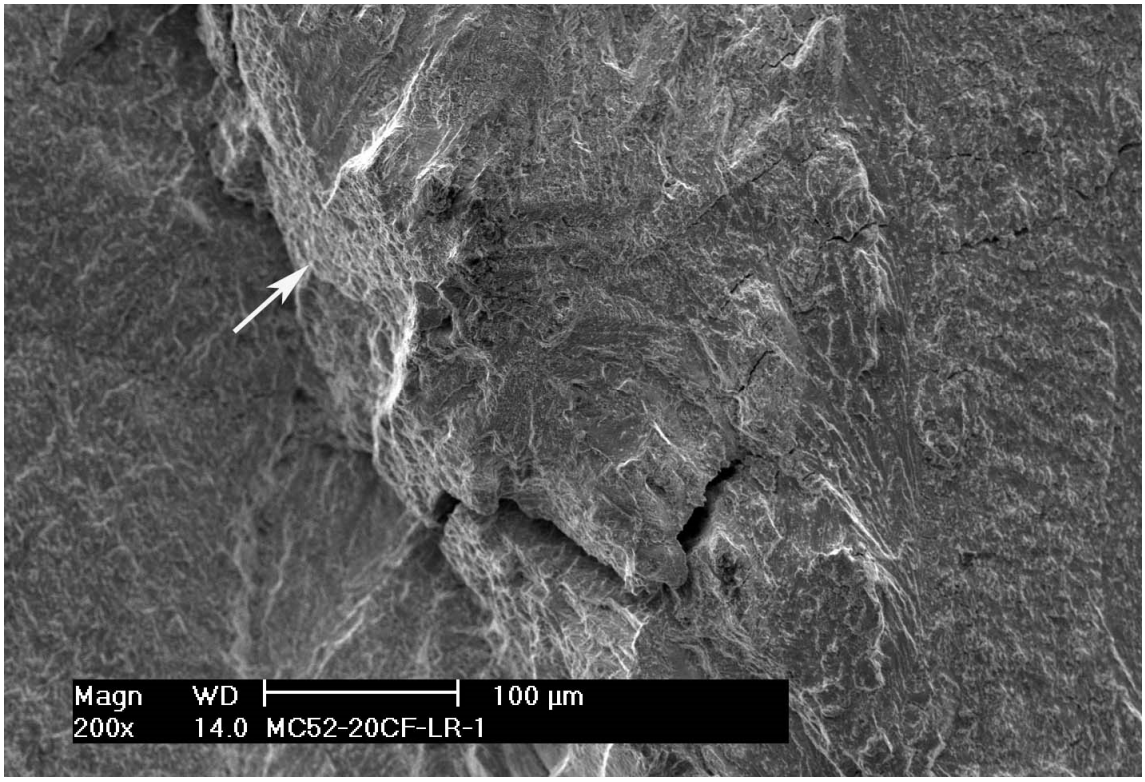

Figure 113 Fracture surface of Alloy 52 specimen MC52-20CF-CR-1 tested in simulated PWR environment, detail at location 3 in Figure 112. The arrow points to a plane of ductile fracture. Crack advance is from bottom to top.

During a conference call with the research sponsor, it was recommended that LR orientation be tested instead of a repeat test on the CR orientation. For this cold-forged piece of tubing, the LR orientation is in the forging plane, hence the level of deformation would be uniform in the testing plane. In the framework of a butt weld, the CR orientation corresponds to a circumferential crack and the LR orientation corresponds to an axial crack, Figure 114.

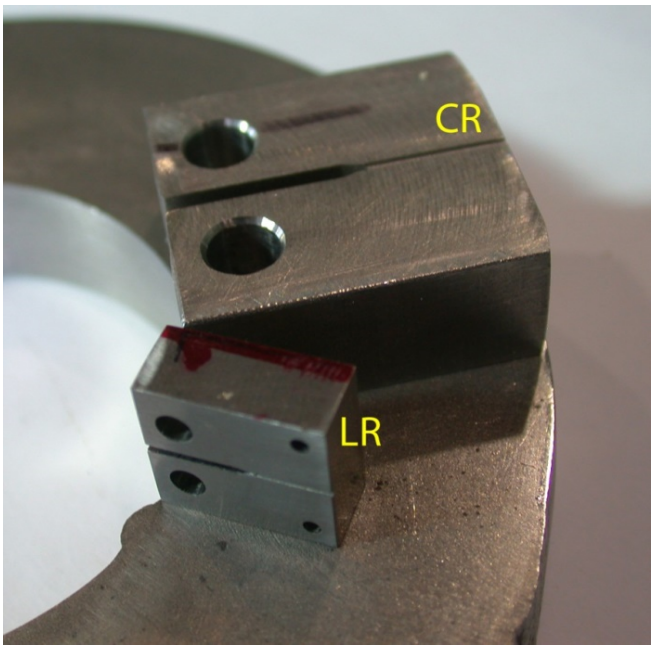

Figure 114 CT specimens in the CR and LR orientations. For a butt weld, the CR orientation corresponds to a circumferential crack, and the LR orientation corresponds to an axial crack.

3.4.3 Specimen MC52-20CF-LR-1, 20% cold-forged weld produced by MHI

In preparation for this test, two 1/4T CT specimens were machined from the 20% cold-forged weld in the LR orientation (Figure 115), and the first one was loaded in the system.

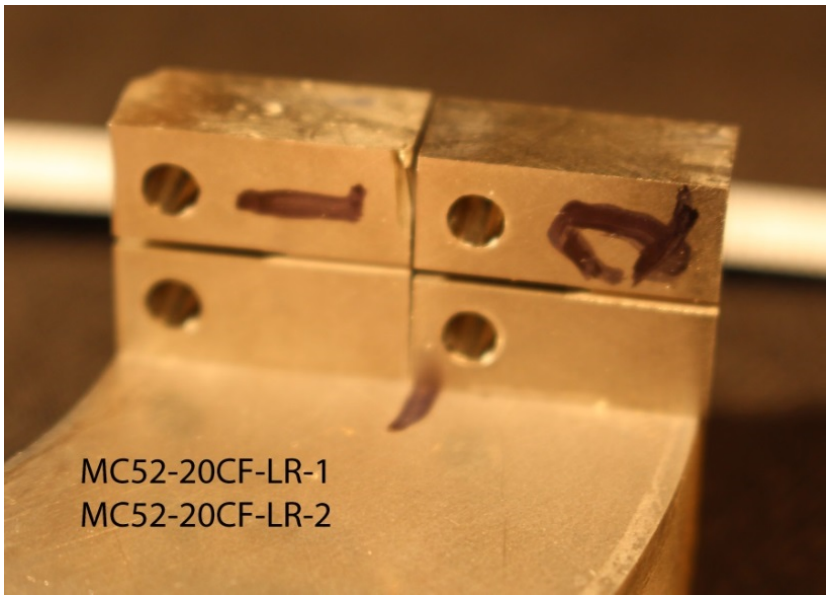

Figure 115 1/4T CT specimens in LR orientation made from Alloy 52 weld cold-forged by 20%.

Given the limitation on K imposed by the use of a 1/4T CT specimen, the test on MC52-20CF-LR-1 will focus on two stress intensity factor regimes: low, approx. 10 MPa $m^{1/2}$ and moderate, approx. 20 MPa $m^{1/2}$. The testing conditions are given in Table 23, and the changes in crack length and K_{max} with time are shown in Figure 116.

The precracking was started at a slightly higher K than the target 10 MPa $m^{1/2}$ in order to facilitate the initiation of crack propagation from the machined notch. Once that was accomplished, the stress intensity factor was gradually reduced to slightly below the target, and the known fatigue behavior for this weld was reproduced in test periods Pre a and Pre b. These were followed by transitioning and constant load. Several “no/low” SCC growth determinations were made thru test period 12 at a stress intensity factors of up to approx. 14.5 MPa $m^{1/2}$. Next, the stress intensity factor was increased to 20 MPa $m^{1/2}$, and a low SCC CGR was measured in test period 16. Next, the stress intensity factor was further increased to 25 MPa $m^{1/2}$ and a low SCC CGR was measured. Next, it was decided to increase the stress intensity factor to 30 MPa, and extended transitioning steps were undertaken. The response observed in test periods 26-28 where the CGRs decrease almost proportionally with decreasing the loading frequency, suggest that growth is driven primarily by fatigue, and hence the SCC CGR is low. Next, the specimen was set at constant load for the final test period (29). The resulting rate was slow, however, approximately 1000 h into the test period, two small (1 micron) jumps were observed (Figure 116j and Figure 116k). In order to check for the formation of ligaments (that might otherwise mask the true crack extent), cyclic loading was briefly introduced in test period 30. Upon measuring a similar rate as previously, constant loading was resumed for the final determination of the test.

Table 23 Crack growth data for specimen MC52-20CF-LR-1 in PWR water[a].

Test Period	Test Time, h	Temp. °C	Load Ratio R	Rise Time, s	Down Time, s	Hold Time, s	K_{max}, MPa·m$^{1/2}$	ΔK, MPa·m$^{1/2}$	CGR_{env}, m/s	Estimated CGR_{air}, m/s	Crack Length, mm
Pre aa	29.0	320.9	0.08	0.5	0.5		11.4	10.5	2.59E-09	1.01E-08	5.844
Pre bb	31.0	320.9	0.09	0.5	0.5		10.6	9.6	1.99E-09	7.07E-09	5.854
Pre cc	46.0	321.0	0.10	100	100		10.6	9.5	2.95E-11	3.45E-11	5.855
Pre dd	53.0	321.0	0.08	0.5	0.5		9.4	8.6	1.28E-09	4.43E-09	5.867
Pre ee	70.0	321.0	0.09	100	100		9.4	8.6	3.27E-11	2.23E-11	5.869
Pre a	73.0	320.9	0.09	0.5	0.5		9.5	8.7	3.55E-09	4.65E-09	5.886
Pre b	77.0	320.9	0.09	2	2		9.6	8.7	1.58E-09	1.20E-09	5.895
1	94.0	320.9	0.49	120	12		9.7	4.9	8.34E-12	5.03E-12	5.897
2	166.0	320.9	0.48	600	12		9.5	4.9	4.90E-14	9.76E-13	5.897
3	366.0	320.7	0.49	600	12	7,200	9.6	4.9	3.00E-13	7.64E-14	5.898
4	678.0	320.9	1.00	0	0		9.7	0.0	no growth	-	5.898
5	696.0	321.0	0.50	120	12		12.5	6.2	3.50E-11	1.36E-11	5.900
6	747.0	321.1	0.50	600	12		12.5	6.3	9.21E-12	2.78E-12	5.902
7	847.0	321.2	0.50	600	12	7,200	12.4	6.2	1.27E-12	2.05E-13	5.903
8	1,174.0	321.3	1.00	0	0		12.5	0.0	no growth	-	5.903
9	1,192.0	321.3	0.50	120	12		14.5	7.2	6.55E-11	2.28E-11	5.906
10	1,263.0	321.3	0.49	600	12		14.6	7.5	1.73E-11	5.39E-12	5.911
11	1,460.0	321.3	0.50	600	12	7,200	14.7	7.3	2.52E-12	4.09E-13	5.913
12	1,865	321.2	1.00	0	0		14.8	0.0	1.50E-12	-	5.916
13	1,869	321.5	0.50	120	12		19.8	9.9	1.78E-10	8.20E-11	5.920
14	1,942	321.3	0.50	600	12		19.9	9.9	4.35E-11	1.81E-11	5.931
15	2,013	321.4	0.50	600	12	7,200	20.0	10.0	7.90E-12	1.44E-12	5.934
16	2,414	321.8	1.00	0	0		20.0	0.0	1.56E-12	-	5.937
17	2,420	321.9	0.50	120	12		24.4	12.2	3.08E-10	2.15E-10	5.944
18	2,485	321.9	0.50	600	12		24.7	12.3	8.82E-11	4.48E-11	5.964
19	2,610	321.8	0.50	600	12	7,200	24.8	12.4	9.71E-12	3.50E-12	5.970
20	3,088	321.8	1.00	0	0		24.8	0.0	1.24E-12	-	5.972
21	3,230	323.0	0.50	600	12	7,200	24.9	12.5	9.08E-12	3.65E-12	5.977
22	3,257	322.0	0.50	600	12	0	25.0	12.5	6.15E-11	4.71E-11	5.981
23	3,302	321.8	0.50	600	12	7,200	25.0	12.5	8.53E-12	3.62E-12	5.983
24	3,324	321.7	0.50	120	12	0	29.8	14.9	7.78E-10	4.84E-10	6.040
25	3,395	321.7	0.50	600	12	0	30.1	15.1	1.88E-10	1.02E-10	6.087
26	3,450	321.8	0.50	600	12	7,200	30.2	15.1	1.89E-11	7.88E-12	6.093
27	3,732	321.7	0.50	600	12	14,400	30.3	15.2	1.06E-11	4.18E-12	6.104
28	3,874	320.4	0.50	600	12	28,800	30.1	15.0	6.74E-12	2.02E-12	6.109
29	4,953	319.9	1.00	0	0		30.5	0.0	1.72E-12	-	6.116
30	4,956	320.1	600	12			30.3	15.2	4.36E-10	1.03E-10	6.121
31	5,718	320.1	1.00	0	0		30.8	0.0	1.15E-12	-	6.124

[a]Simulated PWR water with 2 ppm Li, 1000 ppm B, and 2 ppm. DO<10 ppb. Conductivity was 21±3 μS/cm, and pH 6.4.

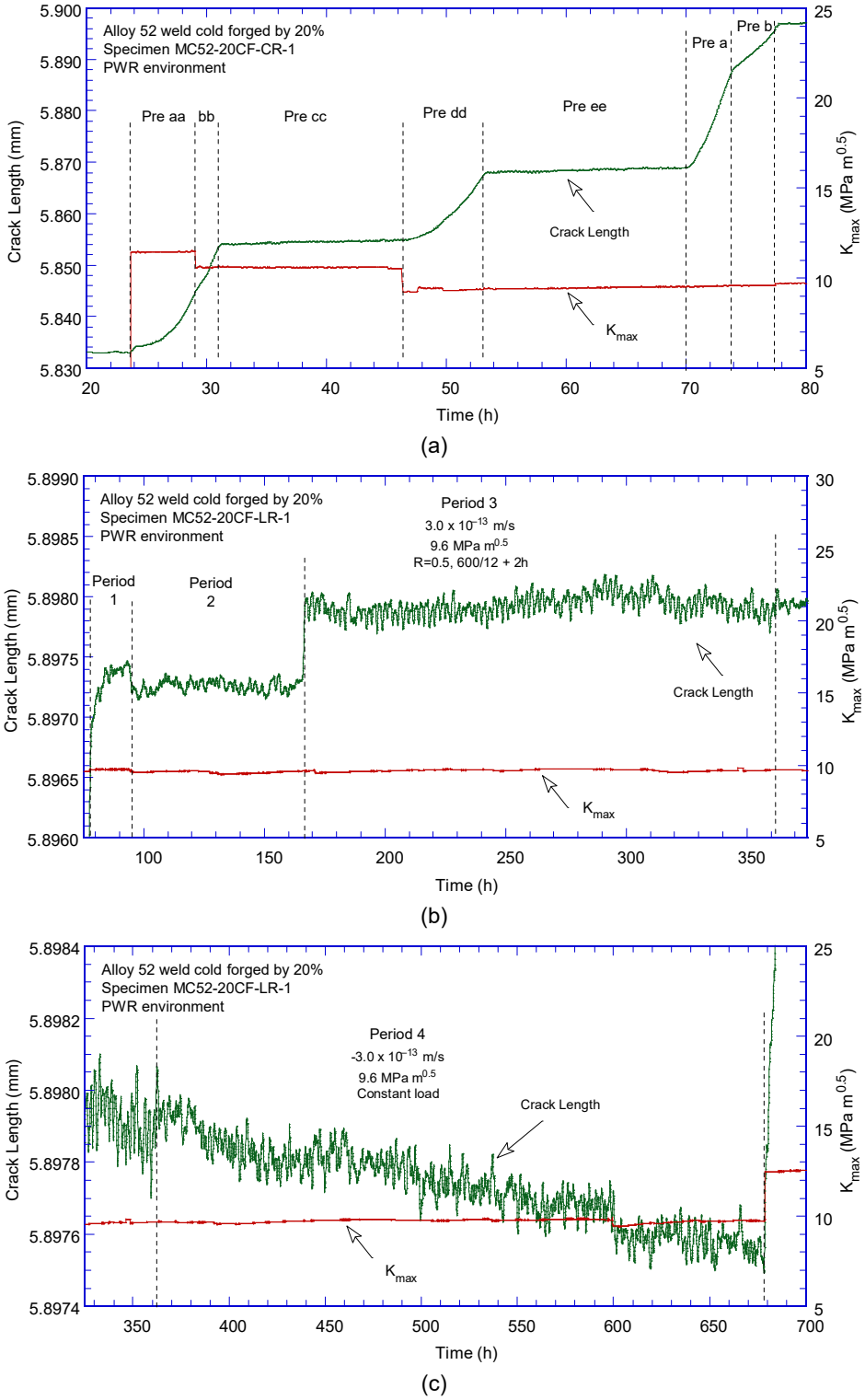

Figure 116 Crack–length–vs.–time for specimen MC52-20CF-LR-1 in simulated PWR environment during test periods (a) precracking, (b) 1-3, (c) 4, (d) 5-7, (e) 8, (f) 9-12, and (g) 9-16, (i) 25-28, (j) 29-30, and (k) detail in test period 29.

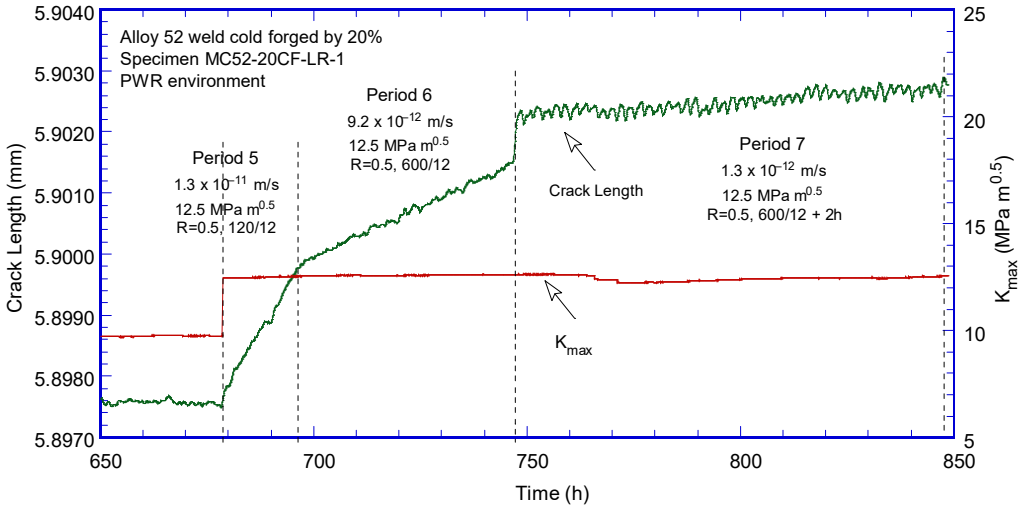

(d)

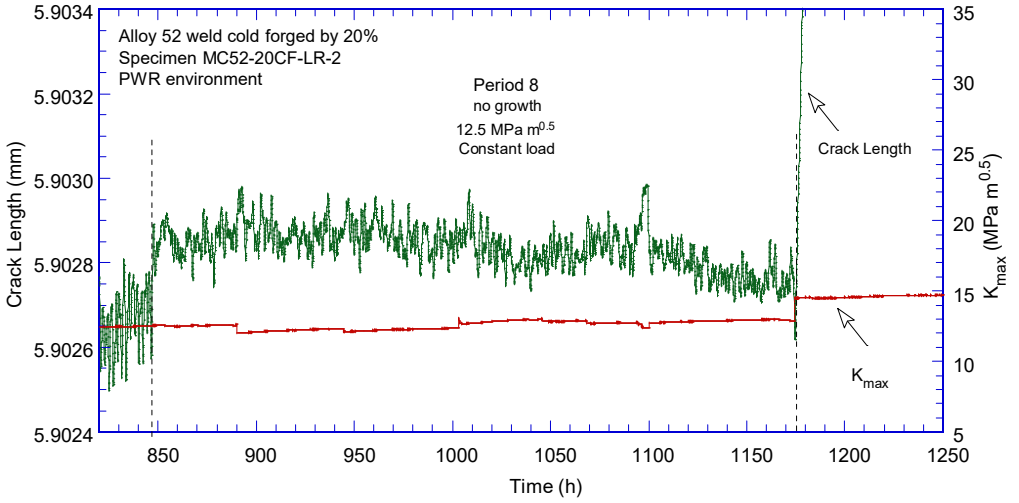

(e)

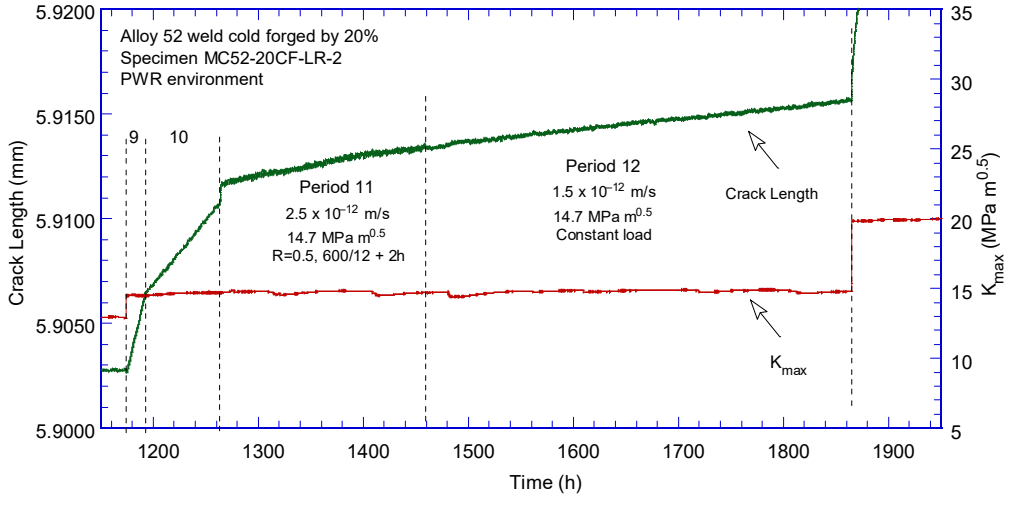

(f)

Figure 116 (cont.)

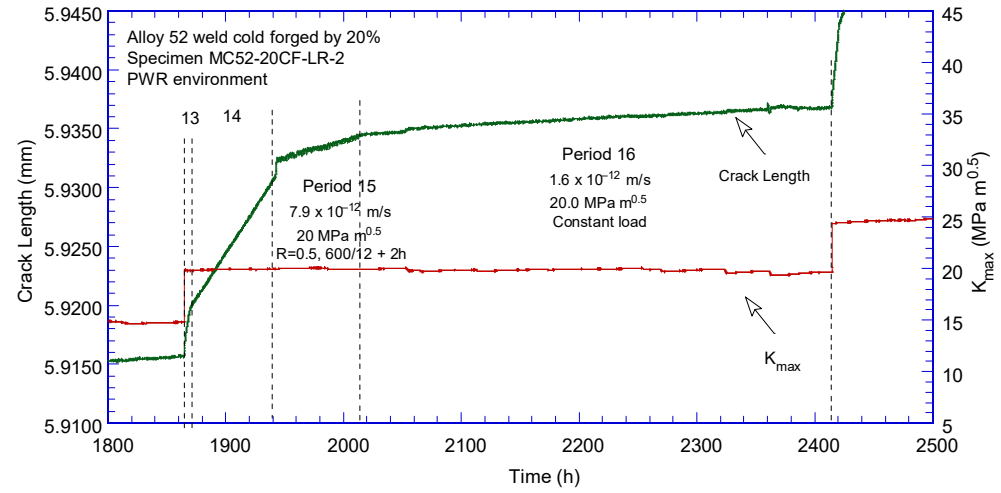

(g)

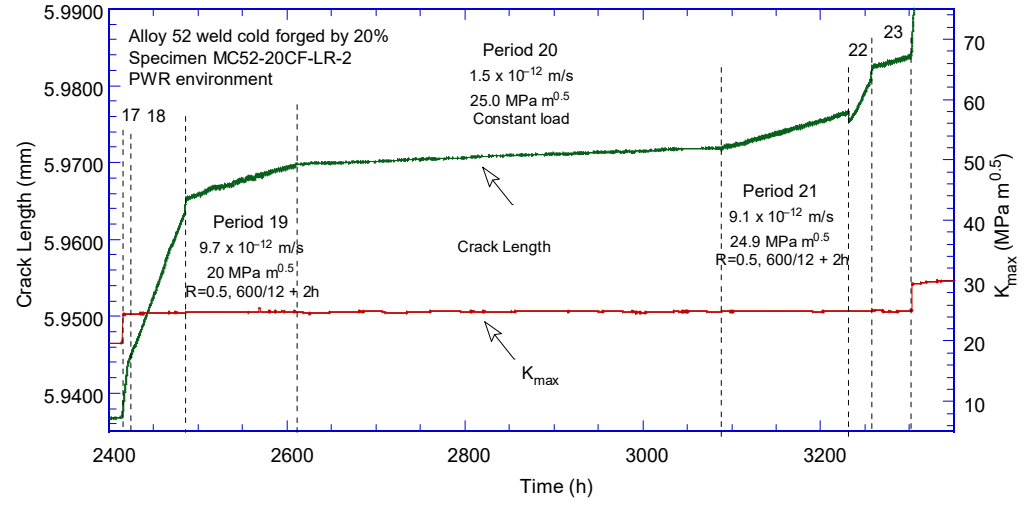

(h)

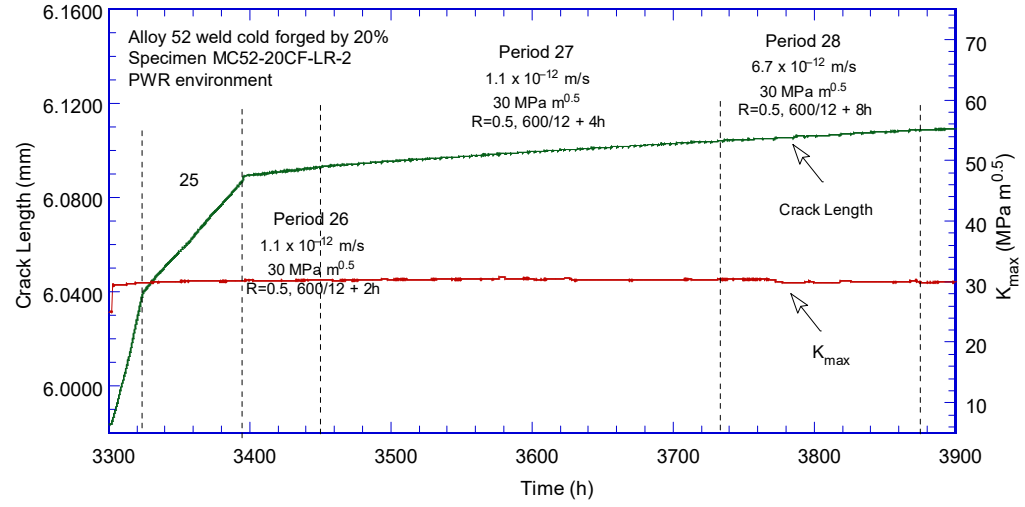

(i)

Figure 116 (cont.)

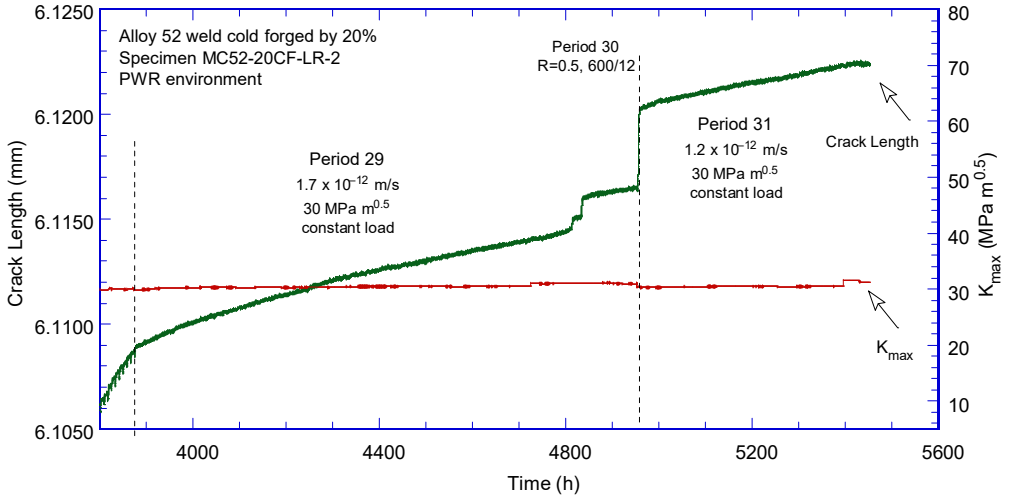

(j)

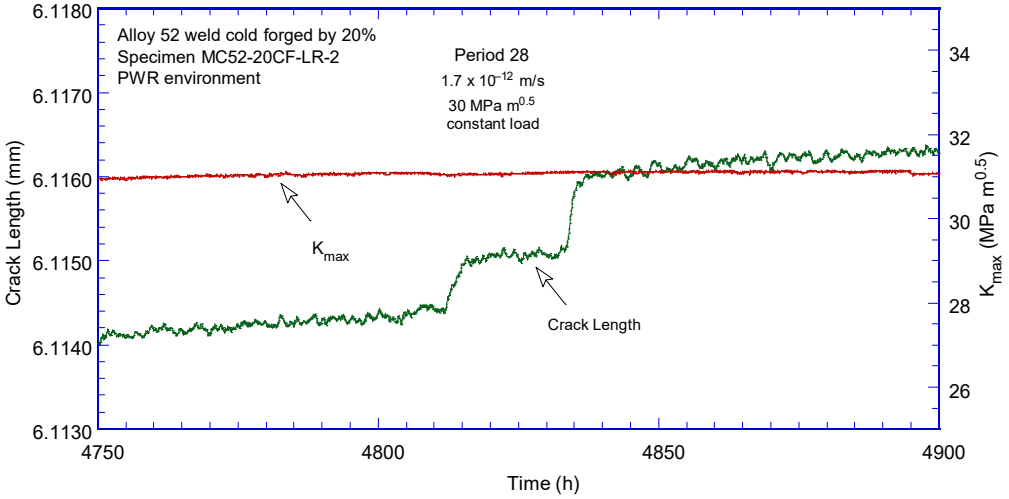

(k)

Figure 116 (cont.)

Figure 117 summarizes the cyclic CGR data obtained on this specimen, and attempts to put this data into perspective. Figure 117a (or Figure 117b at higher magnification) provide a comparison between the current specimen and the specimen tested previously. Both specimens are from the 20% cold-forged weld, and the only difference is in the test plane orientation: LR in the current specimen vs. CR in the previous specimen. Data obtained from the current specimen is shown with different colors corresponding to the gradually increasing stress intensity factors. Overall, the data sets are in very good agreement, and the implications are discussed below.

As described in the previous sections, this Alloy 52 weldment was tested in both the as-welded and a similar 20% cold-forged condition previously. Both specimens were in the CR orientation. A comparison of the two resulting data sets (Figure 109) has shown that, surprisingly, the cyclic CGR response for the cold forged specimen was lower than that of the as-welded specimen. The effect of cold forging appears to be completely opposite from that of cold-rolling where 26% cold-rolling of Alloy 690 led to an approximately 10x increase in the cyclic CGR response.

Nevertheless, unlike rolling which was parallel to the testing plane for the Alloy 690 in the ST orientation, cold-forging was normal to the testing plane in the CR orientation for the Alloy 52 weldment.

In the current test of Specimen MC52-20CF-LR-1, the test plane coincides with the deformation plane, and one would expect the cyclic response to be higher than that for the weld in the as-welded condition. However, as described previously, the current test was initiated at a fairly low stress intensity factor and the cyclic response was expected to mirror that observed for the Davis-Besse Alloy 600 specimen that was also tested at low K [28]. Both Davis-Besse alloys tested at ANL have shown the unique feature that crack propagation was IG irrespective of the loading condition, and that included aggressive 1-2 Hz fatigue loading. However, at low K (14 MPa $m^{1/2}$) the environmental enhancement was found to be retarded (Figure 117c), and the fracture mode was mixed IG-TG. It was only after K was increased to 17 and then to 19 MPa $m^{1/2}$ that that the fracture mode changed to completely IG and the environmental enhancement regained the prior high levels. In short, there was an expectation that the current specimen showed a low environmental enhancement at lower Ks. However, as Figure 117a (or Figure 117b) seem to suggest, the environmental enhancement is unchanged as the stress intensity factors increase to 30 MPa $m^{1/2}$. The implication is that in the current test, transitioning to IG SCC has not occurred.

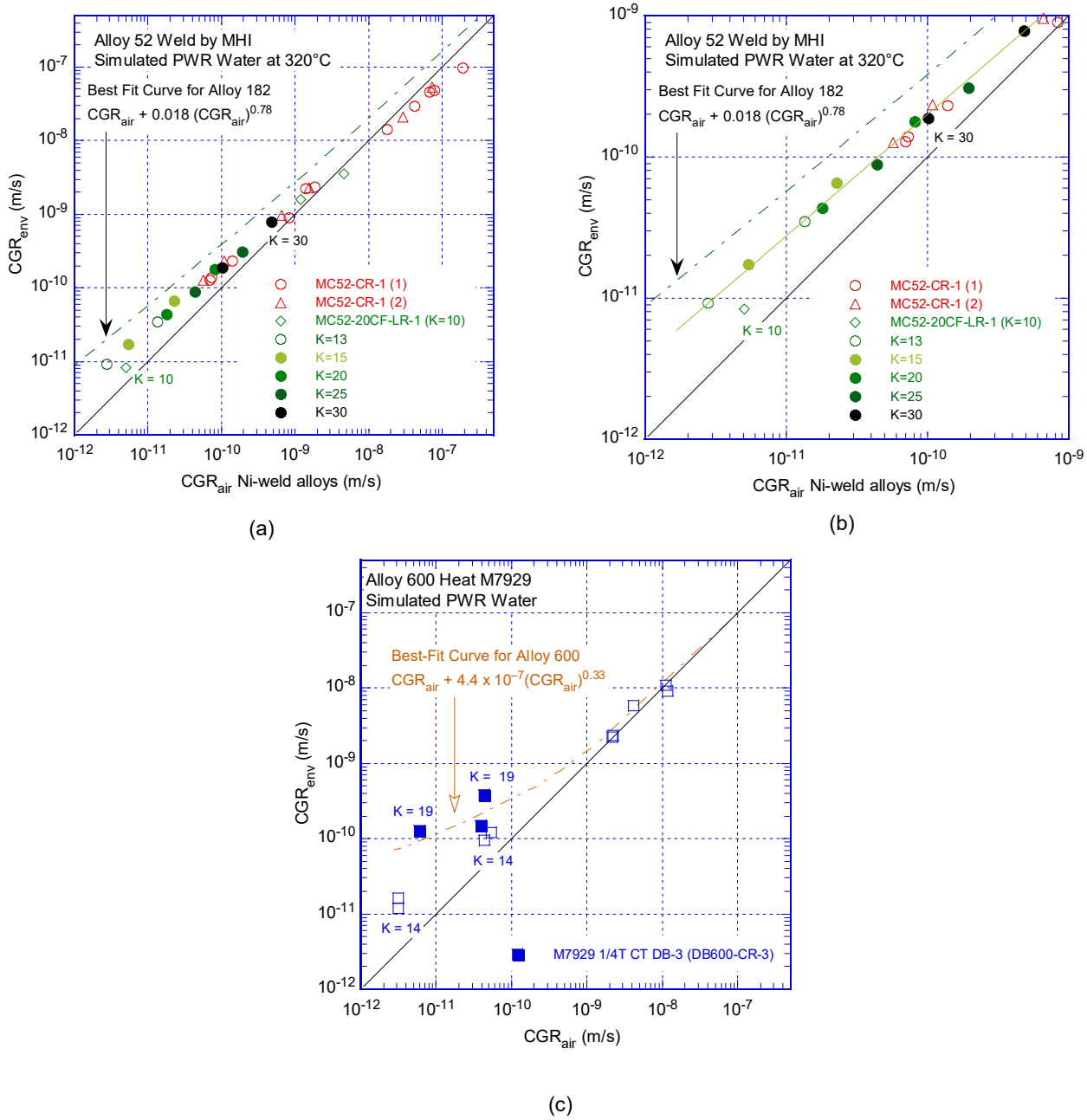

Figure 117 Cyclic CGR data for (a, b) Alloy 52 specimen MC52-20CF-LR-1 (cold forged by 20%) vs. the same weld in the as-received condition, and (c) Alloy 600 Heat M7929 from the Davis-Besse replacement head [28]. Stress intensity factors are indicated in the figure.

Figure 118 summarizes the SCC CGR data obtained on this Alloy 52 weld produced by MHI in the as-welded and 20% cold-forged (CF) conditions. The CGRs obtained from test periods where some cycling was always present (estimate from cycle + hold or the difference between CGRs with the hold time at K_{max} and K_{min}) are shown with open symbols and appear to be slightly higher than those measured at constant load (solid symbols), but overall all the SCC

CGRs are very small. From the current test, one data point resulting from cycle+hold in test period 7 was included. The “no growth” data points resulting from test period 4 and 8 were not included in the plot.

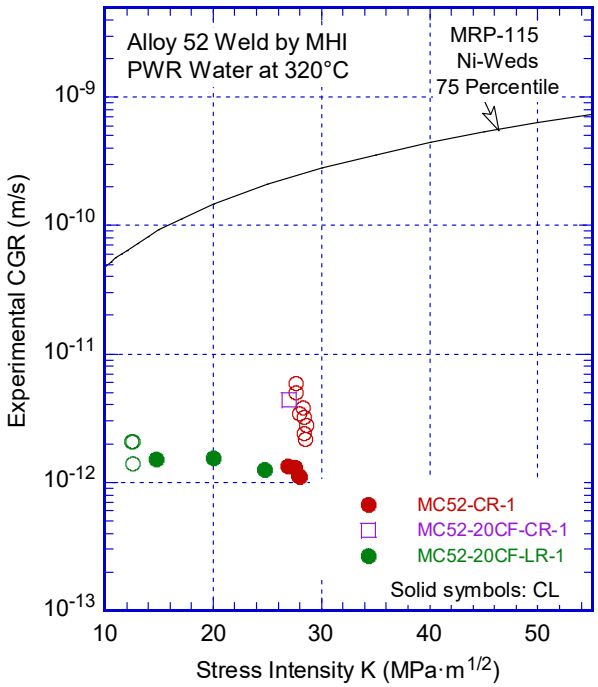

Figure 118 SCC CGR data in simulated PWR environment for Alloy 52 weld produced by MHI in the as-welded and 20% cold-forged (CF) conditions.

The fracture surface of the specimen is shown in Figure 119. The total measured crack is 0.337 mm, which is 14% larger than the DC-potential measured extension (0.291 mm), hence no correction was made to the data shown in Table 23. Nevertheless, one also notes that a few localized “fingers” extend perhaps twice the average extension.

The fracture surface was also examined in the SEM, Figure 120. As suspected, the fracture morphology of this specimen was primarily TG. As such, Figure 120b taken at location 1 in Figure 120a shows a TG fracture mode with striations typical of environmental fatigue. Surprisingly, even the “finger” at location 2 in Figure 120a does not exhibit the IG/interdendritic fracture mode that one usually associated with SCC “fingered” growth along the dendritic grains in welds. As such, the low/no growth CGR response recorded throughout this test are constant with the fracture appearance.

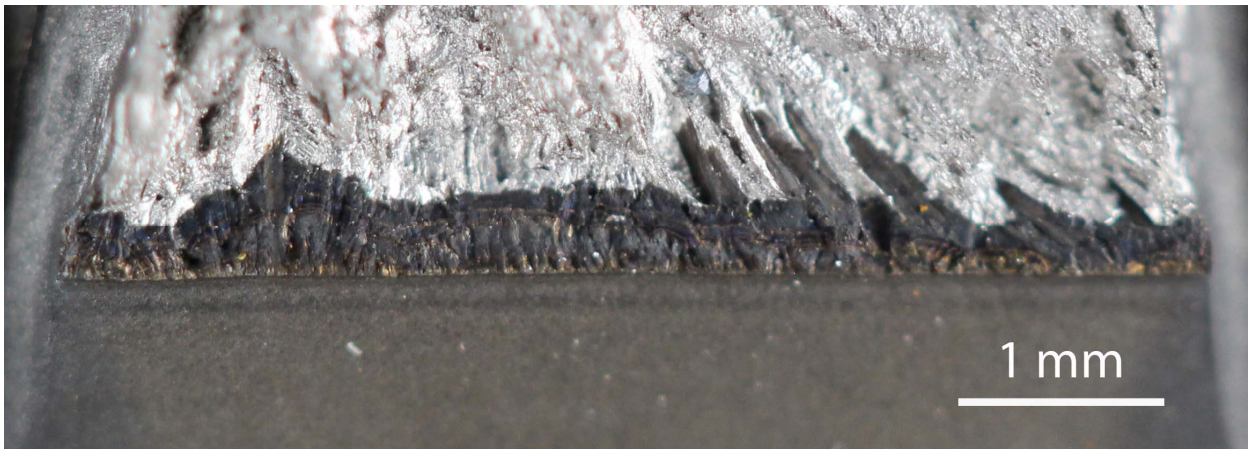

Figure 119 Fracture surface of Alloy 52 specimen MC52-20CF-LR-1 tested in simulated PWR environment. Crack advance is from bottom to top.

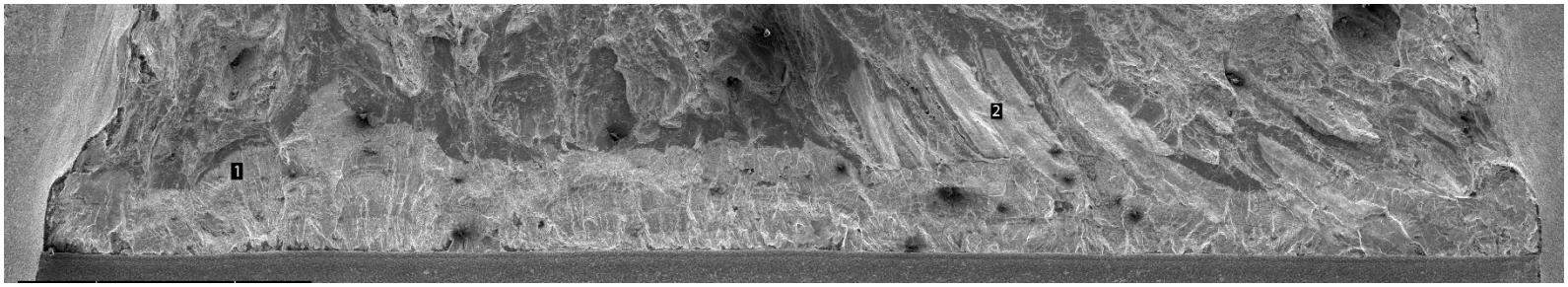

(a)

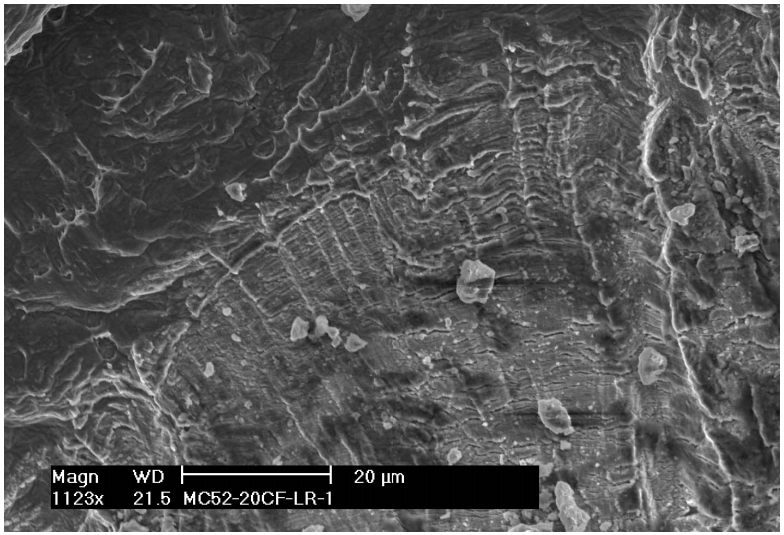

(b)

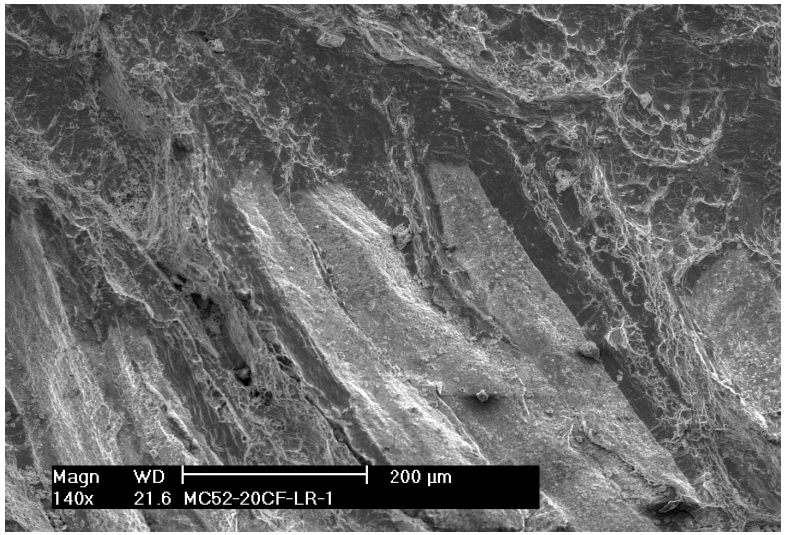

(c)

Figure 120 (a) Fracture surface of Alloy 52 specimen MC52-20CF-LR-1 tested in simulated PWR environment. (b) detail at locations 1, and (c) detail at location 2. Crack advance is from bottom to top.

4 DISCUSSION

The section summarizes and discusses the cyclic and SCC CGR results obtained on the Alloy 52/152 weldments. A comparison with the industry-proposed disposition curves is made. Hence, in the following discussion, SCC CGRs reported as “no growth” have not been included in the plots as such data cannot be used for the disposition of cracks assumed to be growing.

4.1 Cyclic CGR Response of Alloys 52/152 and variants

Cyclic CGRs for Alloys 52/152 are compared with CGR correlations for Ni-welds developed previously at ANL [22]. The relationship between cyclic CGR response and fracture morphology is investigated.

4.1.1 Dedicated Cyclic CGR Curves for high-Cr Alloy 52/152 Welds and Variants

The objective of this section is to compare the cyclic CGRs for Alloys 52/152 obtained in this program with the CGR correlations for Ni-welds developed previously at ANL [22], and to explore the possibility of developing a dedicated Alloys 52/152 cyclic CGR curve.

The fatigue CGR (da/dN) curve for Ni–alloy weld metals, e.g., Alloys 182, 82, 152, and 52, was developed at ANL [22] based on a database that was inadequate to establish the effects of stress ratio R, cyclic frequency, and stress intensity factor range ΔK on the CGRs. Consequently, the functional forms for the effects of frequency, R, and ΔK in Eq. (2) were assumed to be the same as those for Alloy 600. The temperature dependence of the constant C was determined from data sets that were normalized for the effects of R and ΔK (Figure 121), resulting in a fourth-order polynomial dependence of temperature T (°C) expressed by Eq. (5).

The estimated–vs.–experimental fatigue CGRs for Ni–alloy weld metals (Alloys 182, 82, 152, and 52) at various temperatures are shown in Figure 122. The estimated values show good agreement with the experimental results.

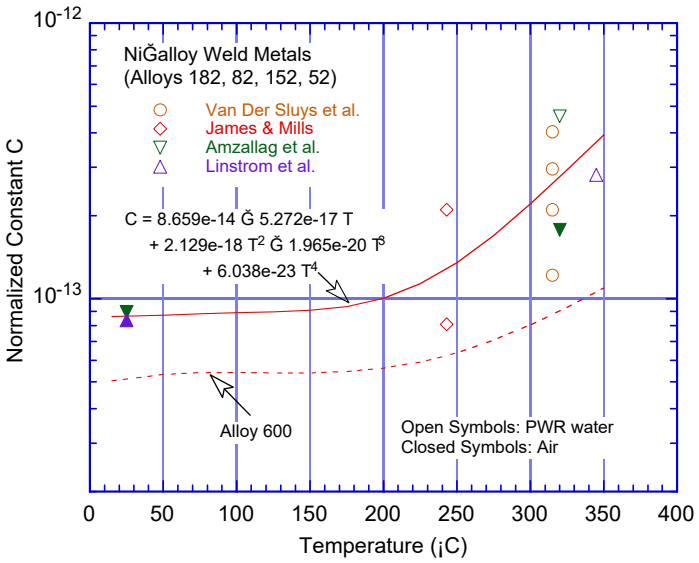

Figure 121 Variation of normalized constant C for Ni–alloy welds with temperature [22].

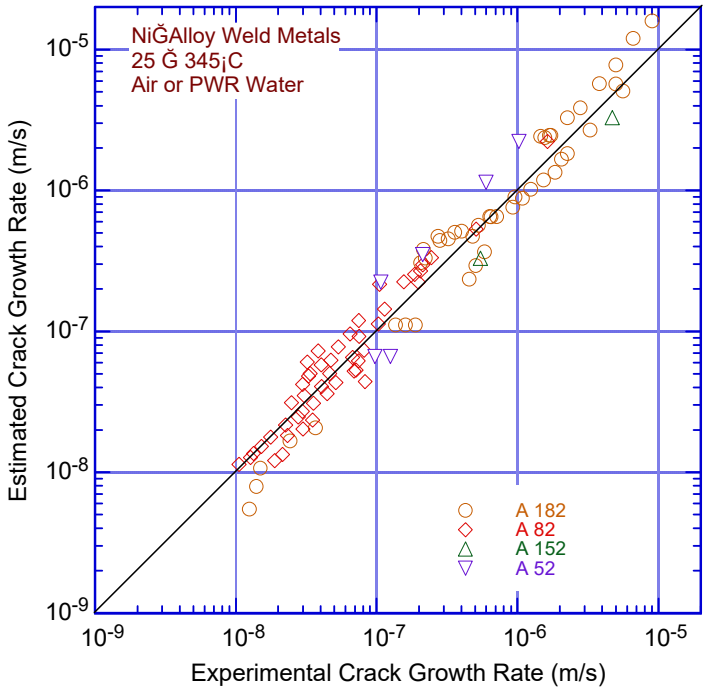

Figure 122 Estimated–vs.–experimental values of fatigue CGR of Ni–alloy weld metals in air and PWR environment at temperatures between 25 and 345°C [22].

Since the publication of NUREG/CR-6921 (2006), the fatigue CGR database has not changed, as no dedicated fatigue CGR program has started anywhere. Hence, the functional forms for the effects of frequency, R, and ΔK are still unknown for Alloys 52/152. The vast majority of the cyclic CGR data generated worldwide are a byproduct of SCC CGR testing programs in high temperature water where specimens are most often tested in parallel using servo-mechanical loading systems that are unsuitable for generating high quality fatigue CGR data.

The data generated in this program comes from single specimen tests using servo-hydraulic loading, however, it is limited to 320°C. Hence, it cannot be used to verify or alter the temperature dependence shown in Figure 121. Nevertheless, the data generated in this program can be used to assess the suitability of the cyclic CGR equations developed more than a decade ago. As such, Figure 123 shows all the cyclic CGR data generated at ANL for this report. The fatigue data (10^{-8}-10^{-7} m/s) for all specimens appears to be in excellent agreement with the behavior predicted by Eq. (2) and (5). The only exception appears to be the 20% cold-forged specimen MC52-20CF-CR-1 where the test plane was normal to the forging plane; the reason for the discrepancy is unknown, however, one notes that the specimen of the same heat tested in the as-welded condition behaved as expected. The environmental effect curve – developed using mostly Alloys 82/182 – Eq. (7) seems to bound most of the data. Consistently, some of the highest levels of environmental enhancement are for Alloy 152 heat WC04F6 (blue symbols) which yielded high levels of IG fracture. Several conditions from the EPRI-produced high heat input weld specimen HHEP52M-TS-1 (red symbols) show high levels of environmental enhancement, and it is unclear at this stage whether that is a local or a more generalized effect for these welds. Two more tests on high heat input welds are in progress.

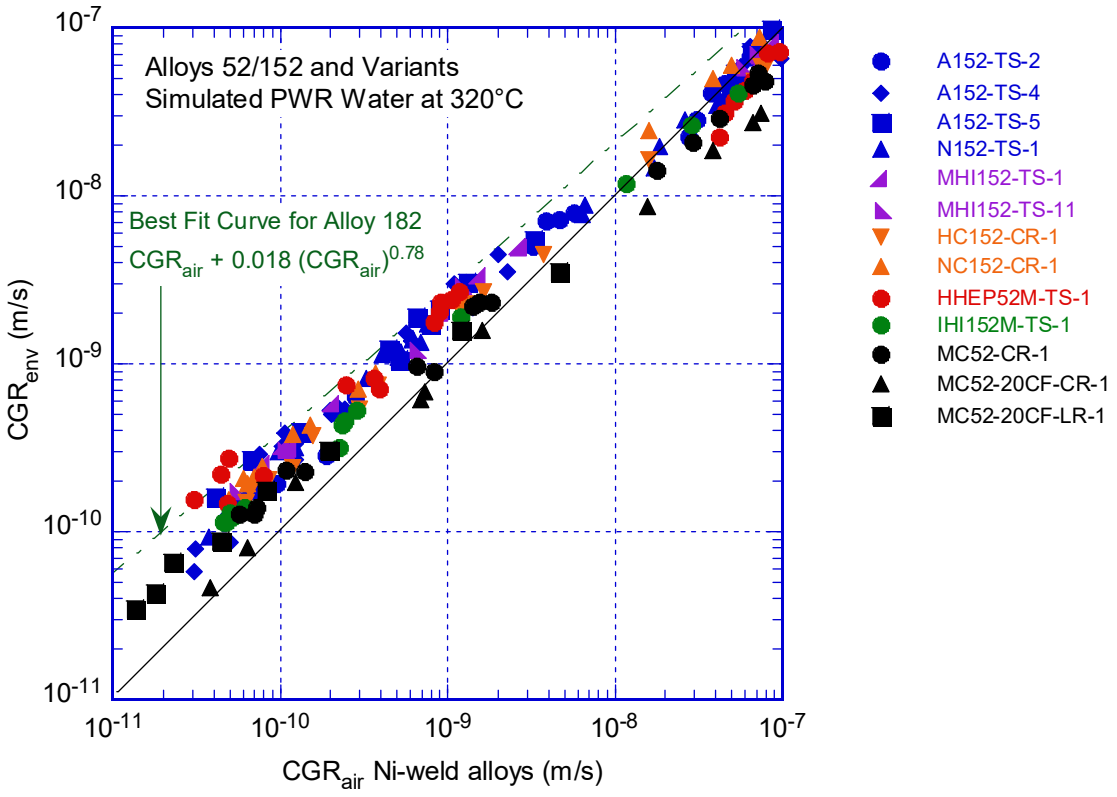

Figure 123 Cyclic CGRs for all Alloy 52/152 and variant welds tested in the ANL program.

4.1.2 Effect of Fracture Morphology on Cyclic CGR response for high-Cr Alloy 52/152 Welds and Variants

Almost all modern SCC CGR testing involves a transitioning stage. The purpose of this stage is to induce a change in the fracture mode from fatigue TG to IG SCC. The general approach to transitioning is identical at all laboratories, and it fundamentally relies on the concept of superposition described previously, Eq. (1). Essentially, during "transitioning" the mechanical/corrosion fatigue component is gradually reduced with the expectation that the fracture mode changes from fatigue TG to IG, and the "gentle" cyclic CGR asymptotes to an SCC CGR. Loading waveforms with hold times, termed "cycle + hold" or generic "partial periodic unloading" (PPU) are often used. The objective of the following analysis is to determine whether (PPU) CGR response reflects the fracture morphology. Equally important is to determine the relationship between SCC CGRs obtained under constant load (CL) and PPU.

In order to determine whether a correlation between PPU response and crack morphology exists or not, the PPU CGR data on Alloy 52/152 obtained at ANL is plotted against the IG fraction in Figure 124. These data span a wide range of SCC susceptibilities, from resistant heats (no IG fracture) to IG SCC–susceptible heats (nearly complete IG fracture). Figure 124a shows one such cycle + hold condition (R=0.5, 600s rise/12s down + 2 h hold) for all weld specimens tested at ANL, and the trend suggests that cyclic response detects rather reliably the occurrence of IG SCC. In the superposition framework described previously, one understands that the occurrence of IG SCC and SCC growth is the reason for the overall higher CGRs

measured at the higher %IG. Figure 124b shows the resulting SCC CGR components after the fatigue and corrosion fatigue components were subtracted (the "PPU" CGRs are shown with yellow symbols in the figure), and the SCC CGRs measured under constant load (shown with solid green symbols). As one would expect, low IG specimens have no/low SCC CGR components as the overall response is driven by fatigue. In light of Eq. (1), it is hopefully obvious that in such "no growth" conditions even the most "gentle" fatigue "PPU" data will always result in a higher CGR than the no/low growth CL determinations. Nevertheless, Figure 124b shows that at higher levels of IG engagement – perhaps over 70% - the PPU and CL CGR responses show consistency, as expected. Some low/no growth response at constant load still exists, but these data should be treated carefully, especially when they contradict both CL and PPU CGR data obtained in the context of the same specimen. In other words, these are likely cases of crack arrest or off-plane cracking and should be probed accordingly.

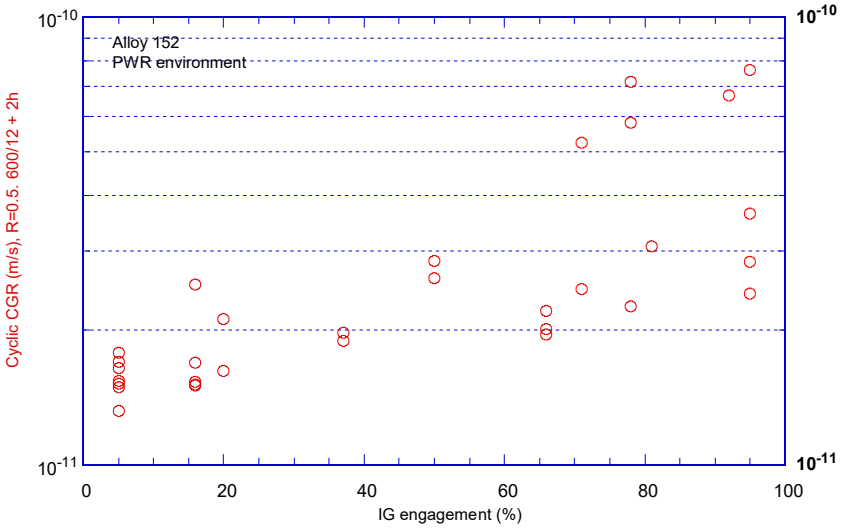

(a)

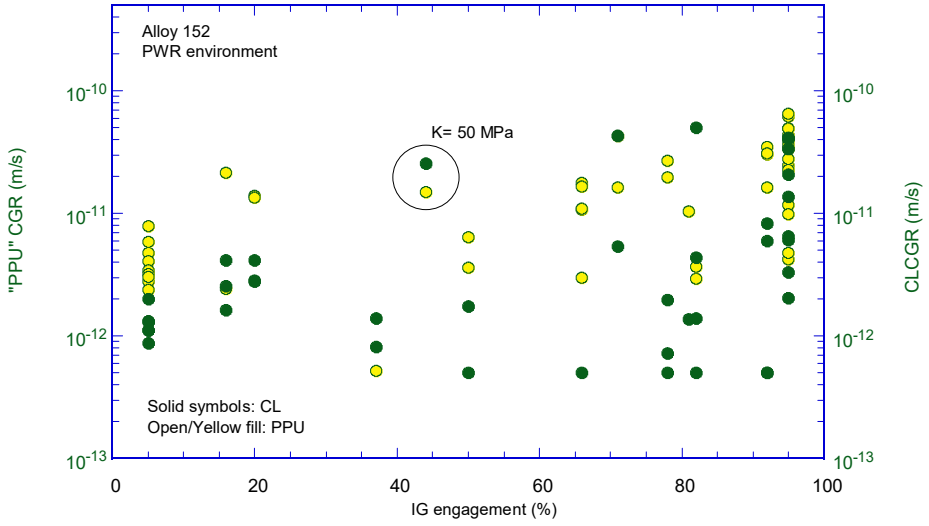

(b)

Figure 124 (a) Cycle + hold (R=0.5, 600 rise, 12 down + 2 h hold) response, and (b) PPU and constant load CGRs as a function of IG fraction in Alloy 52/152 specimens tested at ANL in simulated primary water at 320ºC.

4.2 SCC CGR Response of Alloys 52/152 and variants

The SCC CGR data obtained in this program on Alloy 52/152 and variant welds is presented and discussed in the framework of the SCC CGR disposition curves proposed by the industry.

4.2.1 SCC CGR Disposition Curves Proposed by Industry

The SCC CGR disposition curve (MRP-115) was proposed by industry in 2004 [1] and has since provided a benchmark for all SCC CGR data generated on Alloy 82/182, and even for the high-Cr Alloys 52/152 and variants. More recently, a similar effort [13] was made for high-Cr Ni-base Alloys 690 and 52/152. As the data did not display any dependencies typical of SCC growth such as K or temperature, these were assumed to exist and, moreover, be identical to those for Alloys 600 and 182. The improved resistance to SCC for the high-Cr alloys was captured by factors on improvement (FOI) applied to Eq. (8) and Eq. (9): 38 for Alloy 690 and 324 for Alloy 52/152. As such, as Figure 125 shows, the SCC CGR average for 75% of the Alloy 52/152 heats should be in the 10^{-13} m/s range. Of concern with this outcome is that there was no actual data to support the assumed dependencies or the proposed curve. The MRP-386 curve relies on a database of which 60% of the data were obtained at 350-360°C to which the assumed temperature dependency was applied. Most of this data was low/no growth.

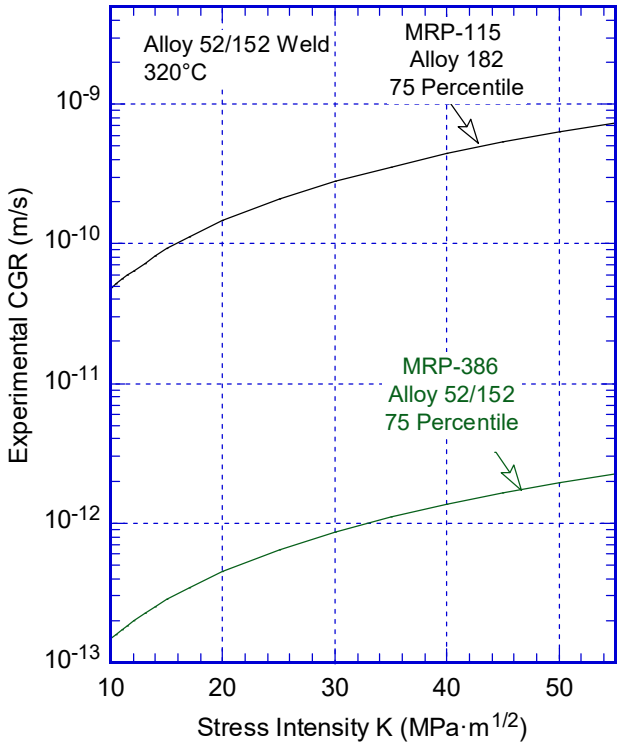

Figure 125 The proposed disposition curves for Alloys 182 [1] and 52/152 [13].

In order to explore whether the application of the temperature dependence to low/no growth data generated at 350-360°C resulted an artificially low disposition curve, Figure 126 shows only the SCC CGRs from the MRP-386 database that were generated at 320-325°C and so they

did not require a temperature correction. For the ANL data (Figure 126a), the MRP-386 bounds 7% of the data points, and for the data obtained elsewhere (Figure 126b), the MRP-386 bounds 33% of the data points. While this discussion should be in terms of heats and not individual data points, the low bounding percentages seem to suggest that the MRP-386 is not conservative. Several areas of concern with the underlying rationale leading to the development of this curve will be discussed next.

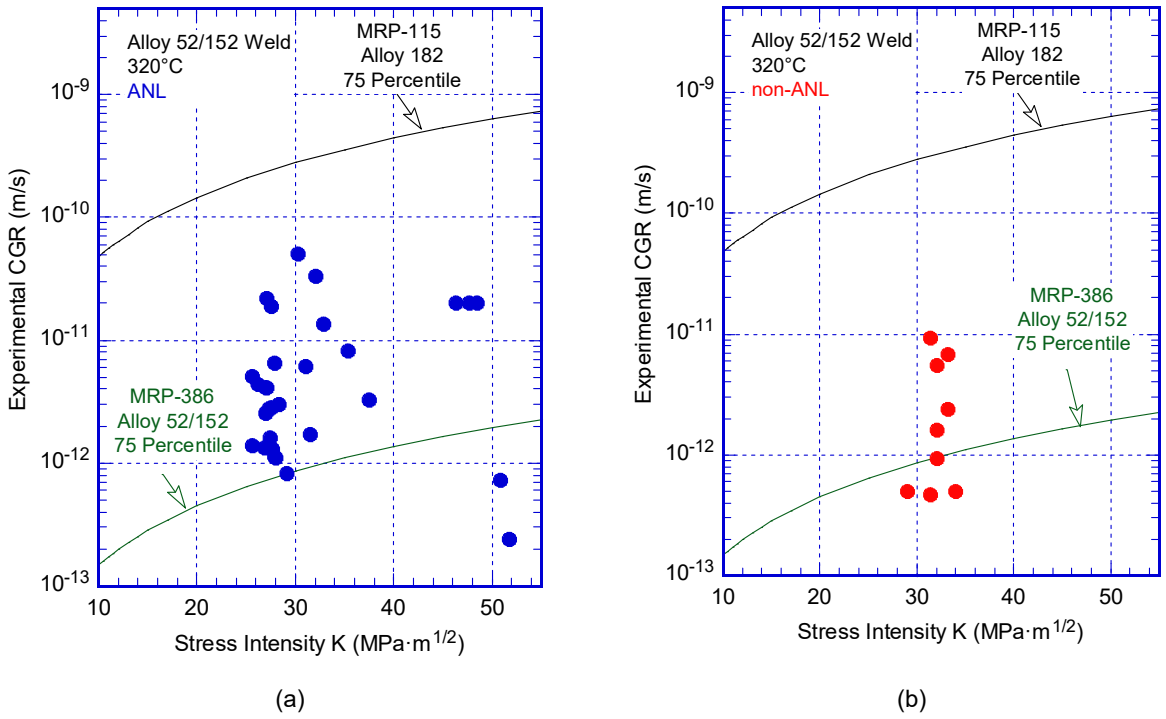

Figure 126 SCC CGRs from the MRP-386 database generated at 320-325C at (a) ANL, and (b) elsewhere. The proposed disposition curves for Alloys 182 [1] and 52/152 [13] are included.

The primary concern is that the proposed curves (and resulting FOIs) for Alloy 690/152 are not representative of intergranular (IG) SCC growth like the original or the recently-revised Alloy 600/182 curves are. As such, while every effort was made for the original (MRP-55 and MRP-115) and the revised 600/182 curves (MRP-420) to be re presentative of IG SCC growth by imposing a lower limit for the %IG, and correcting the CGRs for %IG, the current Alloy 690/152 analysis makes no differentiation between the assumed-to-be-existing transgranular (TG) SCC growth and IG SCC growth. Even if TG SCC were to exist as a degradation mode for the alloys at hand, IG and TG processes are kinetically different, hence comparing TG SCC and IG SCC CGRs is essentially an apples to oranges comparison.

There seems to be no evidence that TG SCC even exists in any of the alloys at hand. In the previous Alloy 600/182 efforts, TG fracture was considered "unrepresentative morphology" [1] as TG SCC growth was never demonstrated to occur. The same appears to be true for Alloys 690/152. The fact that mixed TG and IG fracture is often found in multi–stage tests does not constitute proof for the existence of TG SCC growth, as it is not clear under which loading conditions the said TG fracture occurred. By contrast, the lack of TG SCC in the single condition, bolt loaded specimens (where loading in not ambiguous) seems to be a far more

compelling argument against the existence of TG SCC. In such tests, TG SCC growth, if it were to occur, it would develop readily and easily from the TG fatigue precrack with no need for "transitioning" to another fracture mode. Yet, not a single case of TG SCC growth in Alloys 690/152 or 600/182 resulting from an unambiguous single-condition test was ever reported.

As described previously, unlike the Alloy 600/182 databases, the current Alloy 690/152 databases are a collection of assumed-to-be-existing TG SCC and IG SCC CGR data. Also unlike the Alloy 600/182 databases, the Alloy 690/152 data was not corrected for %IG despite strong evidence that %IG influences the measured CGR by as much as a factor 100, and that significantly higher CGRs were measured in both the base metals and the welds at levels of IG higher than 70-80% (see for example Figure 124).

In addition to disregarding the effect of the IG morphology on the CGRs, IG SCC - derived dependencies were applied to the assumed-to-be-existing TG SCC CGR data. In the published version of MRP-386, those dependencies were limited to the temperature correction, and the authors also decided to impose a lower limit of $1\ 10^{-12}$ m/s for the application of the Alloy 600 IG SCC- derived temperature dependency. The authors did not provide a serious explanation as to what the basis for their choice might have been. In addition to the above, one important thing to keep in mind is that in the absence of any evidence for the existence of TG SCC growth, many of the low/no growth CGRs in the database are likely resistivity/electronics drifts, essentially noise from the DC-potential CGR measuring system. The fact that these "rates" fail to display the widely-known temperature and hydrogen dependencies of SCC growth supports the idea that they are indeed electronic drifts/noise. These noise "CGR" data do not belong in a SCC CGR database, much less have artificial dependencies applied to them. Even if TG SCC were to exist, it is not at all clear why temperature, hydrogen, and other dependencies would be similar to those developed from IG SCC growth data. In fact, they should not be as the governing, rate-limiting processes, i.e., the dislocation kinetics at grain boundaries vs. the matrix are different.

In summary, the practice of indiscriminately lumping together assumed-to-be-existing TG and IG SCC CGRs, and applying IG SCC-derived dependencies to TG SCC CGRs and/or electronic drift/noise "CGRs" does not appear to be technically sound. The outcome of any analysis – whether curves or FOI – will essentially reflect what is in the database, and for the case at hand the outcome is likely not representative of a growing SCC crack.

4.2.2 SCC CGR Response of Alloy 152 Weldments Produced by ANL and MHI

Figure 127 summarizes the SCC CGR data for two ANL-produced Alloy 152 weldments (heat WC04F6 was used in both). Figure 127a includes all the data obtained in these tests, irrespective of the extent of the crack advance. SCC CGRs obtained under constant load are shown with solid symbols, while those obtained at constant load with periodic unloading or PPU are shown with open symbols. There seems to be a good agreement between that data obtained at CL and the data obtained from PPU conditions, especially for the data with the longer crack extensions. In Figure 127b a criterion on crack advance was imposed, namely that it be at least 10x the resolution, and in this case there is a very good agreement between the data obtained under CL and PPU. In either case, the data points resulting from the test on specimen N152-TS-1 appear to be in good agreement with the A152 data set.

This data set shown in Figure 127b also meet most of the selection criteria of EPRI MRP-115 [1], including the minimum IG-engagement, and frequency of periodic unloading criteria. The

crack advance falls short on the required 0.5 mm, but it is comparable to that in a few cases. The minimum crack length criterion imposed (10x resolution) helps with the level of uncertainty of these data points. Hence, this data set can be compared to the proposed disposition curve for Alloys 182/82.

The SCC CGR data from the test on A152-TS-5, obtained at various K levels was used to determine the K dependence for Alloy 152. A functional dependence similar to that proposed in MRP-115 seems to describe the data reasonably well (R^2 = 0.37). The resulting SCC CGR amplitude is approx. 8.8 1 10^{-14} m/s (see Eq. (9)), and the implication of this finding is that this current heat of Alloy 152 has an average SCC CGR approximately 17x lower than the disposition curve for Alloy 182. It should be emphasized that this Alloy 152 dataset is representative of IG SCC, just like the MRP-115 curve, so the comparison is an apples to apples comparison.

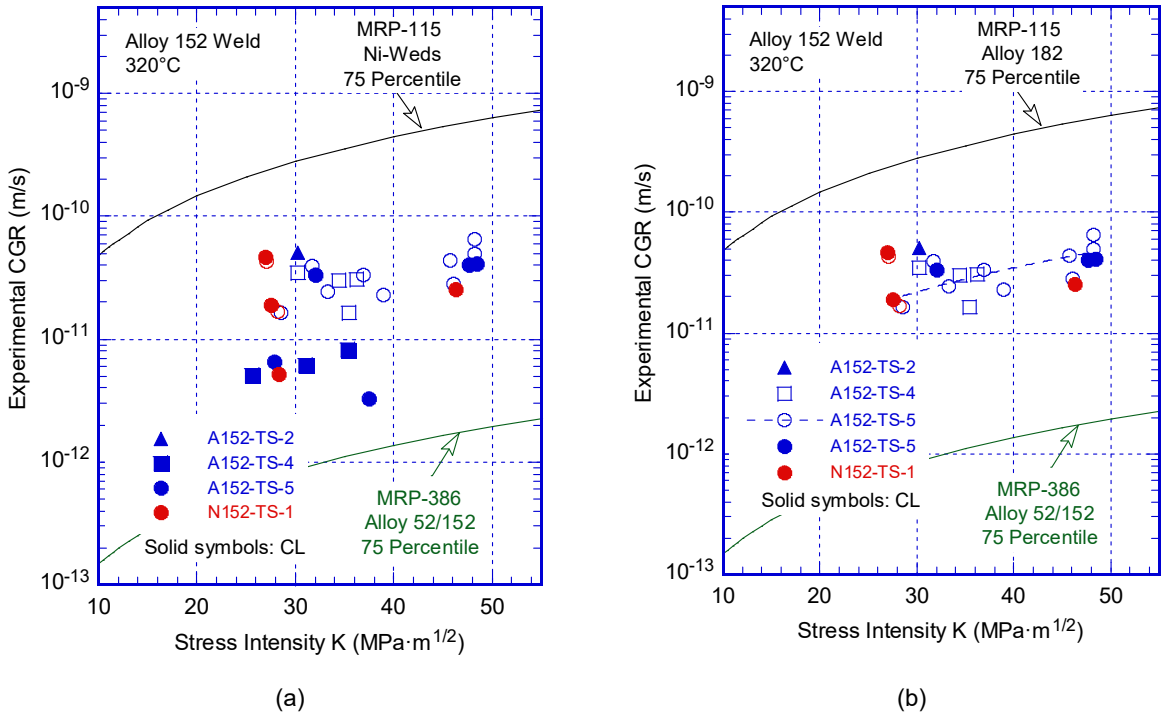

Figure 127 SCC CGRs for Alloy 152 weldments (heat WC04F6) produced at ANL: (a) all CL and PPU data, and (b) only data for which the crack advance is 10x resolution. The proposed disposition curves for Alloys 182 [1] and 52/152 [13] are included.

Another weldment that yielded moderate to high levels of IG fracture during testing was the Alloy 152 mock-up weld produced by MHI, Figure 128. One of the two specimens that were tested was a 1T CT, and this allowed testing at both moderate and relatively high stress intensity factors. Testing at moderate K resulted in a moderate IG engagement, and in the larger specimen was confined to one half of the fracture surface. The reason for this is unclear, but the more modest %IG in these regions is likely reflected in the lower SCC CGRs. The SCC CGRs at constant load were relatively small, and in agreement with the rates obtained in test periods that involved some cycling. Testing at a higher K resulted in substantial IG engagement (80%) that was spread uniformly across the specimen width. The resulting SCC CGRs at

constant load were still small, and contradictory to the moderate CGRs obtained during test periods that involved some cycling. The latter actually approach the rates measured in the ANL-produced welds. The discrepancy between CL and PPU CGRs is not entirely surprising given the amount of finger-like growth, but additional testing on IG SCC -vulnerable heats is perhaps warranted.

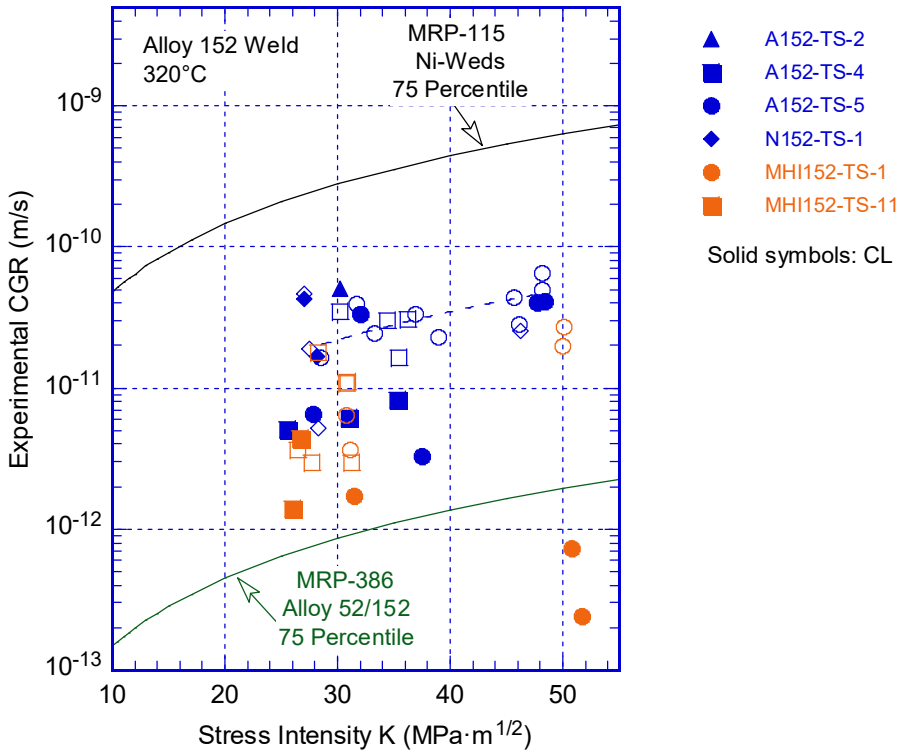

Figure 128 SCC CGRs for Alloy 152 weldment produced by MHI for "Kewaunee" reactor. The proposed disposition curves for Alloys 182 [1] and 52/152 [13] are included in the figure.

Occasionally, materials with suspected vulnerabilities have been tested in common with other laboratories. As such, ANL made available to other laboratories sections of the Alloy 152 weld (designation N152) produced with heat code WC04F6 at ANL Central Shops. Additional testing was conducted at both GE and PNNL.

A comparison of the cyclic CGR response obtained at the ANL, GE and PNNL is shown in Figure 129. Figure 129a shows the comparison of CGR responses obtained during precracking at the three labs. While the ANL data is obtained in-situ (in 320°C water, using the regular test frame and loading system), the PNNL and GE specimens are precracked in ambient air prior using a fixture other than their regular test frame. Nevertheless, as Figure 129a shows, the expected fatigue CGR response during precracking was reproduced at all three laboratories, so the expectation for the fatigue response of this weld is clear. Next, Figure 129b provides a comparison of the CGR responses obtained in high temperature water. The GE and PNNL data shown in this figure are obtained during the CGR tests using their usual test fixtures and loading system (just like the ANL data). One observes that the data obtained in the regular CGR test

frames at GE and PNNL does not reproduce the fatigue response they measured previously in air, using a different “precracking” setup (Figure 129a). Also, while the data sets obtained in water by both GE and PNNL are similar (unsurprising since both laboratories use essentially identical “GE-designed” test facilities and CGR measurement software), they are both substantially lower than the ANL data. This outcome was totally unexpected given the higher test temperatures at GE and PNNL (360°C) vs. ANL (320°C). The lower CGR response during the test suggests that the loading systems do not reach the intended peak loads. Hence, it is very likely that it is the loading system – servo-hydraulic (ANL) vs. servo-electric (GE and PNNL) that is largely responsible for the observed difference.

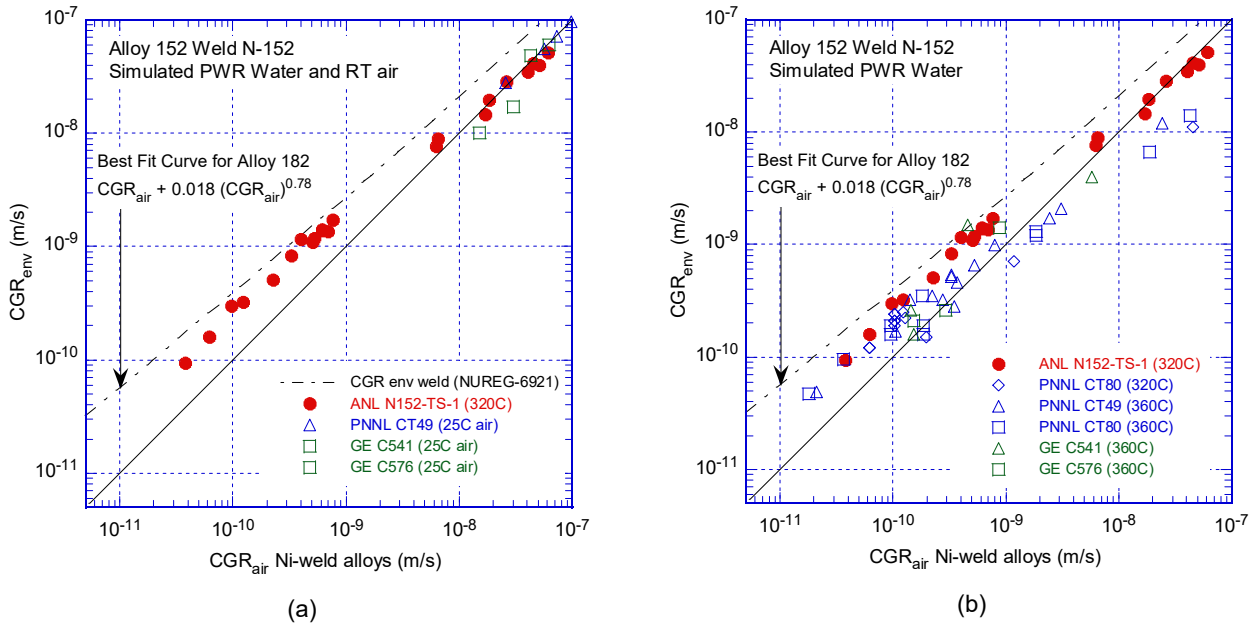

Figure 129 Cyclic response obtained in ANL, GE and PNNL tests on the same Alloy 152 weld heat WC04F6: (a) precracking in 320C water (ANL) and RT air (GE, PNNL), and (b) testing in 320ºC water (ANL) and 360ºC water (PNNL, GE).

While the cyclic CGR responses described in the previous paragraph are clearly not suitable for establishing the CGR correlations discussed in Section 4.1.1, the immediate implication from an SCC CGR test management perspective is that key pieces of information typically used to guide it may be unavailable or unreliable. For example, the CGR of 5.2 10^{-11} m/s under cycle + hold conditions (test period 14, Table 12) – judged by superposition to be a clear indication of IG propagation in the ANL test – was never reproduced in either the GE or PNNL tests despite using the same loading waveforms and higher test temperatures. If one were to trust the CGR response, the lower response may mean a lack of IG engagement, however, both laboratories reported moderate-high (35-75) %IG in the MRP-386 database [13].

For the purpose of this comparison, only the specimen with the highest reported %IG will be discussed. This is specimen c541 tested at GE. According to the MRP-386 database [13], the proportion of IG on the fracture of this specimen is 75%. However, this specimen was also sent to PNNL for additional examination, Figure 130. The analysis by PNNL found the %IG in this specimen to be between 14-40%. While it is not the purpose of this discussion to re-analyze fractographic information, it is worth noting that if the PNNL analysis is right, under MRP-115 rules, such low levels of %IG would have screened out the respective test result.

Another equally important observation is that approximately 25% of the sample (right side) did not engage at all, and the likely culprit seems to be the unbroken ligament shown with the red arrow in Figure 130a. The presence of such a large ligament must have affected the DC potential reading and the CGR response (both cyclic and SCC).

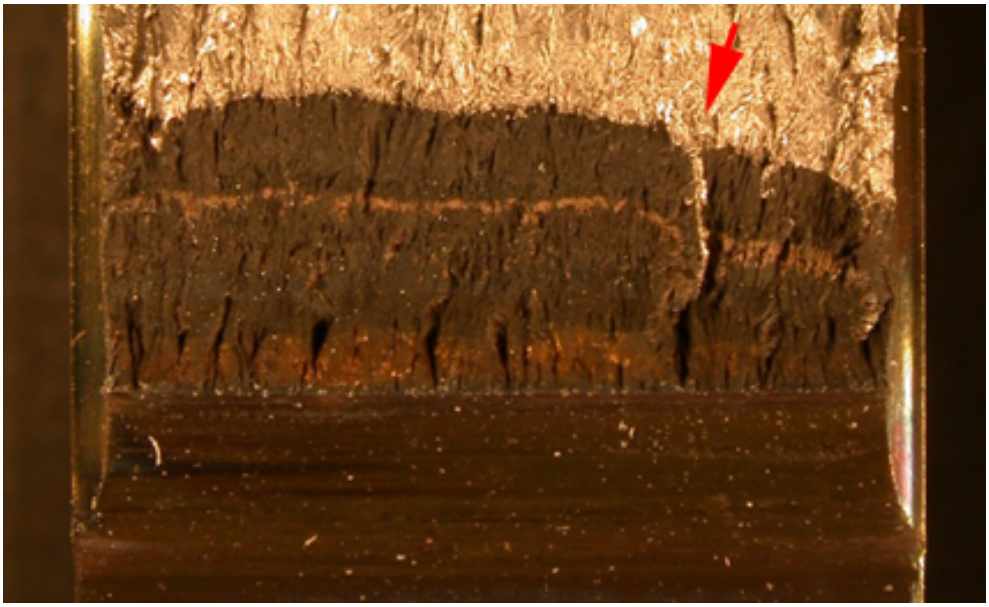

(a)

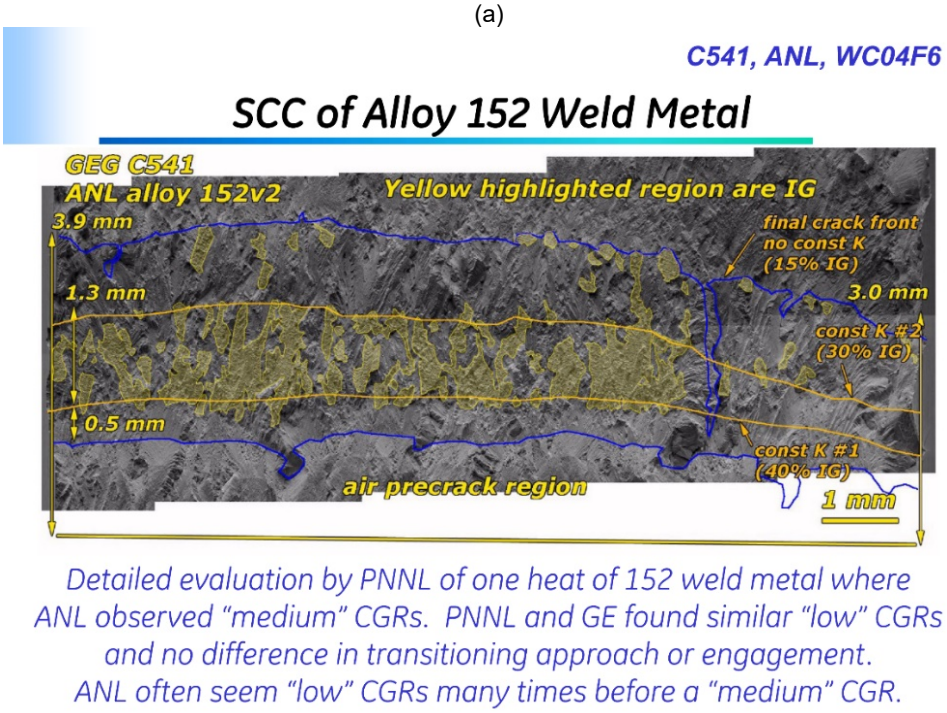

(b)

Figure 130 Fracture surface of Alloy 152 weld specimen C541 tested at GE and analyzed at (a) GE and (b) PNNL.

Finally, the SCC CGR comparison is provided in Figure 131. The SCC CGR data generated at ANL is in disagreement with the data generated at GE and PNNL. Despite the apparently large differences in %IG, GE and PNNL SCC CGR data are in agreement with each other. This, along with the apparent lack of K and temperature dependence, do not describe the widely known and accepted IG SCC behavior. Yet, the GE and PNNL data shown in Figure 131 were adjusted for temperature just as was done in order to generate the MRP-386 curve [13]. As such, Figure 131 illustrates how data obtained at high temperatures as well as the application of an unproven temperature dependence were critical for determining the large FOI of the MRP-386 curve [13].

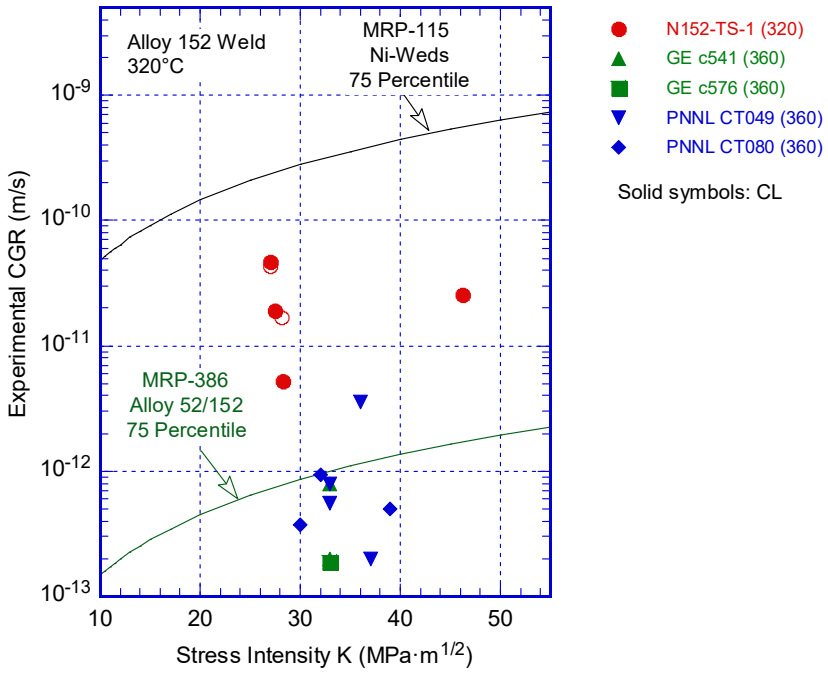

Figure 131 SCC CGR response obtained in ANL, GE and PNNL tests on the same Alloy 152 weld heat WC04F6. Proposed disposition curves for Alloys 182 [1] and 52/152 [13] are included in the figure.

4.2.3 Activation Energy for SCC growth in Alloy 152 Weld

As described in Section 3.1.1, at the end of the test on Specimen A152-TS-5, a temperature change was made to observe its effect on the SCC CGR, Figure 132. The fracture mode was verified to remain IG, hence the outcome can be compared to similar data for Alloy 182.

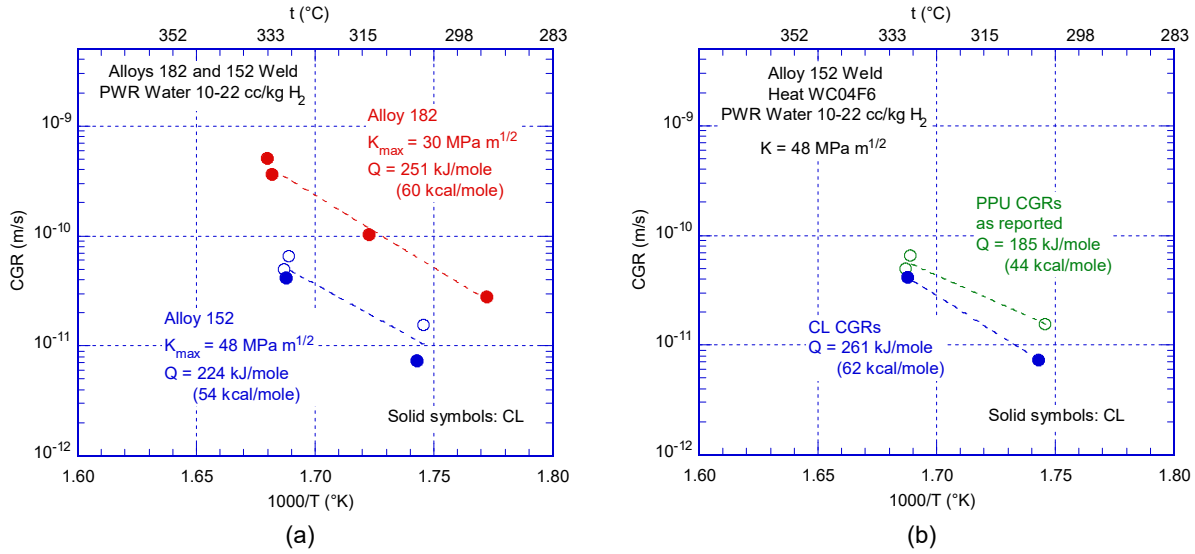

Figure 132 SCC CGRs as a function of 1/T: (a) Alloy 152 and Alloy 182, and (b) Alloy 152 CL and PPU SCC CGRs.

Figure 132a shows the resulting SCC CGRs at two temperatures as well as Alloy 182 data obtained previously [7]. The Alloy 152 data consists of both CL and PPU SCC CGRs while the Alloy 182 data was obtained at constant load, Figure 133. At first sight, there seems to be a very good agreement between the two data sets. However, one has to question the exclusive use of CL for such determinations. For example, while the SCC CGR response seen in Figure 133 appears to be extremely "well-behaved", or perhaps because of that, no attempt was made to correct the CL CGR response at the end of each test period. This could have been accomplished by introducing a short cyclic period at the end of each test to break the ligaments, and straighten the fracture surface. Instead, the resulting 5x fractography correction was applied at the end of the test, uniformly across all test periods. Arguably, this approach is likely to have affected the lower SCC CGRs disproportionately, resulting in a larger activation energy than would have been the case otherwise. As such, for the current results, it is interesting to observe (Figure 132b) that if one selects only the CL SCC CGRs, the activation energy remains similar to that for Alloy 182 determined from under CL, while if one selects the PPU SCC CGRs the resulting activation energy becomes closer to the accepted value for Alloys 600/182.

Based on the limited data here, it would be unwise to quote a value for the activation energy. However, it is important to point out that under IG SCC conditions, the SCC CGR responds to temperature in a manner largely consistent with that of a thermally-activated process, essentially, consistent with the widely known and accepted behavior of IG SCC.

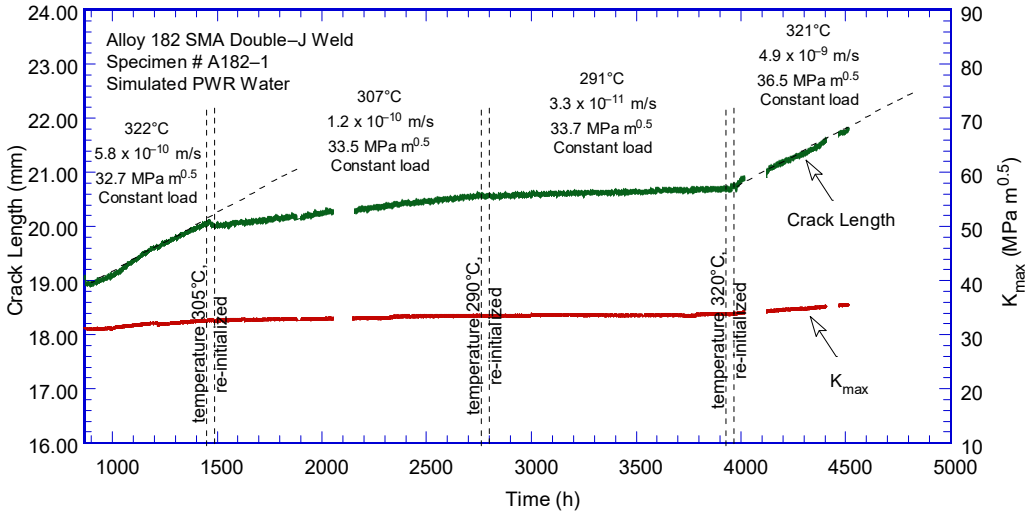

Figure 133 SCC CGR response to temperature changes for Alloy 182 weld specimen A182-TS-1 in simulated PWR environment [7].

4.2.4 Effect of the Welding Parameters on the SCC CGR response in Alloy 52/152 and Variants

In order to conduct a systematic study on the effect of welding parameters on the SCC CGR response, three weldments were made by ANL Central Shops with the same Alloy 152 heat code and in the same geometry (see Section 2.4). Figure 134 summarizes the results. SCC CGR data obtained for the NC152-CR-1 weld specimen produced using “normal” welding parameters is shown alongside SCC CGR data obtained for the HC152-CR-1 weld specimen produced with high current, and the HH152-CR-1 weld specimen produced with high heat input. Also included for comparison are data obtained from the A152 series, and the proposed disposition curves for Alloys 182 [1] and 52/152 [13]. Overall, the data from the A152 series appears more susceptible to SCC than the welds produced for the study of the welding parameters. The welding parameters tested do not seem to affect the SCC CGR response. It is interesting to note that despite the spotty IG engagement and low SCC CGRs obtained on these two Alloy 152 weld specimens, the proposed Alloys 52/152 curve [13] still does not bound any of the data.

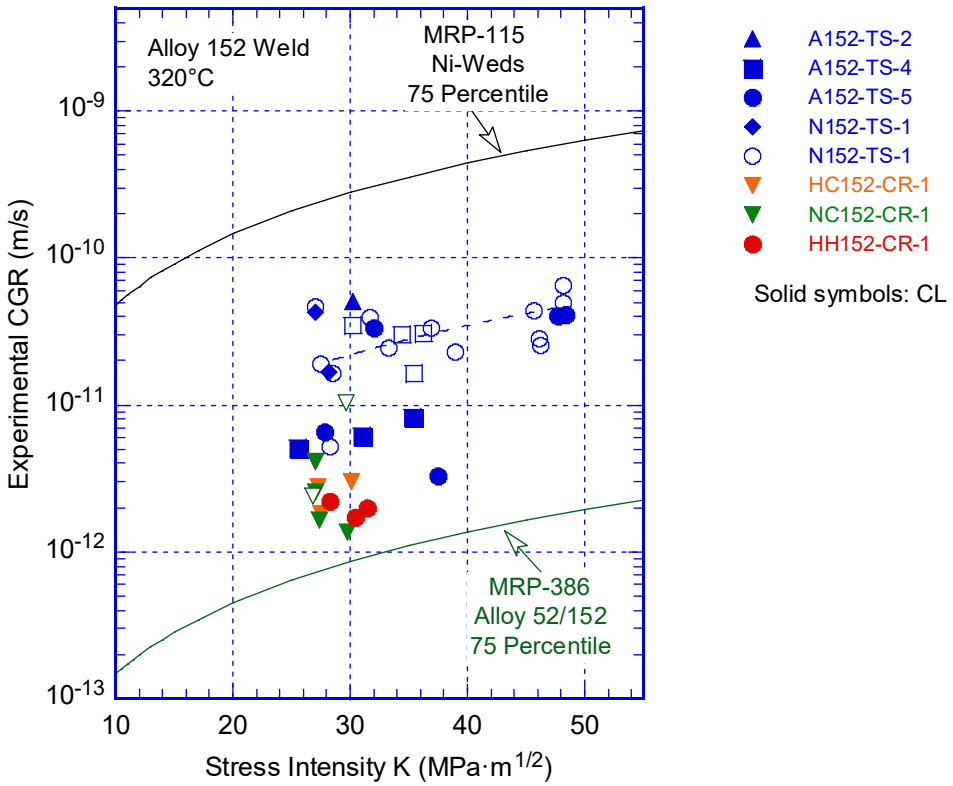

Figure 134 SCC CGRs vs. stress intensity factors for high current Alloy 152 weld specimens NC152-CR-1 ("normal") and HC152-CR-1 ("high current") in simulated primary water. Also included are data from Alloy 152 A152 and N152 welds produced using "normal" welding parameters. The proposed disposition curves for Alloys 182 [1] and 52/152 [13] are included in the figure.

In addition to the ANL-produced welds, testing also involved an Alloy 52M weld produced at EPRI with high heat input. Overall, the weld appears to be resistant, however, some concerns remain in the high stress intensity regime. As such, one SCC CGR measurement – conducted over an extended period of time to increase the confidence in the reported rate – was close to those reported for the "susceptible" Alloy 152 heat used in the early ANL-produced weldments, Figure 135.

The singular data point on specimen HHEP52M-TS-2 shown in Figure 135 highlights two additional, likely important issues:

1) The lack of SCC CGR data at high stress intensity; while the proposed disposition curves extend beyond 50 MPa $m^{1/2}$, the actual data points in this regime are extremely scarce (1%).
2) The SCC CGR data at high intensity would help establish the much-needed dependencies on stress intensity factor, temperature, dissolved H_2, etc.

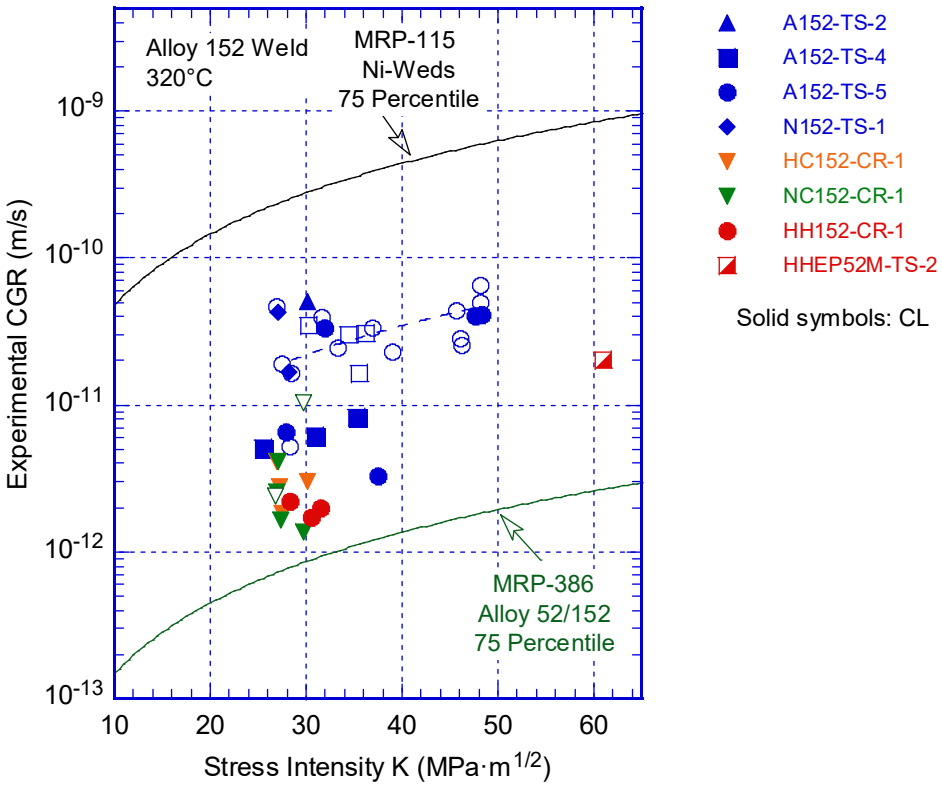

Figure 135 SCC CGRs vs. stress intensity factors for high current Alloy 52M weld "high heat input" weld specimen HHEP52M-TS-2 produced by EPRI. Also included are data from Alloy 152 A152 and N152 welds produced using "normal" welding parameters. The proposed disposition curves for Alloys 182 [1] and 52/152 [13] are included in the figure.

Also tested was an Alloy 152M weldment produce by IHI. For this weld, the initial weld filler had to be abandoned because of weldability issues experienced during production. Hence, the SCC CGR test was deigned to sample both regions. In both regions, no SCC susceptibility was detected, and the IG-less fracture surface confirmed the findings.

4.2.5 Effect of Cold Work on the SCC CGR response in Alloy 52/152 and Variants

The effect of cold-work was evaluated on an Alloy 52 weld produced by MHI on a piece of Alloy 690 CRDM tubing. Tests were conducted on both as-welded conditions and 20% cold-forged (CF) conditions. Figure 136 summarizes the SCC CGR data obtained on these weldments. For context, SCC CGR data obtained for the Alloy 152 ANL-produced weldments A152 and N152 series as well as the proposed disposition curves for Alloys 182 [1] and 52/152 [13] are included. As before, the CGRs obtained from test periods where some cycling was always present ("PPU") are shown with open symbols and appear to be slightly higher than those measured at constant load (solid symbols), but overall all the SCC CGRs are very small. The SCC CGR response is consistent with the predominantly TG fracture morphology for these specimens. Moreover, given the lack of IG fracture and the fact that the SCC CGRs in the 12-20 MPa $m^{1/2}$ range do not show any K-dependence, these data may not even be real SCC CGRs, but noise from the DC potential. Since these were obtained at 320°C, they were not

adjusted for temperature. However, the fact that the proposed Alloys 52/152 curve [13] still does not bound any of these data suggests that many similar, potentially "noise" data points went into the development of the curve.

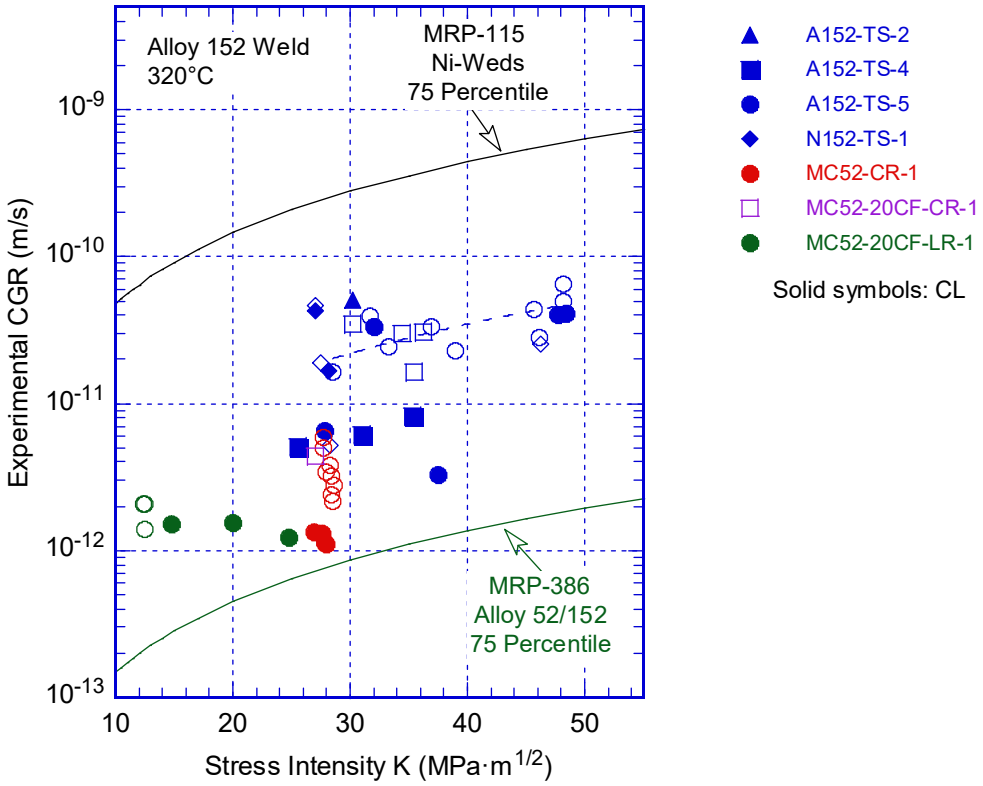

Figure 136 SCC CGR data in simulated PWR environment for Alloy 52 weld produced by MHI in the as-welded and 20% cold-forged (CF) conditions. The proposed disposition curves for Alloys 182 [1] and 52/152 [13] are included in the figure.

5 CONCLUSIONS

This report summarizes testing performed at ANL to investigate the SCC susceptibility of Ni-base Alloy 52/152 and variant welds. The main findings of this report are as follows:

An Alloy 152 weld heat (WC04F6) used in the production of two early weldments by ANL Central Shops was found to be particularly susceptible to IG SCC. As such, testing in a primary water environment resulted in significant proportions of IG morphology. For these specimens, there seems to be a good agreement between that data obtained at CL and the data obtained from PPU conditions, especially for the data with the longer crack extensions. When a criterion on crack advance was imposed, namely that it be at least 10x the resolution to reduce some of the uncertainties associated with the SCC CGRs, the data set appeared to exhibit a functional dependence similar to that for Alloys 82/182. This data set is representative of IGSCC, just like the Alloy 82/182 curve, and was found to have an average SCC CGR approximately 17x lower than the disposition curve for Alloy 182. In addition, these SCC CGRs also exhibited a response to temperature change consistent with that observed for Alloy 182, suggesting that the activation energy for IGSCC growth of Alloy 152 is similar to that of Alloy 182. SCC CGR testing of an Alloy 152 mock-up produced by MHI for the Kewaunee reactor was found to occasionally result in elevated levels of IG fracture, especially at higher stress intensity factors. The SCC CGR for this latter weldment were not as high as those measured for the ANL-produced welds.

A systematic study on the effect of welding parameters on the SCC CGR response was conducted on three weldments produced by ANL Central Shops with the same Alloy 152 heat code and in the same geometry. Specifically, the study involved a weld produced using "normal" welding parameters (qualified to ASME IX), one produced using "high current", and another produced using a "high heat input". SCC CGR testing of these welds resulted in a low IG fractions and low SCC CGRs. The welding parameters tested do not seem to affect the SCC CGR response. In addition to the ANL-produced welds, testing also involved an Alloy 52M weld produced at EPRI with high heat input. Overall, the weld appears to be resistant, however, some concerns remain in the high stress intensity regime. As such, one SCC CGR measurement – conducted over an extended period of time to increase the confidence in the reported rate – was similar to those reported for the "susceptible" Alloy 152 heat used in the early ANL-produced weldments. This singular data point highlights two additional, likely important issues: i) the lack of SCC CGR data at high stress intensity, and ii) the potential of such data to help establish the much-needed dependencies on stress intensity factor, temperature, dissolved H_2, etc.

Also tested was an Alloy 152M weldment produced by IHI with two fillers, one of which exhibited weldability problems. SCC CGR testing covered areas produced with both of these fillers, and no SCC susceptibility was detected. The IG-less fracture surface confirmed the findings.

The effect of cold-work was evaluated on an Alloy 52 weld produced by MHI on a piece of Alloy 690 CRDM tubing. Tests were conducted on both as-welded conditions and 20% cold-forged (CF) conditions, and all the SCC CGRs were found to be very small. The SCC CGR response is consistent with the predominantly TG fracture morphology for these specimens.

The results are discussed in the framework provided by the industry-proposed disposition curves for Alloys 182 [1] and 52/152 [13]. It was found that the Alloy 52/152 SCC CGR disposition curve proposed in MRP-386 [13] bounds hardly any data (7%) presented in this

report. In order to generate Alloy 52/152 curve, it was assumed that the underlying CGR data had dependencies which they were never demonstrated to possess. As such, the MRP-386 curve [13] relies on a database of which 60% of the data were obtained at 350-360°C, and to which an unproven dependence on temperature was applied, thus resulting in an artificially low curve. By contrast, the ANL data were obtained at 320°C, hence, they did not need to be adjusted for temperature.

6 REFERENCES

1. Materials Reliability Program: Crack Growth Rates for Evaluating Primary Water Stress Corrosion Cracking (PWSCC) of Alloy 82, 182, and 132 Welds (MRP-115), EPRI, Palo Alto, CA: 2004. 1006696.

2. Materials Reliability Program: Resistance of Alloys 690, 52 and 152 to Primary Water Stress Corrosion Cracking (MRP-237, Rev. 1): Summary of Findings From Completed and Ongoing Test Programs Since 2004. EPRI, Palo Alto, CA: 2008. 1018130.

3. Materials Reliability Program: Resistance of Alloys 690, 152, and 52 to Primary Water Stress Corrosion Cracking (MRP-237, Rev.2): Summary of Findings Between 2008 and 2012 from Completed and Ongoing Test Programs. EPRI, Palo Alto, CA: 2013. 3002000190

4. Materials Reliability Program: Resistance to Primary Water Stress Corrosion Cracking of Alloy 690 in Pressurized Water Reactors (MRP-258). EPRI, Palo Alto, CA: 2009. 1019086.

5. Alexandreanu, B., Y. Yang, Y. Chen, and W. J. Shack, “Stress Corrosion Cracking in Nickel-Base Alloys 690 and 152 Weld in Simulated PWR Environment - 2009,” NUREG/CR–7137, ANL–10/36, June 2012.

6. Dunn, D., Alexandreanu, B., Toter, W., “Shielded Metal Arc Welding Parameters for Primary Water Stress Corrosion Cracking Test Materials,” Technical Letter Report ML13171A113, June 2013.

7. Alexandreanu, B., O. K. Chopra, and W. J. Shack, “Crack Growth Rates and Metallographic Examinations of Alloy 600 and Alloy 82/182 from Field Components and Laboratory Materials Tested in PWR Environments,” NUREG/CR–6964, ANL–07/12, May 2008.

8. Material Documentation Report for Consumers Power Midland (620-0012-51) and TMI-2 (620-0006-51) Reactor Vessel Lower Head Material, The Babcock & Wilcox Company, BAW-2071, January 1989.

9. American Society for Testing and Materials, “Standard Test Method for Measurement of Fatigue Crack Growth Rates,” ASTM E647-08, DOI 10.1520/E0647-08, West Conshohocken, PA, 2008.

10. American Society for Testing and Materials, “Standard Test Method for Determining a Threshold Stress Intensity Factor for Environment-Assisted Cracking of Metallic Materials,” ASTM E1681-03, DOI 10.1520/E1681-03R08, West Conshohocken, PA, 2008.

11. Electric Power Research Institute, “PWR Primary Water Chemistry Guidelines,” Volume 1, Revision 4, EPRI, Palo Alto, CA, 1999.

12. Electric Power Research Institute, “Materials Reliability Program (MRP) Crack Growth Rates for Evaluating Primary Water Stress Corrosion Cracking (PWSCC) of Thick-Wall Alloy 600 Materials (MRP-55),” Revision 1, 1006695, Palo Alto, CA, 2002.

13. Electric Power Research Institute, “Recommended Factors of Improvement for Evaluating Primary Water Stress Corrosion Cracking (PWSCC) Growth Rates of Thick-Wall Alloy 690 Materials and Alloy 52, 152, and Variants Welds (MRP 386),” Palo Alto, CA, 2017: 3002010756.

14. Ruther, W. E., W. K. Soppet, and T. F. Kassner, “Corrosion Fatigue of Alloys 600 and 690 in Simulated LWR Environments,” NUREG/CR-6383, ANL-95/37, April 1996.

15. Ruther, W. E., W. K. Soppet, T. F. Kassner, and W. J. Shack, “Environmentally Assisted Cracking of Alloys 600 and 690 in Simulated LWR Water,” in Environmentally Assisted Cracking in Light Water Reactors, Semiannual Report, January 1998-July 1998, NUREG/CR-4667, Vol. 26, ANL-98/30, pp. 25-32, March 1999.

16. Chopra, O. K., W. K. Soppet, and W. J. Shack, “Effects of Alloy Chemistry, Cold Work, and Water Chemistry on Corrosion Fatigue and Stress Corrosion Cracking of Nickel Alloys and Welds,” NUREG/CR-6721, ANL-01/07, April 2001.

17. Cassagne, T. B., and A. Gelpi, “Crack Growth Rate Measurements on Alloy 600 Steam Generator Tubes in Steam and Primary Water,” Proc. of the Fifth Intl. Symp. on Environmental Degradation of Materials in Nuclear Power Systems--Water Reactors, American Nuclear Society, La Grange Park, IL, pp. 518-524, 1991.

18. Foster, J. P., W. H. Bamford, and R. S. Pathania, “Initial Results of Alloy 600 Crack Growth Rate Testing in a PWR Environment,” Proc. of the Seventh Intl. Symp. on Environmental Degradation of Materials in Nuclear Power Systems-Water Reactors, NACE International, Houston, TX, pp. 25-39, 1995.

19. Magdowski, R., F. Vaillant, C. Amzallag, and M. O. Speidel, “Stress Corrosion Crack Growth Rates of Alloy 600 in Simulated PWR Coolant,” Proc. of the 8th Intl. Symp. on Environmental Degradation of Materials in Nuclear Power Systems--Water Reactors, S. M. Bruemmer, ed., American Nuclear Society, La Grange Park, IL, pp. 333-338, 1997.

20. Le Hong, S., C. Amzallag, and A. Gelpi, “Modeling of Stress Corrosion Crack Initiation on Alloy 600 in Primary Water of PWRs,” Proc. of the Ninth Intl. Symp. on Environmental Degradation of Materials in Nuclear Power Systems--Water Reactors, F. P. Ford, S. M. Bruemmer, and G. S. Was, eds., Minerals, Metals, and Materials Society, Warrendale, PA, pp. 115-122, 1999.

21. Raquet, O., and G. Santarini, “Stress Corrosion Crack Propagation Rate of Alloy 600 in the Primary Water of PWR Influence of a Cold Worked Layer,” Proc. of the Ninth Intl. Symp. on Environmental Degradation of Materials in Nuclear Power Systems--Water Reactors, F. P. Ford, S. M. Bruemmer, and G. S. Was, eds., Minerals, Metals, and Materials Society, Warrendale, PA, pp. 207-213, 1999.

22. Alexandreanu, B., O. K. Chopra, and W. J. Shack, “Crack Growth Rates of Nickel Alloys from the Davis-Besse and V. C. Summer Power Plants in a PWR Environment,” NUREG/CR–6921, ANL–05/55, November 2006.

23. Alexandreanu, B., O. K. Chopra, and W. J. Shack, “Crack Growth Rates of Nickel Alloy Welds in a PWR Environment,” NUREG/CR–6907, ANL–04/3, May 2006.

24. Alexandreanu, B., Chen, Y., Natesan, K., and Shack, W. J., SCC Behavior of Alloy 152 Weld in a PWR Environment, 15th International Conference on Environmental Degradation of Materials in Nuclear Power Systems – Water Reactors, Cheyenne Mountain Resort, Colorado Springs, Colorado, August 7-11, 2011.

25. Van Der Sluys, W. A., B. A. Young, and D. Doyle, “Corrosion Fatigue Properties on Alloy 690 and some Nickel–Based Weld Metals,” Assessment Methodologies for Preventing Failure: Service Experience and Environmental Considerations, PVP Vol. 410-2, ed., R. Mohan, American Society of Mechanical Engineers, New York, pp. 85–91, 2000.

26. Psaila–Dombrowski, M. J., C. S. Wade, J. M. Sarver, W. A. Van Der Sluys, and P. E. Doherty, “Evaluation of Weld Metals 82, 152, 52, and Alloy 690 Stress Corrosion Cracking and Corrosion Fatigue Susceptibility,” Proc. of the 8th Intl. Symp. on Environmental Degradation of Materials in Nuclear Power Systems-Water Reactors, S. M. Bruemmer, ed., American Nuclear Society, La Grange Park, IL, pp. 412–421, 1997.

27. Alexandreanu, B., Chen, Y., Natesan, K., and Shack, “Primary Water Stress Corrosion Cracking of High-Chromium, Nickel-Base Welds Near Dissimilar Metal Weld Interfaces,” NUREG/CR–7226, ANL–16/10, January 2018.

28. Alexandreanu, B., Chen, Y., Natesan, K., and Shack, “Crack Growth Rate Testing of Alloy 600 Nozzle Sections from the Replacement Pressure Vessel Head at Davis-Besse Reactor, ANL–12/21, February 2012.

NRC FORM 335
(12-2010)
NRCMD 3.7

U.S. NUCLEAR REGULATORY COMMISSION

BIBLIOGRAPHIC DATA SHEET

(See instructions on the reverse)

1. REPORT NUMBER
(Assigned by NRC, Add Vol., Supp., Rev., and Addendum Numbers, if any.)

NUREG/CR-7276

2. TITLE AND SUBTITLE

Primary Water Stress Corrosion Cracking of High Chromium, Nickel-Base Welds - 2018

3. DATE REPORT PUBLISHED

MONTH	YEAR
April	2023

4. FIN OR GRANT NUMBER

5. AUTHOR(S)

B. Alexandreanu, Y. Chen, and K. Natesan

6. TYPE OF REPORT

Technical

7. PERIOD COVERED (Inclusive Dates)

8. PERFORMING ORGANIZATION - NAME AND ADDRESS (If NRC, provide Division, Office or Region, U. S. Nuclear Regulatory Commission, and mailing address; if contractor, provide name and mailing address.)

Argonne National Laboratory
Argonne, IL 60439

9. SPONSORING ORGANIZATION - NAME AND ADDRESS (If NRC, type "Same as above", if contractor, provide NRC Division, Office or Region, U. S. Nuclear Regulatory Commission, and mailing address.)

Office of Nuclear Regulatory Research
Division of Engineering
U.S. Nuclear Regulatory Commission
Washington, DC 20555

10. SUPPLEMENTARY NOTES

11. ABSTRACT (200 words or less)

This report presents the results of a confirmatory research program conducted with the purpose of evaluating the susceptibility of Nickel-base Alloy 52/152 and variant welds to stress corrosion cracking (SCC). Several areas have been of particular interest: heat to heat variability, the effect of welding parameters, and the effect of cold work on SCC CGR response. A systematic study on the effect of welding parameters on the SCC CGR response was conducted on three weldments produced by ANL Central Shops with the same Alloy 152 heat code and in the same geometry. Also tested was an Alloy 152M weldment produced by IHI with two fillers, one of which exhibited weldability problems. The effect of cold-work was evaluated on an Alloy 52 weld produced by MHI on a piece of Alloy 690 CRDM tubing. Tests were conducted on both as-welded conditions and 20% cold-forged (CF) conditions. Overall, these results support the excellent SCC resistance of the high Cr welds in the as-welded condition.

12. KEY WORDS/DESCRIPTORS (List words or phrases that will assist researchers in locating the report.)

Alloy 690
Nickel alloys
Cold work
Stress corrosion cracking

13. AVAILABILITY STATEMENT

unlimited

14. SECURITY CLASSIFICATION

(This Page)
unclassified

(This Report)
unclassified

15. NUMBER OF PAGES

16. PRICE

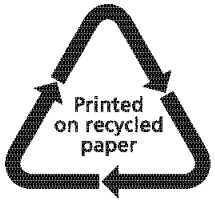

Federal Recycling Program

UNITED STATES
NUCLEAR REGULATORY COMMISSION
WASHINGTON, DC 20555-0001

OFFICIAL BUSINESS

NUREG/CR-7276

Primary Water Stress Corrosion Cracking of High-Chromium Nickel-Base Welds - 2018

April 2023